Sudan University of Science and Technology

College of Graduate Studies

Morphological and Immunohistochemical Study on the Cranial Cervical Ganglion of Dromedary Camel (*Camelus dromedarius*)

دراسة مورفولوجية و كيمياء نسيجية مناعية للعُقدة العصبية العنقية القحفية في الجمل وحيد السنام

By:

Amira Ibrahim Ahmed Abu-Alhassan

B.V.Sc. (1999), University of Nayala

M.V.Sc. (2007), University of Khartoum

A thesis Submitted to the Sudan University of Science and Technology in Fulfillment of the Requirements for Doctor of Philosophy in Veterinary Anatomy

Supervisor: Professor Hassan Ahmed Ali
Department of Biomedical Sciences, College of Veterinary Medicine,
Sudan University of Science and Technology

Co-Supervisor: Dr. Rasha Babikir Yasin Mohammed

Department of Anatomy, College of Veterinary Medicine,

University of Bahri

February, 2019

DEDICATION

To the soul of my father

To my mother Fatima, to my husband Alkhatim

&lovely kids Ahmed, Ehab, Awab & Eyad

To my brothers & sisters

with great love

ACKNOWLEDGEMENTS

First of all, I thank Allah for providing me with health and strength to conduct this work.

I wish to express my deepest thanks and gratitude to my supervisor Prof. Hassan Ahmed Ali for his interest, valuable advices, helpful supervision and suggestions in all aspects of this study.

Sincere thanks are also extended to my co-supervisor Dr. Rasha Babikir Yasin for her advices, suggestions, encouragement and continued support during this study.

Sincere thanks and appreciation for Prof. Gasim Badri, the Vice chancellor of the Ahfad University for Women (AUW) for his kindness, paternal support and financial support. My appreciation is also extended to my colleagues and staff members of the School of Medicine, AUW, for their encouragement and support.

I would like to thank Dr. Zarroug Hassan Ibrahim, College of Agriculture and Veterinary Medicine, Qassim University, KSA, Dr. Mortada Mahjoup, College of Veterinary Medicine, University of Bahri, Dr. Sara Abd Elrahman Shaa aldin, School of Medicine, AUW, Dr. Abd Erahman Ahmed Ali, Faculty of Veterinary Medicine, King Faisal University, KSA, for their unlimited help and encouragement throughout this study.

My thanks are also extended to the rest of the staff members of the Department of Anatomy, Faculty of Veterinary Medicine, University of Khartoum for their cooperation during the study.

At Last, my sincere thanks are also extended to my husband Alkhatim and all members of my family for their great help and continued support.

Published papers extracted from this thesis

1- Amira-Abualhassan, I.A.; Ali, H.A.; Yasin, R.B. (2019).
An Anatomical Study of the Cranial Cervical Ganglion of the Dromedary Camel (*Camelus dromedarius*). Journal of Science and Technology. (in press).

2- Amira-Abualhassan, I.A.; Ali, H.A.; Yasin, R.B.; Ibrahim, Z.H. (2019). Microscopic studies on the cranial cervical ganglion of the dromedary camel (*Camelus dromedarius*). Journal of Agricultural and Veterinary Science, **12** (1). (in press)

List of Abbreviations

ABC	avidin-biotin peroxidase complex
ANMA	anti-neurofilament monoclonal antibodies.
AUW	Ahfad University for Women
CCG	cranial cervical ganglion
NFs	neurofilaments subunits
NSE	neuron specific enolase
PBS	phosphate buffer saline
PGN	principal ganglionic neuron
PGP 9.5	protein gene product 9.5
SCG	superior cervical ganglion
SGC	satellite glial cell
SIF	small intensely fluorescent
TEM	transmission electron microscope

Abstract

Anatomical, histological, ultrastructural, and immunohistochemical studies were carried out on the cranial cervical ganglion (CCG) of the one-humped dromedary camel (*Camelus dromedarius*).

Twenty-eight CCG were collected from adult animals of both sexes and different ages during the period of November 2015 to June 2016, from Al-Salam slaughterhouse, Sudan, and processed for histological, ultrastructural, and immunohistochemical techniques.

Six heads of dromedary camels were used to investigate the position and topography of the CCG. The average weight, length, width and thickness (Mean ± SD) of the right CCG were 0.6±0.08 g, 16.33±1.41 mm, 7.0±1.03 mm and 3.03±0.54 mm, respectively, whereas average weight, length, width and thickness of the left CCG were 0.53±0.09 g, 16.65±1.21 mm, 7.21±0.82 mm and 3.21±0.37 respectively.

The CCG of the camel was located ventral to the atlas and dorsal to the pharynx on the rostrolateral surface of the longus capitis muscle. The CCG was white in colour and triangular or fusiform in shape. The main branches of the CCG were the internal and external carotid nerves in addition to the jugular nerve.

Histological samples collected from ten adult camels were fixed in 10% neutral buffered formalin and conventionally processed for hematoxylin and eosin (H&E) and some special stains.

The CCG was surrounded by dense connective tissue capsule measuring about 155.92±19.43 μm. The capsule was composed of three layers.

The CCG was divided into several ganglionic lobules by connective tissue septa. Each lobule was further subdivided into several ganglionic units which were formed of different types of cells that included the principal ganglionic

neurons (PGNs), satellite glial cells (SGCs), Schwann's cells, small intensely-fluorescent (SIF) cells, mast cells, microglial cell, fibroblasts and pericytes.

The principal ganglionic neurons (PGNs) showed significant differences between the diameters ($p<0.05$) and as a result it had been divided into three types: small, medium and large-sized neurons. All the PGNs showed large cytoplasm with Nissl's substances and peripheral lipofuscin granules.

Satellite glial cells (SGCs) surrounding the PGNs, together with the collagen fibres formed the glial capsule. The small intensely-fluorescent (SIF) cells showed dark centrally located nuclei and pale cytoplasm.

The ultrastructure of the PGNs in the CCG showed an eccentric nucleus with one or two nucleoli, chromatin and heterochromatin granules, and nuclear envelope with pores. The cytoplasm was pale and contained numerous mitochondria, Golgi apparatus, smooth and rough endoplasmic reticulum, free ribosomes, lysosomes, neurofilaments and microtubules.

The ultrastructure of the SGCs showed an irregular, eccentric nucleus, faint cytoplasm with numerous mitochondria, rough endoplasmic reticulum, Golgi complex, lysosomes as well as neurofilaments and microfilaments.

The ultrastructure of the Schwann cells showed pale cytoplasm with numerous mitochondria, rough endoplasmic reticulum in addition to the presence of 1-5 homogeneous, dense bodies. The Schwann cell measured about 46.47±1.46 µm in width and about 67.20±2.01 µm in length.

The ultrastructure of the mast cell showed the small irregular nucleus which contained heterochromatin. The cell membrane had many cytoplasmic processes. The cytoplasm was packed densely staining granules and showed few organelles. The mast cell measured 88.04±3.09 µm in width and about 94.07±2.67 µm in length.

The ultrastructure of the microglial cell showed irregular nucleus with clumps of chromatin. The cytoplasm was dark and contained fine granules and

numerous mitochondria. The measurements of the microglial cell measured 53.15±2.09 µm in width and about 68.75±1.88 µm in length.

The stromal components of the CCG consisted of the neuropil and the blood vessels.

The ultrastructure of the neuropil in the CCG showed both myelinated and nonmyelinated axons in addition to dendrites showing dilatations containing densely packed dark mitochondria. The axoplasm of the myelinated axons was formed of neurofilaments, microtubules, smooth endoplasmic reticulum, small mitochondria and covered with basal membrane, whereas that of the nonmyelinated axons was covered by plasmalemmal folds of Schwann cells and their axoplasms contained mitochondria, neurofilament and microtubules.

Numerous axodendritic synapses and few axosomatic synapses of the neuropils were observed throughout the ganglionic units.

Two types of of vasculature were observed in the stroma; the first type was numerous with different sizes and composed of a single layer of endothelium with many basally accumulated micropinocytotic vesicles. The second type was few in number and larger in size and composed of an inner endothelial lining and an outer layer of smooth muscles.

The immunopositive reactions for S-100 protein were observed in the cytoplasm of large and intermediate sized PGNs, SGCs and Schwann's cells in addition to myelinated and non-myelinated nerve fibres.

The PGNs and myelinated and unmyelinated axons positively reacted with anti-neurofilaments monoclonal antibodies (ANMA).

المُستخَلص

أُجري هذا البحث لدراسة التشريح العياني و التركيب النسيجي و البنية المستدقة و كيمياء النسيج المناعية للعُقدة العصبية العنقية القحفية في الجمل وحيد السنام.

أُخذت هذه العينات من الحيوانات البالغة من الجنسين بمختلف الاعمار و ذلك خلال الفترة من نوفمبر 2015 الى يونيو 2016 من مسلخ السلام بالسودان و تمت معالجتها بالطرق النسيجية وطرق التركيب النسيجي المستدق و الكيمياء النسيجية المناعية.

تم أستخدام ست من رءوس الأبل وحيد السنام لمعرفة التموضع و طبوغرافية العقدة العصبية العنقية القِحفية. وجد أن متوسط الوزن، الطول، العرض والسُمك للعُقدة العصبية العنقية القِحفية اليمنى 0.6 جرام، 1.41±16.33 ملم، 1.03±7.0 ملم و 0.54±3.03 ملم على التوالي، 0.08±يساوي بينما وجد أن متوسط الوزن، الطول، العرض والسمك للعُقدة العصبية العنقية القحفية اليسرى يساوي 1.21±16.65 جرام، 0.82±7.21 ملم و 0.37±3.21 ملم على التوالي. 0.09±0.53

تتموضع العقدة العصبية العنقية القحفية بطنياً للفهقة (الحاملية) و ظهرياً للبلعوم في السطح الخطمي الوحشي للعضلة الطويلة الرأسية. العُقدة العصبية العنقية القحفية بيضاء اللون و مثلثة أو مغزلية الشكل. تشمل الفروع الرئيسية للعُقدة العصبية العنقية القِحفية الأعصاب السباتية الداخلية و الخارجية بالإضافة للعصب الوداجي.

جُمعت عينات نسيجية من عشر من الأبل البالغة ثم حُفظت في 10 % فورملين متعادل و من ثم صبغها بواسطة صبغة الهيماتوكسلين و الايوزين و بعض الصبغات الخاصة الأخرى.

تحاط العُقدة العصبية العنقية القحفية بمحفظة من النسيج الضام الكثيف يبلغ متوسط سمكها حوالي 19.43±155.92 ميكرومتر وتتكون المحفظة من ثلاث طبقات.

تقسم العُقدة العصبية العنقية القحفية الى عدد من الفصيصات العُقدية بواسطة حواجز من النسيج الضام. قسم كل فصيص الى عدد من الوحدات العُقدية و التي تتكون من أنواع مختلفة من الخلايا تشمل العُصبونات العُقدية الرئيسية، خلايا السآتل الدِبقية ، خلايا شُفان، الخلايا الصغيرة كثيفة التألق، الخلايا البدينة، خلايا الدِبق الصغير، الأورمات الليفية و الخلايا الحولية.

و عليه ($p<0.05$)اظهرت العُصبونات العُقدية الرئيسية اختلافاً معنوي بين اقطارها قسمت هذه الخلايا الى عُصبونات صغيرة، متوسطة و كبيرة الحجم. كما اظهر هيولي كل هذه الأنواع من الخلايا حبيبات نسل وحبيبات ليبوفكسين طرفية.

تكون خلايا السآتل الدِبقية المحيطة بالعُصبونات العقدية الرئيسية مع الألياف الكلاجينية المحفظة الدِبقية. أظهرت الخلايا الصغيرة كثيفة التألق أنوية مركزية غامقة اللون و هيولي باهت.

أوضح التركيب النسيجي المُستدق للعُصبونات العُقدية الرئيسية في العُقدة العصبية العنقية القحفية أنوية طرفية لها نوية أو أثنتان، حبيبات كروماتينية، حبيبات كروماتينية مغايره و غشاء نووي مثقب كما أن لها هيولي باهت يحتوي على عدد من المتقدرات، جهاز جولجي، شبكة هيولية باطنة ملساء و محببة، رِيباسات حرة، جُسيْمات حَالة، خيوط عصبية و أنيبيبات.

أظهر التركيب النسيجي المُستدق خلايا السآتل الدِبقية أنوية غير منتظمة طرفية و هيولي باهت يحتوي على عدد من المتقدرات، جهاز جولجي، شبكة هيولية باطنة محببة و جُسيْمات حالة بالأضافة الى خيوط عصبية و خييطات.

أظهر التركيب النسيجي المُستدق لخلايا شُفان هيولي باهت يحتوي على عدد من المتقدرات و شبكة هيولية باطنة محببة بالاضافة الى وجود 1-5 من الأجسام الكثيفة المتجانسة. بلغت ابعاد . ميكرومتر 67.20±2.01 ميكرومتر و طولها 46.47±1.46 عرض خلايا شُفان

أوضح التركيب النسيجي المُستدق للخلايا البدينة أنوية صغيرة غير منتظمة الشكل تحتوي على حبيبات كروماتينية مغايره. لغشاء الخلية زوائد هيولية متعددة، كما يُظهر الهيولي تكدس 88.04±3.09حبيبات كثيفة الصبغة و قليلاً من العضِيات. بلغ قياس عرض الخلايا البدينة حوالي ميكرومتر. 94.07±2.67ميكرومتر و طولها حوالي

أظهرَ التركيب النسيجي المُستدق لخلايا الدِبق الصغير نواة غير منتظمة ذات لُزن كروماتينية. الهيولي داكن اللون و يحتوي على حبيبات دقيقة و الكثير من المتقدرات. بلغَ قياس عرض خلايا الدِبق الصغير 53.15 ميكرومترو و طولها 68.75 ميكرومتر.

تتكون المكونات السدوية للعُقدة العصبية العنقية القحفية من اللِبد العصبي و الاوعية الدموية.

أظهرَ التركيب النسيجي المستدق للبد العصبي مزيجاً من المحاوير النخاعينية و غير النخاعينية بالاضافة الى تغصنات تظهر توسعات تحتوي على متقدرات غامقة تتكدس بكثافة. تتكون جِبلة المحوار النخاعيني من خيوط عصبية، أنيبيبات، شبكة هيولية باطنة ملساء، متقدرات صغيرة و تغطى بغشاء قاعدي, بينما تحتوي جِبلة المحوار غير النخاعيني على متقدرات، خيوط عصبية، أنيبيبات و تغطى بطيات غمدية بلازمية لخلايا شُفان.

تمت ملاحظة عدد من التشابكات المحوارية التغصنية و المحوارية الجسدية للِبد العصبي خلال الوحدات العُقدية.

تمت ملاحظة نوعين من أوعية دموية في السدى، النوع الأول وهو الأكثر انتشاراً ذو أحجام مختلفة و يتكون من طبقة واحدة من الخلايا البطانية ذات حويصلات إحتسائية صغيرة قاعدية التراكم. النوع الثاني وهو قليل العدد، كبير الحجم و يتكون من طبقة داخلية من الخلايا البطانية و طبقة خارجية من العضلات الملساء.

في هيولي العُصبونات العقدية الرئيسية S-100لوحظ التفاعل المناعي الموجب للبروتين المحاوير النخاعينية و كبيرة و متوسطة الحجم، خلايا السآتل الدِبقية و خلايا شُفان بالاضافة الى غير النخاعينية.

العُصبونات العُقدية الرئيسية و المحاوير النخاعينية و غير النخاعينية تفاعلت إيجابياً مع مضادات الأجسام المضادة وحيدة النسيلة للخيوط العصبية.

Table of Contents

List of Tables

List of Text Figures

INTRODUCTION

The autonomic nervous system consists of a vast range of nerves and ganglia connected to the central nervous system on one side and to the viscera on the other side. The sympathetic cervical chain lies dorsal to the vagus nerve and ventral to the transverse processes of the cervical vertebrae and prevertebral muscles. Two ganglia are present in the neck region, the cranial cervical ganglion and the caudal cervical ganglion or stellate ganglion (which includes the uppermost thoracic sympathetic ganglion); a small intermediate (middle) cervical ganglion is sometimes present (Gabella, 1976; Hedger and Webber, 1976; Baljet and Drukker, 1979).

The cranial cervical ganglion (CCG) contains the neurons from which the postganglionic nerve fibres arise. These nerve fibres carry the sympathetic innervation to structures in the head such as the mucosa, smooth muscles, glands, and eyes (Luebke and Wright, 1992; Hubbard, Robinson, Schmidt, Rohen, Tamm and Kaufman, 1999; Hayakawa, Itoh, Miki, Kaneto, Tomiyama and Takeuchi, 2000; Ladizesky, Cutrera, Boggio, Mautalen and Cardinali, 2000). The neurophysiology of the CCG has been studied in the guinea pigs (Purves and Wigston, 1983; De Castro, Sanchez-Vives, Munoz-Martinez and Gallego, 1995).

On the other hand, the CCG's role in some neuropathies is clearly seen in Horner's syndrome as described by Bell, Atweh and Possenti (2001) in human and by Morgan and Zanotti (1989), Boydell (1995), Melian, Morales, Espinosa de los Monteros, and Peterson (1996) and Panciera, Ritchey, Baker and Di Gregorio (2002) in dogs and cats.

Several studies have been published on the role of CCG of stroke-prone rats in relation to the innervation of cerebral vessels (Cardinali, Vacas and Gejman, 1981; Sadoshima, Busija and Brody, 1981; Sadoshima and Heistad, 1982; Coutard, Mertes, Mairose, Osborne-Pellegrin and Michel 2003).

However, the diagnosis and therapy of other animal neuropathies which are related to CCG such as epilepsy (Kokaia, Cenci, Elmer, Nilsson, Kokaia, Bengzon and Bjorklund, 1994) and stroke (Shaibani, Khawar, Shin, Cashen, Schirf, Rohany, Kakodkar and Carroll, 2006; Palmer, 2007) are still unclear to most neuroscientists and neurologists of large mammals.

During the last twenty years, the CCG of different mammals has been thoroughly studied using electrophysiological, immunohistochemical and biochemical techniques, because of its role in the innervation of the intracranial organs such as cerebral vessels, pineal gland and the eye (Miolan and Niel, 1996).

The anatomy of the CCG of the camel had been studied by Cui-sheng, Wang and Xie (1998) and Nourinezhad, Mazaheri and Biglari (2015). However, Abdel-Magied (1995) studied the fine structure of the nerve endings and junctions in the CCG of the dromedary camel.

To our knowledge, the available literature lacked information about the histology, histometry and immunohistochemistry of the CCG of the dromedary camel.

The current study was undertaken to provide a better knowledge and understanding to study morphology and immunohistochemistry of the CCG in the dromedary camel.

Objectives:

The main objectives of this research are to:

1- Investigate the gross anatomy of the CCG and its branches in the dromedary camel.
2- Study the histological components and histometry of the CCG of dromedary camel.
3- Study the ultrastructure of the CCG of dromedary camel using transmission electron microscopy.
4- Detect the localization of the neurofilaments protein and S-100 protein, in the CCG of the dromedary camel using immunohistochemical techniques.

CHAPTER ONE
LITERATURE REVIEW

1.1. Gross anatomy

1.1.1. Topography of the cranial cervical ganglion

The CCG of the horse, dog and cat is located at the most cranial part of the cervical region, close to the base of the skull and represented the cranial portion of the sympathetic trunk which runs parallel to the vagus nerve forming the vagosympathetic trunk (Fioretto, de Abreu, de Souza Castro, Guidi and Ribeiro, 2007).

In donkey, the CCG is located at the cranial extremity of each cervical sympathetic trunk, and lies close by opposite to the internal carotid artery. Each ganglion is related to the caudal face of the guttural pouch and is located ventral to atlantoccipital articulation (Ozgel, Kurtul and Dursun, 2004).

The CCG of bovine is positioned rostral and medioventral to the jugular process extremity and placed ventromedial to the ventral margin of the large tympanic bulla (Nourinezhad, Mazaheri and Saberifar, 2016).

Najafi, Soltanalinejad and Dehghani (2011) described in buffalo, a well-developed CCG located in the dorsal region of the base of epiglottic cartilage, ventromedial to the tympanic bulla and ventral to the atlantic fossa, and medial to the occipital artery.

In white yak, the CCG is located on the rostrolateral surface of the longus capitis muscle and it is partially covered by the tympanic bulla and the stylohyoideus muscle (Shao, Ding, Xie, Yu, Saberi, and Wang, 2007; and Shao, Ding and Wang, 2011).

In goat, the CCG is located ventral to the tympanic bulla, cranioventral to the atlas, ventromedial to the jugular process of the occipital bone and lateral to the longus capitis muscle. It is related to the vagus and hypoglossal nerves and the condylar artery laterally, and glossopharyngeal nerve medially (Ari, Soyguder. and Cinaroglu, 2010).

In sheep, the CCG is located medial to the occipitohyoid muscle, ventral to the jugular foramen, lateral to the longus capitis muscle and craniomedial to a common mass composed of the glossopharyngeal, vagal, accessory and hypoglossal nerves and the condylar artery (Turkmenoglu and Dursun, 2003). On the other hand, Najafi and Nejati (2009) reported in the sheep that the CCG was placed cranioventral to the atlas, at the medial aspect of the paramastoid process and dorsal to the base of the epiglottic cartilage and medial to the internal carotid and occipital arteries.

In roe deer, the CCG is located ventral to the atlas, dorsal to the pharynx, medial to the retropharyngeal lymph node and levator veli palatini muscle cranial to the terminal branches of the common carotid artery and between the ascending pharyngeal and the internal carotid arteries (Kabak and Onuk, 2010).

In dog, the CCG is positioned at the cranial region of the neck, covered by the digastricus muscle and related to the hypoglossal nerve (Fioretto, Guidi, Oliveira and Ribeiro, 2003).

In domestic pig, the CCG is positioned cranioventral to the distal ganglion of the vagus nerve, medial to the jugular process, ventral to the atlas, dorsal to the epiglottis (Kabak, Orhan and Haziroglu, 2005).

In guinea pig, the CCG is located caudoventral to the distal ganglion of the vagus nerve, medial to the digastricus and styloglossal muscles, ventrolateral to the longus capitis muscle, ventral to the tympanic bulla, and between the ascending pharyngeal and the internal carotid arteries (Kabak, 2007).

In the bactrian camel, the CCG is located on the rostrolateral surface of the longus capitis muscle, ventral to the sternomastoideus muscle and covered by the mandibular gland (Cui-sheng *et al.*, 1998). They added that the caudodorsal border of the ganglion is parallel to the vagus nerve, while the rostroventral margin ran along the carotid sinus branch of the glossopharyngeal nerve. On the other hand, Nourinezhad *et al.* (2015) reported that the CCG of

the dromedary camel was constantly present caudal to the cranial base at the rostroventral border of the occipital condyle over the caudolateral part of nasopharynx. The CCG is always in close relation to the longus capitis muscle medially, the internal carotid artery rostrolaterally, and the vagus nerve caudally.

1.1.2. Shape and measurements of the cranial cervical ganglion

The weight and dimensions of the CCG vary with the animal species, size and age (Fioretto *et al*., 2007).

The measurements of the width and length of the CCG of the horse are given by Getty (1975) and Fioretto *et al.* (2007). Getty (1975) reported that the CCG of the horse was a fusiform grayish-pink ganglion which was about 2 to 3 cm in length and 3 mm to 1 cm in diameter. On the contrary, Fioretto *et al.* (2007) compared between the young and adult horses and reported 19.6 mm. length and 5.9 mm. width for the ganglion in young horses compared to 26.3 mm. in length and 2.34 mm. in width for the adult ones.

Nourinezhad *et al.* (2016) reviewed that the CCG of the bovine was well developed and oval or roughly spindle in shape. They added that the length and width of the CCG were 20-25 mm and 10-12 mm, respectively.

Najafi *et al.* (2011) reported that in buffalo the CCG was also well developed, fusiform in shape and reddish in color. They compared the mean of weight, length, width, and thickness in male and female buffalo. They concluded that in male, the ganglion was measured (0.230 ± 0.022 gm), (12.42± 0.610 mm), (3.645 ± 0.049 mm) and (3.110 ± 0.032 mm) respectively, whereas in female they measured (0.261 ± 0.033 gm), (10.89 ±0.553 mm), (3.97 ± 0.050 mm) and (4.001 ±0.040 mm) respectively.

In white yak, the CCG is a grayish arciform in structure, with a mean length of 17.3 mm, a width of 8.0 mm and a thickness of 3.9 mm (Shao *et al.,* 2007; Shao *et al.,* 2011).

In calf, sheep and goat, the CCG is about 8-15.15 mm in length, 3-8.5 mm in width and 3- 4.3 mm in thickness respectively (Getty, 1975).

Turkmenoglu and Dursun (2003) and Najafi and Nejati (2009) concluded that the CCG in sheep is was well develop, fusiform or triangular in shape, and reddish to brown in color. Moreover, Najafi and Nejati (2009) added that the weight, length, width and thickness of the ganglion were 0.12±0.01 g, 8.52±0.34 mm, 2.31±0.03 mm and 2.00 0.03 mm, respectively.

In goat, the CCG is rectangular in shape (Ari *et al.,* 2010). They measured the weight, length, width and thickness of the ganglion and reported that they were 9.05 g, 3.16 mm, 2.55 mm and 2.43 mm, respectively.

In roe deer, the CCG is oval in shape and the mean dimensions of its length, width, and thickness are 13.84±0.50 mm, 3.67±0.15 mm and 3.07±0.14 mm, respectively (Kabak and Onuk, 2010).

Fioretto *et al.* (2003) described the CCG in the dog as a fusiform structure, that was measuring 4-6 mm in length and 2-3 mm in width, however, Fioretto *et al.* (2007) reported that the CCG of young dogs was about 3.5 mm. in length and1.8 mm. in width, whereas the CCG of adult ones was about 4.4 mm. in length and 2.34 mm. in width.

In guinea pig, the CCG is oval in shape and the mean length, width and thickness are 3.16±0.28 mm, 1.49±0.14 mm and 1.11±0.14 mm, respectively (Kabak, 2007).

In cat, the CCG is white in colour and roughly spindle-shaped. In young cats, it is about 3.3 mm. in length and 0.8 mm. in width, whereas in adult it is about 3.3 mm. in length and 1.6 mm. in width (Fioretto *et al.,* 2007).

The dimensions of the CCG of the bactrian camel are given by Cui-sheng *et al.* (1998), who concluded that the CCG was a well-developed structure, varying about 15-20 mm in length, 4- 6 mm in width and 3 mm in thickness. On the other hand, the measurements of the dimensions of the CCG of the dromedary camel are given by Nourinezhad *et al.* (2015) who reported that the

CCG was convex on its lateral surface, and its medial side had a tendency toward concavity or flatness, varying about 14–18 mm in length and 6–8 mm in width.

1.1.3. Branches of the cranial cervical ganglion

Nourinezhad *et al.* (2016) mentioned in bovine that the CCG gave off the vascular, visceral, and communicating branches and received the cervical interganglionic branches.

In buffalo, the branches of the CCG include the internal carotid nerve, external carotid nerve and jugular nerve (Najafi *et al*., 2011).

In white yak, the branches of the CCG include the internal and external carotid nerves, the sympathetic trunk and communicating branches to the glossopharyngeal, vagus and hypoglossal nerves (Shao *et al*., 2011).

In goat, the branches of the ganglion are the internal and external carotid nerves, the jugular and laryngopharyngeal nerves and the communicating branches to the vagus and glossopharyngeal nerves (Getty, 1975; Ari *et al.*, 2010).

In sheep, the internal carotid, external carotid and jugular nerves emerge from each ganglion, detach a branch to the thyroid gland and join the glossopharyngeal, hypoglossal and first cervical nerves and their accessories (Getty, 1975; Najafi and Nejati, 2009).

Kabak and Onuk (2010) reported in roe deer that the internal and external carotid and the jugular nerves were the major nerve trunks of the CCG.

In guinea pig, the branches of the CCG include the internal and external carotid nerves, the jugular nerve, in addition to connecting branches to the pharynx, vagus, glossopharyngeal, accessory, cranial laryngeal, first and second cervical nerves and the vessels in the carotid body region (Kabak, 2007).

In dogs, the main branches of the CCG include the internal carotid and external carotid branches (Fioretto *et al.*, 2003).

Cui-Sheng *et al*. (1998) reported that the branches of the CCG of the bactrian camel included the internal carotid nerve, external carotid nerve, jugular nerve and the branches connecting with the glossopharyngeal, vagus, hypoglossal and first cervical nerves. On the other hand, Nourinezhad *et al.* (2015) reported that the branches of the CCG of the dromedary camel included, the internal carotid and external carotid nerves, jugular nerve, cervical interganglionic branch, laryngopharyngeal branch, carotid sinus branch and communicating branches to the vagus, and first spinal nerves.

1.2. Histology

The CCG microstructure is quite similar between young and adults and among the species. It has been divided into distinct compartments or units by capsular septa of connective tissue which was composed of layers of collagen fibers and flattened fibroblasts as in mammalian sympathetic ganglia (Gabella, Trigg and McPhail, 1988; Szurszewski and King, 1989; Szurszewski and Miller, 1994; Miolan and Niel, 1996; Schmidt ,1996; Ribeiro, Elias, Liberti, Guidi, and de Souza, 2002; Kiran, 2002; Gagliardo, Guidi, da Silva, and Ribeiro, 2003, Ribeiro, Davis and Gabella, 2004; Fioretto *et al.*, 2007). Moreover, Gabella (1976) reported that the connective tissue capsule which surrounded the ganglia of the sympathetic trunk was continued with the epineurium of the associated nerves.

In most domesticated mammals, the sympathetic ganglia composed of neurons (principal ganglionic neurons), satellite cells, Schwann cells and connective tissue (Gabella *et al.*, 1988; Kiran, 2002; Fioretto *et al.*, 2007; Eroschenko, 2008).

Aughey, Fredric and Frye (2001) and Eroschenko (2008) reviewed that the ganglion cells (principal ganglion neurons) were generally spindle or circular in shape, large in size and had a distinct nucleus and nucleolus. The neuron bodies were surrounded and supported by satellite glial cells. Moreover,

they added that the neurons in the sympathetic ganglia were evenly distributed, the nucleus was eccentrically placed in the cell.

Mammalian sympathetic ganglion neurons are usually mononucleated, however, cells with two nuclei could be noticed (Smith, 1970; Dalsgaard and Elfvin, 1982; Ribeiro, 2006). Harman (1989), Young and Heath (2000) and Gartner and Hiatt (2011) reviewed the presence of lipofuscin granules in the cytoplasm of the neurons.

Miolan and Niel (1996) and Gabella (2004) concluded that, in addition to the principal ganglion neurons (PGNs), the sympathetic ganglia contained several other cells types which included small intensely fluorescent (SIF) cells, vascular endothelial cells, mast cells, and fibroblasts which were restricted to the thin septa and capsule.

Webster (1975), Pannese (1981), Pomeroy and Purves (1988) and Young and Heath (2000) stated that there were two types of glial cell in most sympathetic ganglia and nerves. The first type was Schwann cells, which enclose axons in the peripheral nerves. The second type was the satellite glial cells (SGCs), which were associated with the neuron cell bodies within the sympathetic ganglia.

The histological structure of the CCG of mature horses, dogs and cats have been described by Fioretto *et al.* (2007). They prefered to describe the structural units of the ganglion as a ganglion complex rather than a ganglion unit.

Some quantitative studies have been published concerning the total number of CCG's neurons in rats (Santer, 2001). Stereologically related changes in the CCG neuron's number have been reported in mammals of varying body weights, such as rats, capybaras and horses (Ribeiro *et al.*, 2004).

1.3. Histometry

A few histometric investigations have been conducted on the capsule of CCG of horses, dogs and cats (Fioretto *et al.*, 2007; Ribeiro *et al.*, 2004;

Ribeiro, 2006). Fioretto *et al*. (2007) reported that during maturation (from young to adults) there was 32.7% increase in the CCG's capsule in dogs, 25.8% in cats and a 33.2% in horses. Ribeiro *et al.* (2004) measured the thickness of the CCG's capsule in adult animals which ranged from15 to 30 μm in rats, 30 to 70 μm in capybaras, to 60 to 80 μm in horses, whereas, Ribeiro (2006) reported that the thickness of the CCG's capsule ranged from 30–50 μm in young capybaras.

On the other hand, Fioretto *et al*. (2007) noticed a positive correlation between advancing age and the increase in the neuronal profile size in the CCG.

1.4. Ultrastructure

Palay and Palade (1955) and Forssman (1964) in rat, Elfvin (1963) in cat, and Heym and Williams (1979) in shrew investigated the fine structure of the PGNs in the sympathetic ganglion. They described the PGNs as polygonal, mononucleated cells with numerous processes. The Golgi apparatus was well represented in the perinuclear region, and the rough endoplasmic reticulum was abundant throughout the perikaryon. Numerous, large spherical and irregular lysosomes were concentrated near the cell center. The neuropil distributed near the PGNs was highly organized and aggregations of small mitochondria are found within large dendritic processes. Glycogen granules were interposed between many of these mitochondria.

Palay and Palade (1955) reported that the Nissl's substance in the rat's PGNs was a composite material constructed of endoplasmic reticulum and fine granules. The first component of the Nissl's substance appeared to be part of the general endoplasmic reticulum of the neuron. The second component was represented by small granules disposed in patterned arrays either in close contact with the outer membranes of the endoplasmic reticulum or scattered in the intervening matrix. Palay and Palade (1955) also noted that the cytoplasm between Nissl's bodies contained numerous mitochondria, lipids and fine filaments. According to Smith (1959) another type of Nissl's bodies comprising

compact masses of particles and devoid of endoplasmic reticular elements was observed in the sympathetic neurons of the lizard.

Several studies were undertaken to study the ultrastructure of the CCG in rabbits, rats, dogs, cats and horses (Causey and Hoffman, 1956; Barton and Causey, 1958; Siegrist, Dolivo, Dunant, Foroglou-Kerameus, de Ribaupierre and Rouiller, 1968; Matthews and Raisman, 1969; Fioretto *et al*., 2007).

Barton and Causey (1958), Matthews and Raisman (1969), Heym and Williams (1979), Case and Matthews (1985), Matthews (1989) and Fioretto *et al.* (2007) reported the presence of small intensely fluorescent cells (SIF) which were clearly distinct from PGNs and other SGCs. Fioretto *et al*. (2007) added that most of the SIF cells form synapsed with the preganglionic fibers, while few of them had synaptic contact with the PGNs.

Gabella (2004) classified the SIF cells into two types; type I with small granular vesicles ranging from 80 to 100 nm and type II with large granular vesicles varying from 150 to 300 nm.

Causey and Hoffman (1956) and Siegrist *et al.* (1968) focused on the ultrastructure of the synaptic area in the CCG. They described a close approximation of axonal and dendritic or somatic double membranes in the synaptic area. On the contrary, Peters, Palay and Webster (1991) studied the fine Structure of synaptic areas of the rat's CCG. They described the synaptic cleft as the intercellular space between the pre- and postsynaptic components. They added that there were two types of synapses; asymmetric synapses with spherical synaptic vesicles and a prominent postsynaptic density, and symmetric synapses lacking a prominent postsynaptic density, and had pleomorphic vesicles (round and elongated).

Dixon (1963) described the ultrastructure of the SGCs in rabbit CCG. He reported that the SGCs surrounding the neuron were not continuous and showed occasional gaps. The cytoplasm of the SGCs contained mitochondria,

microtubules, solid filaments and limited number of vesicles. Axo-somatic synapses were very rare.

In camel, information pertaining to the ultrastructure of the CCG appeared to be scanty. Abdel-Magied (1995) studied the fine structure of the nerve endings and junctions in the CCG of the dromedary camel and reported that the CCG contained cholinergic, aminergic and sensory endings. The cholinergic endings contained numerous small clear vesicles, a few large dense-cored vesicles, and mitochondria. The aminergic endings are characterized by a mixed population of dense-cored vesicles and clear vesicles. The sensory endings are characterized by numerous slender mitochondria and had no synaptic junctions of any kind.

1.5. Immunohistochemistry

Suvarna, Layton and Bancroft (2013) studied the protein targets of antibodies used in immunohistochemical preparations for the demonstration of neuronal elements. They reported the presence of four main groups of protein in the neurons. In group one, the neuronal cytoskeletal proteins consisted mainly of the neurofilaments subunits (NFs**)** which was specifically expressed by mature neurons. In group two, the cytoplasmic proteins included the protein gene product 9.5 (PGP 9.5) and neuron specific enolase (NSE) which were strongly expressed in neurons. In group three, the neuronal nuclear proteins consisted mainly of the neuronal nuclear protein (NeuN) which was a neuron specific DNA binding protein. In group four, proteins were associated with neurosecretory granules which included the synaptophysin and chromogranin.

1.5.A. Neurofilaments

Liem, Yen, Salomon, and Shelanski (1978), Schlaepfer and Freeman, (1978), Dahl (1983), Trojanowski, Obrocka and Lee (1985), Trojanowski, Walkenstein, and Lee (1986) and Lee, Carden, Schlaepfer, and Trojanowski (1987) classified the mammalian neurofilaments subunits (NFs) into three different polypeptides, commonly referred to as the high (NF-H), middle (NF-

M), and low (NF- L), subunits with apparent molecular weights of 200,000 (NF200), 150,000 (NF150) and 68,000 (NF68).

According to Trojanowski *et al.* (1986) the neuronal perikarya of the paravertebral sympathetic ganglia and the trigeminal ganglia in rats exhibit intense immunoreactivity for each of the NFs. They added that all clusters of axons within these ganglia immunostained by each NFs specific antibody.

Lee, Carden, and Trojanowski (1986) investigated the distribution of NFs in the bovine cerebellum, spinal cord, trigeminal ganglion, and trigeminal nerve. They reported that the monoclonal antibodies exhibited weakly or infrequently immunostained reaction in neuronal perikarya, axons and dendrites. After enzymatic dephosphorylation of these tissues, a more extensive distribution of immunoreactivity was seen, especially in axons and dendrites.

Lee *et al.* (1987) mentioned that the neuronal elements within the spinal cord gray matter of the rats were intensely stained for each of the NFs, however, the axons within the white matter were negative or variably immunoreactive. They added that the NFs staining the neuron's perikarya of the dorsal root ganglion were more intense than the principal ganglion neuron's perikarya of the spinal cord.

Trojanowski *et al.* (1985) in bovine, reported that the neurofilaments subunits triplet proteins were present in cerebellar purkinje cells, the perikarya of the basket cells and their axons as well as the axons of cerebellar white matter and the perikarya of other cerebellar neurons.

Kaemmer, Bozkurt, Otto, Junge, Klink, Weis, Sellhaus, O'Dey, Pallua, Jansen, Schumpelick and Klinge (2010) examined the components of the peripheral nervous system in in the rats, pigs and human using immunohistochemical techniques and observed the presence of the NFs triplet proteins in the nerve fibers.

1.5.B. S-100 protein

Sedaghat and Notopoulos (2008) reviewed that the members of the S-100 protein family are calcium binding proteins because of their solubility in a 100% saturated solution with ammonium sulphate at neutral pH. They are multifunctional with a regulatory role in a variety of cellular processes. They exert their actions usually through calcium binding, although Zn^{2+} and Cu^{2+} have also been shown to regulate their biological activity. On the other hand, Donato, Cannon, Sorci, Riuzzi, Hsu, Weber, and Geczy (2013) stated that the S-100 protein family consisted of 24 members which were functionally subdivided into three main subgroups: those only exerted intracellular regulatory effects, those with intracellular and extracellular functions and those which mainly exerted extracellular regulatory effects.

Wolf, Howard, Dong, Voscopoulos, Boeshans, Winston, Divi, Gunsior, Goldsmith, Ahvazi, Chavakis, Oppenheim and Yuspa (2008) and Donato *et al.* (2013) reported that S-100 protein were only expressed in vertebrates. Moreover, they mentioned that it was involved in regulation of protein phosphorylation, transcription factors, Ca^{2+} homeostasis, dynamics of cytoskeleton constituents, enzyme activities, cell growth and differentiation, and the inflammatory response.

Donato *et al.* (2013) reported that the extracellular S-100 protein exerted regulatory activities on macrophages, microglia, neutrophils, lymphocytes, mast cells, articular chondrocytes, endothelial and vascular smooth muscle cells, neurons, astrocytes, Schwann cells, epithelial cells, myoblasts and cardiomyocytes.

Vega, del Valle-Soto, Calzada and Alvarez-Mendez (1991) studied the distribution of S-100 protein and their subunits (alpha and beta) in lumbar dorsal root ganglia of adult rat. They reported that the immunoreaction for the S-100 was observed in the perikarya of some large and intermediate sized neurons, satellite glial cells and Schwann cells.

Cocchia and Michetti (1981) and Gonzalez-Martinez, Perez-Pinera, Diaz -Esnal and Vega (2003) detected the presence of S-100 protein in paravertebral and prevertebral sympathetic ganglia, mainly in the satellite glial cells, intraganglionic Schwann cells and axons.

To our knowledge, no immunohistochemical studies are conducted on the CCG in the dromedary camel.

CHAPTER TWO

MATERIAL AND METHODS

The present study was conducted on twenty-eight cranial cervical ganglia and six heads of dromedary camels (*Camelus dromedarius*) of both sexes. The age of the camels ranged between two to fifteen years (Wilson, 1984). The samples were collected from Al-Salam slaughter-house, Sudan. All specimens were taken from apparently healthy animals, during the period between November 2015 and June 2016.

2.1. Gross Anatomy

2.1. A. Topography

A total of six heads of adult camels were used for the study of the topography of the CCG and its branches. Both sides of each specimen were carefully dissected to observe the shape, location, arrangement and branches of the CCG. A Canon digital camera (Canon Company, Tokyo, Japan) was used for photography.

2.1. B. Weight and Measurements

Six cranial cervical ganglia were used to determine the weight. The whole CCG was carefully dissected out and weighed on a laboratory balance. The length, width and thickness of the ganglia were then measured with a ruler.

2.2. Histology

Samples of CCG were collected from ten heads of camels of both sexes of different ages. The whole ganglia were removed within five minutes after slaughtering the animals. Small pieces of tissues were fixed in different fixatives including 10% formalin, 10% formal saline and 10% neutral buffered formalin (Culling, 1975). The best fixative for the ganglia was found to be 10% neutral buffered formalin.

The specimens were dehydrated in ascending grades of ethyl alcohol, cleared in xylene, embedded in paraffin wax and sectioned by a rotary microtome at 5μ thick (Drury and Wallington, 1980).

The sections were stained with hematoxylin and eosin (H&E) for general histology (Culling, 1975).

Special stains were used for the study of the following components:

1- Masson's trichrome and Van Gieson's stains for collagen fibers (Drury and Wallington, 1980).
2- Verhoeff's stain for elastic fibres (Suvarna *et al.,* 2013).
3- Gomori's silver impregnation method for reticular fibres (collagen type III) (Drury and Wallington,1980; Suvarna *et al.,* 2013).
4- Cresyl fast violet for Nissl's substance (Suvarna *et al.,* 2013).
5- Luxol fast blue with cresyl violet counterstain for myelin sheath (Suvarna *et al.,* 2013).

2.3. Histometry

H&E sections (5 μm thick) from 6 cranial cervical ganglia were used for histometric measurements.

Measurements of the thickness of the capsule of the cranial cervical ganglion and the length and width of the principal ganglion neuron were done. Olympus microscope (CH20-Japan) with ocular micrometer lens X6 was used in this study. The objective lens X40 and X10 were used to measure the thickness after calibrating the ocular scale of the microscope. Nine measurements of each section were taken from each ganglion and the mean value was calculated.

2.4. Ultrastructure

A total of 7 cranial cervical ganglia from both sexes were used. Each ganglion was cut transversely into 6 equal slices (I cm thickness). Each slice was further cut into numerous sections about $1mm^3$.

Samples were fixed in 2.5% glutaraldehyde in cacodylate buffer (pH 7.4) for 48 hours at 4°C. Samples were then washed in 3 changes of cacodylate buffer and post fixed in osmic tetroxide for 90 minutes. They were then washed in 3 changes of cacodylate buffer for 4 hours and dehydrated in ascending

grades of alcohol (30%, 50%, 70%, 90% and 95%) for 10 minutes each and in two changes of absolute alcohol for 10 minutes each. Specimens were cleared in two changes of propylene oxide, 10 minutes each and then infiltrated with epoxy resin for two hours. Finally, Specimens were embedded in fresh resin overnight (Suvarna *et al.*, 2013).

Semi-thin sections were cut at 0.5- 1 μm thick, stained with toluidine blue, and then examined by light microscope. Ultrathin sections were prepared and were stained with uranyl acetate and lead citrate. Stained ultrathin sections were examined and photographed using Phillips CM10 transmission electron microscope (TEM) in the Electron Microscope Unit of Faculty of Veterinary Sciences, University of Pretoria, South Africa.

2.5. Immunohistochemical study

Five samples of cranial cervical ganglia were taken from camels of different ages and sexes. Each ganglion was cut transversely into 6 equal slices (I cm thickness) and fixed in 10% buffered formalin.

2.5.A. Neurofilaments

For neurofilaments immunohistochemical staining, formalin-fixed specimens were dehydrated in ascending grades of ethyl alcohol, cleared in xylene, embedded in paraffin wax. Sections of 5 μm thick were cut and mounted on gelatin-coated slides. After dewaxing, sections were stained for neurofilaments using avidin-biotin complex method (Hsu, Raine and Fanger, 1981; Trojanowski *et al*., 1986). The sections were hydrated through 100%, 96% and 70% alcohol for 3 minutes and rinsed in distilled water. Endogenous peroxidase activity was blocked, using 3% hydrogen peroxide in absolute methanol for 15 minutes and rinsed in distilled water for 3 times. The slides were washed in 0.1 M phosphate buffer saline (PBS) for 10 minutes. The sections were immersed in plastic container filled with Tris/EDTA buffer (pH 9), put in microwave for 21 minutes and then rinsed in distilled water. The sections were washed in buffer solution for 10 minutes. Then incubated with

primary antibody (code M0762, dilution 1:50, Dako Monoclonal Neurofilament clone 2F11) for 30 minutes and then rinsed in distilled water. Sections were washed in buffer solution for 10 minutes followed by incubation in Dako Envision kit for 30 minutes and then rinsed in distilled water. Sections were again washed in buffer solution for 10 minutes. Peroxidase activity was demonstrated with Kit DAB and checked under the microscope. Eventually, sections were rinsed in distilled water, counterstained with haematoxylin, dehydrated in ethanol up to 100%, cleared in xylene and mounted in Entallen. The slides were finally examined using Olympus microscope.

2.5.B. S-100 protein

For S-100 protein immunohistochemical staining, formalin-fixed specimens were dehydrated in ascending grades of ethyl alcohol, cleared in xylene, embedded in paraffin wax. Sections of 5 µm thick were cut and mounted on gelatin-coated slides. After dewaxing, sections were stained for S-100 protein by using avidin-biotin complex method (Hsu *et al.,* 1981; Isobe, Ishioka and Okuyama, 1981; Isobe, Takahashi, and Okuyama, 1984). The sections were hydrated through 100%, 96% and 70% alcohol for 3 minutes and rinsed in distilled water. Endogenous peroxidase activity was blocked, using 3% hydrogen peroxide in absolute methanol for 15 minutes and rinsed in distilled water for 3 times. The sections were immersed in plastic container filled with Citrate buffer (pH 6), put in microwave for 14 minutes and then rinsed in distilled water. All sections were rinsed in Normal Horse serum (dilution 1:10) for 20 minutes. The sections were incubated in primary anti-body dilution 1:2000 for 40 minutes and then rinsed in distilled water for 3 times. The sections were then washed in buffer dilution for 10 minutes, followed by incubation in Dako Envision kit for 30 minutes and then rinsed in distilled water for 3 times. Sections were again washed in (PBS) buffer solution for 10 minutes. Peroxidase activity was demonstrated with Kit DAB for chromogen and checked under the microscope. Finally, sections were rinsed in

distilled water, counterstained with haematoxylin, dehydrated in ethanol up to 100%, cleared in xylene and mounted in Entallen. The slides were examined with Olympus microscope.

2.6. Statistical analysis

Data of the different histometric parameters were statistically analyzed using Student's t-test, and the difference was considered statistically significant at $p<0.05$.

CHAPTER THREE

RESULTS

3.1. Gross Anatomy

The cranial cervical ganglion (CCG) was a well-developed organ disposed ventral to the caudal stylopharyngeal muscle and covered by the mandibular gland. It was lodged between the common carotid artery and the internal carotid artery rostrolateral to the longus capitis muscle. (Figs. 1 and 2). It was related laterally to the vagus nerve and medially to the retropharyngeal lymph node (Fig. 2). It was triangular or fusiform in shape and white in colour.

The main branches of the CCG comprised the internal carotid nerve and jugular nerve at the cranial half of the ganglion, the external carotid nerve at the caudal half of the ganglion (Fig. 3).

The external carotid nerve emerged from the caudal half of the CCG. It ran caudoventrally to the origin of the external carotid artery and reached its medial wall, where it formed the external carotid plexus (Fig. 3).

The internal carotid nerve was subdivided into five branches which emerged from the rostrodorsal end of the CCG. The branches were surrounded by a sheath and ran rostrally radiating to each other along the surface of the longus captis muscle, whereas the jugular nerve originated as a single branch from the dorsal border of the cranial half of the ganglion and near the jugular foramen and it divided into two branches (Fig. 4).

The CCG gave two communicating branches from the caudodorsal border of the ganglion. The first communicating branch to the vagus nerve and the second communicating branch connected the CCG to the ventral branch of the first cervical nerve (Fig. 5).

The cervical sympathetic trunk passed cranially from the stellate ganglion and joined the vagus nerve in a common sheath as a vagosympathetic trunk, then separated from the common trunk and terminated in the caudodorsal part of the CCG (Fig. 5).

The length, width, thickness and weight of the fresh samples of the right and left CCG were shown in Table 1. The length of the right CCG ranged between 14.5-18.5 mm (the mean length was 16.33±1.41 mm), whereas the length of the left CCG ranged between 15.0-18.2 mm (the mean length was 16.65±1.21 mm). The width of the right CCG ranged between 5.8-8.5 mm (the mean width was 7.0±1.03 mm), while the width of the left CCG ranged between 6.0-8.3 mm (the mean length was 7.21±0.82 mm). The thickness of the right CCG ranged between 2.5-4.0 mm (the mean length was 3.03±0.54 mm), whereas the thickness of the left CCG ranged between 2.8-3.8 mm (the mean length was 3.21±0.37 mm). The weight of the right CCG ranged between 0.70-0.49 g (the mean weight was 0.6±0.08 g), whereas the weight of the left CCG ranged between 0.67-0.43 g (the mean weight was 0.53±0.09 g).

Table (1): Showing the length, width, thickness and weight of fresh samples of right and left cranial cervical ganglion (CCG) in the dromedary camel.

Animal No.	Length (mm)		Width (mm)		Thickness (mm)		Weight (g)	
	Right	Left	Right	Left	Right	Left	Right	Left
1	17.3	16.5	7.5	6.7	3.2	3.0	0.70	0.67
2	15.5	17.9	6.2	7.8	2.6	3.5	0.55	0.51
3	18.5	18.2	8.5	8.3	4.0	3.8	0.69	0.62
4	15.9	16.4	6.5	7.0	2.9	3	0.57	0.45
5	14.5	15.0	5.8	6.0	2.5	2.8	0.49	0.43
6	16.2	15.9	7.7	7.5	3.0	3.2	0.60	0.50
Mean ± SD	16.33 ± 1.41	16.65 ± 1.21	7.0 ± 1.03	7.21 ± 0.82	3.03 ± 0.54	3.2 ± o.37	0.6 ± 0.08	0.53 ± 0.09

2.2. Histology

The CCG was surrounded by a capsule of dense irregular connective tissue consisting mainly of dense bundles of collagen fibres (Fig.6). Numerous reticular fibres were observed within the connective capsule in addition to adipocytes (Fig. 7). The capsule was made of three layers; the outer, middle and inner layer (Fig. 8). The outer layer was thick and showed a compact, regular, and parallel arrangement of collagen fibres (Figs. 8 & 9). The middle layer was thick with a moderate cellular content and consisted of scattered or organized bundles of collagen fibres together with myelinated and non-myelinated nerve fibres (Fig. 9). The inner layer was thin and contained loose connective tissue with a few cellular contents (Fig. 10). Flattened nuclei of the fibroblasts were seen between the densely packed collagen fibres (Figs, 9 & 10). Arterioles, venules and blood capillaries were embedded between the connective tissue capsule.

The inner surface of the capsule gave rise to a variable number of thick branching septa. The septa entered the ganglion dividing it into a varying number of ganglionic lobules of different shapes and sizes (Fig. 11, A). The septa consisted of small scattered or organized bundles of collagen fibres together with reticular fibres (Fig. 11, B & C). The vasculature of the septa was made up mainly of capillaries, arterioles and venules (Fig. 11, D).

The ganglionic stroma consisted of scattered or organized bundles of collagen fibres together with reticular fibres (Fig. 12, A & B). Moreover, many capillaries were seen within the ganglionic stroma, as well as myelinated and non-myelinated nerve fibres (Fig. 12, B & C).

The myelinated nerve fibres contained many fascicles and were bounded by an epineurium (Fig. 13, A). Blood vessels of various sizes were seen in the epineurial connective tissue (Fig. 13, B). Each fascicle was surrounded by a perineurium and contained numerous axons which were cylindrical in shape and bearing a smooth outline and a uniform thickness throughout their length

(Fig. 13, B). The single axon was surrounded by an endoneurium of thin connective tissue (Fig. 14, A). Nodes of Ranvier were seen between the internodal segments of the myelinated nerve fibres (Fig. 14, B). Schmidt-Lanterman's clefts which resulted from the oblique incisions in the myelin sheath of the axons were very obvious (Figs. 14, C). These clefts were produced by inclusions of Schwann cell cytoplasm. Schwann cells were observed winding around a single axon forming the myelin sheath (Fig.14, B).

In cross sections, the non-myelinated nerve fibres were tightly packed and Schwann cell nuclei and capillaries were scattered among them (Fig. 15, A). The non-myelinated nerve fibres were seen in parallel alignment with Schwann cells nuclei (Fig. 15, B). Blood capillaries were interspersed among the nerve fibres. Schwann cells were large in size circular or oval in shape (Fig. 15 A, B & C). Their nuclei were large, flattened, rounded, or occasionally irregular (Fig. 15, C).

The vasculature of the ganglionic units was very extensive and made up mainly of blood capillaries. The blood capillaries were restricted to the PGNs rather than around the nerve fibres (Fig. 15, A, B & C).

Dense network of reticular fibres were seen supporting the ganglionic units, as well as the neuropil, capillaries and myelinated and non-myelinated nerve fibres (Fig. 16).

The ganglionic units were composed of various cells types. These cells include PGNs and glial cells. Other cell types, such as small intensely fluorescent cells (SIF), fibroblasts, mast cells and pericytes have been found (Fig. 17).

The PGNs were large in size, circular or oval in shape and the cell bodies and axons were evenly distributed across the ganglion rather than being grouped into clumps (Fig. 18, A). The majority of the PGNs were concentrated at the middle of the ganglion leaving the two terminal ends of the ganglion being made up exclusively of nerve fibres (Fig. 18, B). The PGNs composed

of three types of neurons: small, medium and large neurons. Their average diameters were 77.13±4.099 µm, 127.154±7.444 µm and 250.22±37.154 µm for the small, medium and large neurons respectively. The small PGNs were distributed in the broad middle region of the ganglia, followed by a zone containing a mixture of medium and large PGNs, whereas the terminal parts contained only large PGNs (Fig. 19, A & B). The small-sized PGNs were the most numerous type observed.

All PGNs were mononucleated (Figs. 20, A, B & 21, A & B). The nuclei were eccentric, however, some of them were central in position. The granules were large, spherical and light in colour with finely dispersed chromatin and distinct dark nucleoli (Fig. 20, A). Each neuronal nucleus contained one (Fig. 20, A & B) or two nucleoli (Fig.20, B).

The PGNs contained Nissl's substances (Fig. 21, A). They were scattered throughout the cytoplasm, except the region of the axon hillock. They were coarse and abundant in large PGNs, and fine and few in small PGNs. Moreover, the cytoplasm of the large PGNs contained lipofuscin granules, which were located at the peripheral regions of the cytoplasm (Fig. 21, B).

SGCs were observed encircling the PGNs and their processes (Fig. 22, A), and together with the collagen fibers forming the glial capsule (Fig. 22, B). The number of the SGCs surrounding the neurons were shown in (Table 2). A positive correlation was found between the number of the SGCs and the neuronal size. The small sized PGNs were surrounded by the minimal number of cells which was 5±1.06. The medium-sized PGNs were surrounded by 11±1.58 cells, whereas the large PGNs were surrounded with approximately 19±3.09 satellite glial cells.

The thickness of the glial capsule varied extensively around the perikaryon of each PGN. It was maximal at the level of the nuclei of a SGCs, while it was sharply reduced in areas devoid of the nuclei (Fig. 22, B). The SGCs were either small and flattened (Figs.22, A) or low cuboidal cells (Fig.

22, B). The SGCs were mostly organized around the large PGNs rather than their corresponding small PGNs (Fig.22, A & B).

The glial capsule together with the myelinated and unmyelinated fibers comprised the neuropil wrapping the PGNs. The neuropil was uniformly distributed between the ganglionic units. The thickness of the neuropil was greater around the large PGNs compared to the small PGNs (Fig. 23). Blood capillaries were regularly seen in the neuropil either completely surrounding each PGN, or sometimes aggregated at the poles of the PGN (Fig. 24 A & B).

The SIF cells were of two types; the first type was observed either singly (Fig. 25, A) or sometimes forming clusters, short cords or strands in close proximity to the blood capillaries (Fig. 25, B). The second type of SIF cells was observed within the stroma surrounding the PGNs (Fig. 25, C). The SIF cells were rounded or polyhedral, and sometimes elongated, with a darkly staining, large central nucleus and inconspicuous nucleolus (Fig. 25, A & C). Their cytoplasm lacked the Nissl's bodies and appeared pale and clear.

Pericytes were often seen surrounding the blood capillaries within the connective tissue septa of the ganglionic lobules (Fig. 26, A). Mast cells were observed within the ganglionic stroma containing a large number of cytoplasmic granules (Fig. 26, B). Moreover, nuclei of fibroblasts and Schwann cells associated with nerve fibers bundles were seen at intervals between adjacent groups of PGNs (Fig. 26, C).

Table (2): Showing the average number of satellite glial cells around the different principle ganglion neurons in the cranial cervical ganglion.

Animal No.	Small PGN	Medium PGN	Large PGN
1	16 18 23	12 14 10	5 4 6
2	25 17 18	9 13 11	4 7 4
3	20 16 18	12 9 11	7 5 4
4	19 25 18	12 13 10	4 5 5
5	16 20 16	11 9 10	4 6 5
Total	**285**	**166**	**75**
Mean ± SD	**19± 3.09**	**11± 1.58**	**5± 1.06**

3.3. Histometry

The histometric measurements are summarized in (Tables, 3, 4, 5 and 6), Text-fig. 1 and appendix.

The mean thickness of the capsule of the cranial cervical ganglion was 155.92±19.438 μm.

The mean diameters of the small, medium and large-sized principal ganglion neurons of the cranial cervical ganglion were 77.13±4.099, 127.154±7.444, and 250.22±37.154 respectively.

The mean diameters of the principal ganglion neurons significantly reflected their classification according to the neuronal size into small, medium and large.

Table (3): Showing the thickness (µm) of the capsule of the cranial cervical ganglion.

Animal No. / Sample No.	1	2	3	4	5
1	181.9417	123.6436	196.1861	120.6987	135.5736
2	174.7835	167.0046	194.948	147.4487	124.5118
3	175.333	154.9076	199.8628	142.5518	111.6518
4	164.3926	121.6948	172.2628	154.7037	128.0721
5	162.4574	123.0342	143.9401	168.5695	207.9797
Total	**858.9081**	**690.2847**	**907.1999**	**733.9723**	**707.7889**
Mean± SD	**171.7816± 8.161**	**138.0569± 21.3486**	**181.44± 23.61**	**146.7945± 17.5793**	**141.5578± 38.1263**

Table (4): Showing the dimeter (µm) of the small principal ganglion neurons of the cranial cervical ganglion.

Animal No. / Sample No.	1	2	3	4	5
1	78.05	90.20	73.01	66.68	69.43
2	73.12	87.39	68.17	87.02	75.10
3	96.41	66.86	76.09	94.27	71.16
4	78.01	73.72	82.09	78.91	81.39
5	80.59	63.91	71.04	80.53	65.33
Total	**406.18**	**382.08**	**370.4**	**407.41**	**362.41**
Mean± SD	**81.236± 8.9**	**76.416± 11.89**	**74.08± 5.33**	**81.48± 10.26**	**72.48± 6.09**

Table (5): Showing the dimeter (µm) of the medium-size principal ganglion neurons of the cranial cervical ganglion.

Animal No. / Sample No.	1	2	3	4	5
1	143.05	112.60	100.79	102.42	127.37
2	110.58	131.24	106.80	129.46	109.80
3	133.59	124.72	121.44	143.44	120.85
4	139.63	157.91	124.84	122.54	143.47
5	167.94	121.13	167.08	101.85	114.31
Total	**694.69**	**647.78**	**620.95**	**599.71**	**615.8**
Mean± SD	**138.94± 20.56**	**129.56± 17.22**	**124.19± 25.97**	**119.94± 17.20**	**123.16± 13.16**

Table (6): Showing the dimeter (µm) of the large principal ganglion neurons of the cranial cervical ganglion**.**

Animal No / Sample No	1	2	3	4	5
1	267.99	228.91	342.05	209.87	207.80
2	259.26	262.39	291.22	248.20	217.14
3	231.45	280.76	292.26	232.39	197.72
4	338.09	273.50	248.59	207.90	163.71
5	259.93	235.93	279.04	302.11	177.32
Total	**1356.72**	**1281.49**	**1453.16**	**1199.47**	**963.69**
Mean± SD	**271.34± 39.79**	**256.30± 22.89**	**290.63± 33.72**	**239.89± 38.47**	**192.74± 21.95**

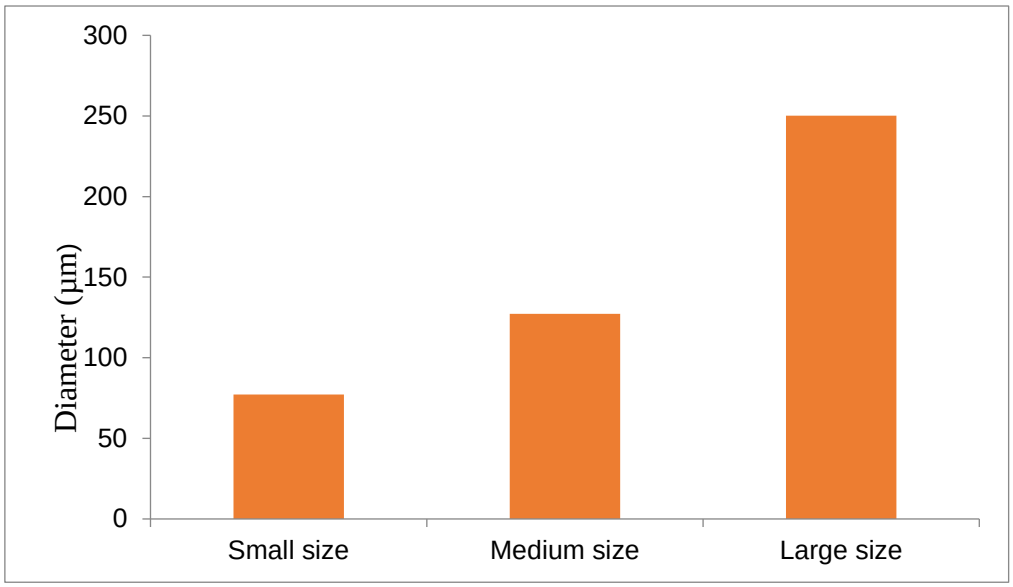

Text-fig.1: Showing the diameters of small, medium and large size principal neurons of cranial cervical ganglia.

3.4. Ultrastructure

The capsule of the CCG composed of several layers of collagen fibres and flattened fibroblasts (Fig. 27, A). Fibroblasts were long, fusiform cells with cytoplasmic processes extending between the bundles of collagen fibres (Fig. 27, B). Organelles such as Golgi apparatus, rough endoplasmic reticulum and mitochondria were seen throughout the cytoplasm of the fibroblasts (Fig. 28). The nuclei of the fibroblasts were flattened or irregular in shape (Figs.27, A & 28). Myelinated and non-myelinated nerve fibres in addition to blood vessels were also observed (Fig. 29, A & B).

The principal ganglion neurons were large in size, circular or more commonly oval-shaped (Fig. 30, A). They showed large, pale and spherical or slightly ovoid nuclei. The nucleus was generally eccentric with one or two well-defined nucleoli (Fig. 30, B & C). The nuclear membrane was a double membraned structure with numerous nuclear pores (Fig. 31, A). The plasma membrane of the PGNs possessed numerous folds. These folds were settled in the intercellular space and displayed shallow irregular grooves (Fig. 31, B).

The cytoplasm of the PGNs was rich in organelles which included granular and smooth endoplasmic reticulum, mitochondria, Golgi apparatus, free ribosomes, lysosomes, centriole and neurofilaments (Figs. 32, A & B).

Smooth endoplasmic reticulum was usually noted throughout the perikaria of the PGNs in association with the rough endoplasmic reticulum (Fig. 33, A), however the rough endoplasmic reticulum predominated and extended to the dendrites (Fig. 33, A). They consisted of flattened, small and loosely packed cisternae which were oriented parallel to each other (Fig. 33, B). Small ribosomes were attached to the outer surface of the membranes of the cisternae, whereas numerous ones of similar size and density were scattered freely between the cisternae (Fig. 34). The peripheral region of the principal ganglion neuron was devoid of rough endoplasmic reticulum, and was occupied

exclusively by free ribosomes, which often were aggregated in the form of small polysomes.

Numerous pale mitochondria with different shapes; filamentous, oval, or spherical were evenly distributed throughout the cytoplasm of the PGNs with special concentration at the perinuclear area (Fig. 35). Their diameters ranged from 0.55±0.13 µm to 1.6±0.49 µm. They possessed an outer smooth membrane and an inner folded one which formed cristae.

The Golgi apparatus was well developed in the perinuclear region of the PGNs. It consisted of several stacks, often parallel to each other. Each stack was enlarged at the ends forming vesicles (Fig. 36).

Large spherical and irregular lysosomes were often noted in the cytoplasm of the of the PGNs (Fig. 37). They appeared as homogeneous, membrane bounded electron-dense bodies, however, some of them showed light vacuoles.

The PGNs contained fine, long threadlike neurofilaments which were scattered throughout the cytoplasm between the rough endoplasmic reticulum and other organelles (Fig. 38). The neurofilaments were regularly seen crossing one another in all directions, but sometimes they were arranged in one direction. They were observed either in the form of loose or dense bundles. Microtubules were also seen distributed throughout the cytoplasm.

The glial capsule was composed of SGCs, dendrites, and connective tissue fibres (Figs. 39).

SGCs were small in size and flattened in shape with numerous cytoplasmic processes intermingled with the dendrites of the principal neurons (Fig. 39). SGCs have large, dark, spherical, ovoid, or irregular and indented nucleus. The nucleus of the SGCs had fine granular chromatin with dense peripheral clumps. It was eccentric with one well-defined nucleolus. The SGCs was surrounded by a basal lamina of variable thickness followed by a narrow rim of cytoplasm. The cell membrane showed numerous folds. Mitochondria,

rough endoplasmic reticulum and Golgi apparatus were prominent organelles in the SGCs (Fig. 40, A & B). Numerous spherical or oval mitochondria were scattered around the nucleus, in addition to compact arrays of granular endoplasmic reticulum (Fig. 40, B). The Golgi apparatus was observed in the perinuclear region. Numerous large spherical or irregular lysosomes scattered throughout the cytoplasm were also observed, as well as neurofilaments and microtubules (Fig. 41, A). These filaments were arranged more or less parallel to each other. Besides being dispersed throughout the cytoplasmic matrix, the neurofilaments often formed capsulated inclusion in the SGCs (Fig. 41, B).

The fibrous constituents, of the neuropil, mainly the myelinated and non-myelinated axons separated by collagen fibrils were usually observed (Fig. 42). Collagen fibrils of the perineurium were noted surrounding the myelinated and unmyelinated axons.

The non-myelinated axons laid in a complicated membrane-lined groove within the Schwann cell either singly or in groups. They were covered by the basal membrane. Plasmalemmal folds of the Schwann cells were observed completely covering the non-myelinated axons. Some non-myelinated axons were located superficially, whereas others were positioned deeply within grooves in Schwann cell cytoplasm (Fig. 43). The axoplasm appeared as a wide area with light cytoplasm. Organelles such as mitochondria, neurofilament and microtubules were seen throughout the axoplasm. A periaxonal space was also observed (Fig. 44).

The myelinated axons were covered by a basal membrane. An outer mesaxon and inner mesaxon were observed consisting of paired dense lines (Fig. 45, A). In the myelinated axons, the myelin sheath appeared as several layers of stacked membranes (Fig. 45, B). Neurofilaments, microtubules, smooth endoplasmic reticulum and small rounded or spherical mitochondria were also found in the axoplasm of the myelinated axons (Fig. 45, C).

Schwann cells were large in size and were estimated to measure about 46.47±1.46 µm in width and about 67.20±2.01 µm in length. They had infoldings or grooves at their surfaces and were surrounded by a basal lamina. Organelles such as rough endoplasmic reticulum and free ribosomes were seen throughout the cytoplasm of the Schwann cells (Fig. 46, A). Schwann cells cytoplasm contained one to five homogeneous, dense bodies (Fig. 46, B). The nuclei of Schwann cells were large, flattened, rounded or ellipsoid. Occasionally, they were irregular in shape (Fig. 46, C).

The dendrites in the neuropil were extensions of the cell body of the PGNs. They were either connected to the SGCs or lying free in the neuropil (Fig. 47, A). Organelles such as mitochondria, endoplasmic reticulum and microtubules were seen in dendrites (Fig. 47, B).

The dendrites in the neuropil also contained densely packed dark and cylindrical mitochondria interspersed with one or more patches of neurofilaments, and microtubules. Many clear vesicles were also observed. (Fig. 48, A & B).

Two types of synapses were observed in the neuropil; axodendritic and axosomatic synapses. The Axodendritic synapses (Fig. 49, A) were seen throughout the ganglionic units of the cranial cervical ganglion between the presumptive axon terminal and the base or terminal end of a large dendrite. The axon terminal contained small clear-synaptic vesicles (50.18±3.01 µm in width and 61.29±2.03 µm in length), and some large dense-cored vesicles (70.49±2.07 µm in width and 83.75±1.29 µm in length) in addition to few mitochondria. The dendrites showed many microtubules, mitochondria, and a few tubules of smooth endoplasmic reticulum. (Fig. 49, B & C)

Axosomatic synapses (Fig. 50) were observed throughout the ganglionic units of the cranial cervical ganglion on the surface of the soma of a PGN. Most of the axon terminals contained some small clear-synaptic vesicles, some large dense-cored vesicles and a few mitochondria.

Mast cells were observed within the stroma of the ganglionic units or in the neuropil in the vicinity of the small vessels. They were large in size and measured about 88.04±3.09 µm in width and about 94.07±2.67 µm in length. They were spindle or irregular in shape with few organelles (Fig. 51, A, B & C). The nuclei of mast cells were relatively small, flattened or irregular in shape. They were centrally located and showed peripheral heterochromatin. The cytoplasm was packed with round or oval densely staining granules (Fig. 51, A, B & C).

Microglial cells were observed within the stroma of the ganglionic units or in the neuropil adjacent to the PGN (Fig. 52, A & B). They were large in size and were estimated to measure about 53.15±2.09 µm in width and about 68.75±1.88 µm in length. They were irregular in shape with many cytoplasmic processes. They had dark cytoplasm with fine granules and numerous mitochondria. They had large, central, flattened or irregular nucleus with clumps of chromatin. A centriole was occasionally observed within the cytoplasm ((Fig. 52, B).

The CCG was highly vascular and it showed two types of vasculature; the first type which resembled blood capillaries was numerous in number with different sizes consisting of a single layer of endothelium only. Its endothelial cells were characterized by a large, elongated nucleus and many basally accumulated micropinocytotic vesicles (Fig. 53, A). The luminal surface of the endothelial cells possessed numerous processes. Pericytes were observed surrounding the basal membrane (Fig. 53, B). The second type was few in number, larger and composed of an inner endothelial lining in addition to an outer layer of smooth muscle cells (Fig. 53, C).

3.5. Immunohistochemistry

3 .5. A. Neurofilaments

The capsule of the CCG negatively reacted to the anti- neurofilaments monoclonal antibodies (ANMA) except for that seen in nerves traversing each

ganglion capsule. The walls of the arteries and veins within the capsule were also negative (Fig. 54, A). The septa and their blood vessels of the CCG did not show any immunoreactivity to the neurofilaments except for that seen in nerves traversing the connective tissue (Fig. 54, B & C).

A variable intensity of ANMA reactivity was observed in the CCG mainly in the PGNs and their axons. The perikarya of PGNs exhibited variable intensity of immunoreactivity for ANMA. The large and medium-sized PGNs strongly reacted to the ANMA (Fig. 55, A), whereas the small PGNs possessed low immunoreactivity (Fig. 55, B). The nuclei within PGNs were negative for ANMA staining (Fig. 55, A **&** B).

The cytoplasm of the small intensely fluorescent (SIF) cells showed moderate reactivity to the ANMA, whereas their nuclei were strongly positive (Fig. 56, A **&** B).

In the neuropil, the myelinated and nonmyelinated axons within the connective tissue of the glial capsule were strongly positive with the ANMA (Fig. 57). The basal lamina of the outer surface of the glial capsule was weakly positive to ANMA. SGCs showed either weak or negative reactivity for the ANMA, however, their nuclei were usually negative (Fig. 57).

In the ganglionic unit stroma, a strong ANMA positive reaction was observed in the axons of the myelinated and nonmyelinated nerve fibres (Fig. 58, A & B). The endoneurium and perineurium showed negative reactivity (Fig. 59).

The cytoplasm of Schwann cells was either negative or reacted weakly to ANMA, whereas their nuclei were negative (Fig. 60).

Table (7): A summary of the immunohistochemical reactivity of the cranial cervical ganglia for the anti-neurofilament monoclonal antibodies (ANMA).

Tissue / Reactivity	Negative (-)	Weak (±)	Moderate (+)	Strong (++)	Very strong (+++)
C. T. capsule	√				
Blood vessel	√				
Non-myelinated axon					√
Myelinated axon					√
Myelin sheath	√				
PGN nucleus	√				
Large PGN. cytoplasm					√
Medium PGN cytoplasm					√
Small PGN cytoplasm			√		
Neuropil basal lamina		√			
SGC nucleus	√				
SGC cytoplasm	√	√			
Schwann cell nucleus	√				
Schwann cell cytoplasm	√	√			
SIF nucleus					√
SIF cell cytoplasm		√			

3.5. B. S-100 protein

The capsule of the CCG negatively reacted to the anti S-100 protein (Fig. 61) except in the nerves traversing the ganglion capsule. The walls of the blood vessels within the capsule were also negative. The septa of the CCG did not show any reactivity for anti S-100 protein except for that seen in the nerves traversing the connective tissue of the septa (Fig. 62, A & B).

In the ganglionic unit stroma, a strong S-100 protein positive reaction was observed in the nerve fibers (Fig. 63). Myelinated and non-myelinated nerve fibres were strongly positive for S-100 protein (Fig. 64). Capillaries within the ganglionic unit stroma showed either weak positive or negative reaction to the anti- S-100 protein (Fig. 65).

A strong immunoreactivity for S-100 protein was observed in the cytoplasm of Schwann cells, however their nuclei were negative (Fig. 66).

Negative to weak immunoreactivity for S-100 protein was observed in the different PGNs. Neuronal perikarya and the nuclei of the small and medium-sized PGNs were negative for - S-100 protein (Fig. 67, A), while the neuronal perikarya of the large-sized PGNs showed weak immunoreactivity (Fig. 67, B).

In the neuropil, the glial capsule was strongly positive for the S-100 protein. A strong immunoreaction for S-100 protein was also detected in the cytoplasm of the SGCs (Fig. 68).

The cytoplasm and nuclei of the SIF cells showed negative reactivity for the S-100 protein (Fig. 69).

Table (8): A summary of the S-100 protein immunoreactivity in the cranial cervical ganglia**.**

Tissue / Reactivity	**Negative (-)**	**Weak (±)**	**Moderate (+)**	**Strong (++)**	**Very strong (+++)**
C. T. capsule	√				
Blood vessel	√				
non-myelinated axon					√
myelinated axon					√
Myelin sheath					√
PGN nucleus	√				
Large PGN cytoplasm		√			
Medium PGN cytoplasm	√				
small PNG cytoplasm	√				
SGC nucleus	√				
SGC cytoplasm					√
Schwann cell nucleus	√				
Schwann cell cytoplasm				√	
SIF cell nucleus	√				
SIF cell cytoplasm	√				

FIGURES

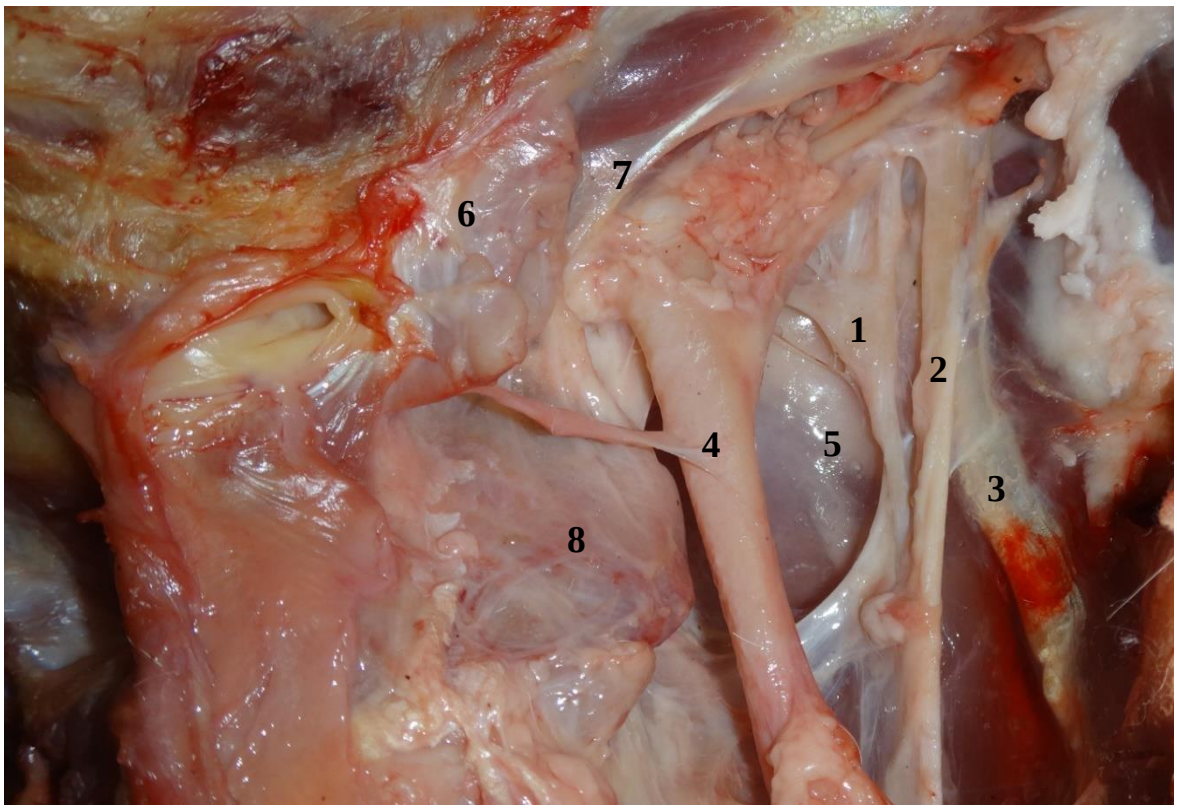

1

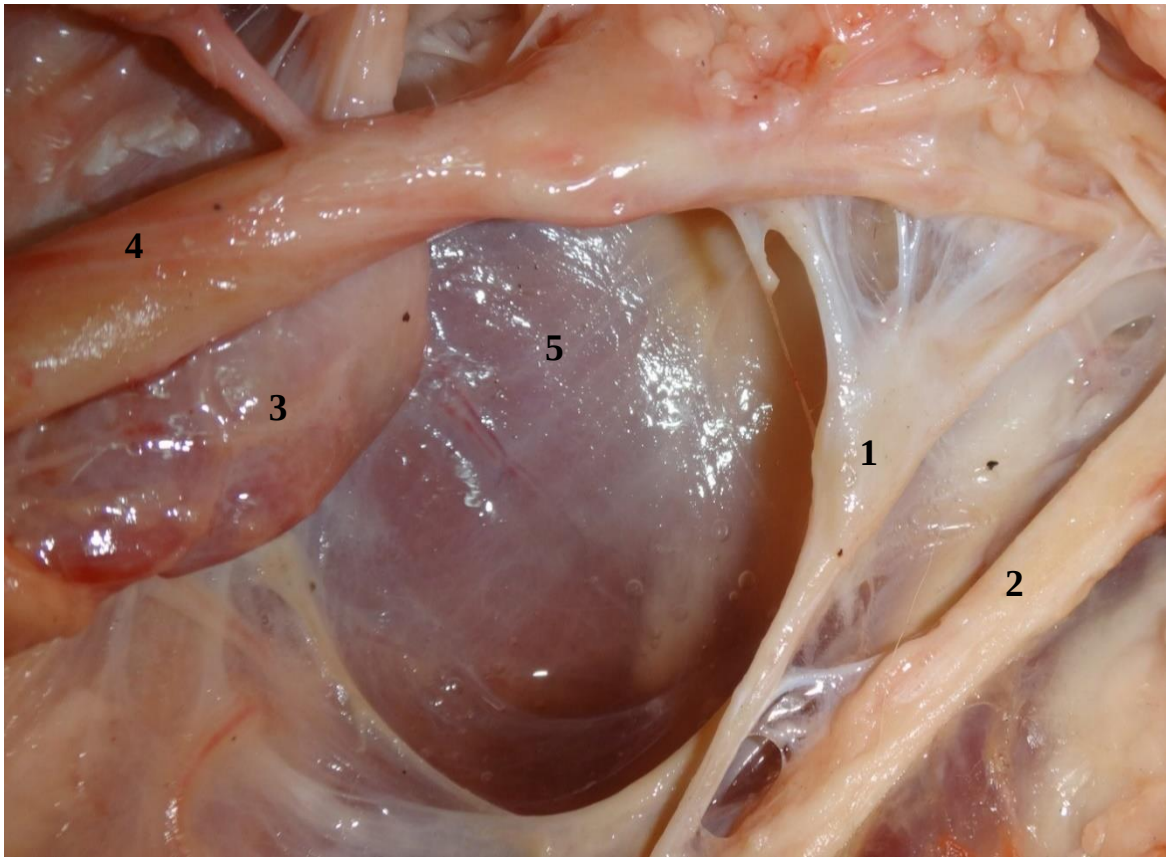

2 Figure 1: The cranial cervical ganglion in dromedary camel (**1**), vagus nerve (**2),** internal carotid artery (**3**), external carotid artery (**4**), longus captis muscle (**5**), mandibular gland (**6**), stylohyoid bone (**7**) and caudal stylopharyngeal muscle (**8**).

Figure 2: The cranial cervical ganglion in dromedary camel (**1**), vagus nerve (**2**), retropharyngeal lymph node (3), external carotid artery (**4**) and longus captis muscle (**5**).

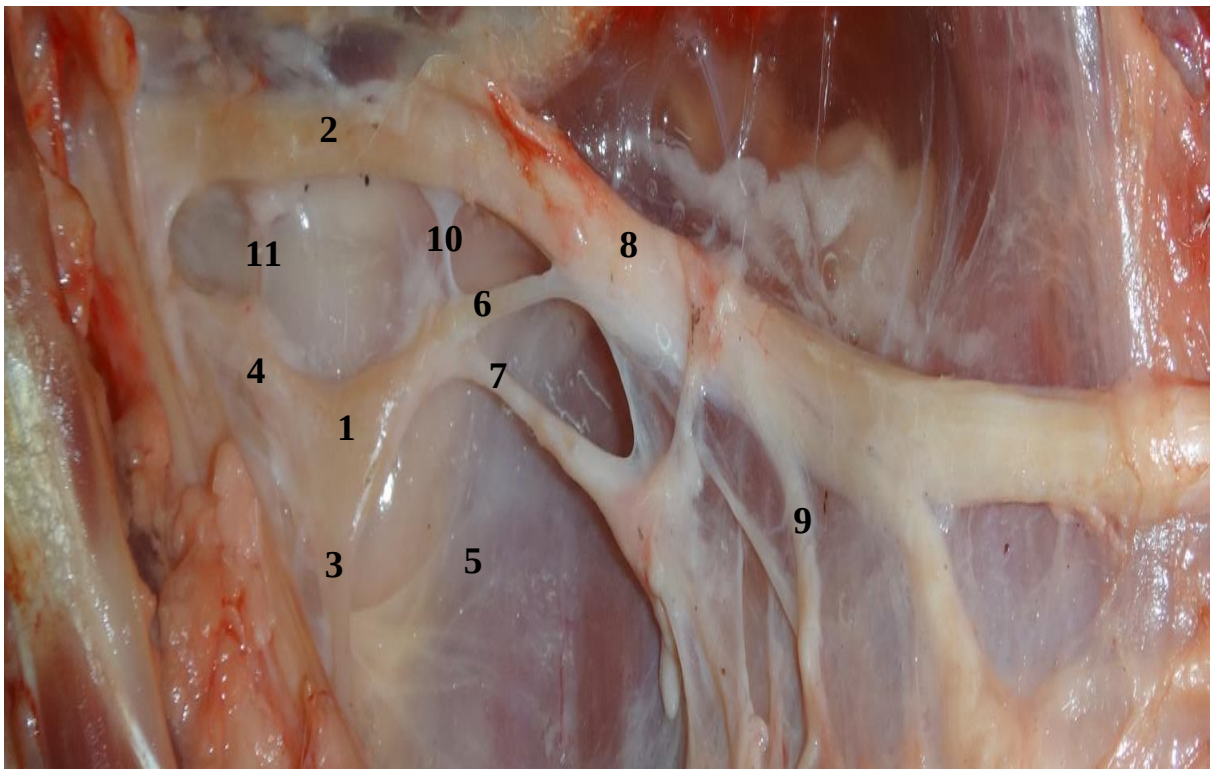

3

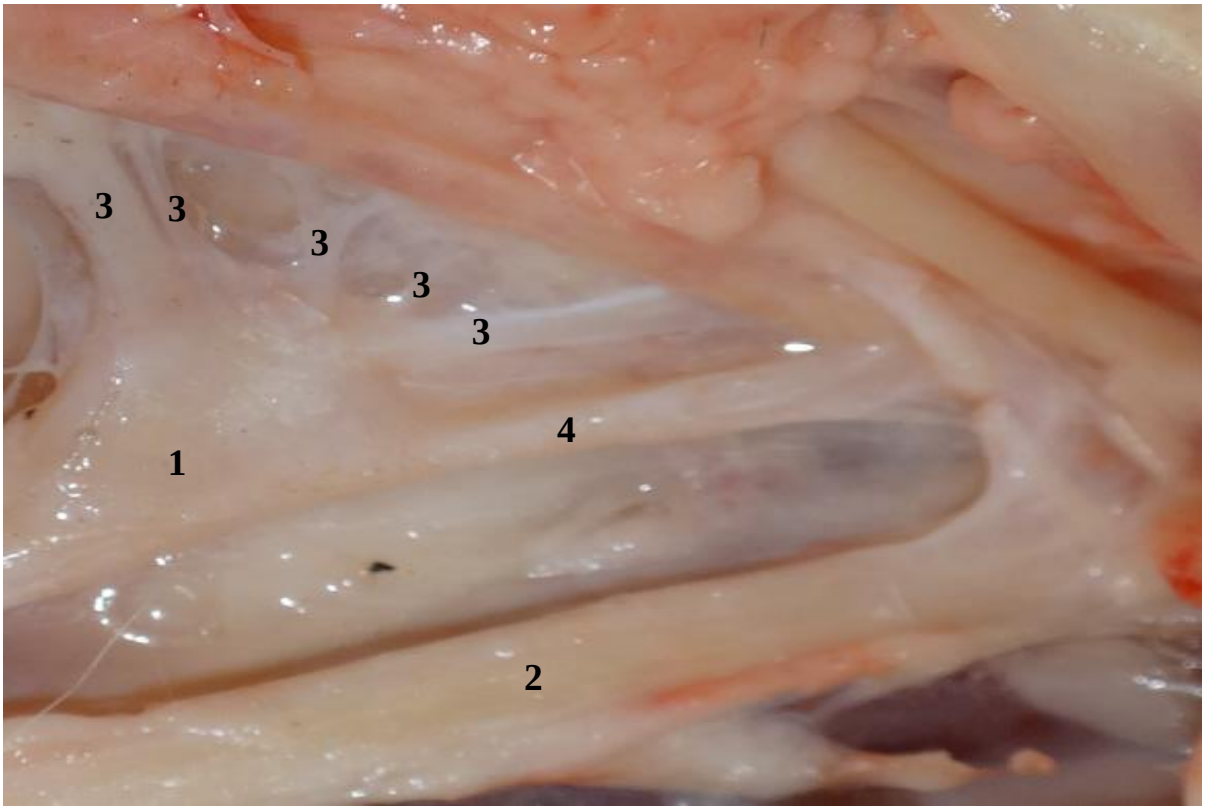

4

Figure 3: Medial view of cranial cervical ganglion (**1)**, vagus nerve (**2**), internal carotid nerve (**3**), jugular nerve (**4**), longus captis muscle (**5**), sympathetic trunk (**6**), external carotid nerve (**7**), vagosympathetic trunk (**8**), cranial laryngeal nerve of vagus nerve (**9**), communicating branch between the cranial cervical ganglion and the ventral branch of the first cervical nerve (**10**) and communicating branches to the vagus nerve (**11**).

Figure 4: Medial view of the cranial half of the cranial cervical ganglion (**1)**, vagus nerve (**2**), branches of the internal carotid nerve (**3**) and jugular nerve (**4**).

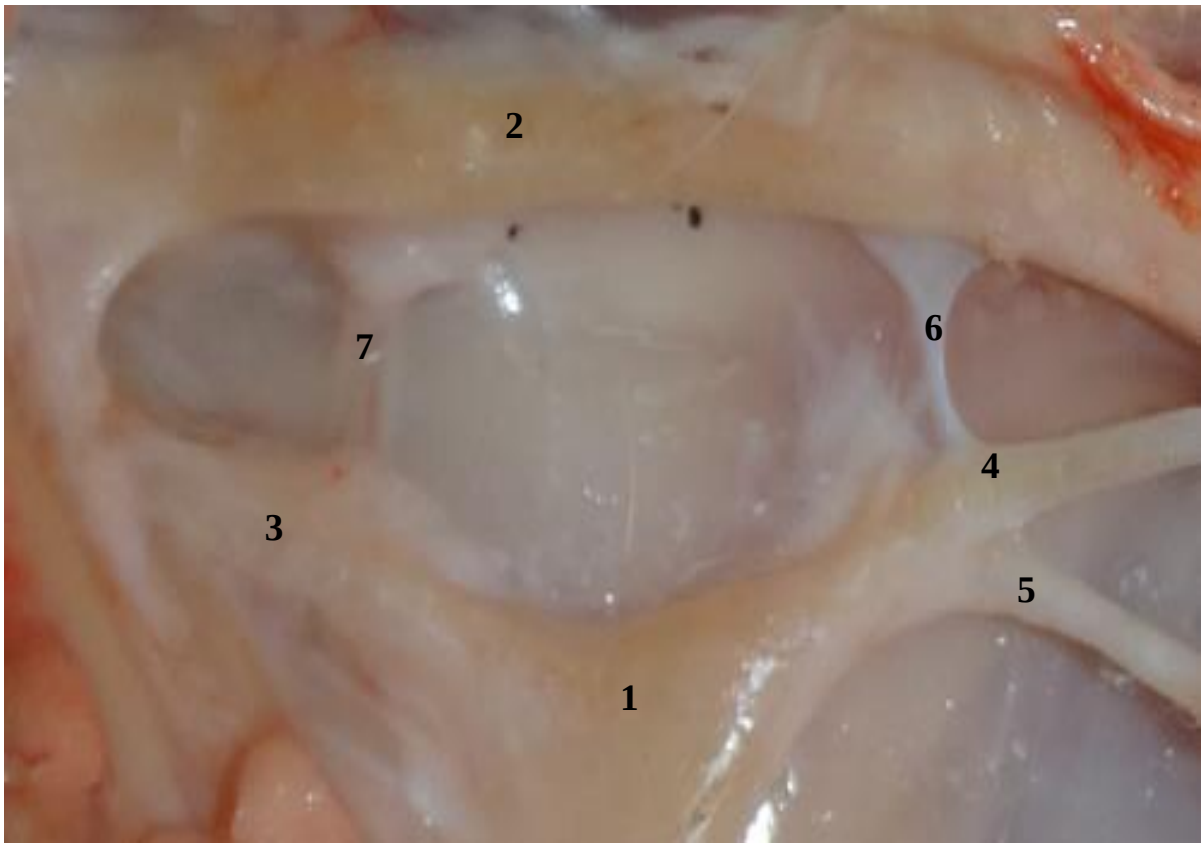

5

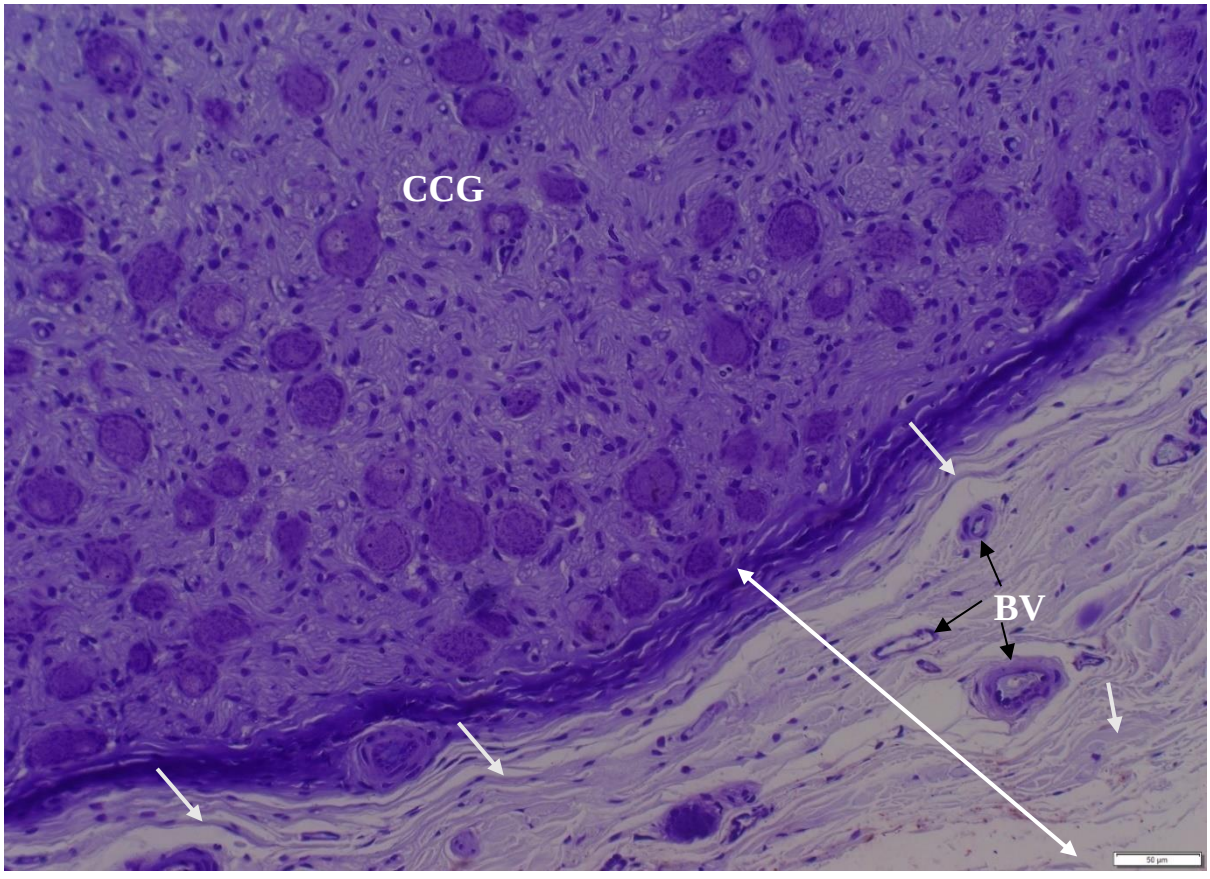

6

Figure 5: View of caudodorsal border the cranial cervical ganglion (**1)** in dromedary camel**,** vagus nerve (**2**), jugular nerve (**3**), sympathetic trunk (**4**), external carotid nerve (**5**), **c**ommunicating branch between the cranial cervical ganglion and the ventral branch of the first cervical nerve (**6**), communicating branches to the vagus nerve (**7**).

Fig. 6: A photomicrograph of the cranial cervical ganglion **(CCG**) showing the capsule (**white double headed arrow**) with collagen fibers (**white arrows**) and blood vessel (**BV**). Luxol fast blue with cresyl violet counterstain. Image bar= 50μm.

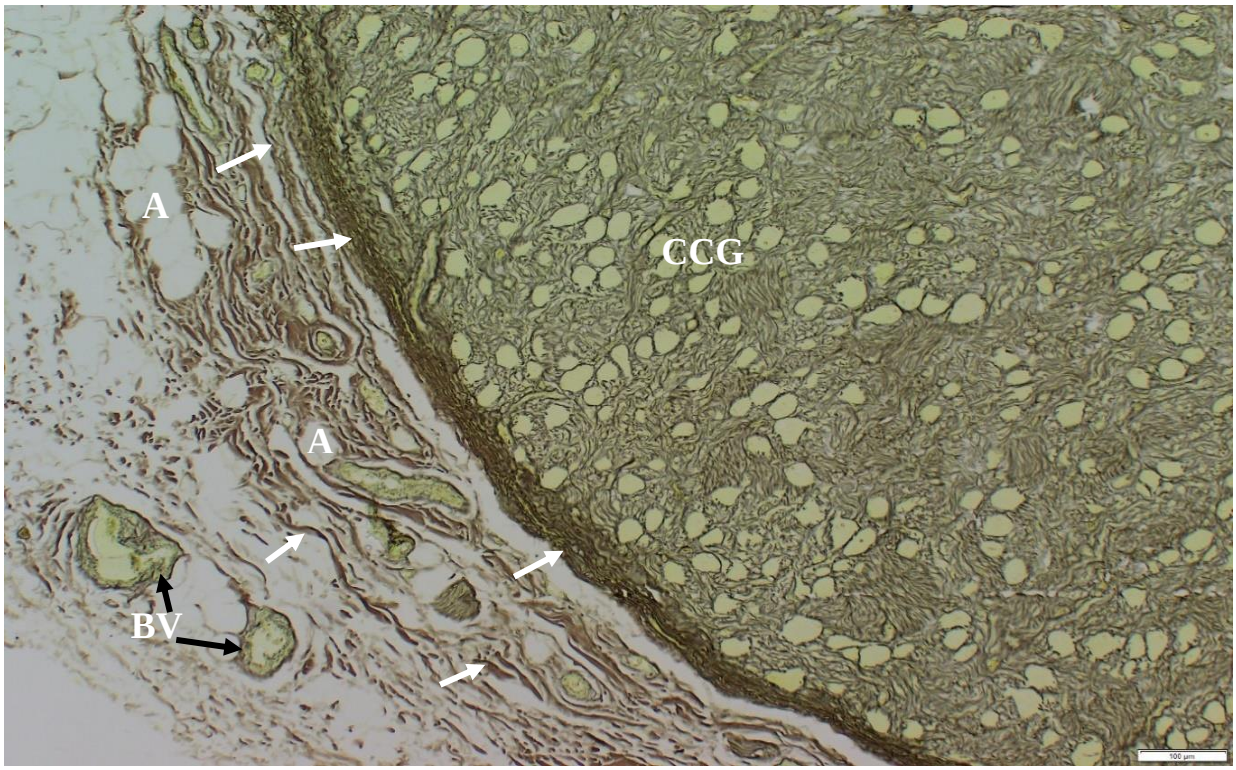

7

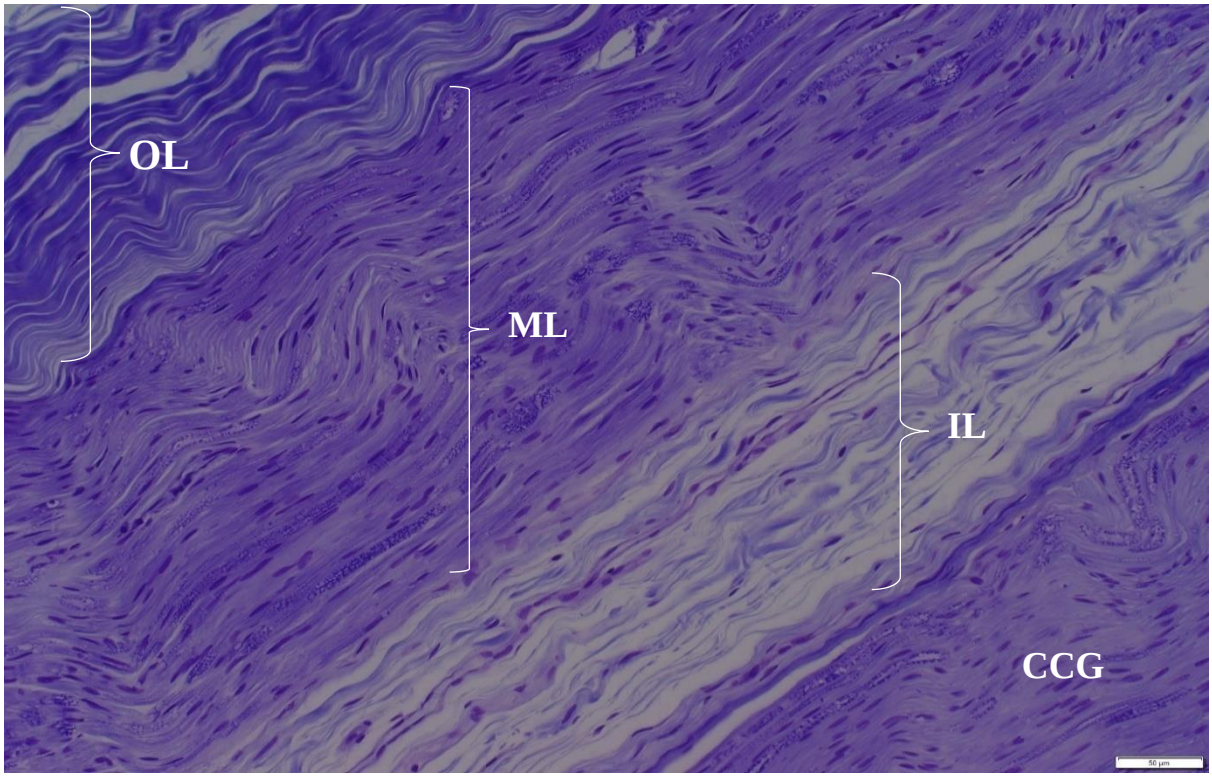

8

Fig. 7: A photomicrograph of the cranial cervical ganglion **(CCG)** showing the capsule containing large amount of reticular fibers (**white arrows**), adipocytes (**A**) and blood vessel (**BV**). Gordon and Sweet stain. Image bar= 100μm.

Fig. 8: A photomicrograph of the cranial cervical ganglion (**CCG**) showing the layers of the capsule. **OL**: the outer layer; **ML**, the middle layer; **IL**, the inner layer. Luxol fast blue with cresyl violet counterstain. Image bar= 50μm.

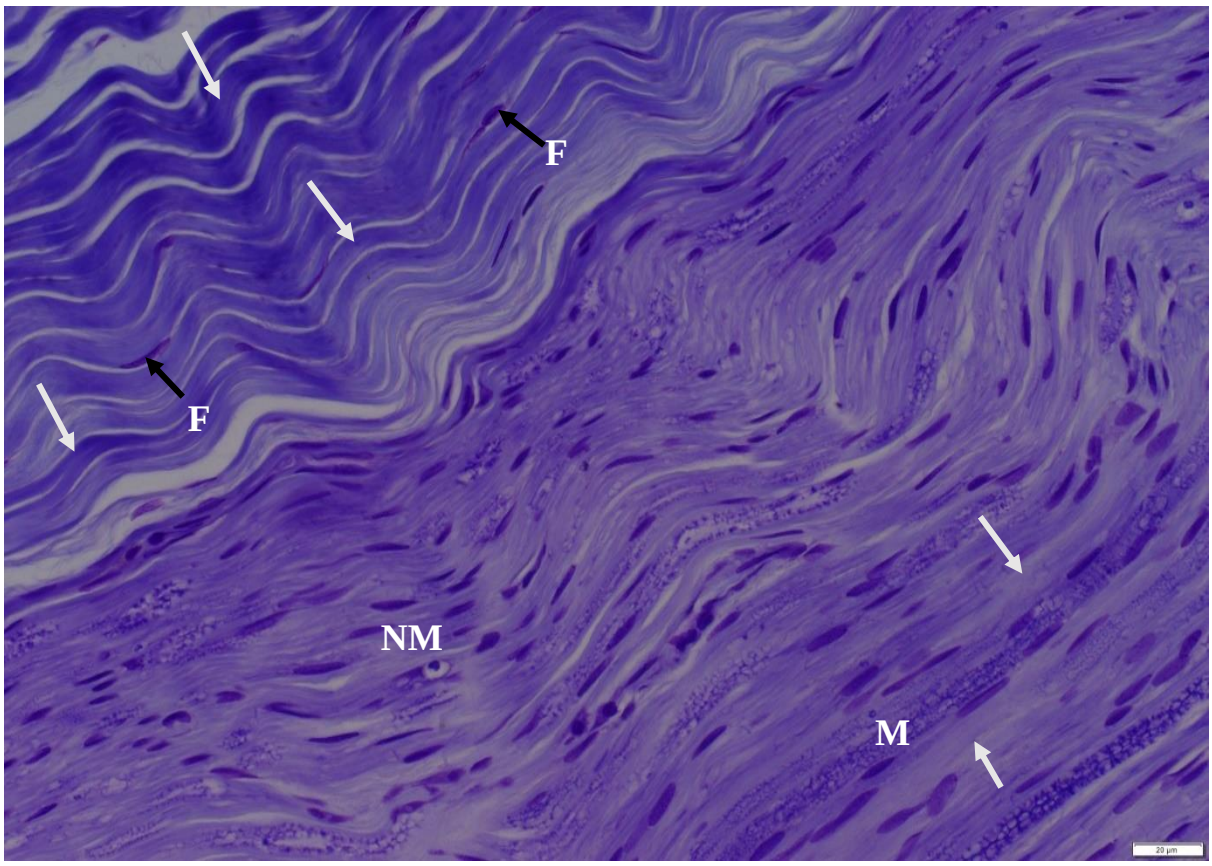

9

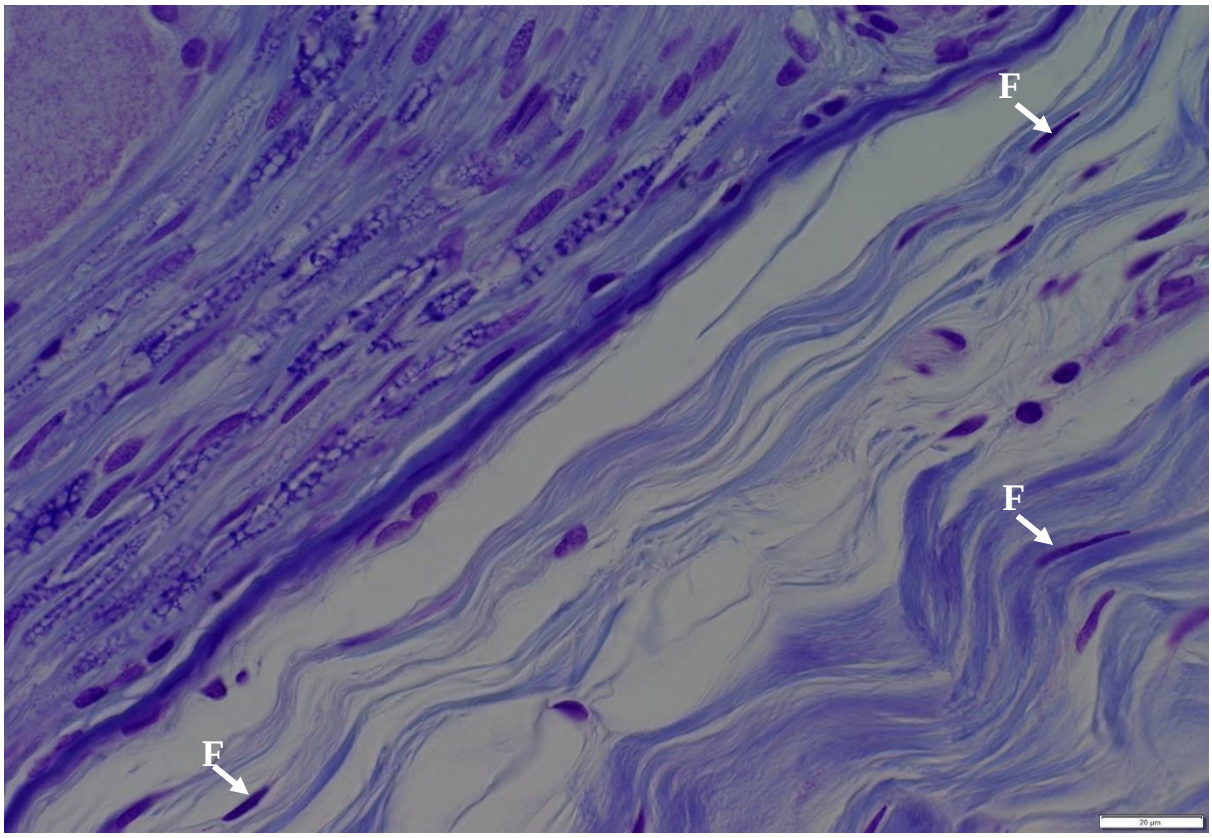

10

Fig. 9: A photomicrograph of the CCG capsule showing the outer and middle layers consisting of thick bundles of collagen fibres; the fibroblast nuclei (**F**) are elongated in the direction of collagen fibres (**white arrows**), myelinated **(M**) and non-myelinated nerve fibres (**NM**) scattered between the collagen fibres. Luxol fast blue with cresyl violet counterstain. Image bar= 20μm.

Fig. 10: A photomicrograph of the cranial cervical ganglion capsule showing the inner layer of capsule consisting of loose connective tissue; the fibroblast nuclei (**F**). Luxol fast blue with cresyl violet counterstain. Image bar= 10μm.

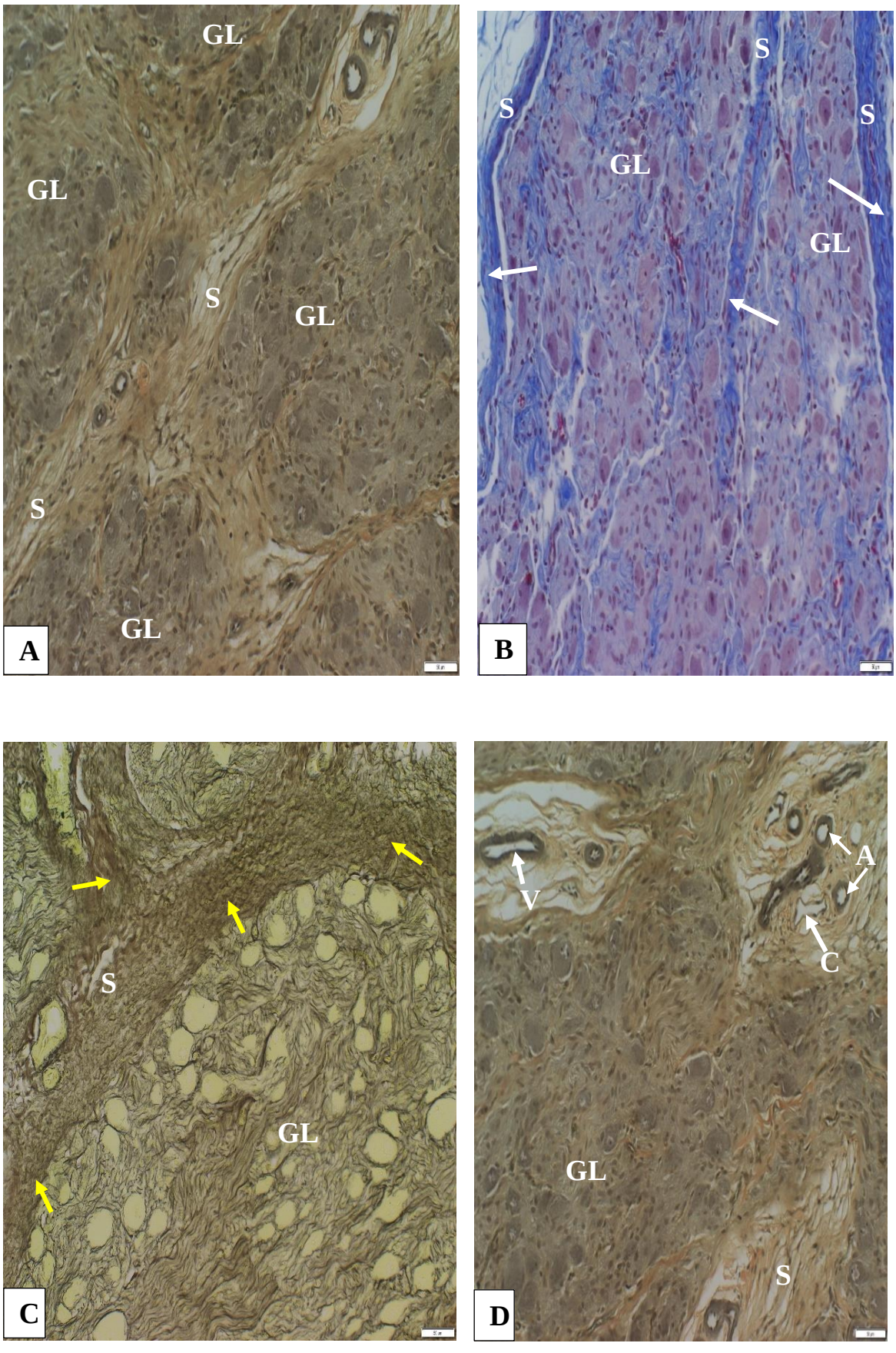

11

Fig. 11. A, B, C & D. Photomicrographs of the CCG; **A:** showing the ganglionic lobule (**GL**) and septa **(S).** Verhoff's stain. Image bar= 50μm.
B: Showing the ganglionic lobule (**GL**), septa **(S)** and collagen fibers (**white arrows**). Masson's Trichrome stain. Image bar= 50μm.
C: Showing the ganglionic lobule (**GL**), septa **(S)** and reticular fibers (**yellow arrows**). Gordon and Sweet stain. Image bar= 50μm. **D:** Showing the arteriole (**A**), venule (**V**) and capillary (**C**) present also in the septa. Verhoff's stain. Image bar= 20μm.

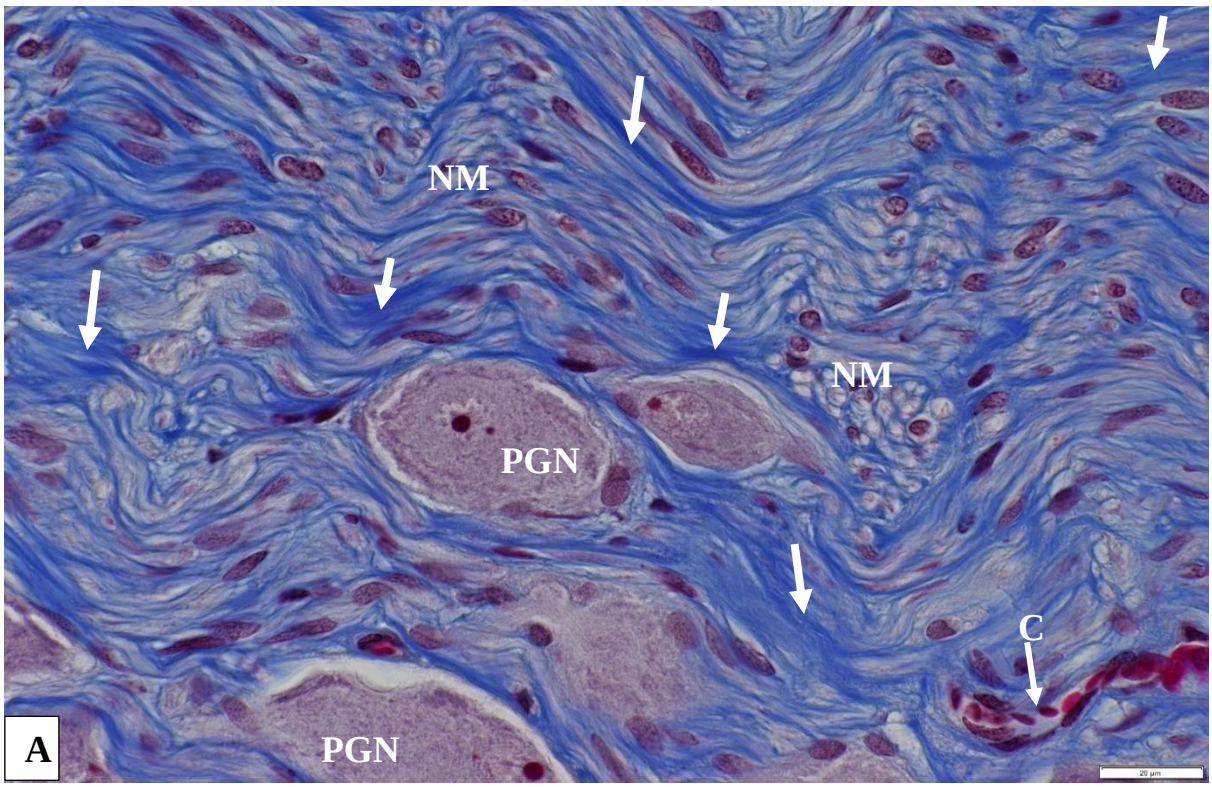

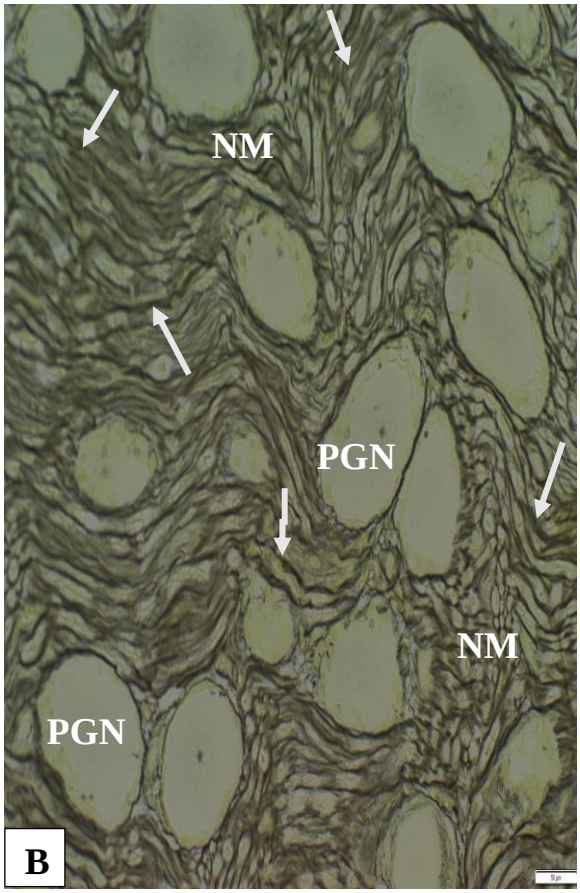

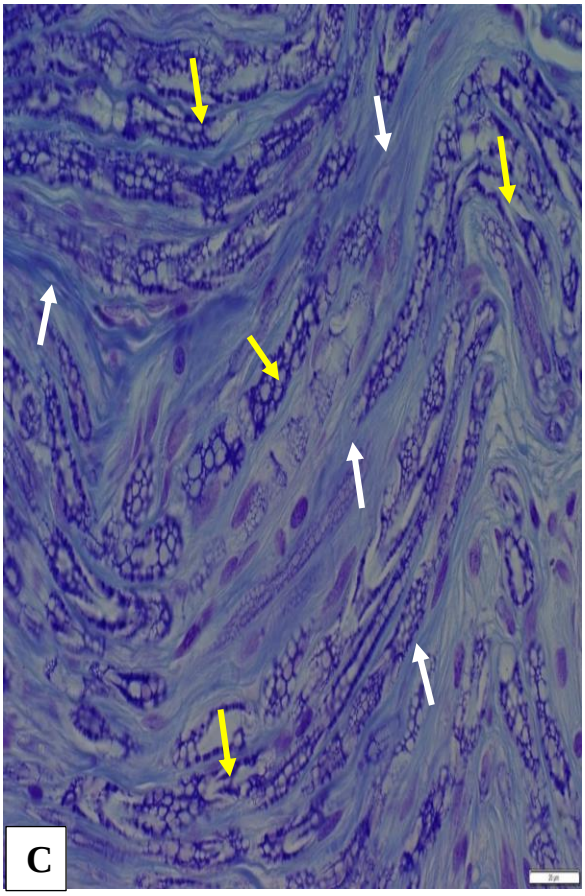

12

Fig. 12. A, B & C. A: Photomicrographs of the CCG ganglionic stroma; **A:** showing the collagen fibres **(white rrows),** scattered within the stroma and surrounding the principal ganglion neuron **(PGN)**, non-myelinated nerve fibres **(NM)** and capillaries **(C)**. Masson's Trichrome stain. Image bar= 20μm. **B**: showing large amount of reticular fibres (**white arrows)** within the stroma and surrounding the base of the principal ganglion neuron **(PGN)** and non-myelinated nerve fibres (**NM)**. Gordon and Sweet stain. Image bar= 50μm. **C:** showing the collagen fibres **(white arrows)** scattered within the stroma and surrounding the myelinated nerve fibres (**yellow arrows).** Luxol fast blue with cresyl violet counterstain. Image bar= 20μm.

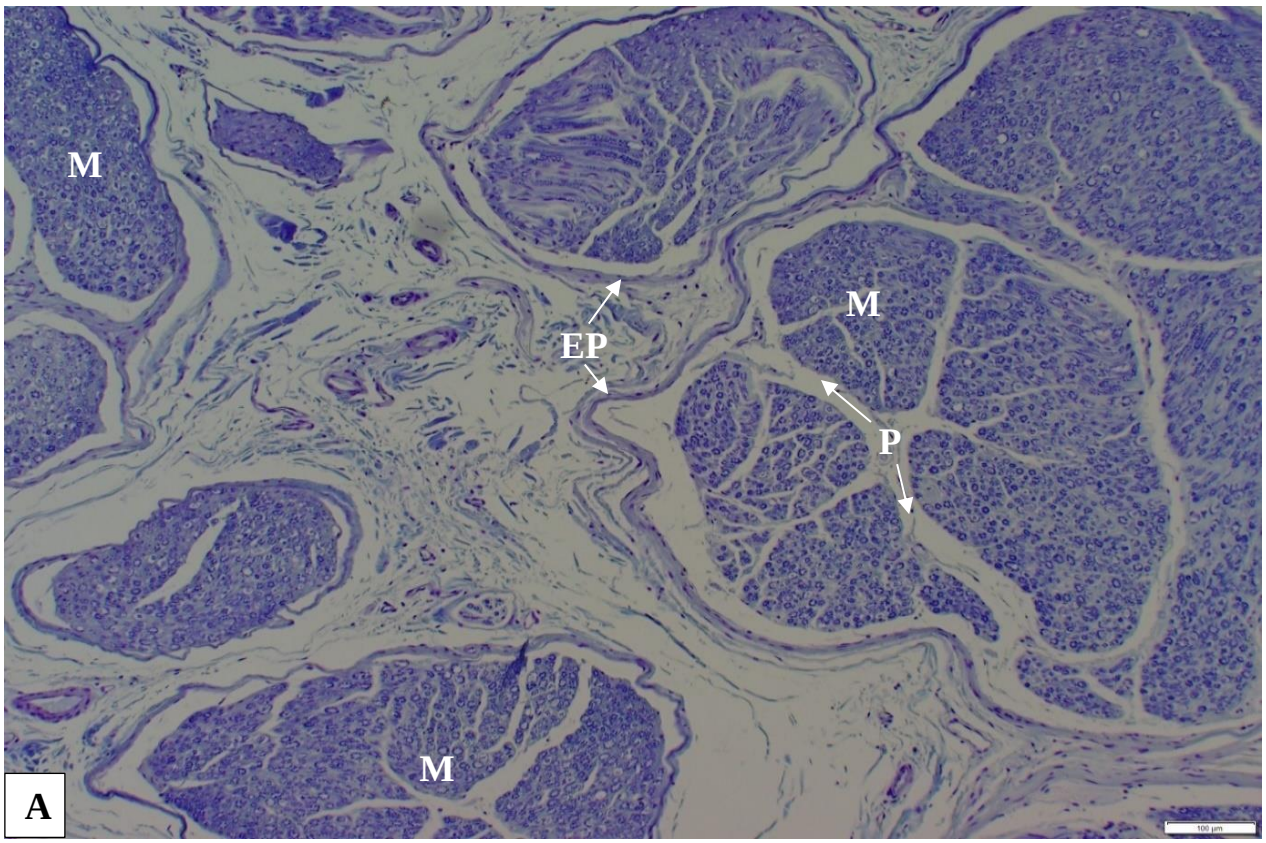

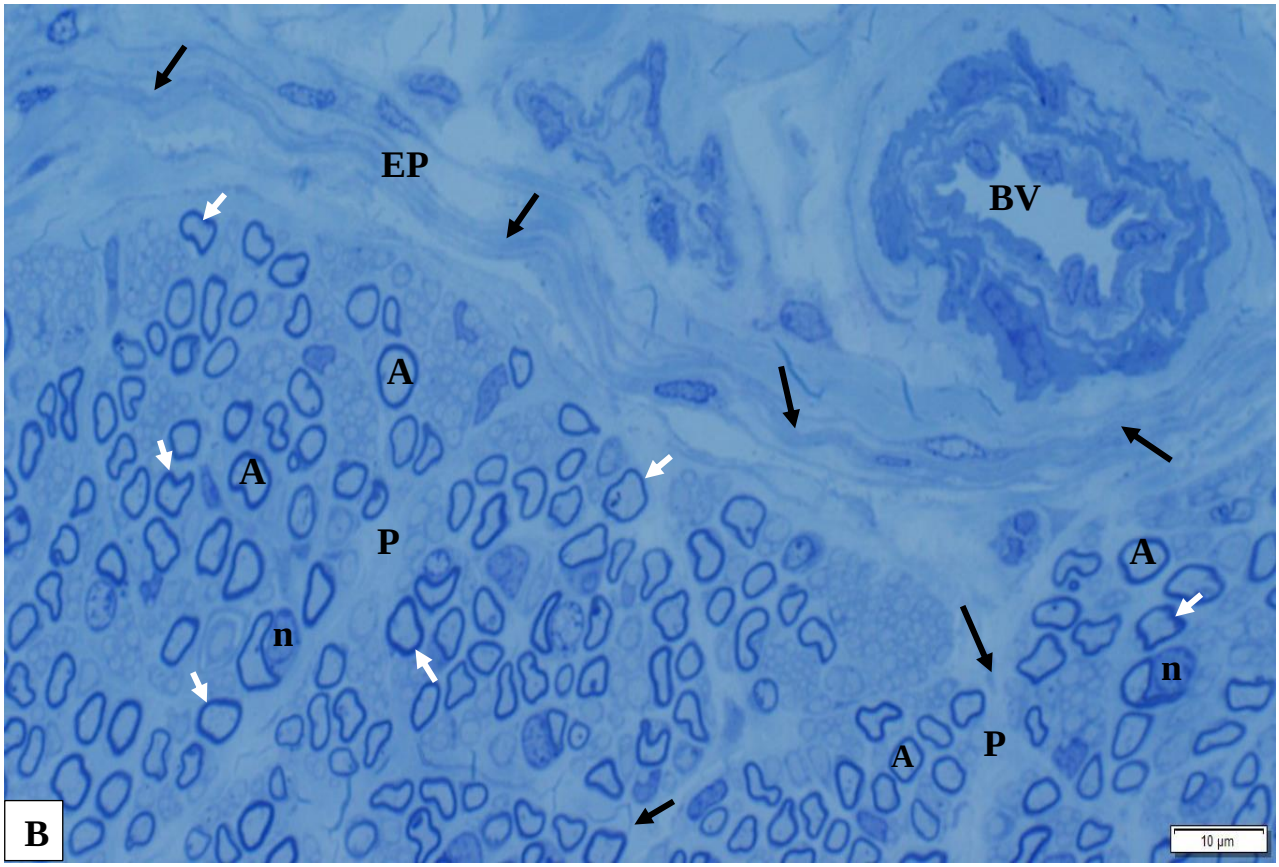

13

Fig. 13. A & B. Photomicrographs of the CCG; **A:** showing the fascicle of myelinated nerve fibres (**M),** epineurium **(EP)** and perineurium (**P).** Luxol fast blue with cresyl violet counterstain. Image bar= 100μm.

B: showing the fascicle of myelinated nerve fibres (**M),** epineurium **(EP),** perineurium (**P),** collagen fibres **(black arrows)**, myelin sheath **(white arrows**), Schwann cell nuclei **(n), and** blood vessel (**BV).** Semi-thin section stained by Toluidine blue. Image bar= 10μm.

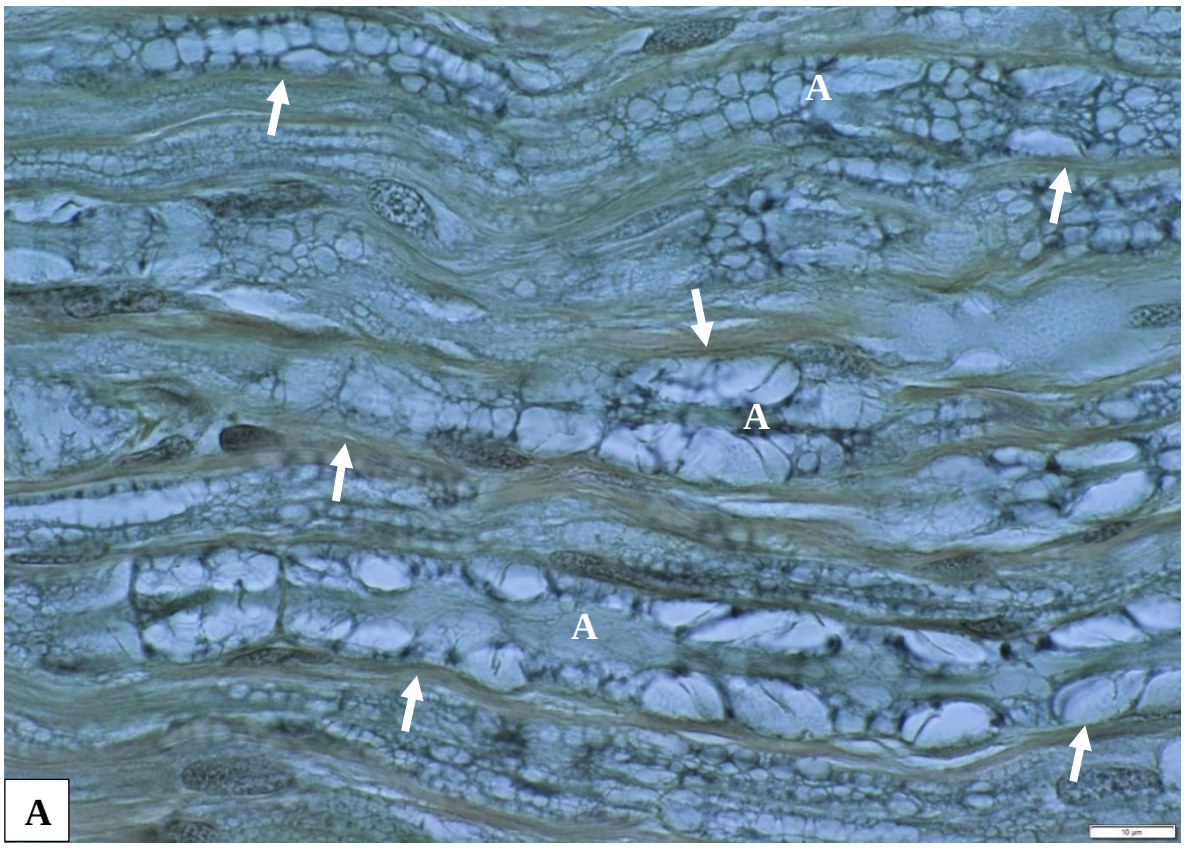

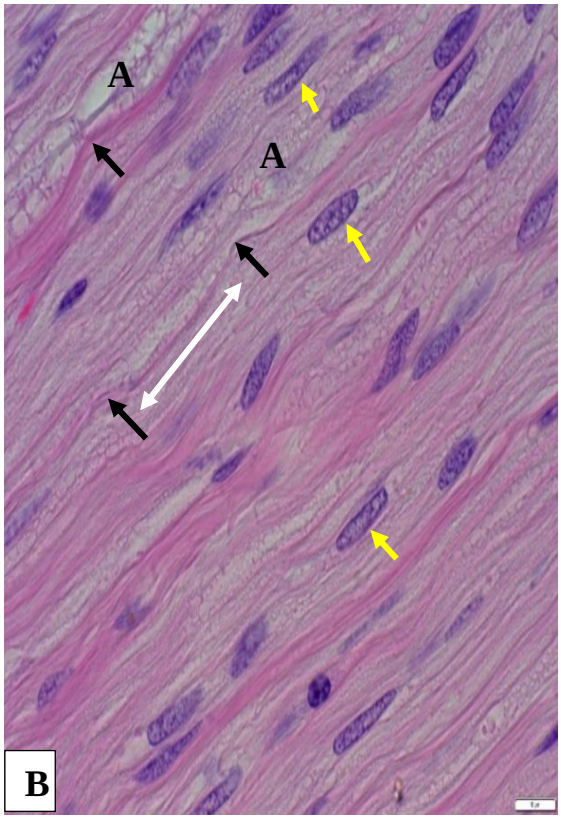

14

Fig. 14. A, B & C. Photomicrographs of the CCG; **A:** showing the myelinated axon (**A**) surrounded by the endoneurium **(white arrows).** Verhoff's stain. Image bar= 10μm. **B:** Showing myelinated axon **(A**), nodes of Ranvier **(black arrows)**, internode (**white double headed arrow**), and Schwann cells nuclei **(yellow arrows)**. H & E stain. Image bar= 10μm. **C:** Showing axon (**A**), Schmidt-Lanterman clefts **(white arrows)** in the myelin sheath of the axons. Gomori's stain. Image bar= 10μm.

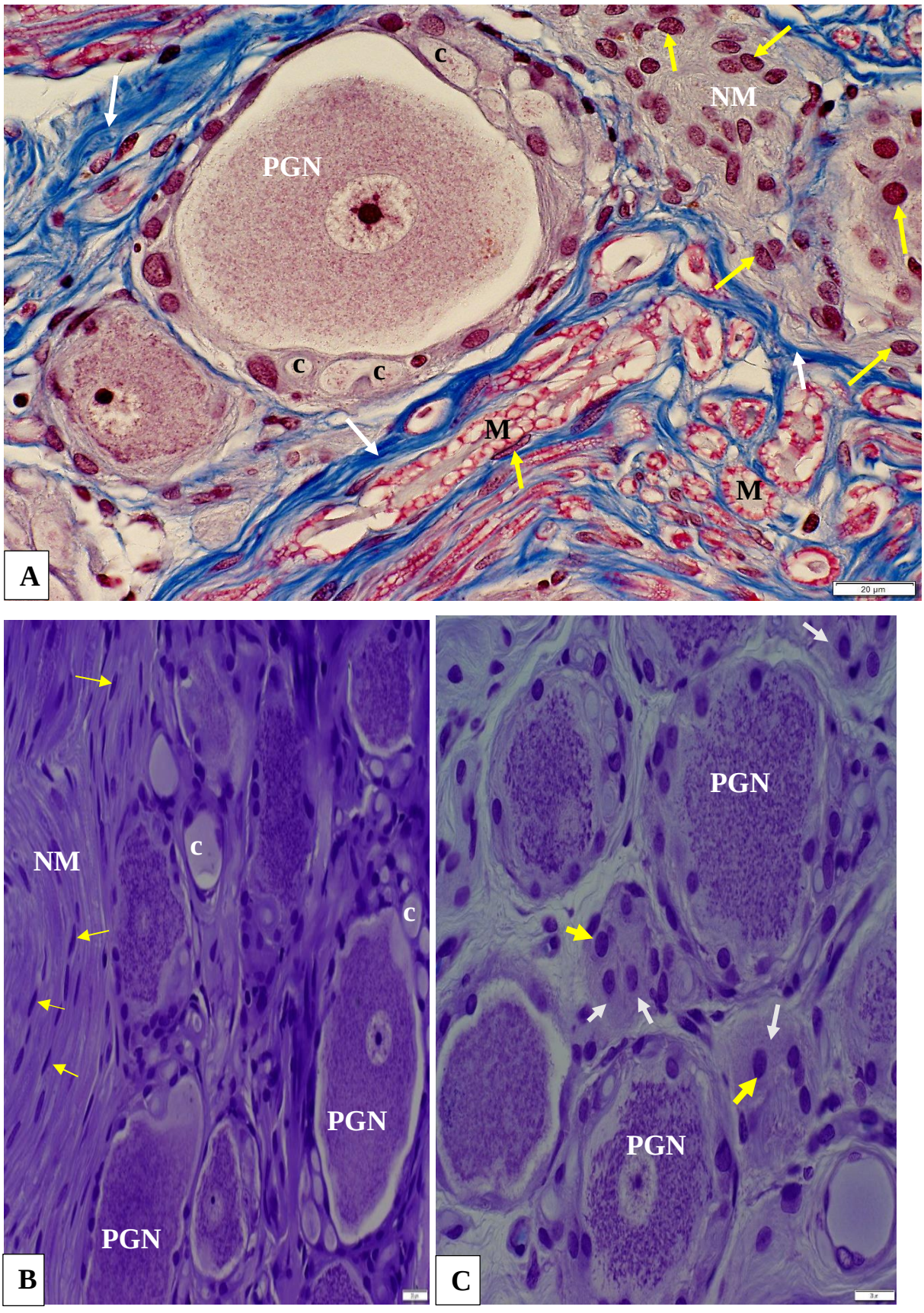

15

Fig. 15, A, B & C. Photomicrographs of the CCG ganglionic stroma; **A:** showing the principal ganglion neuron **(PGN),** non-myelinated nerve fibres (**NM**), myelinated nerve fibres (**M),** collagen fibres **(white arrows)** blood capillary **(c)** and Schwann cell nuclei (**yellow arrows)**. Masson's trichrome stain. Image bar= 20μm. **B:** showing the non-myelinated nerve fibers (**NM),** Schwann cells nuclei **(yellow arrows),** principal ganglion neuron **(PGN)** and capillaries **(c).** Cresyl fast violet stain. Image bar= 20μm. **C:** showing the principal ganglion neuron **(PGN),** Schwann cells (**white arrows**), Schwann cell nuclei (**yellow arrows).** Note that, Schwann's cells nuclei are large, flat or rounded in shape. Luxol fast blue with cresyl violet counterstain. Image bar= 20μm.

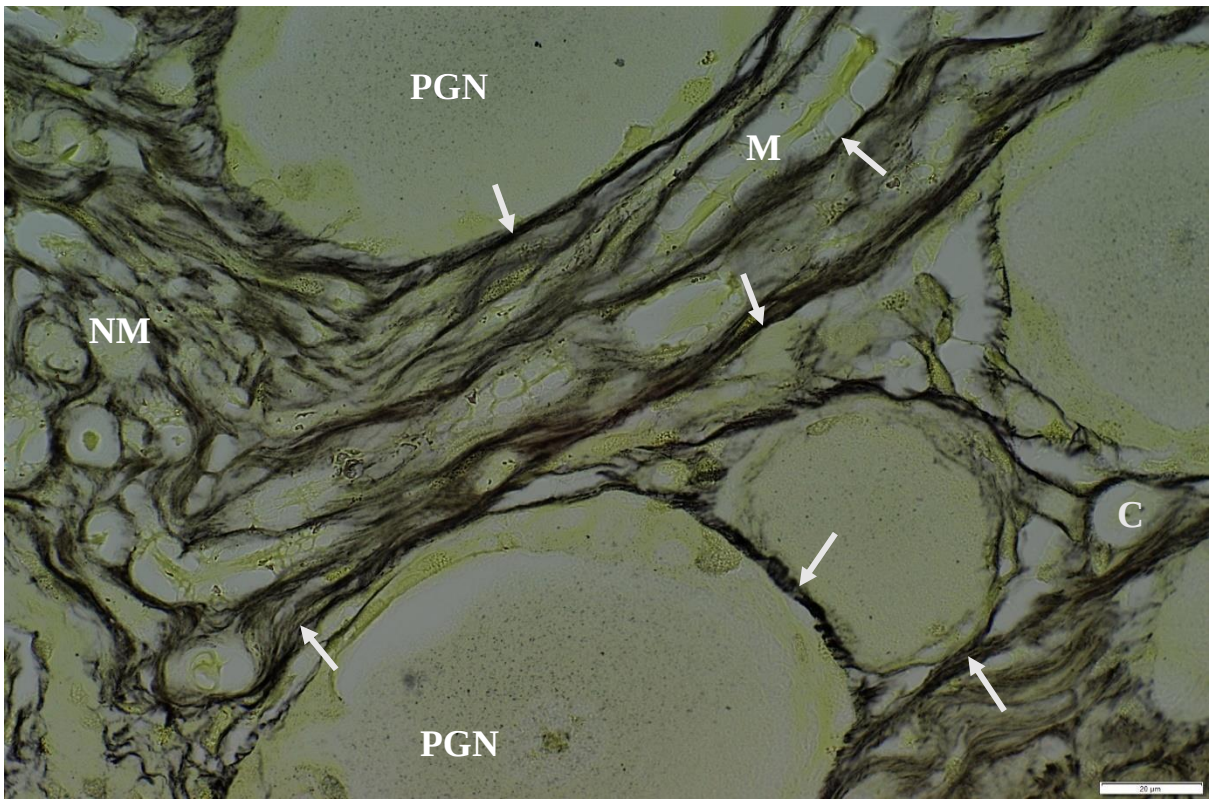

16

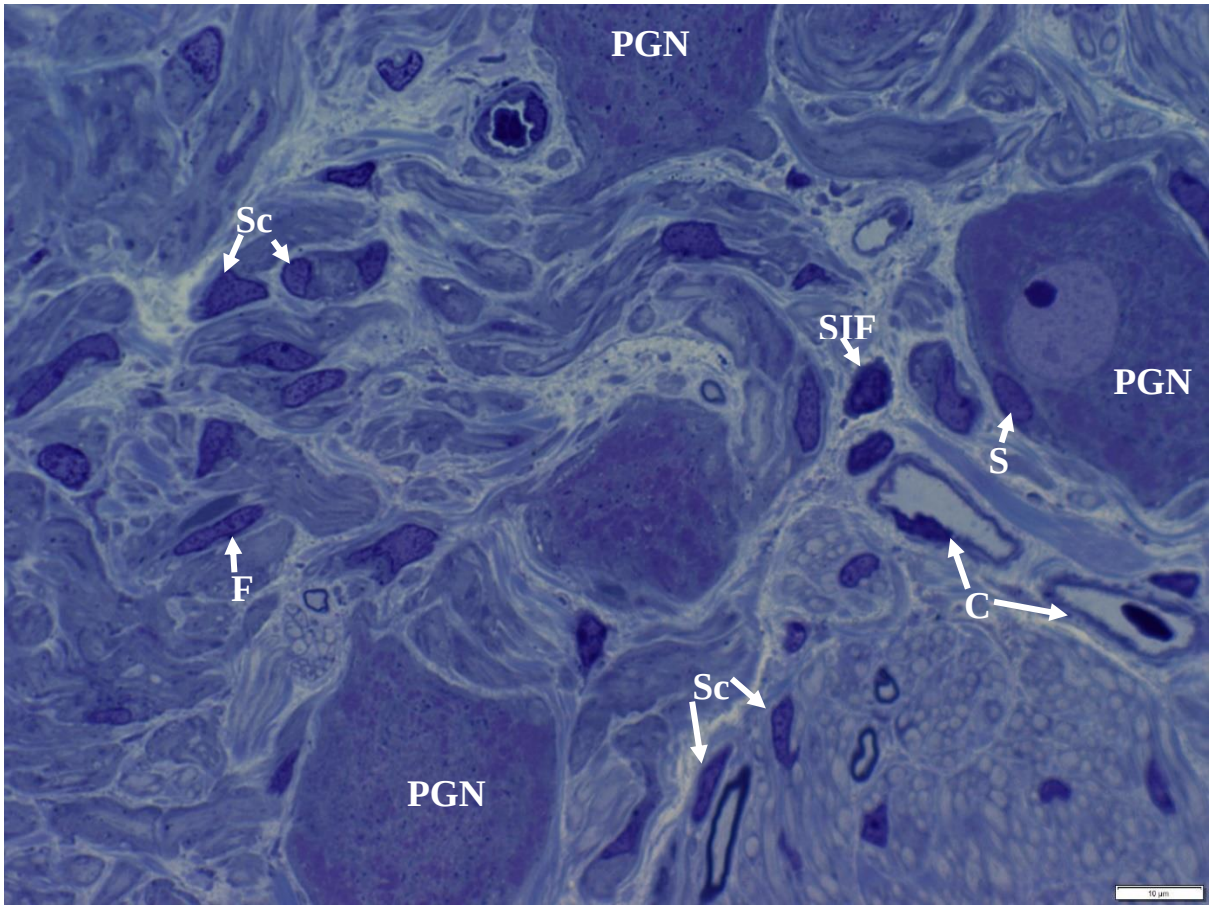

17

Fig. 16: A photomicrograph of the CCG showing the ganglionic unit consisting of large amount of reticular fibres (**white arrows**), principal ganglion neuron (**PGN**), capillaries (**C**), myelinated (**M**) and non-myelinated (**NM)** nerve fibres. Gordon and Sweet**.** Image bar= 20μm.

Fig. 17: A photomicrograph of the ganglionic units showing the principal ganglion neurons **(PGN),** small intensely fluorescent cell **(SIF),** Schwann cell **(Sc),** satellite glial cell **(S),** fibroblasts **(F)** and blood capillary **(C)**. Semi-thin section stained by Toluidine blue. Image bar= 10μm.

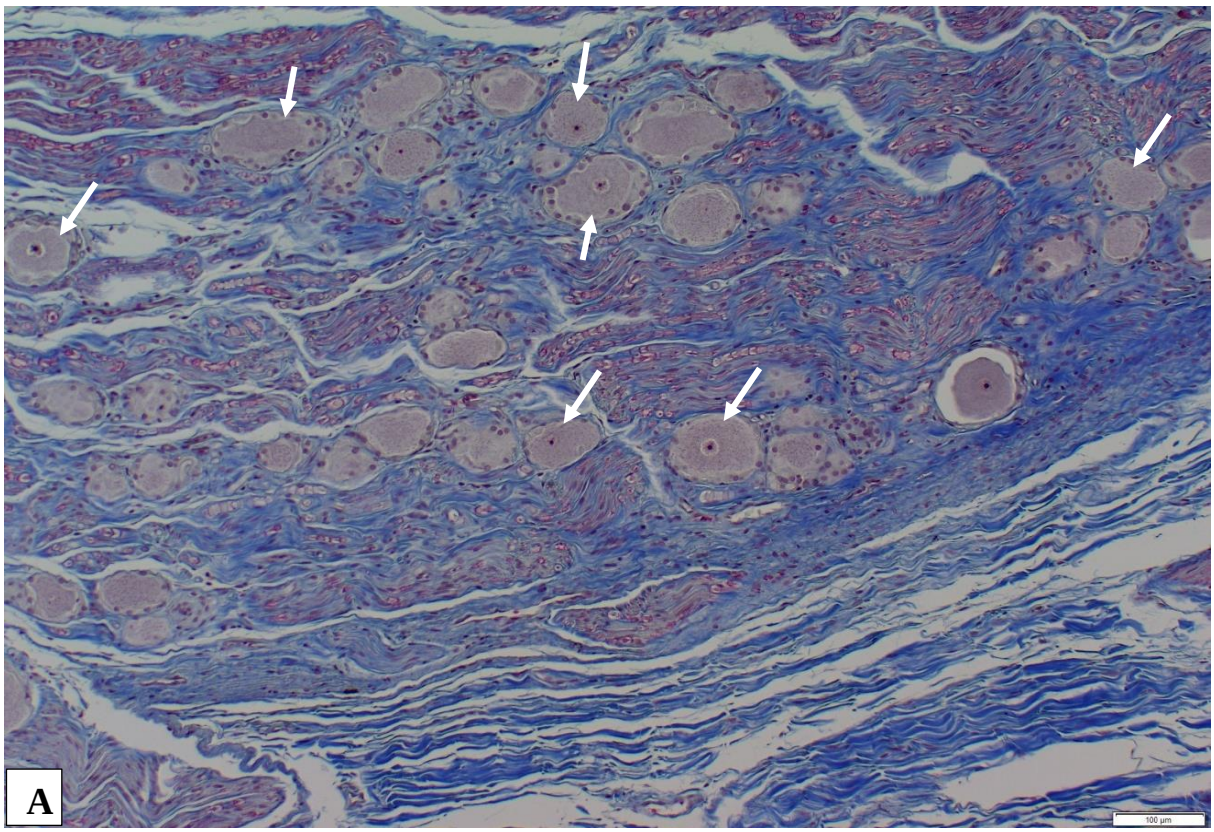

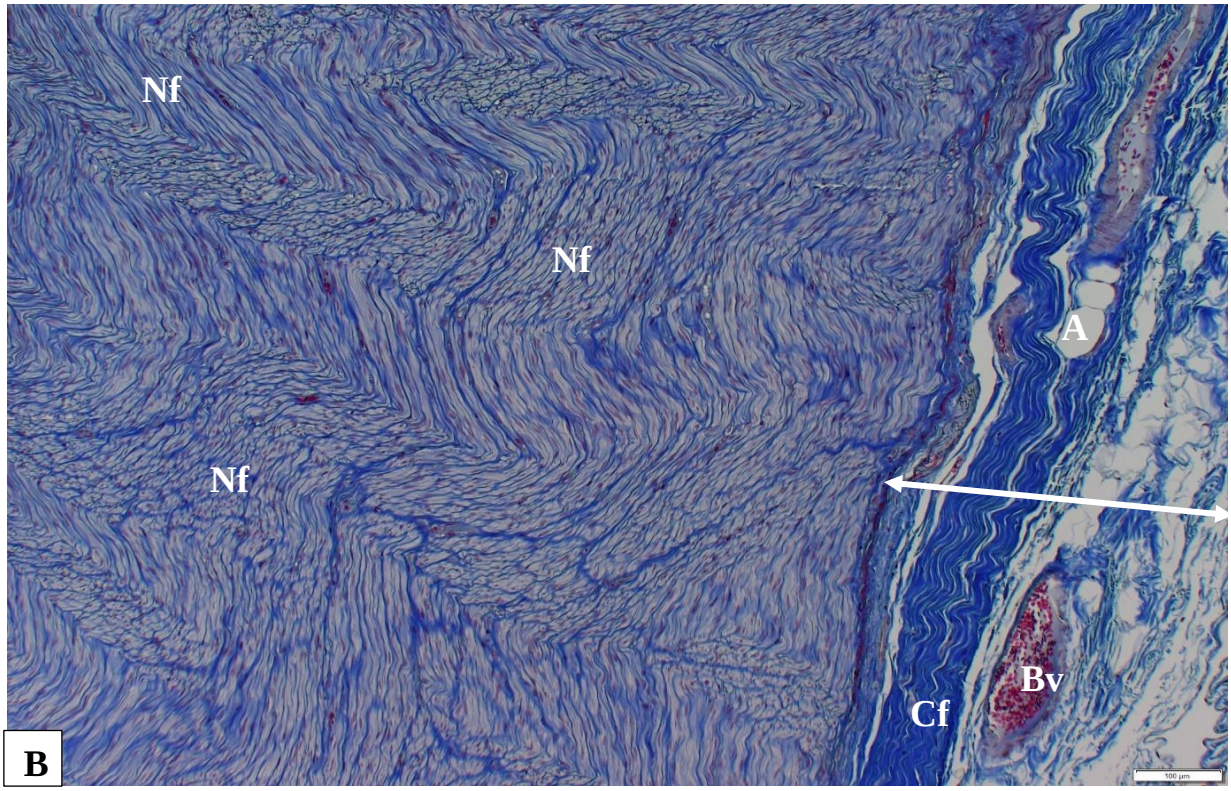

18

Fig. 18: A & B: Photomicrographs of the CCG; **A:** Showing the distribution of the principal ganglion neurons (**white arrows**). They are large in size, circular or oval in shape. Masson's trichrome stain. Image bar= 100μm. **B:** Showing the terminal end of the CCG being made up exclusively of nerve fibres **(Nf**). capsule: (**white double headed arrow**); collagen fibres: (**Cf**); blood vessel: (**Bv**); adipocytes: (**A**). Masson's trichrome stain. Image bar= 100μm.

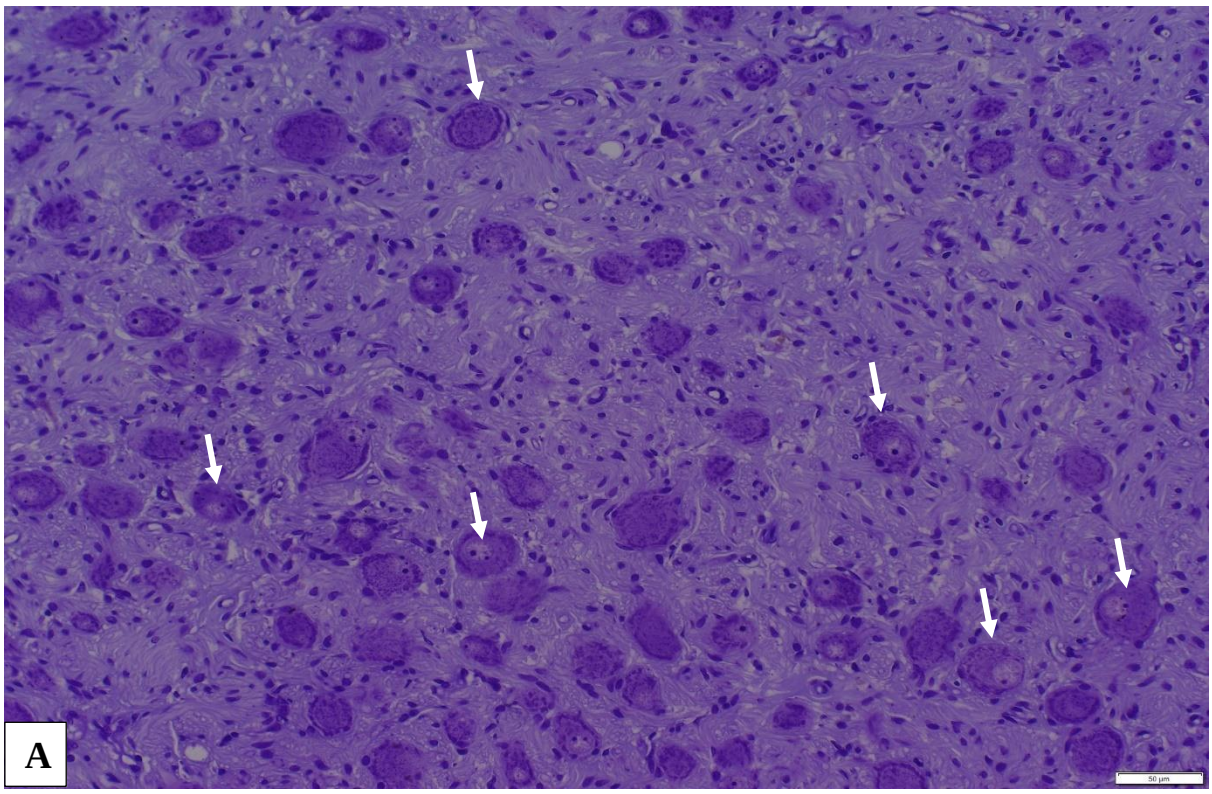

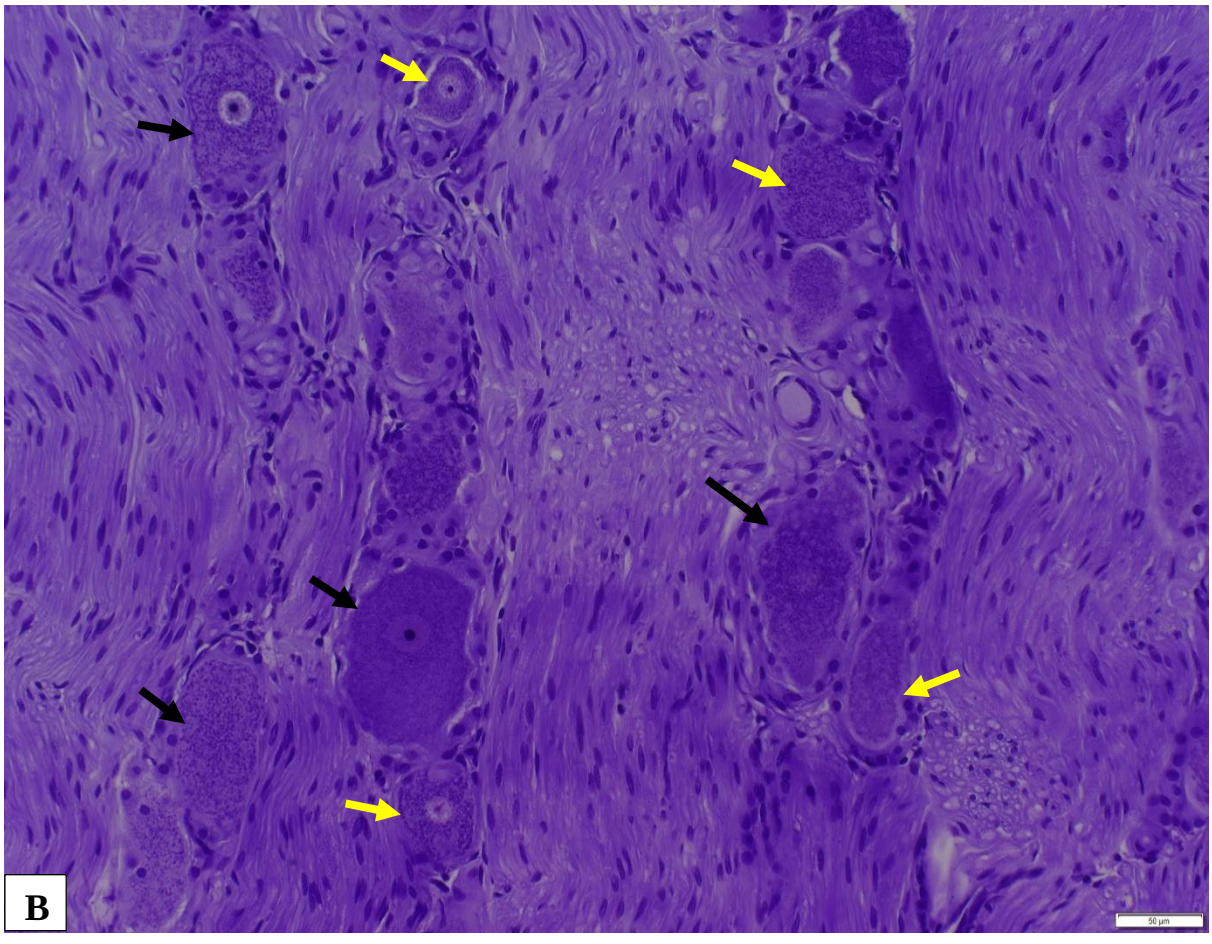

19

Fig. 19: A & B. Photomicrographs of the CCG; **A:** showing the broad middle region with small principal ganglion neurons **(white arrows)**. Cresyl fast violet stain. Image bar= 50μm.

B: Two types of principal ganglion neurons are identifiable in the next zone; the medium-sized principal ganglion neurons **(yellow arrows)** and large-sized principal ganglion neurons **(black arrows)**. Cresyl fast violet stain. Image bar= 50μm.

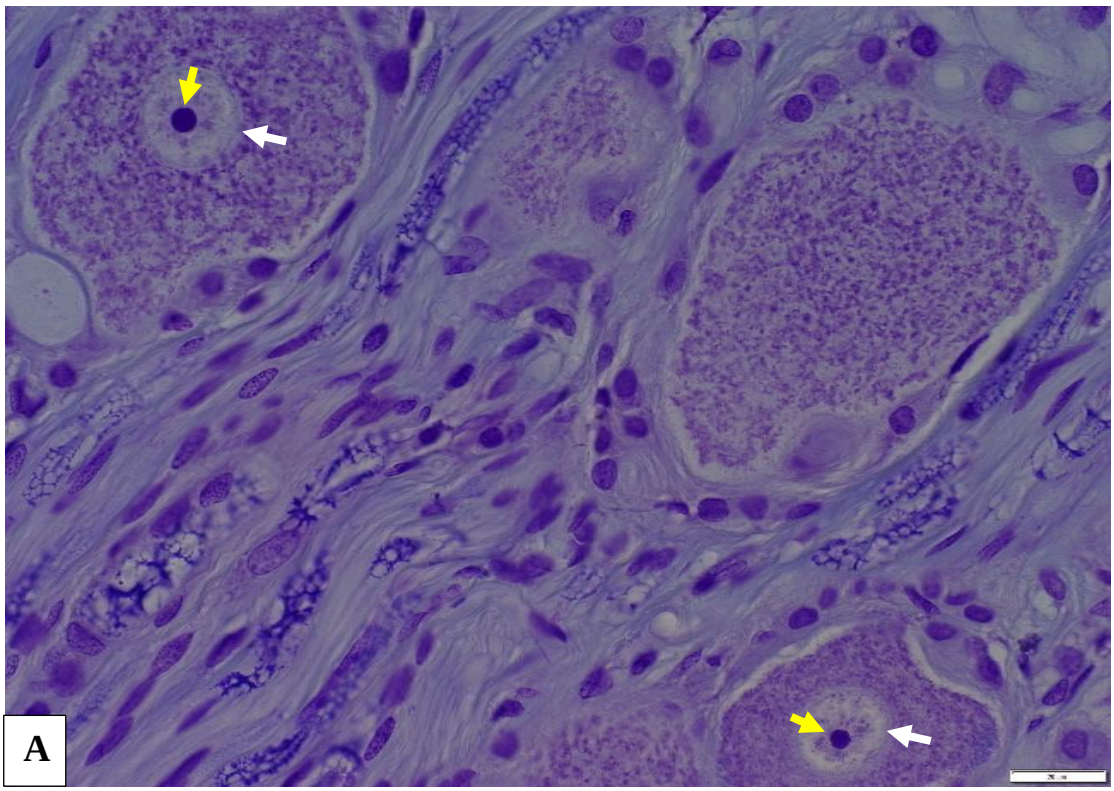

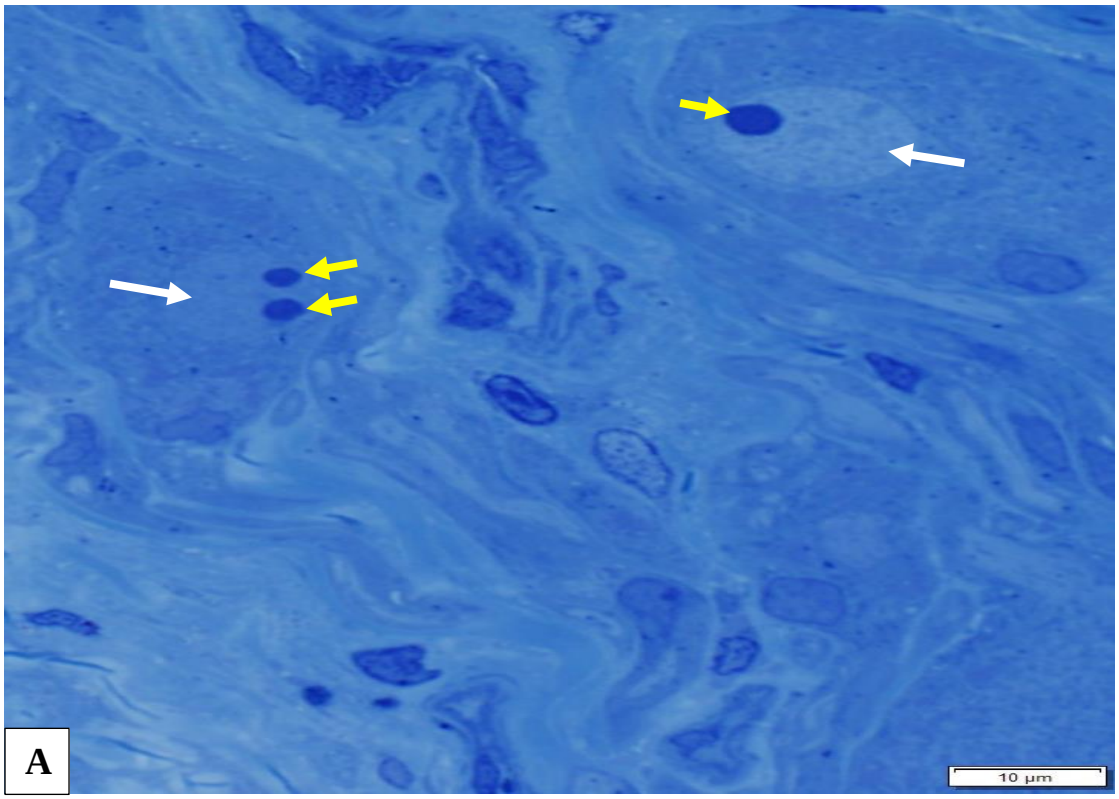

20

Fig. 20: A & B. Photomicrographs of the CCG; **A:** Showing the nuclei of the principal ganglion neurons (**white arrows**) and the nucleoli (**yellow arrows**). Note that the PGN showing large spherical and light nucleus. Luxol fast blue with cresyl violet counterstain. Image bar= 20μm.

B: The nucleus (**white arrows**) with two dark nucleoli (**yellow arrows**). Semi-thin section stained by Toluidine blue. Image bar= 10μm.

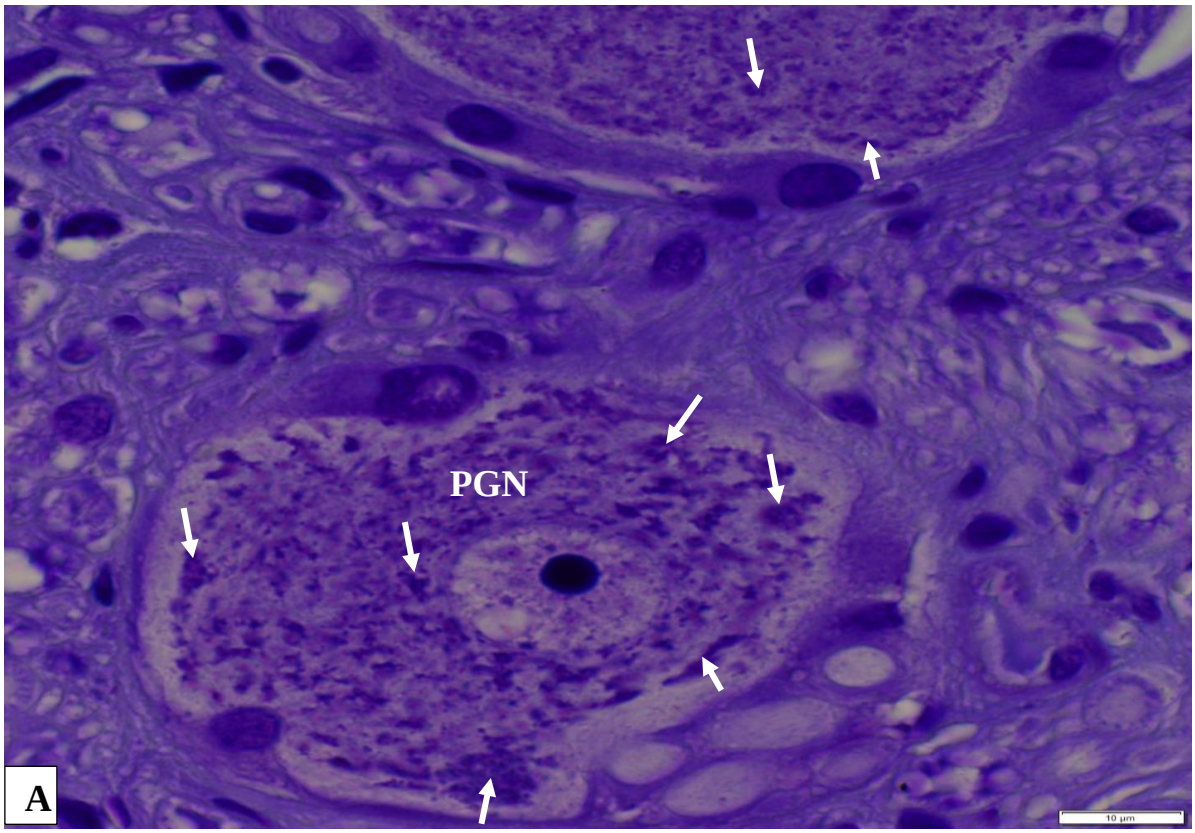

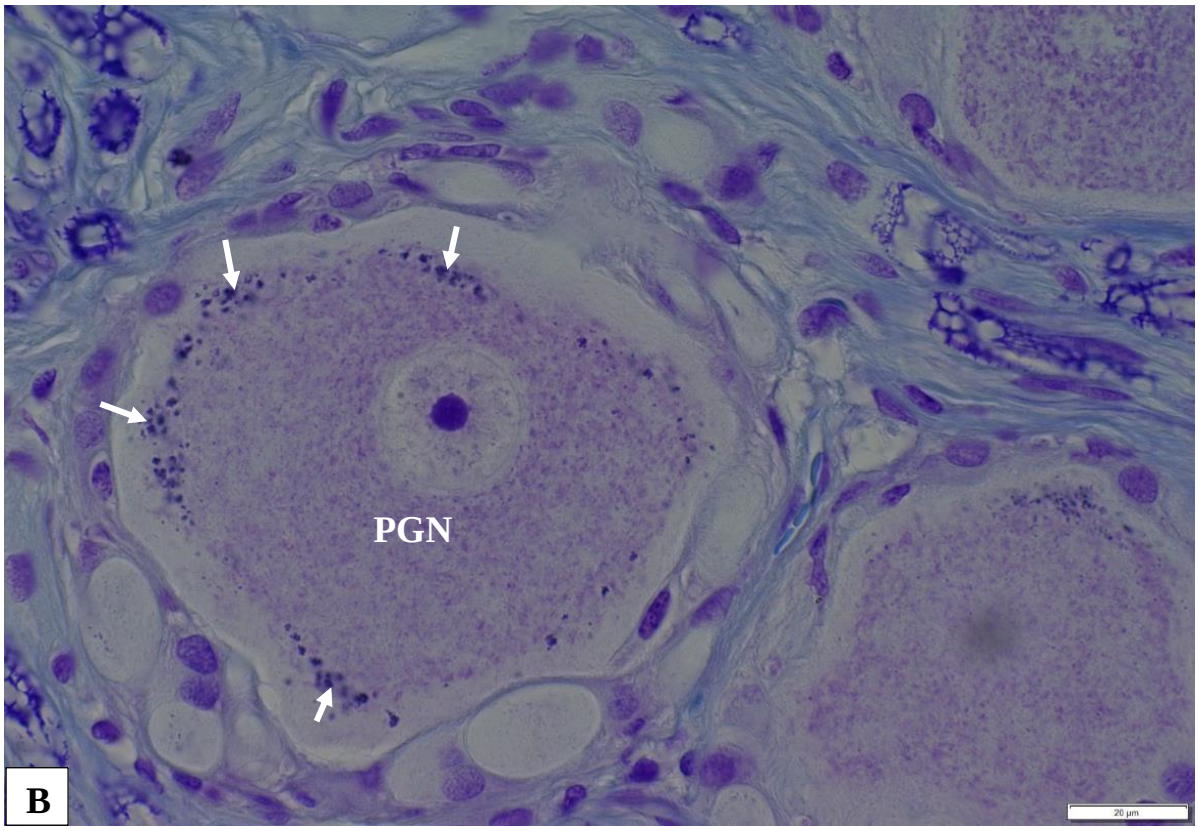

21

Fig. 21: A & B. Photomicrographs of the CCG showing the large principal ganglion neurons **(PGN)**. **A:** Showing the fine Nissl's substance filling the cytoplasm of the large PGN (**white arrows**). Cresyl fast violet stain. Image bar= 10μm. **B:** Showing coarse peripheral spherical lipofuscin granules (**white arrows**). Luxol fast blue with cresyl violet counterstain. Image bar= 20μm.

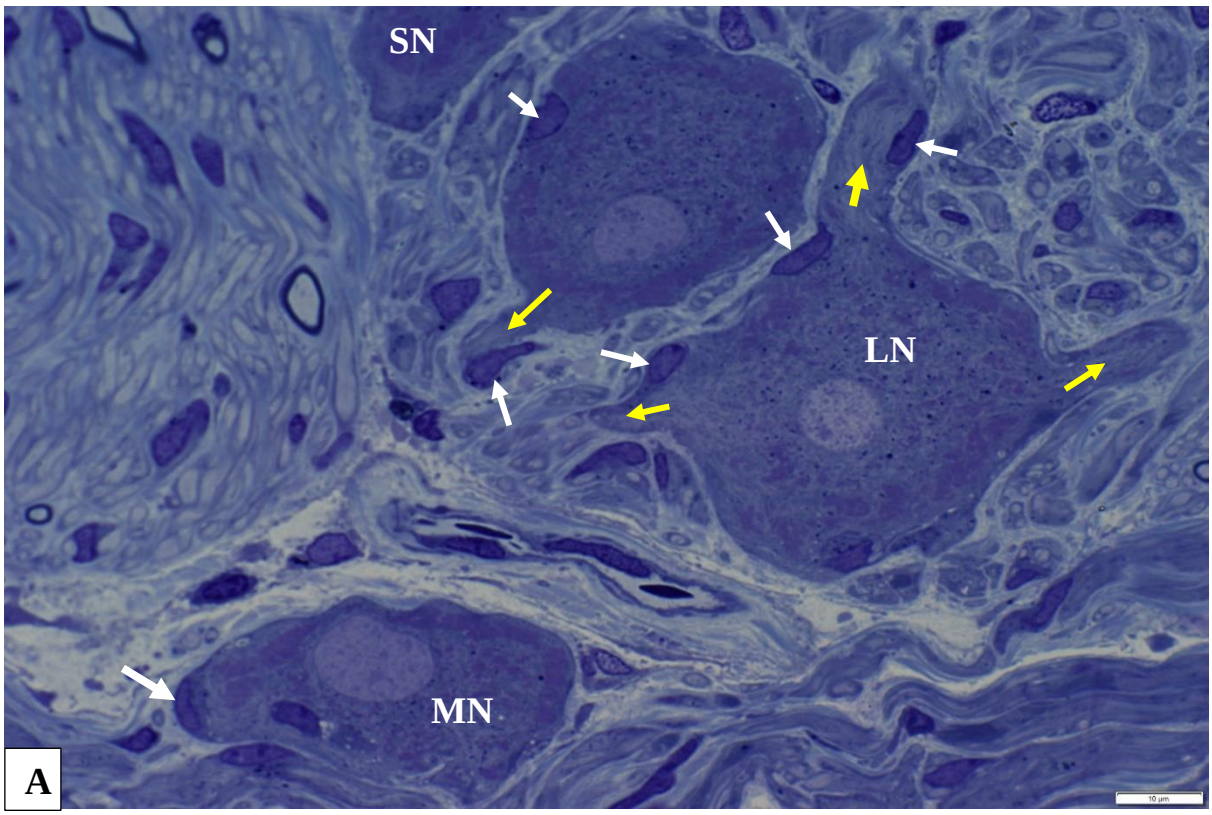

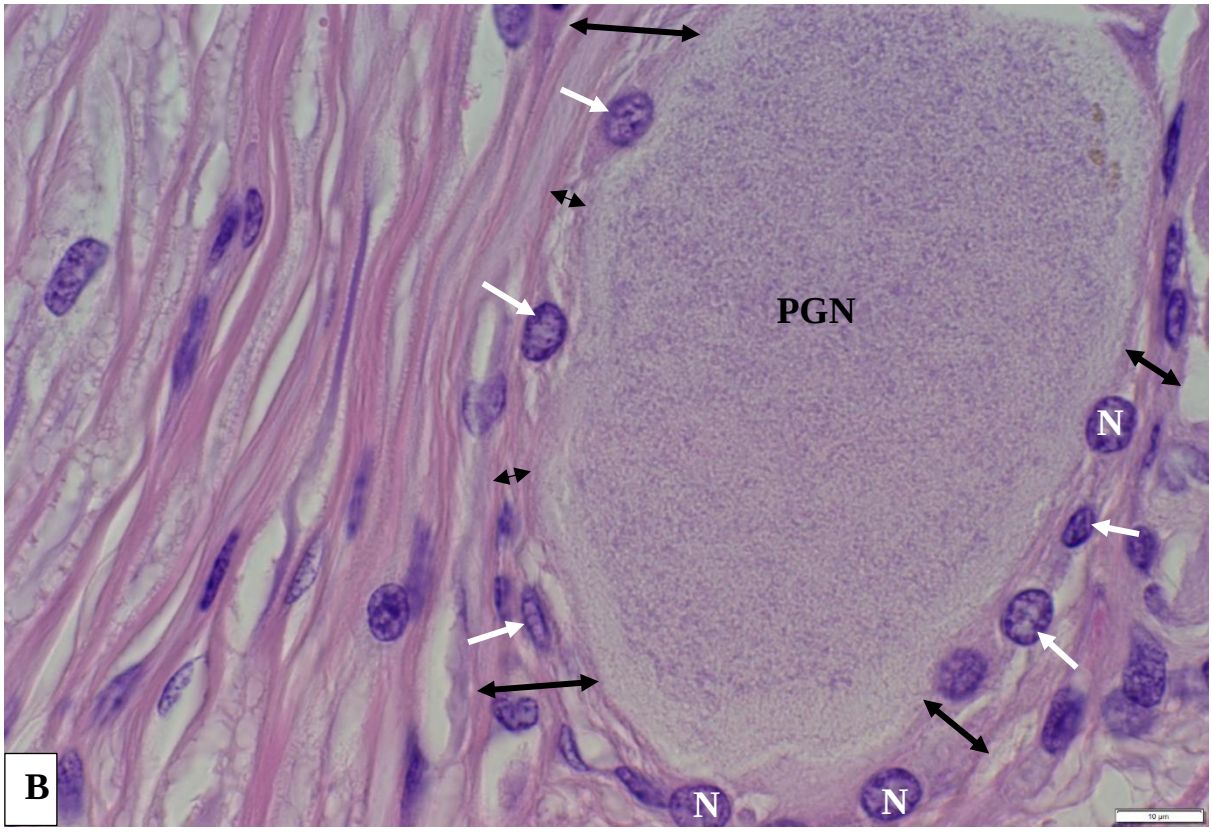

22

Fig. 22: A &B. Photomicrographs of the CCG; **A:** Showing the satellite cell **(white arrows)** surrounding the bodies of the small **(SN)**, medium **(MN)**, large principal ganglion neurons **(LN)** and their cytoplasmic processes **(yellow arrows)**. Note the flat nuclei of the satellite glial cells. Semi-thin section. Toluidine blue stain. Image bar= 10μm. **B:** Showing the satellite glial cells **(white arrows)** and glial capsule (**black double headed arrows**) surrounding the large principal ganglion neurons **(PGN).** Note the spherical nuclei of the satellite glial cells (**N**). H & E stain. Image bar= 10μm.

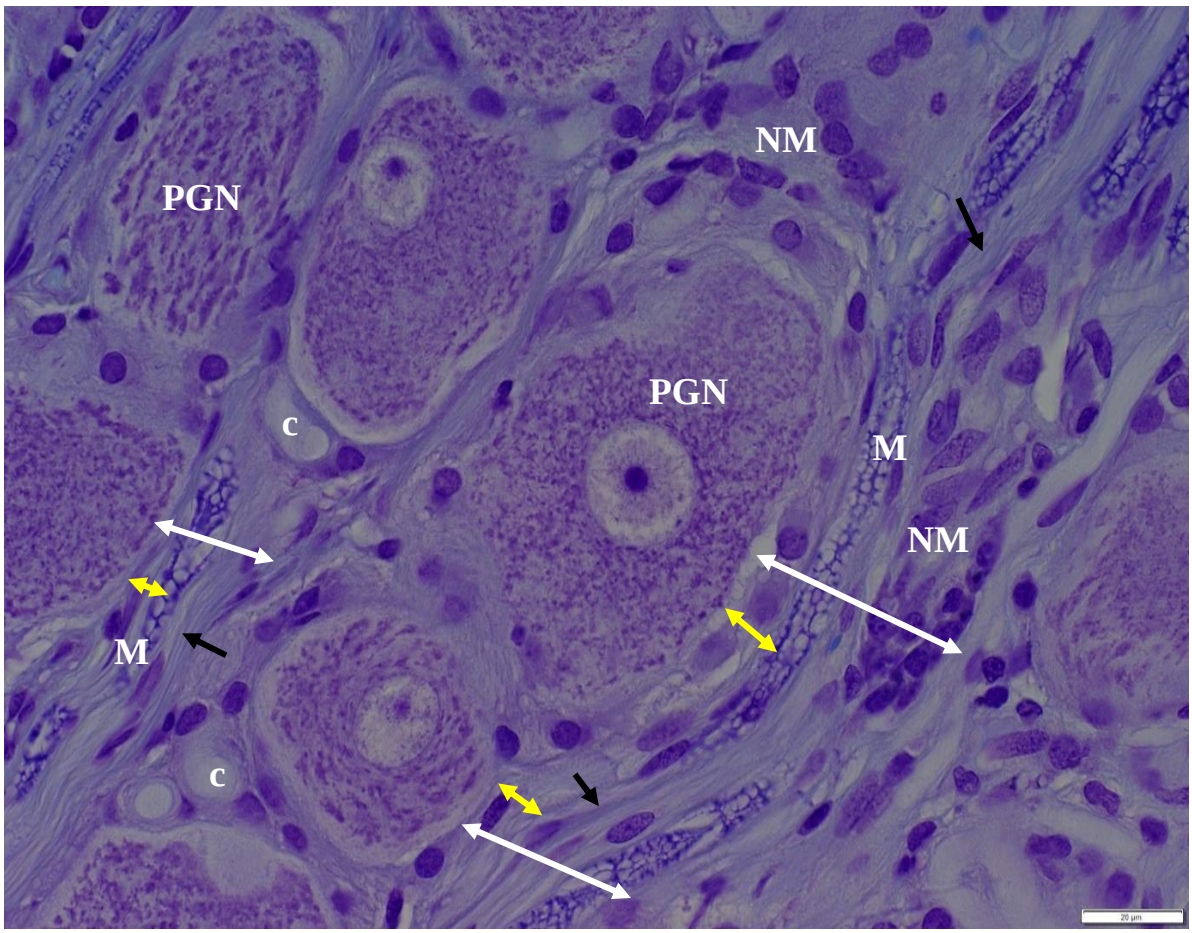

23

Fig. 23: A photomicrograph of the CCG showing the glial capsule (**yellow double headed arrows**) and neuropil **(white double headed arrows)** surrounding the principal ganglion neurons **(PGN).** Collagen fibres **(black arrows),** myelinated nerve fibres (**M),** non-myelinated nerve fibres (**NM)** and blood capillary **(c)**. Note the difference in the thickness of the neuropil around the small and large neurons. Luxol fast blue with cresyl violet counterstain. Image bar= 20µm

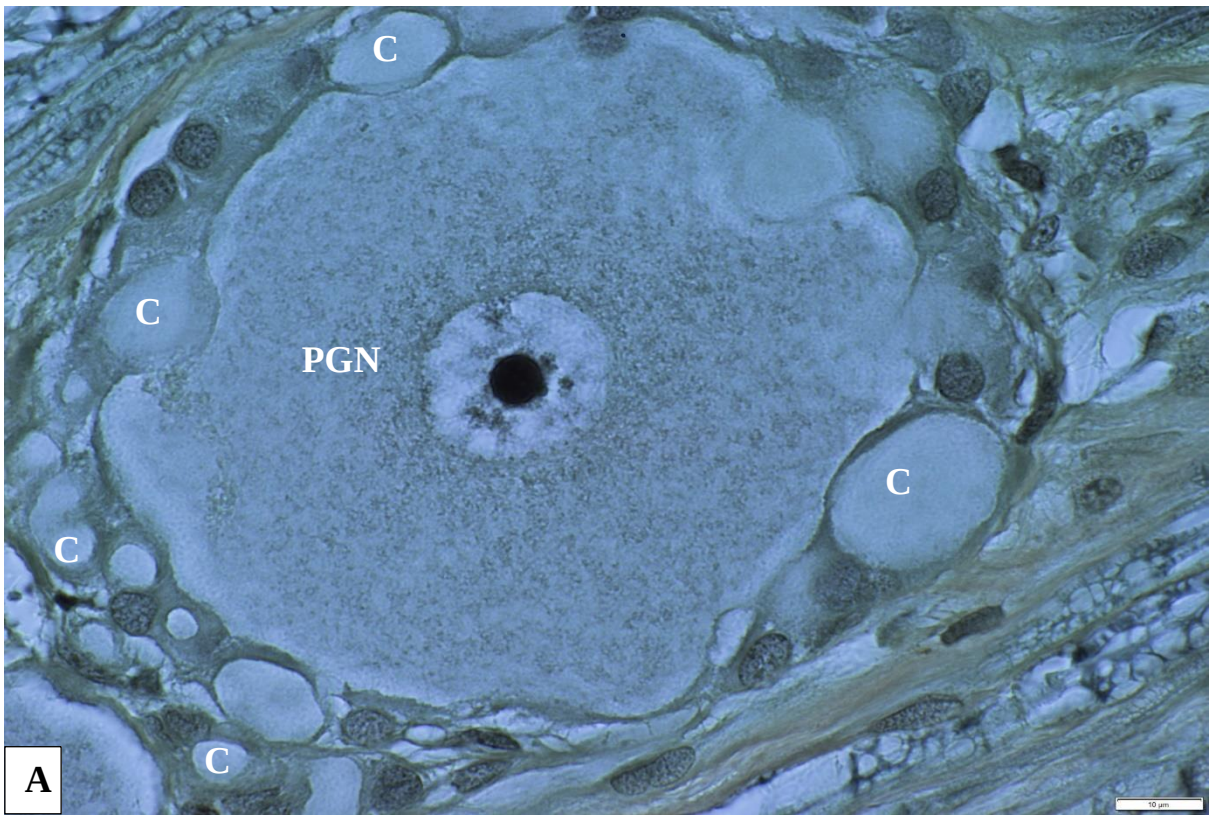

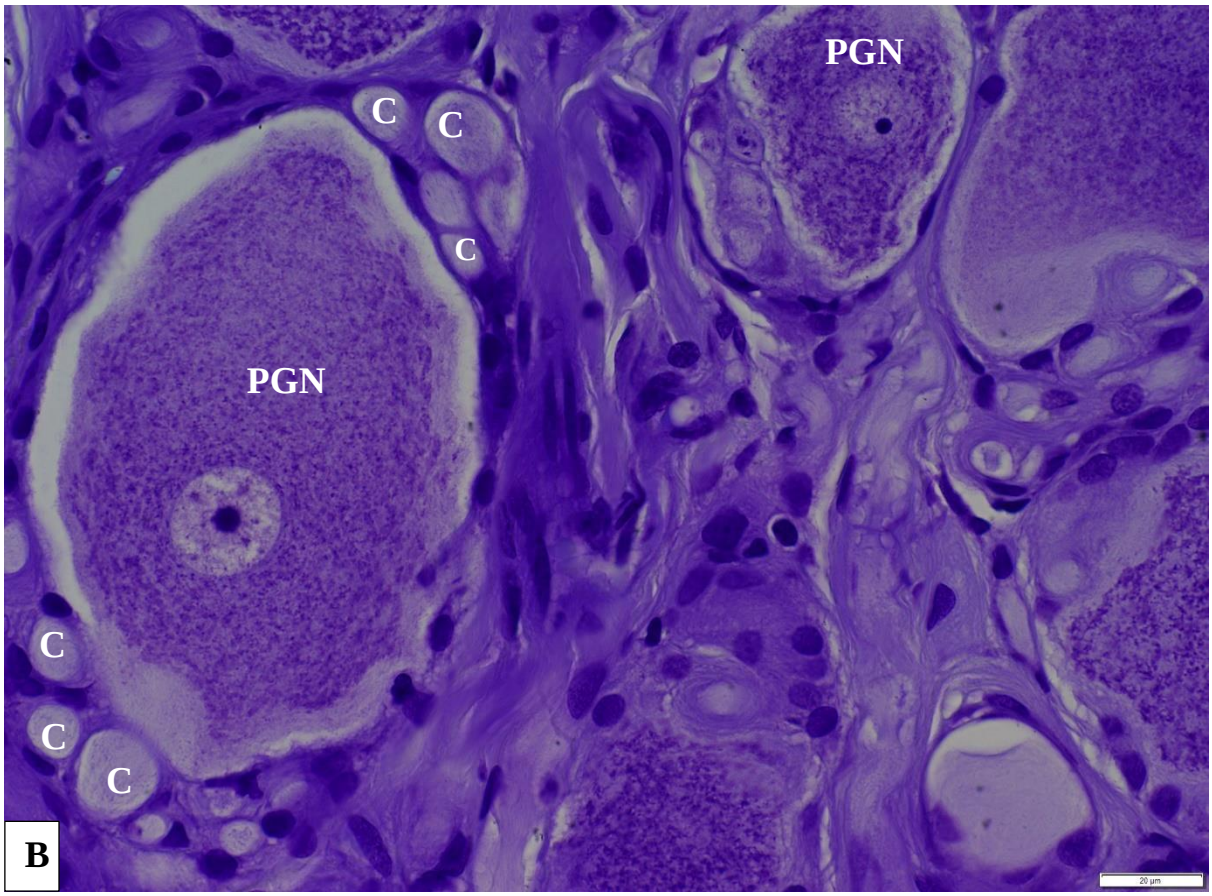

24

Fig. 24: A & B: Photomicrographs of the CCG showing blood capillaries **(C)** in the neuropil surrounding each principal ganglion neuron **(PGN).**

A: The blood capillaries completely surrounding the neurons. Verhoff's stain. Image bar= 10μm. **B:** The blood capillaries are aggregated at the poles of the principal ganglion neuron. Cresyl fast violet stain. Image bar= 20μm.

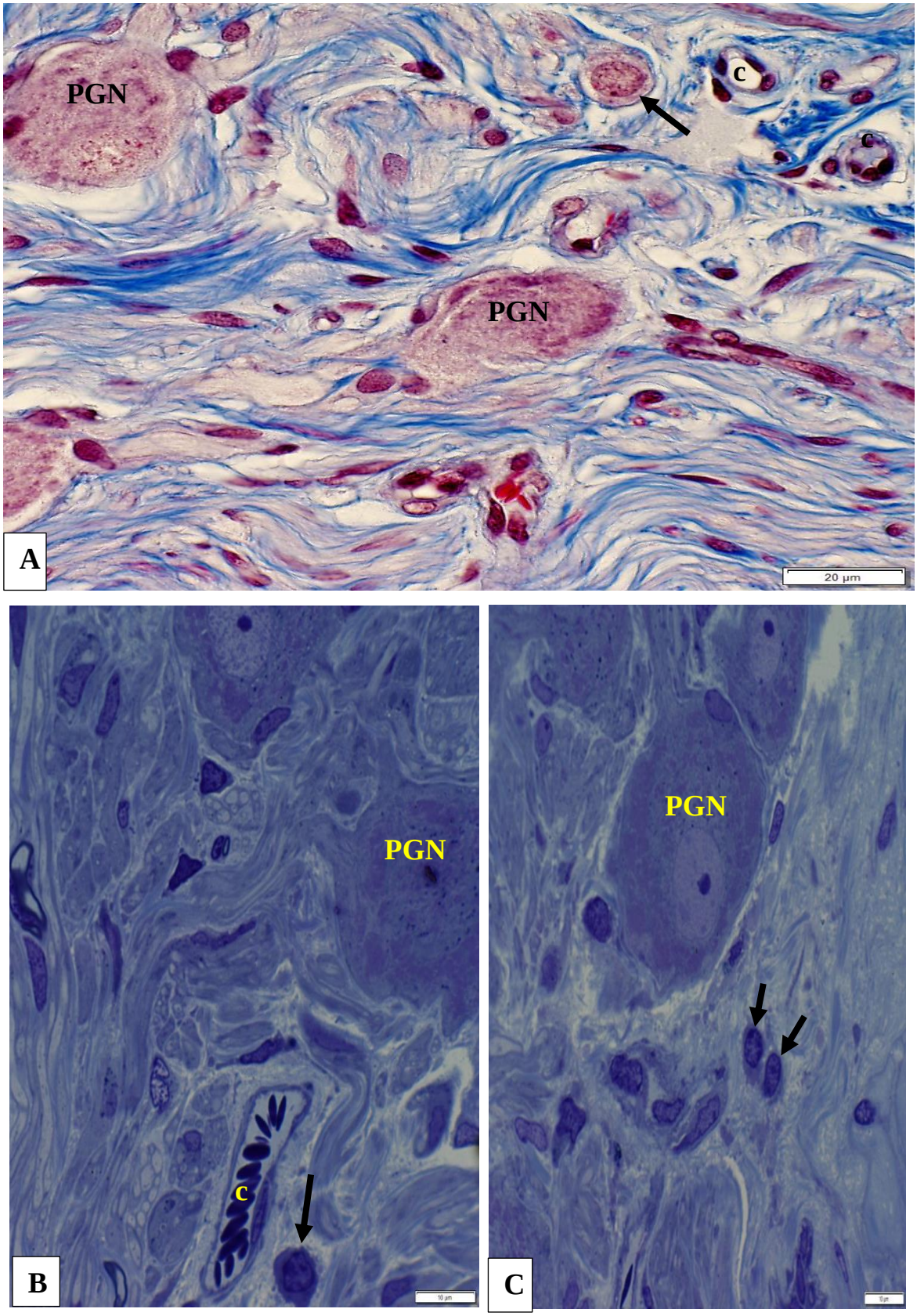

25

Fig. 25: A, B & C: Photomicrographs of the CCG showing small intensely fluorescent cells (**black arrow**), principal ganglion neuron **(PGN),** blood capillary **(c).**

Note: A & B: Showing the location of the small intensely fluorescent cells adjacent to the blood capillaries. **A:** Masson's trichrome stain. Image bar= 20μm. **B**: Semi-thin section stained by toluidine blue. Image bar= 10μm. **C:** The location of the small intensely fluorescent cells is adjacent to the principal ganglion neuron. Semi-thin section stained by toluidine blue. Image bar= 10μm.

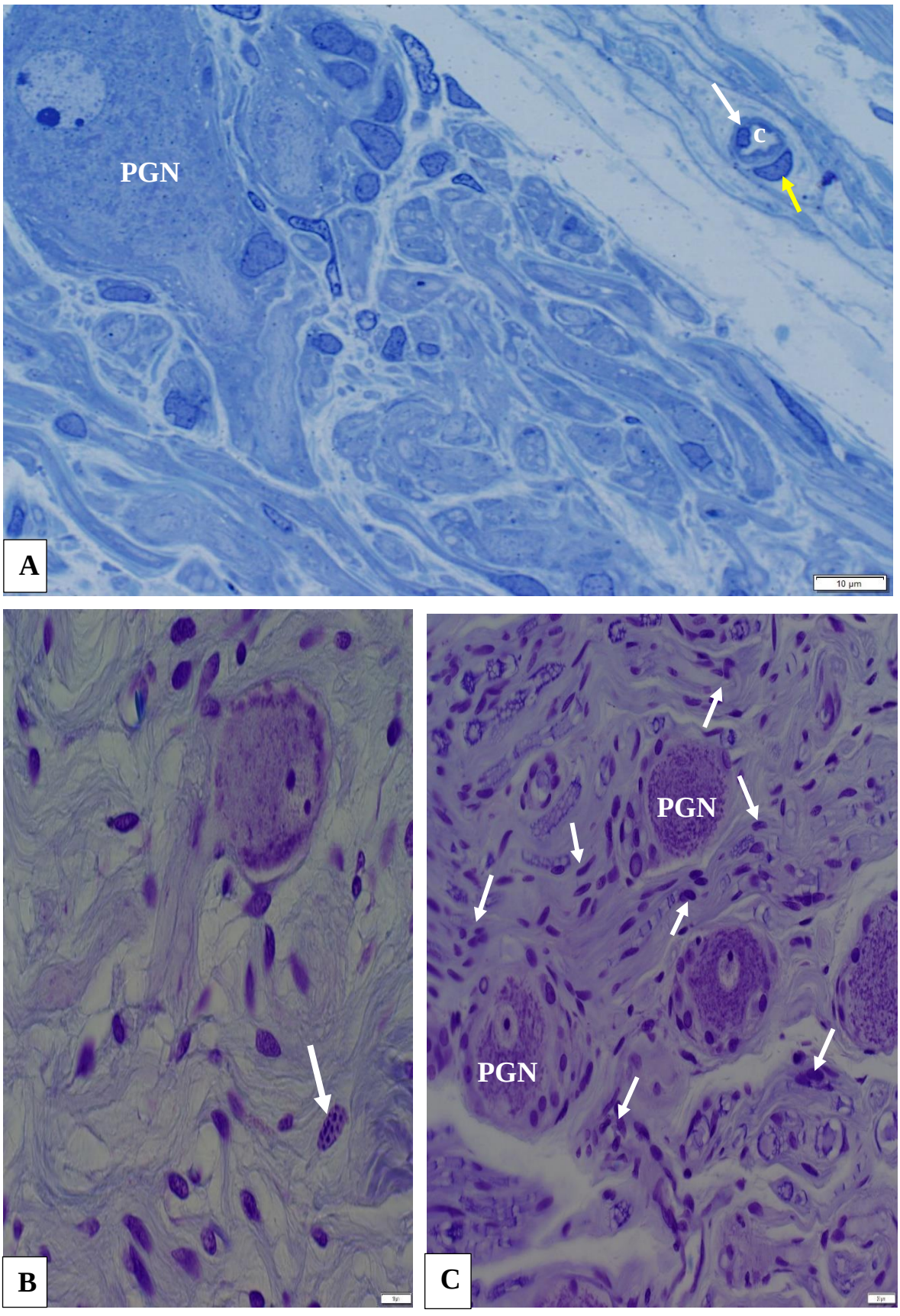

26

Fig. 26: A & B. Photomicrographs of the CCG; **A:** showing a pericyte (**yellow arrow**), endothelial cell (**white arrow**), principal ganglion neuron **(PGN),** blood capillary **(c).** Semi-thin section stained by toluidine blue. Image bar= 10μm. **B:** Showing the mast cell **(white arrow**). Luxol fast blue with cresyl violet counterstain. Image bar= 10μm. **C:** Showing the nuclei of the fibroblasts and Schwann cells (**white arrow**) and principal ganglion neuron **(PGN).** Luxol fast blue with cresyl violet counterstain. Image bar= 20μm.

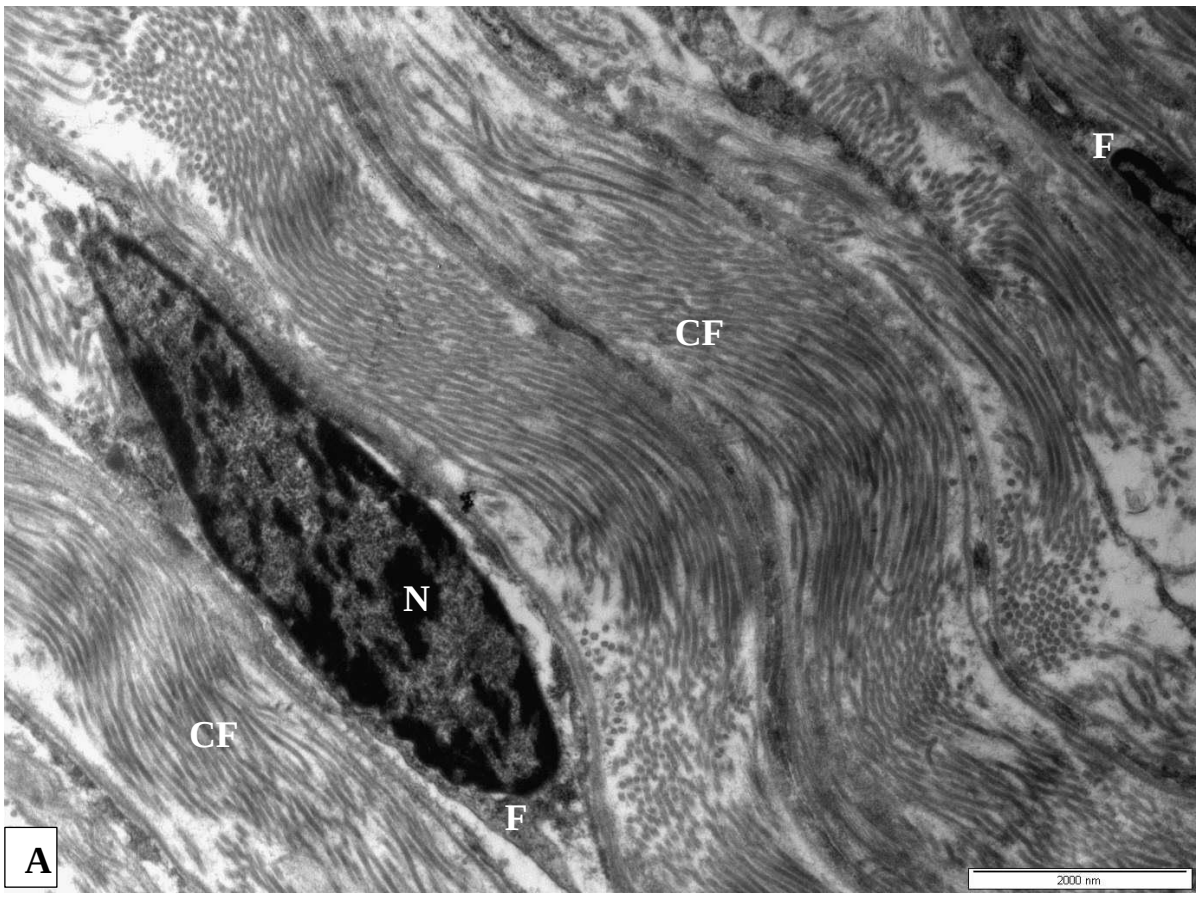

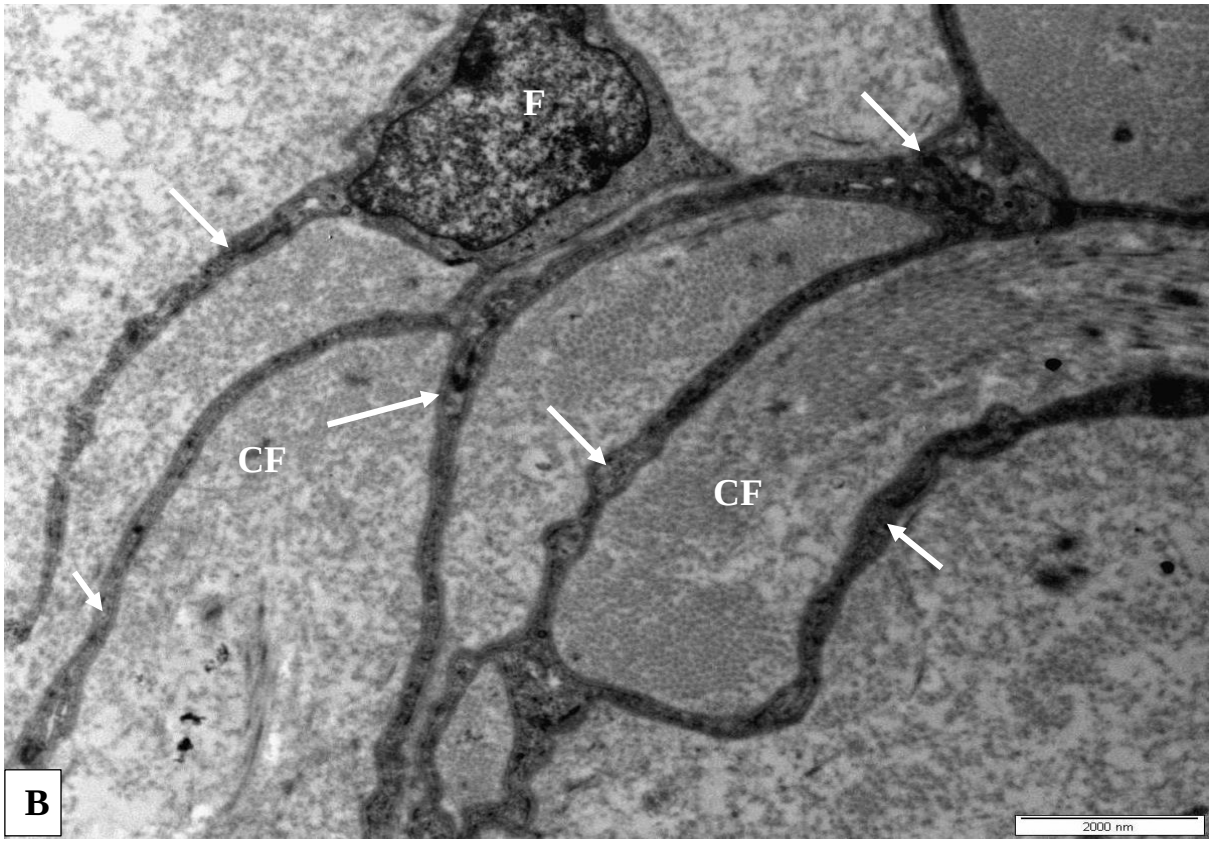

27

Figs. 27: A & B. A: Transmission electron micrographs of the CCG's capsule showing the collagen fibrils (**CF)**, fibroblast (**F**) with flattened nucleus (**N**). **B:** The collagen fibrils (**CF**) and fibroblast (**F**) with cytoplasmic processes (**white arrows**). Image bar= 2000 nm.

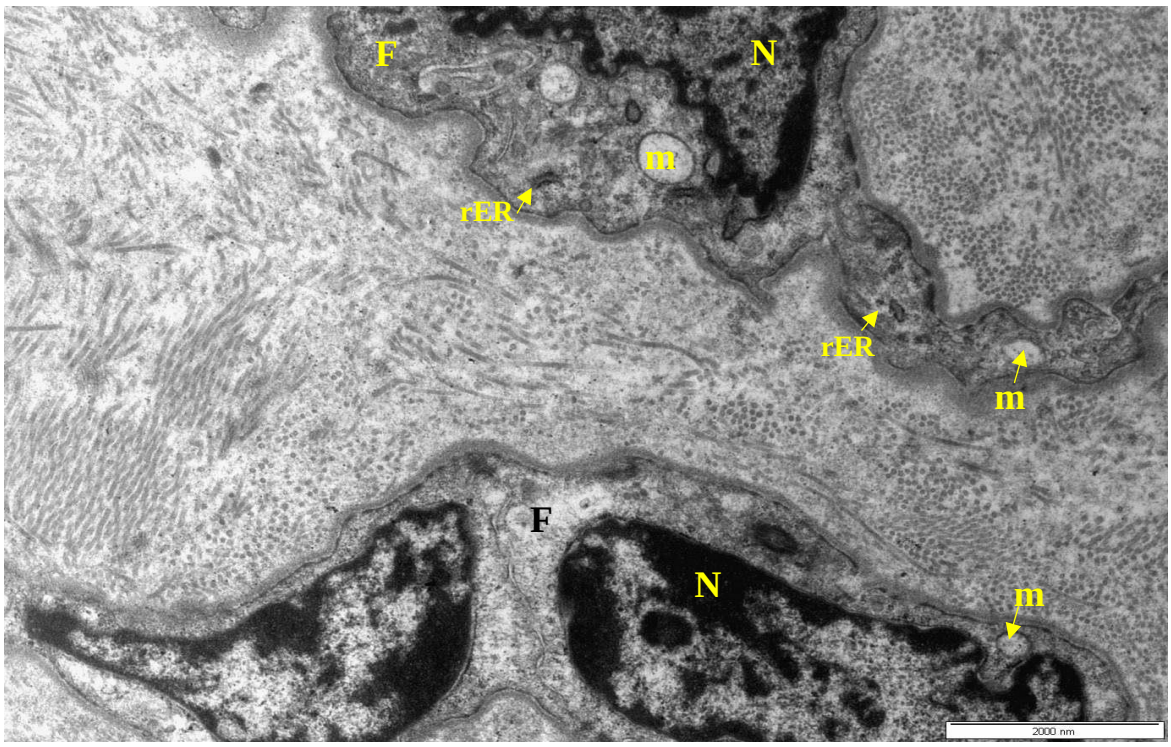

28

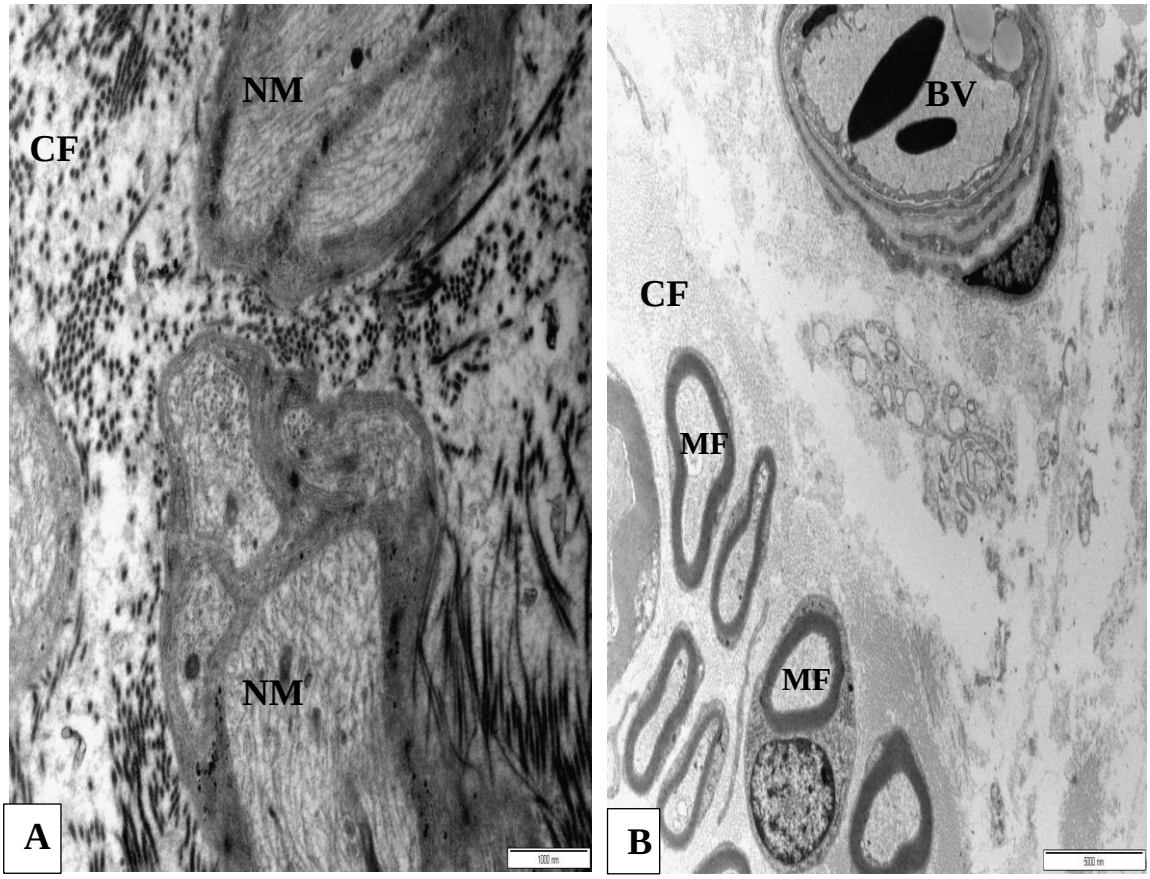

29

Fig. 28: Transmission electron micrograph of the CCG's capsule showing the cytoplasm of the fibroblast (**F**) displaying numerous mitochondria (**m**), and rough endoplasmic reticulum (**rER**). Note the light cytoplasm of the fibroblast and the nucleus (**N**). Image bar= 2000 nm.

Figs. 29. A & B: Transmission electron micrographs of the CCG capsule; A: Showing the collagen fibrils (**CF**) and non-myelinated nerve fibres (**NM**). Image bar= 1000 nm. **B**: Showing the collagen fibrils (**CF**), myelinated nerve fibres (**MF)** and blood vessel (**BV**). Image bar= 5000 nm.

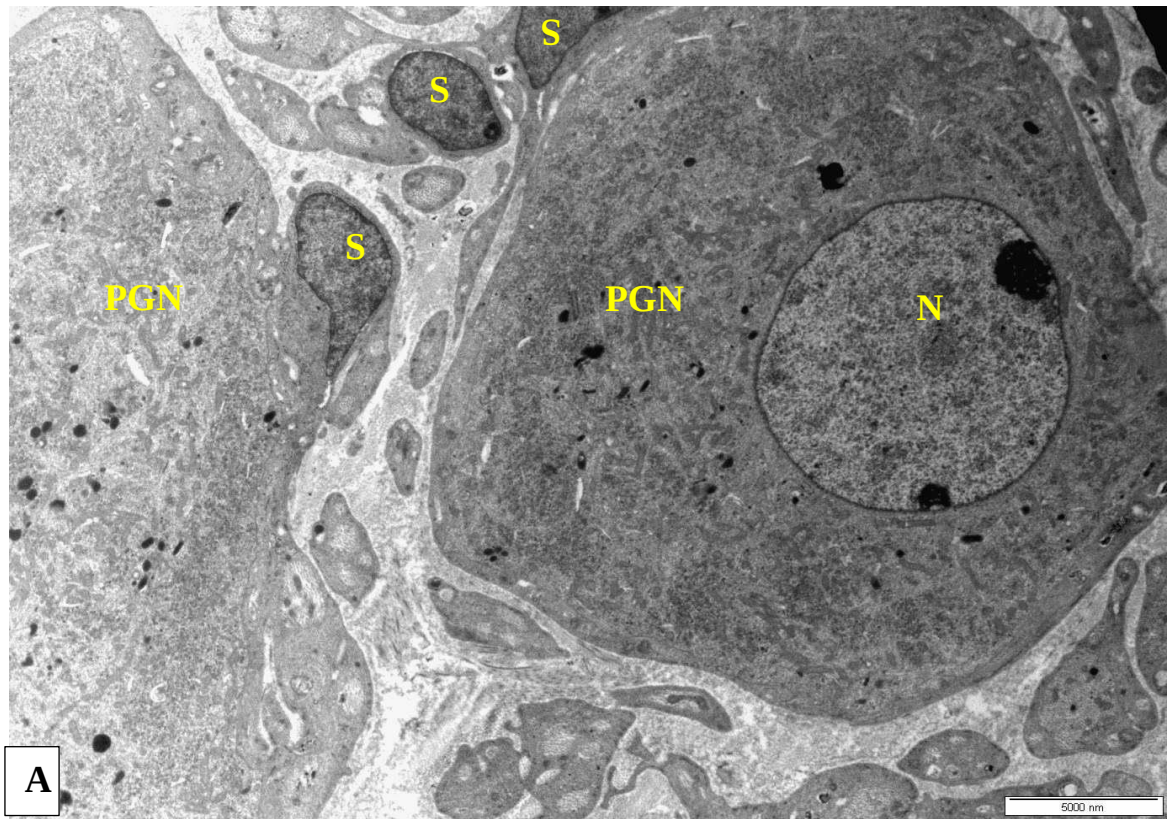

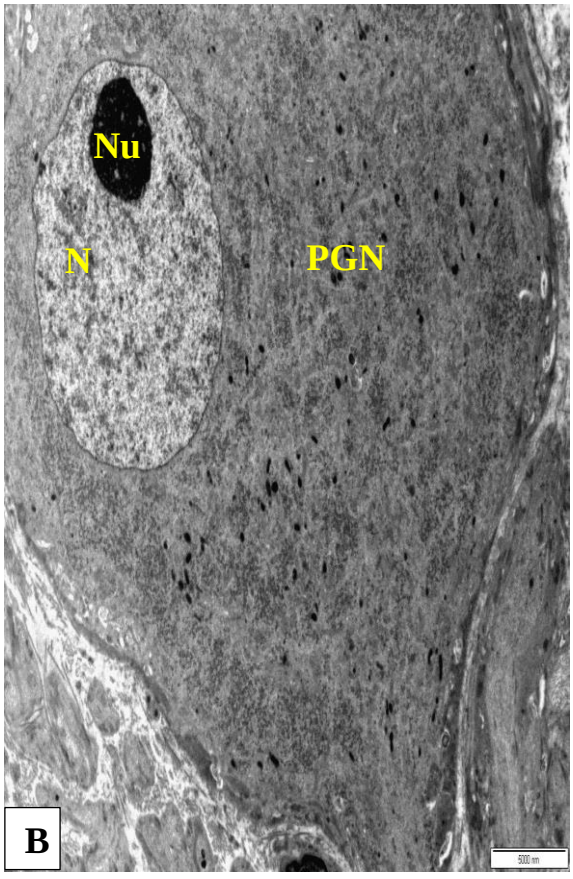

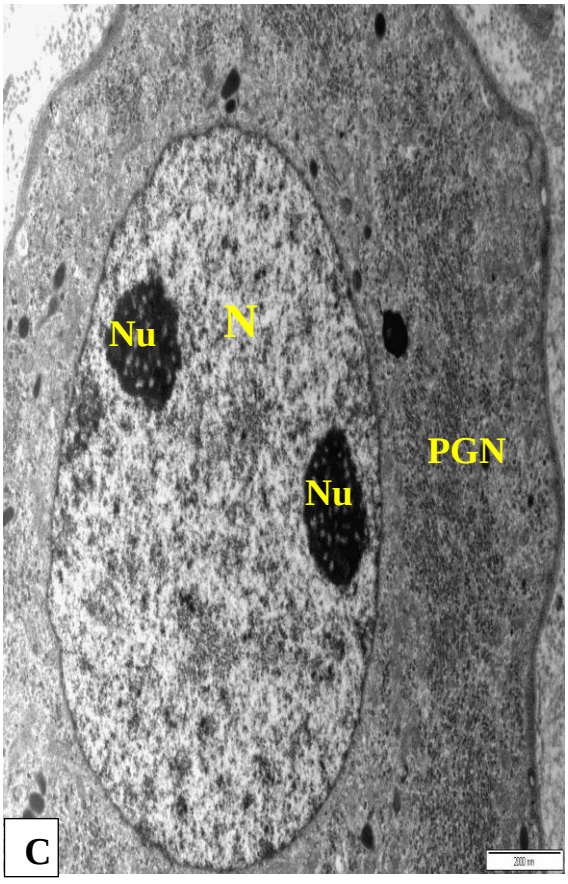

30

Figs. 30. A, B & C: Transmission electron micrographs of the CCG; **A:** Showing the principal ganglion neurons (**PGN**) has eccentric spherical nucleus (**N**) and satellite glial cells (**S**). Image bar= 5000 nm. **B:** Showing the principal ganglion neuron (**PGN**) with eccentric nucleus (**N**) and one nucleolus (**Nu**). Image bar= 5000 nm. **C:** Showing the principal ganglion neuron (**PGN**) with eccentric nucleus (**N**) and two nucleoli (**Nu**). Image bar= 2000 nm.

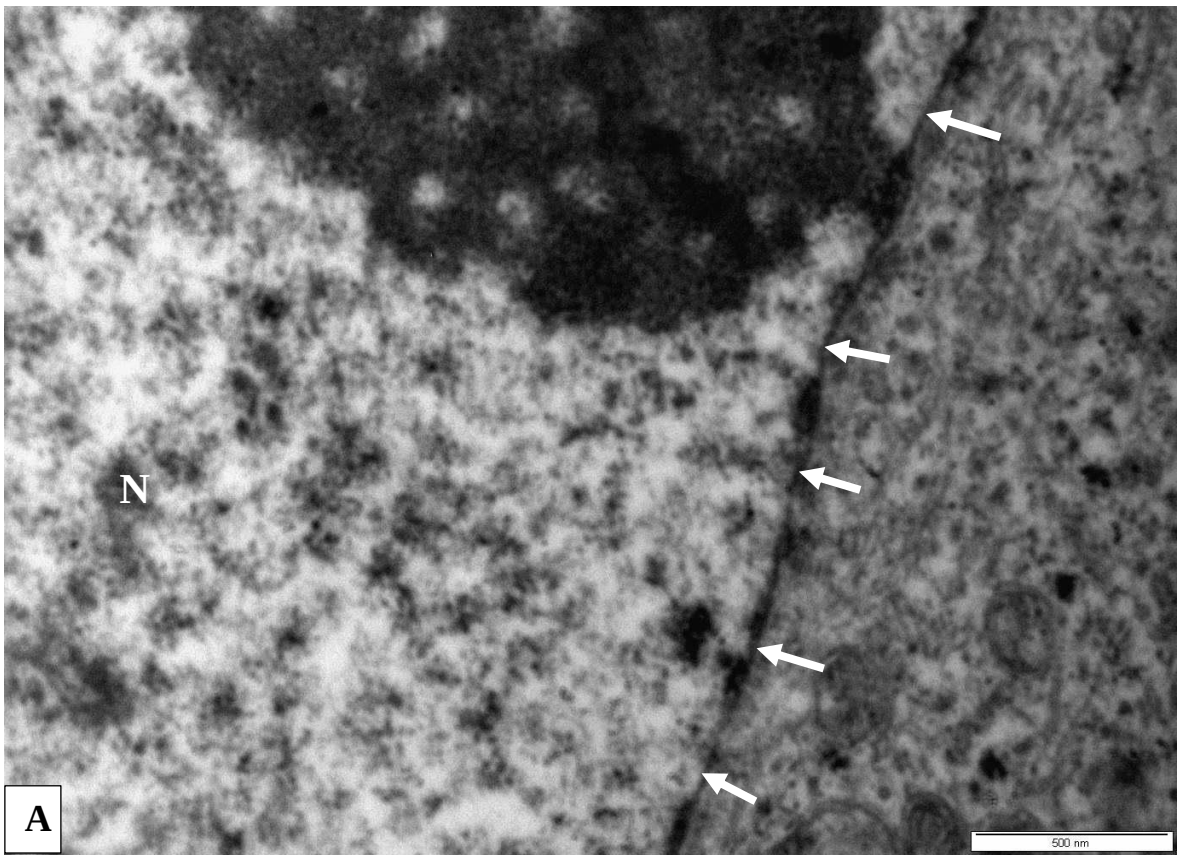

31

Fig. 31: A & B: A: Transmission electron micrographs of the principal ganglion neuron in the CCG showing the nucleus (**N**) and nuclear membrane with nuclear pores (**white arrows**). Image bar= 500 nm. **B:** showing the plasma membrane of the principal ganglion neuron possessing numerous folds (**black arrows**). Principal ganglion neuron: (**PGN**). Satellite glial cells: (**S**). Image bar= 2000 nm.

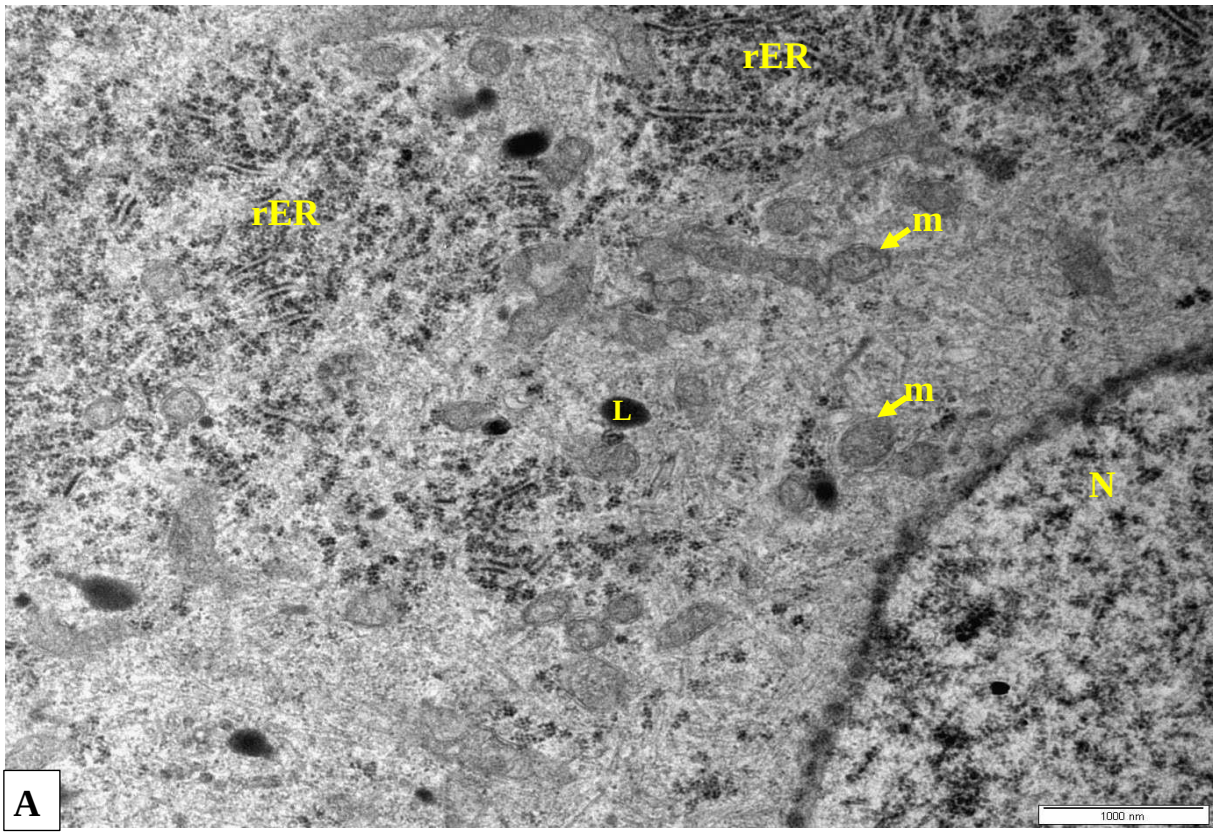

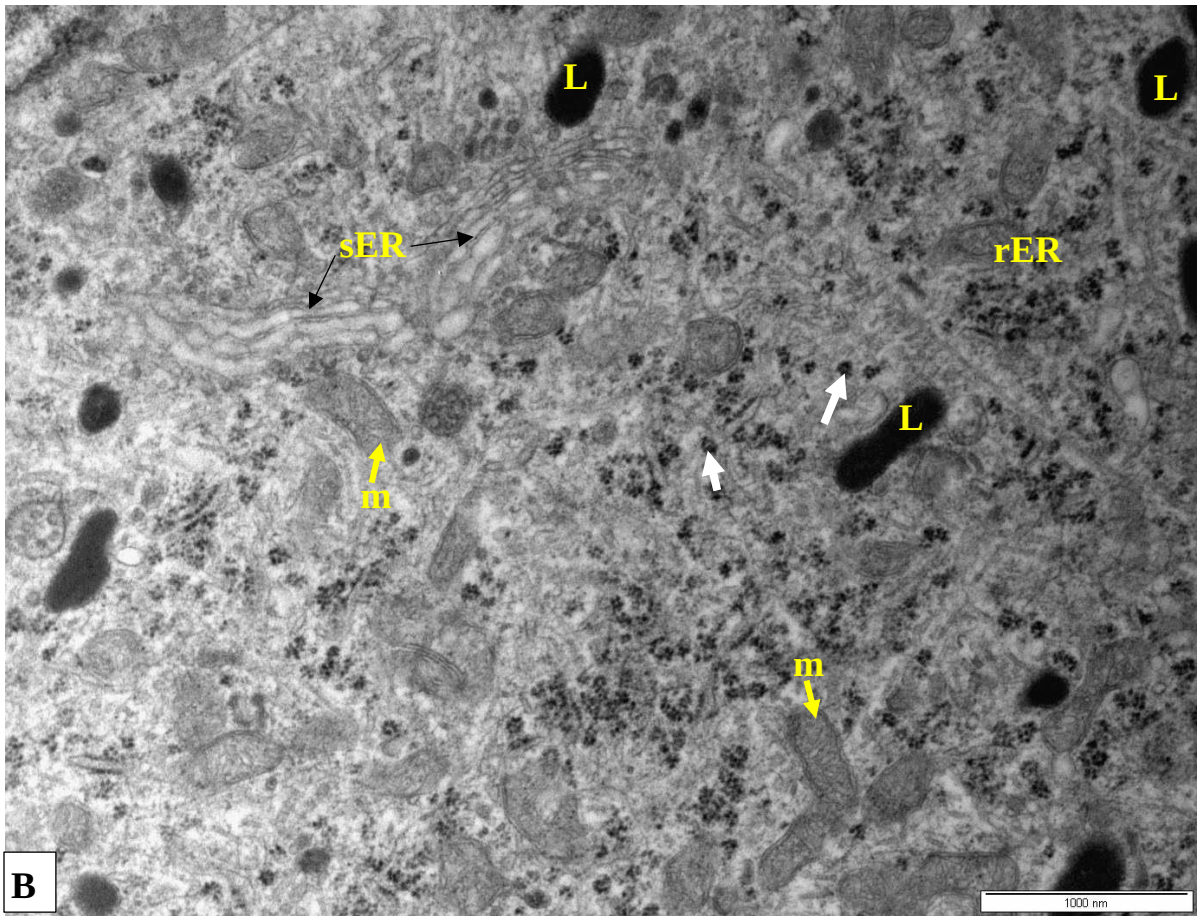

32

Fig. 32: A & B: Transmission electron micrographs of the principal ganglion neuron in the CCG showing the smooth endoplasmic reticulum (**sER**), rough endoplasmic reticulum (**rER**), dense secondary lysosomes (**L**), mitochondria (**m**) and ribosomes (**white arrows**). Image bar= 1000 nm.

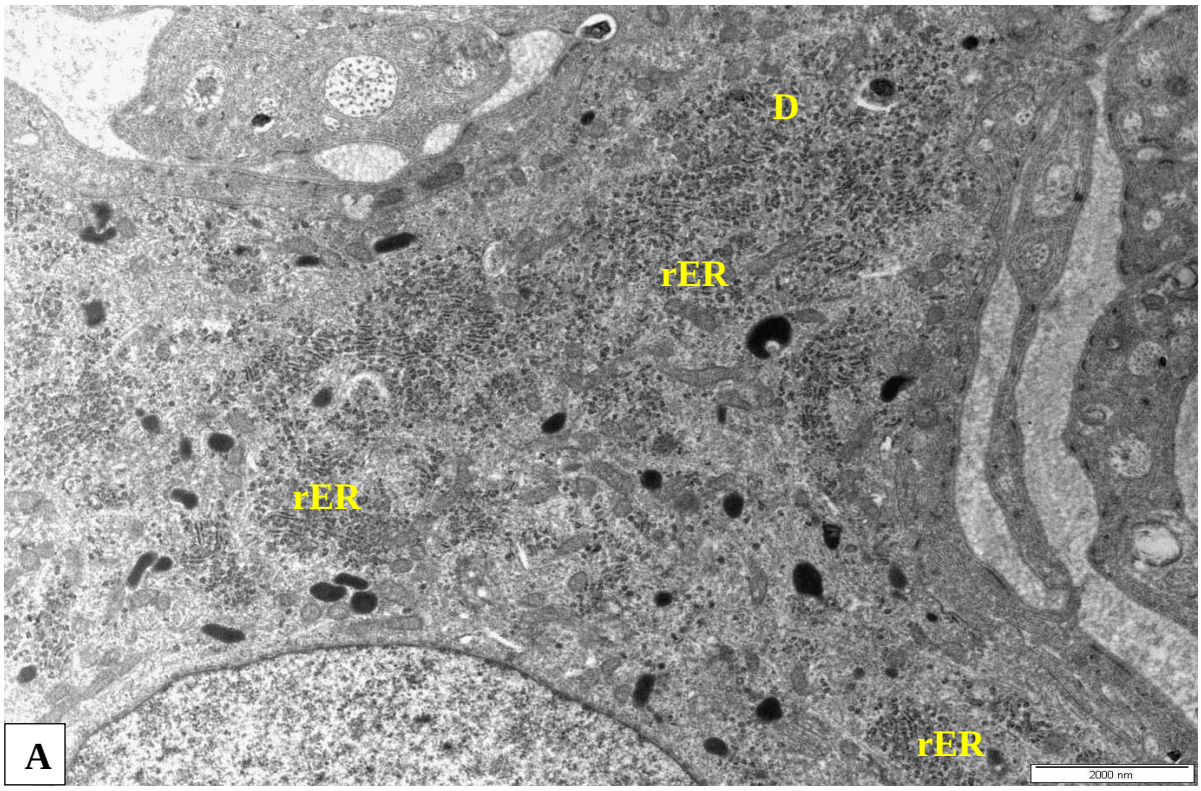

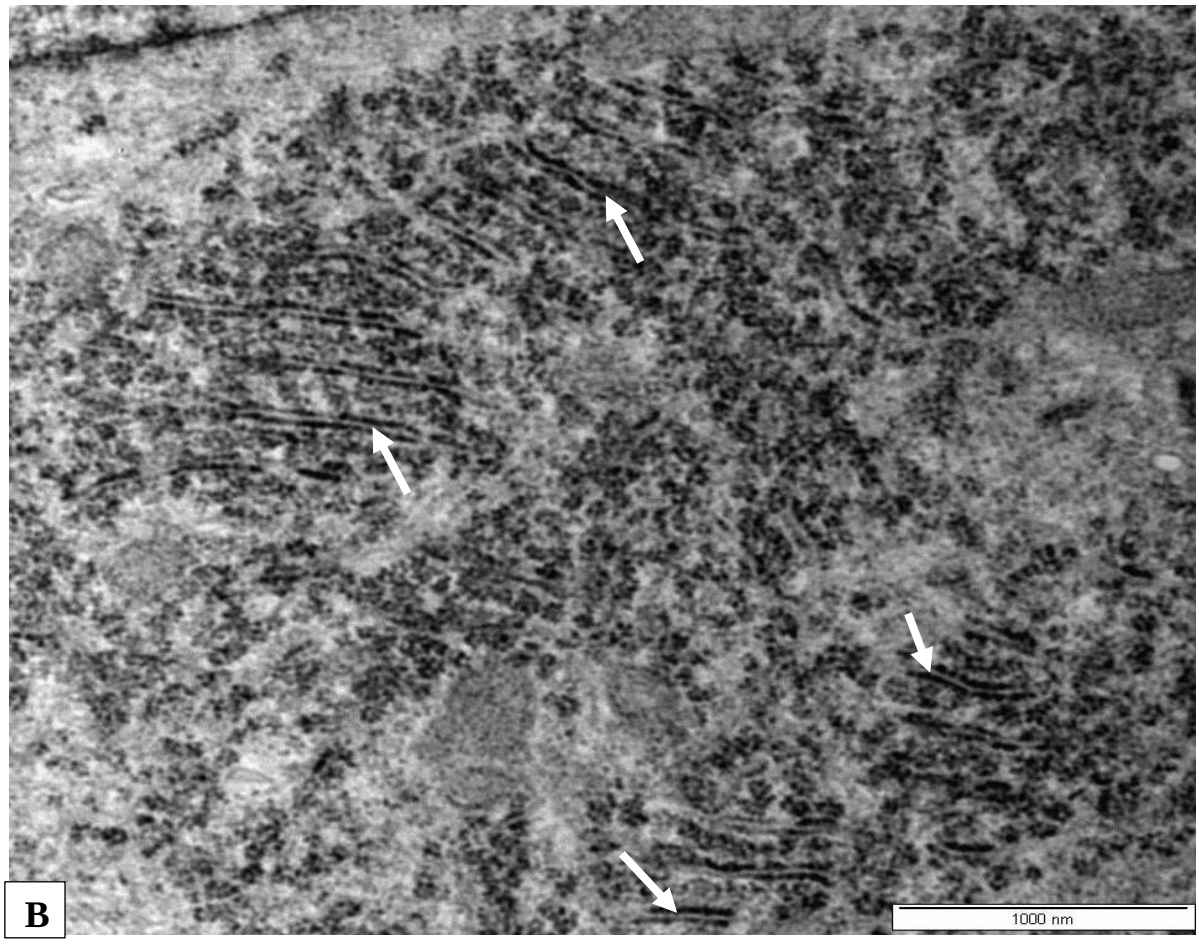

33

Fig. 33: A & B: A: Transmission electron micrographs of the CCG showing the perikaryon of the principal ganglion neuron containing numerous cisternae of rough endoplasmic reticulum (**rER**). Note the extension of the (**rER**) to the dendrites (**D**). Image bar= 2000 nm.

B: Higher magnification of the cisternae of rough endoplasmic reticulum (**white arrows**). Image bar= 1000 nm.

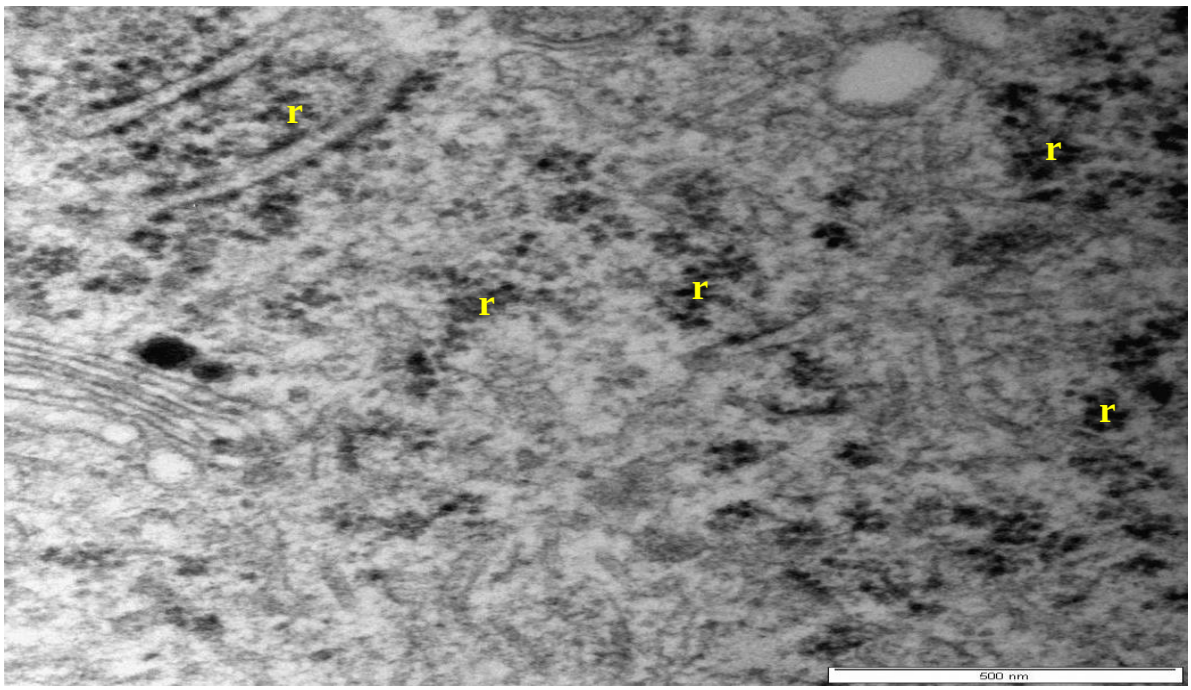

34

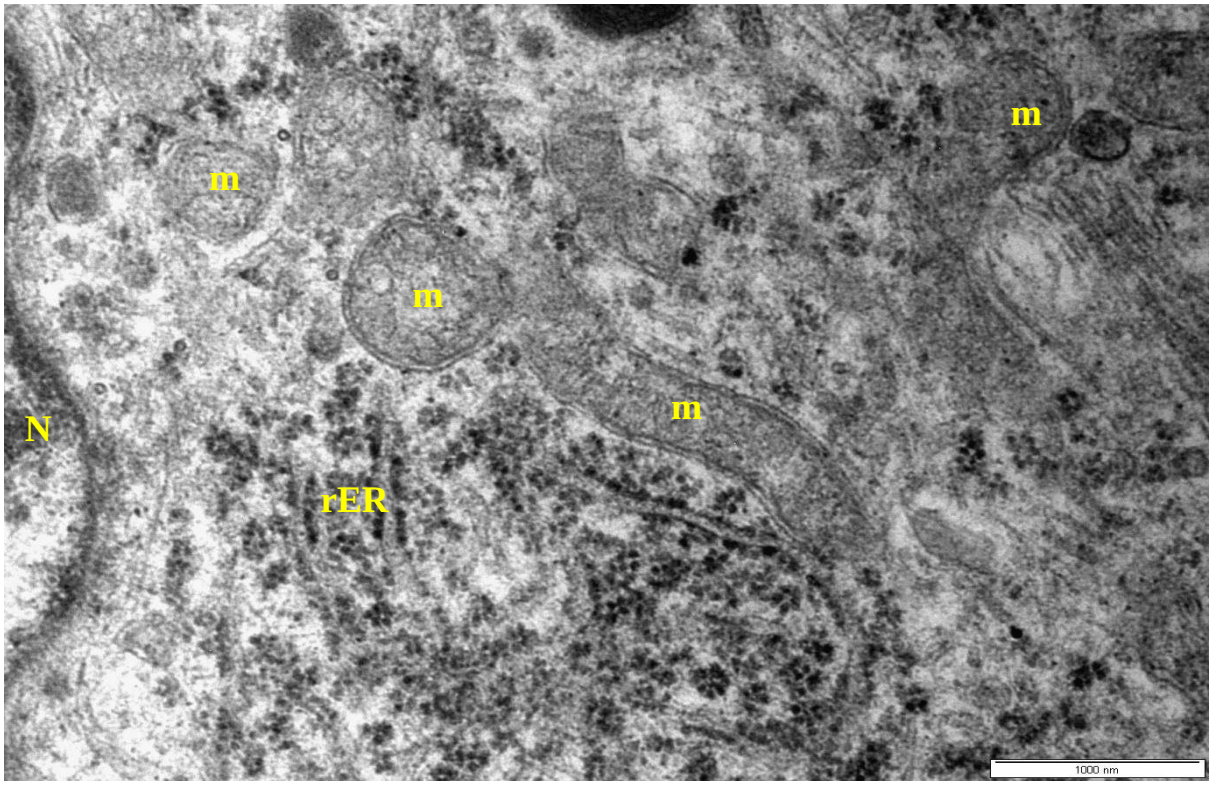

35

Fig. 34: Transmission electron micrograph of the CCG showing the perikaryon of the principal ganglion neuron displaying many ribosomes (**r**). Image bar= 500 nm.

Fig. 35: Transmission electron micrograph of the CCG showing the perikaryon of the principal ganglion neuron. The PGN exhibits different shapes and sizes of supra-nuclear mitochondria (**m**). Nucleus: **(N)**. Rough endoplasmic reticulum (**rER**). Image bar= 1000 nm.

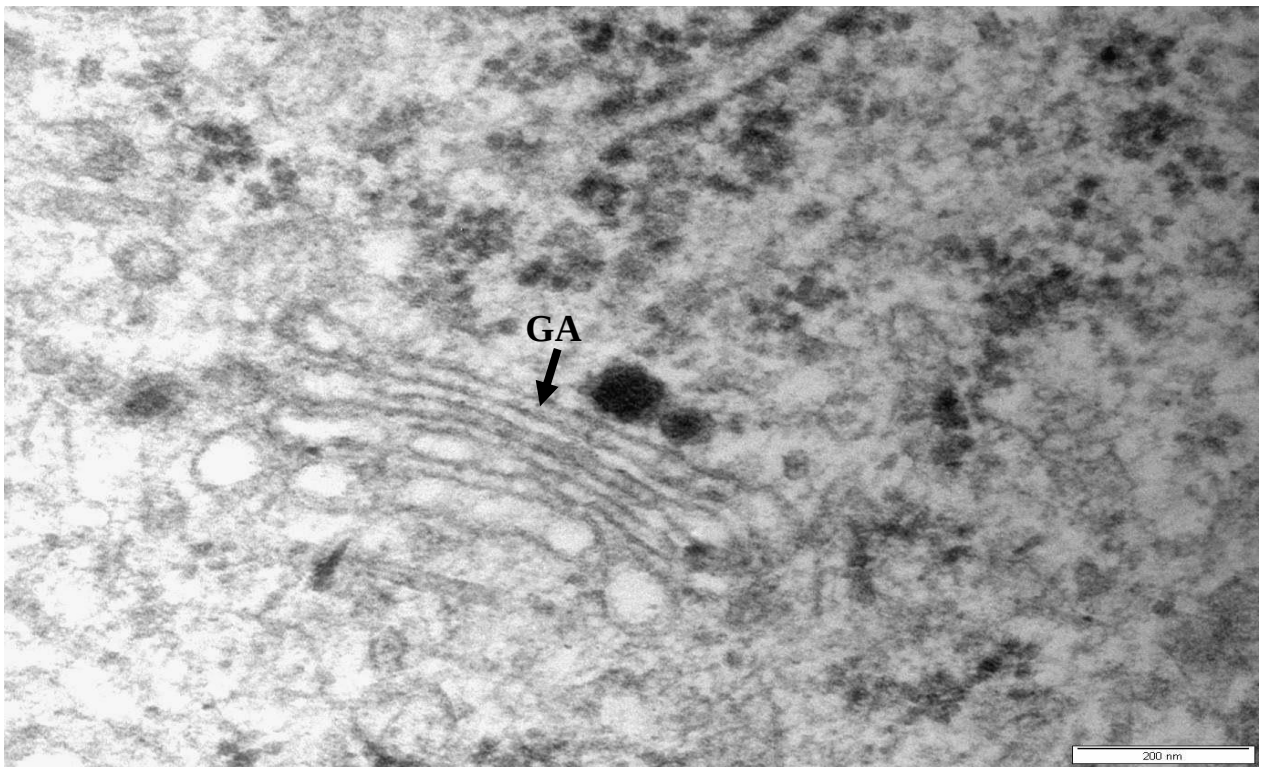

36

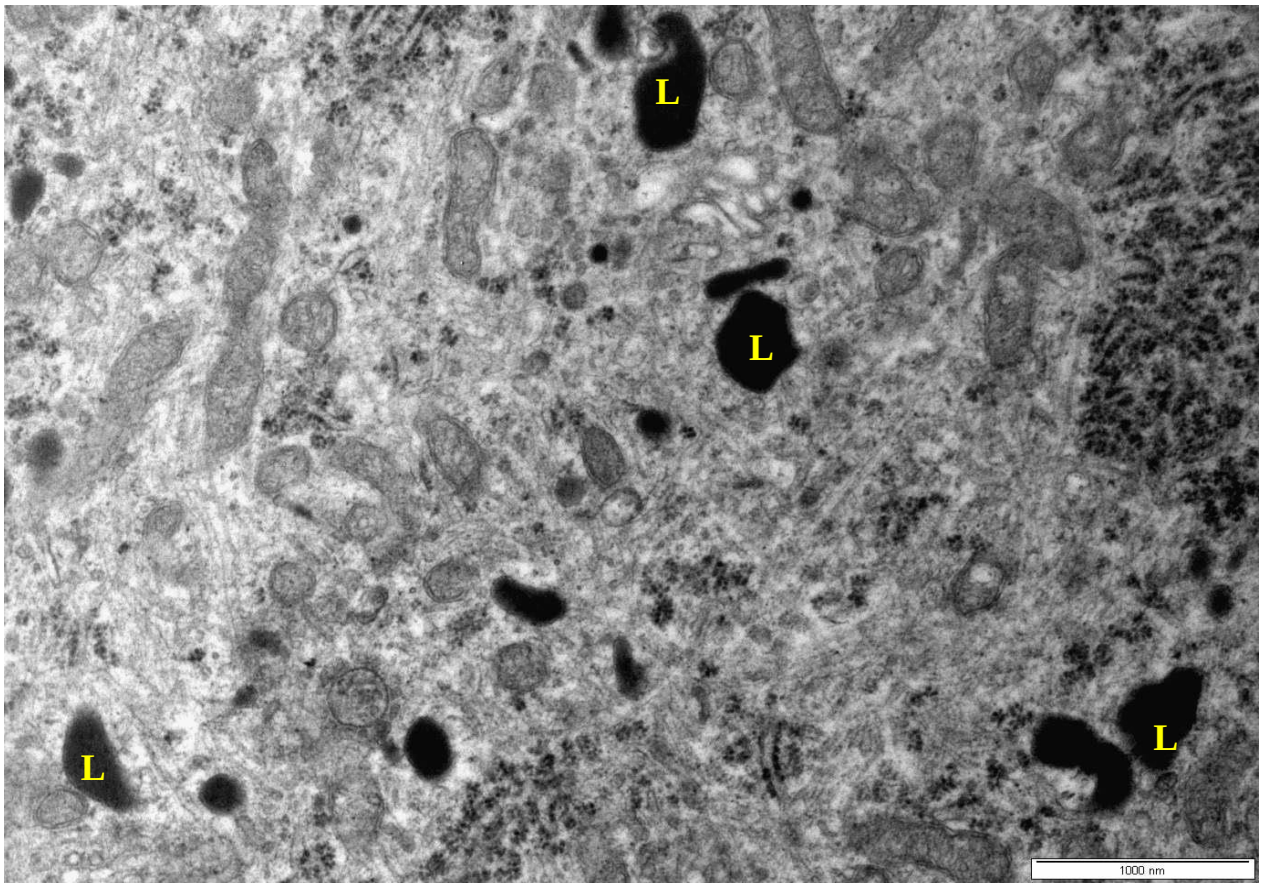

37

Fig. 36: Transmission electron micrograph of the CCG showing the perikaryon of the principal ganglion neuron displays the Golgi apparatus (**GA**). Note that the Golgi apparatus is highly developed and forms a continuous network. Image bar= 200 nm.

Fig. 37: Transmission electron micrograph of the CCG showing the perikaryon of the principal ganglion neuron displaying numerous lysosomes (**L**). Image bar=1000 nm.

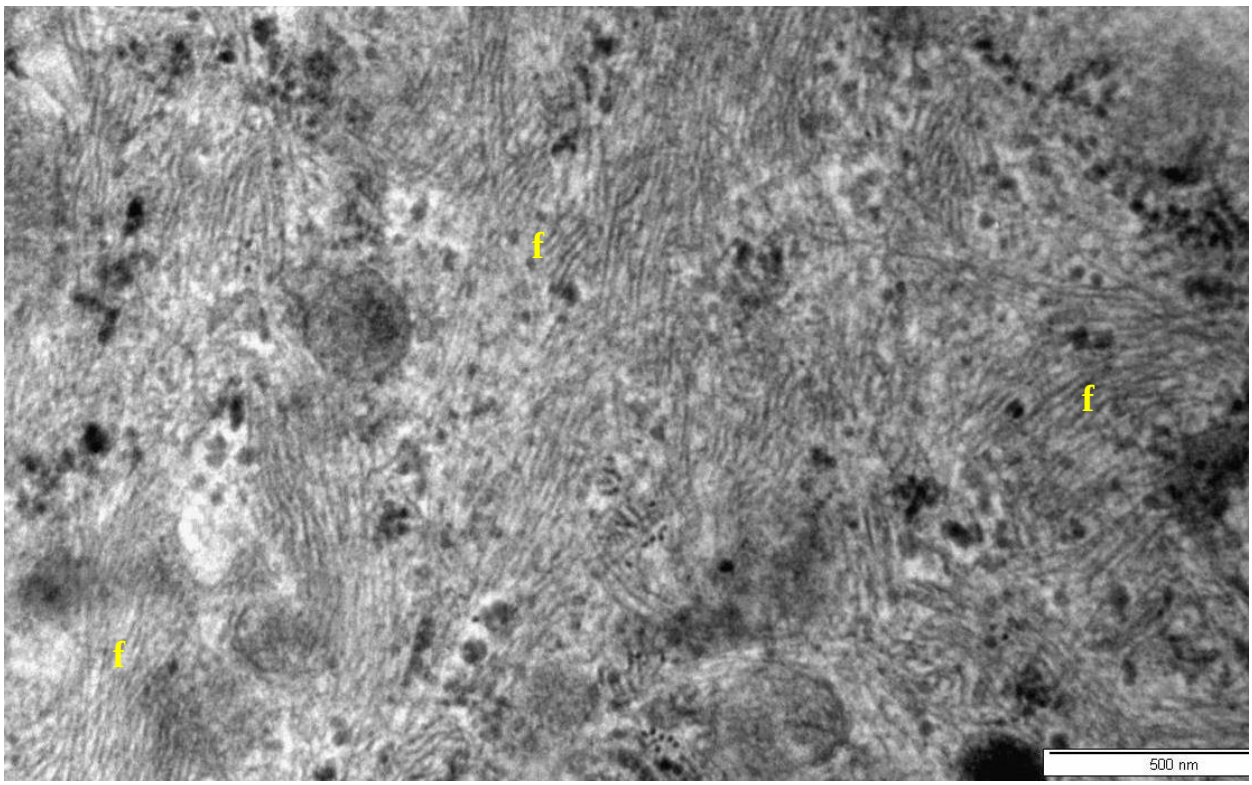

38

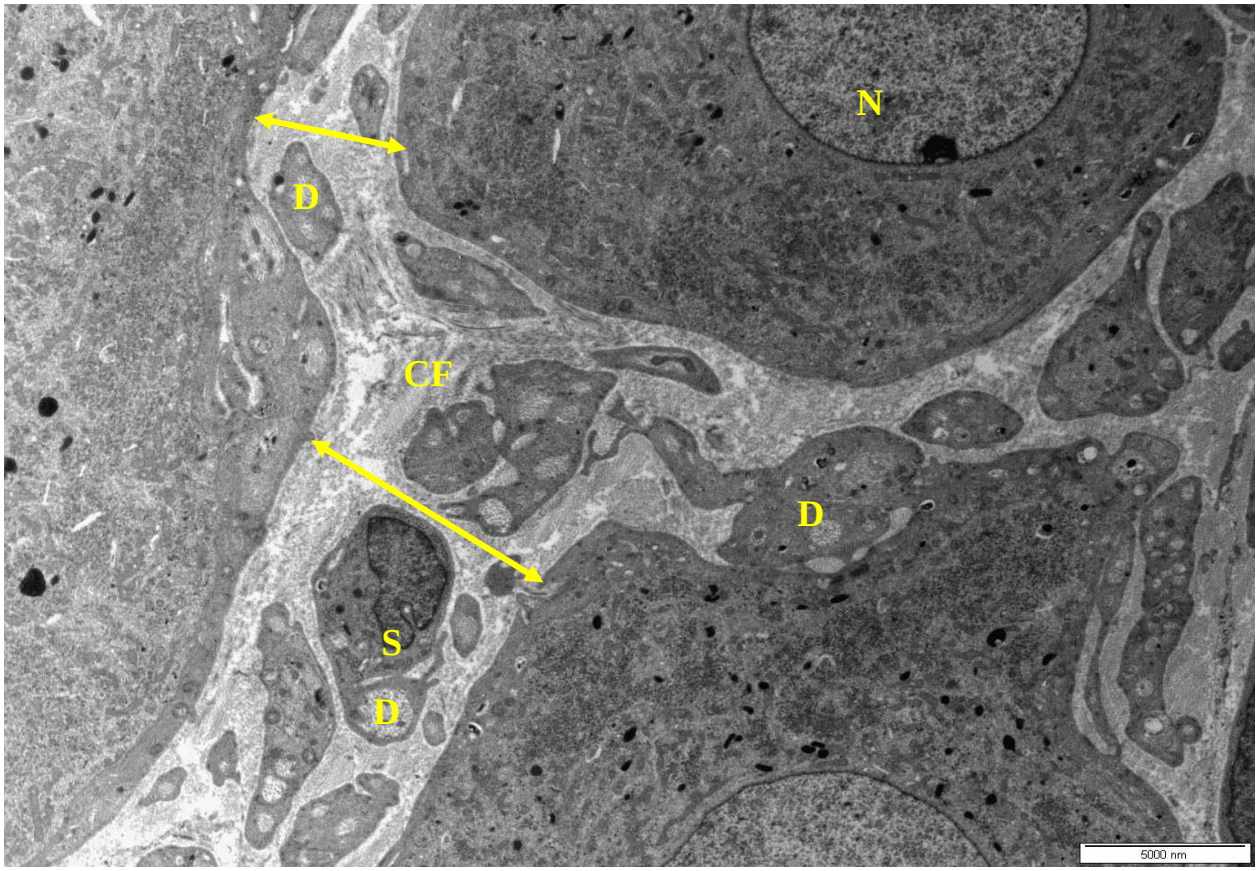

39

Fig. 38: Transmission electron micrograph of the CCG showing the perikaryon of the principal ganglion neuron. The PGN is studded with large amount of neurofilament (**f**). Image bar= 500 nm.

Fig. 39: Transmission electron micrograph of the CCG showing the glial capsule **(yellow double headed arrows)** with satellite glial cell (**S**), dendrites (**D**) and collagen fibrils (**CF**) surrounding the principal ganglion neuron (**PGN**). Image bar= 5000 nm.

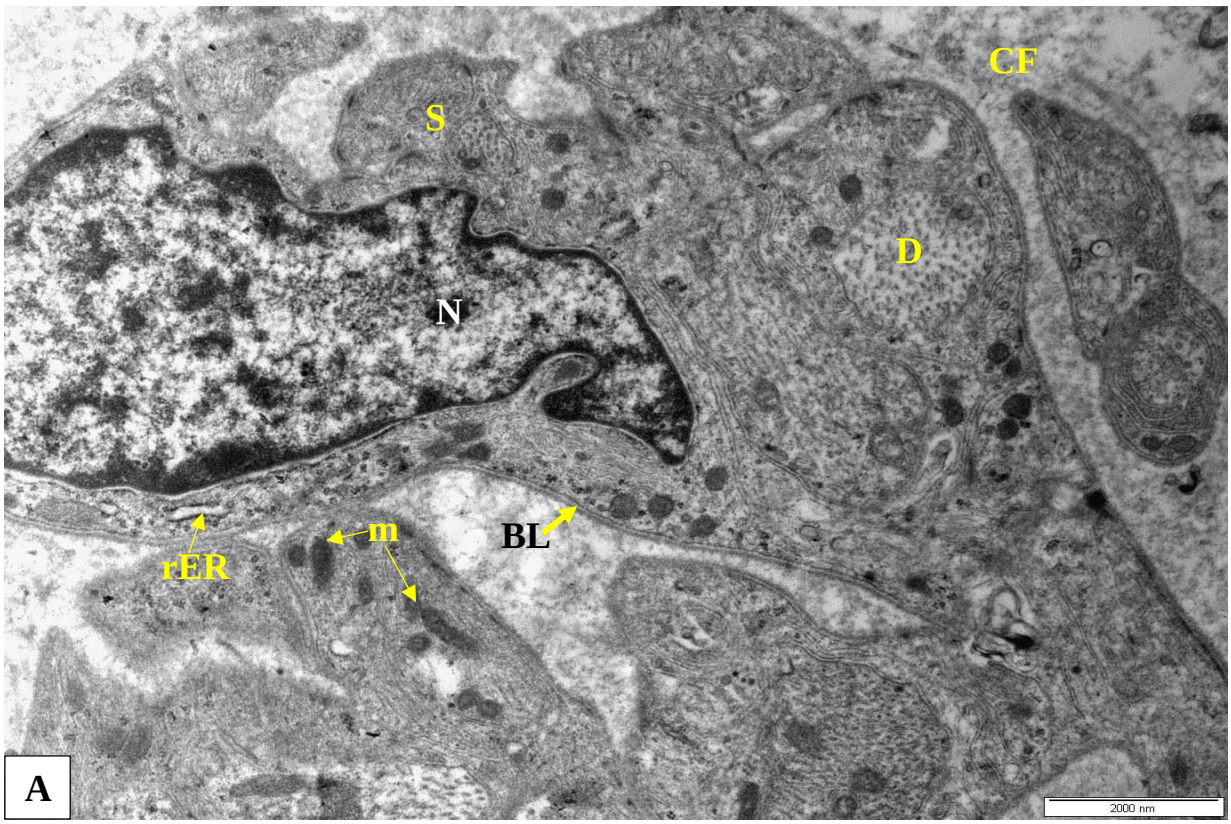

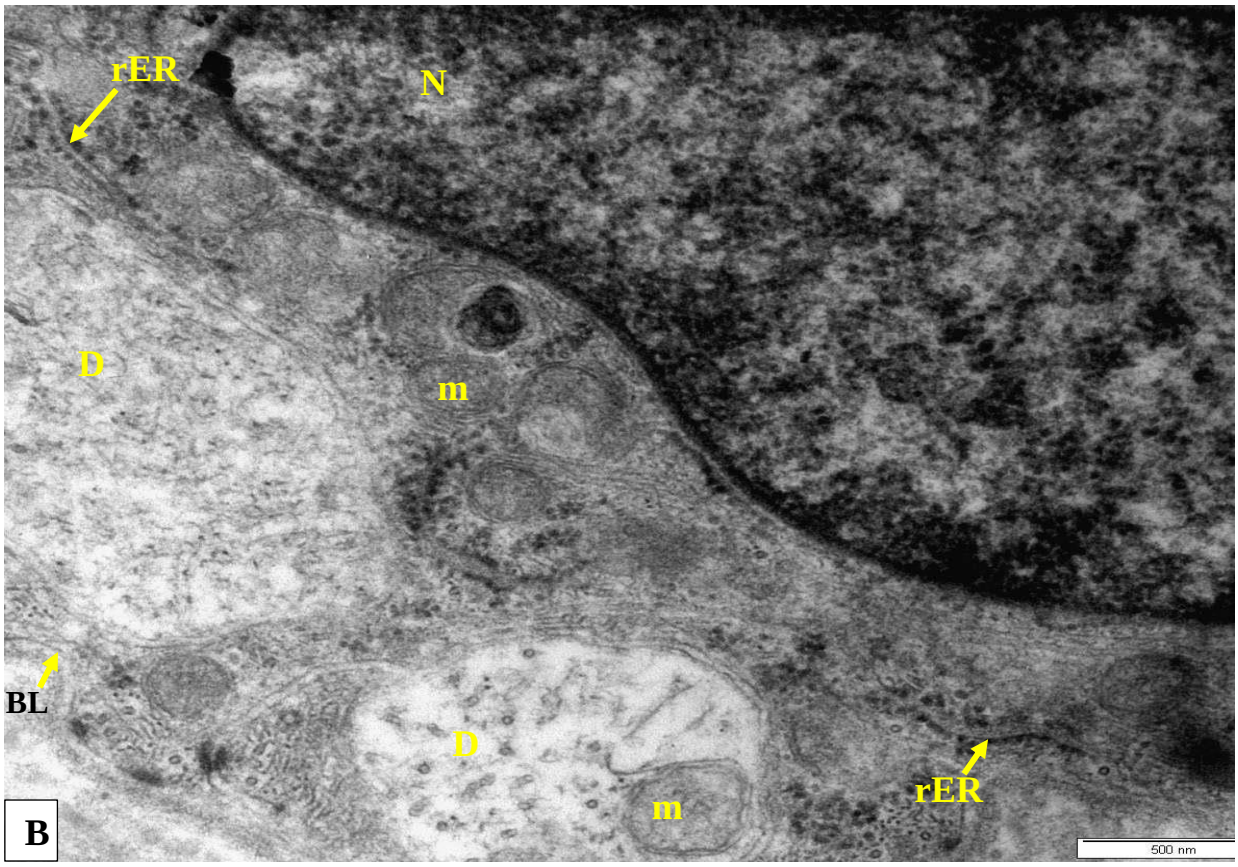

40

Fig. 40: A & B. Transmission electron micrographs of the CCG showing the neuropil; **A:** A satellite glial cell showing cisternae of rough endoplasmic reticulum (**rER**), nucleus (**N)** with heterochromatin, mitochondria (**m**), basal lamina (**BL**), collagen fibrils (**CF**), and dendrite (**D**). Image bar= 2000 nm. **B:** Showing a satellite glial cell's cytoplasm with rough endoplasmic reticulum (**rER**), nucleus (**N)** and mitochondria (**m)**. Basal lamina: (**BL**). Dendrites: (**D**). Image bar= 1000 nm.

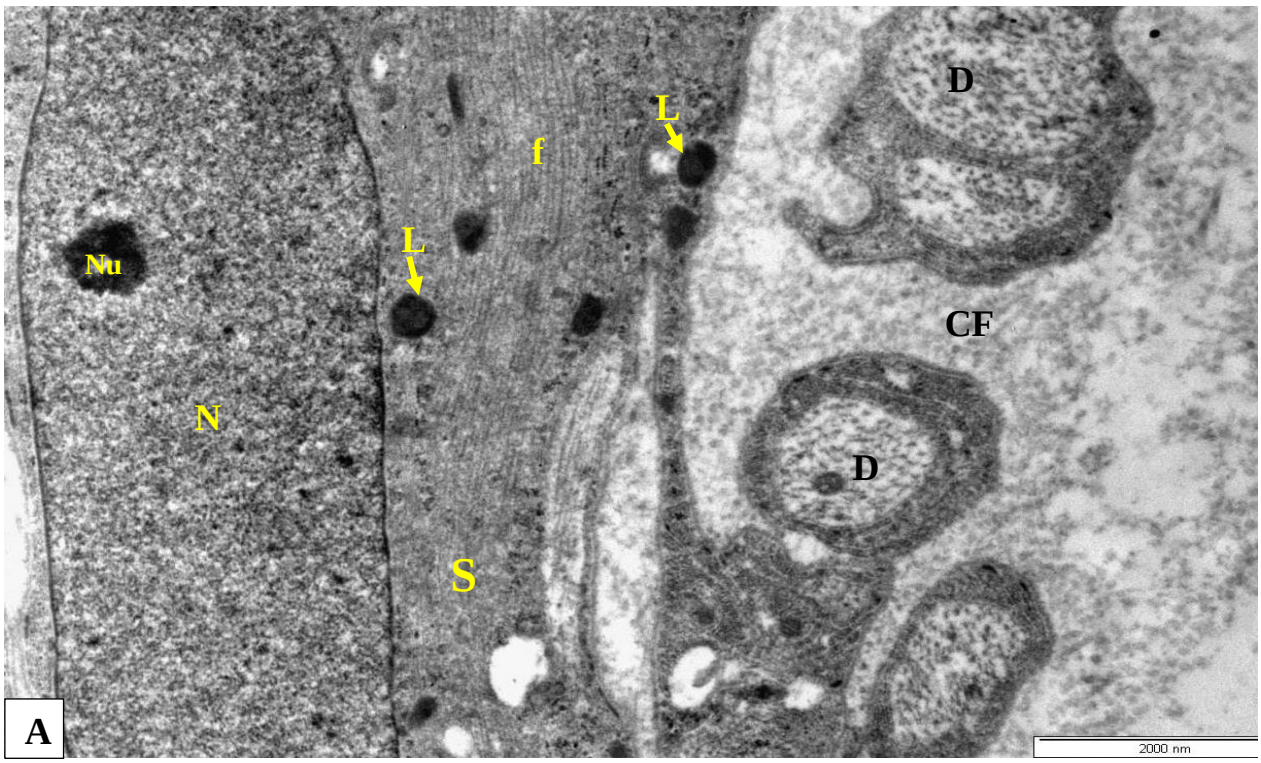

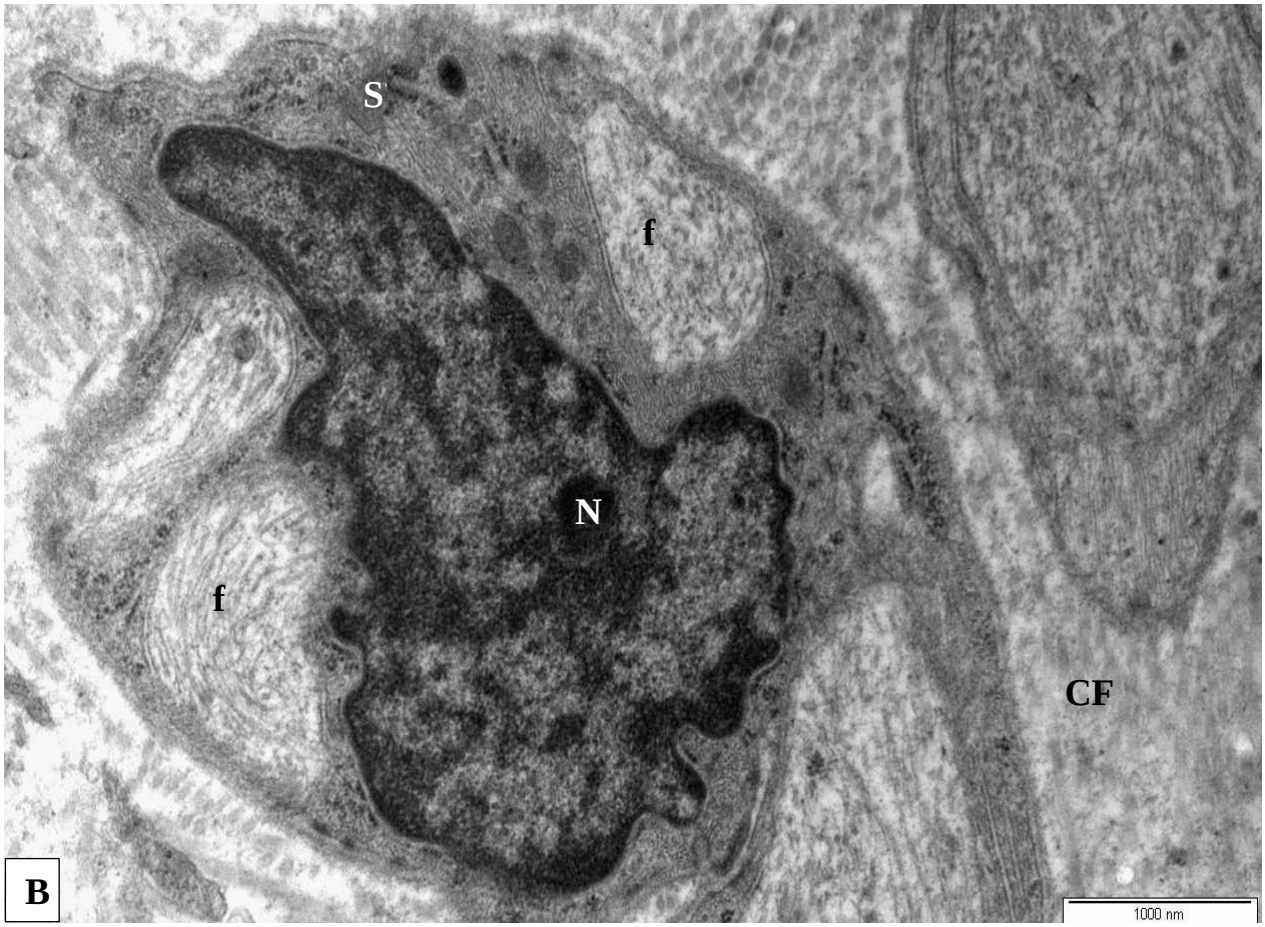

41

Fig. **41: A & B.** Transmission electron micrographs of the neuropil of the CCG; **A:** Showing satellite glial cell (**S**), nucleus (**N**), nucleolus (**Nu**), neurofilaments (**f**), lysosomes (**L**), dendrites (**D**) and collagen fibrils (**CF**). Image bar= 2000 nm. **B:** Showing the satellite glial cell (**S**) and collagen fibrils (**CF**) in the glial capsule. Encapsulated neurofilaments: (**f**). Image bar= 2000 nm.

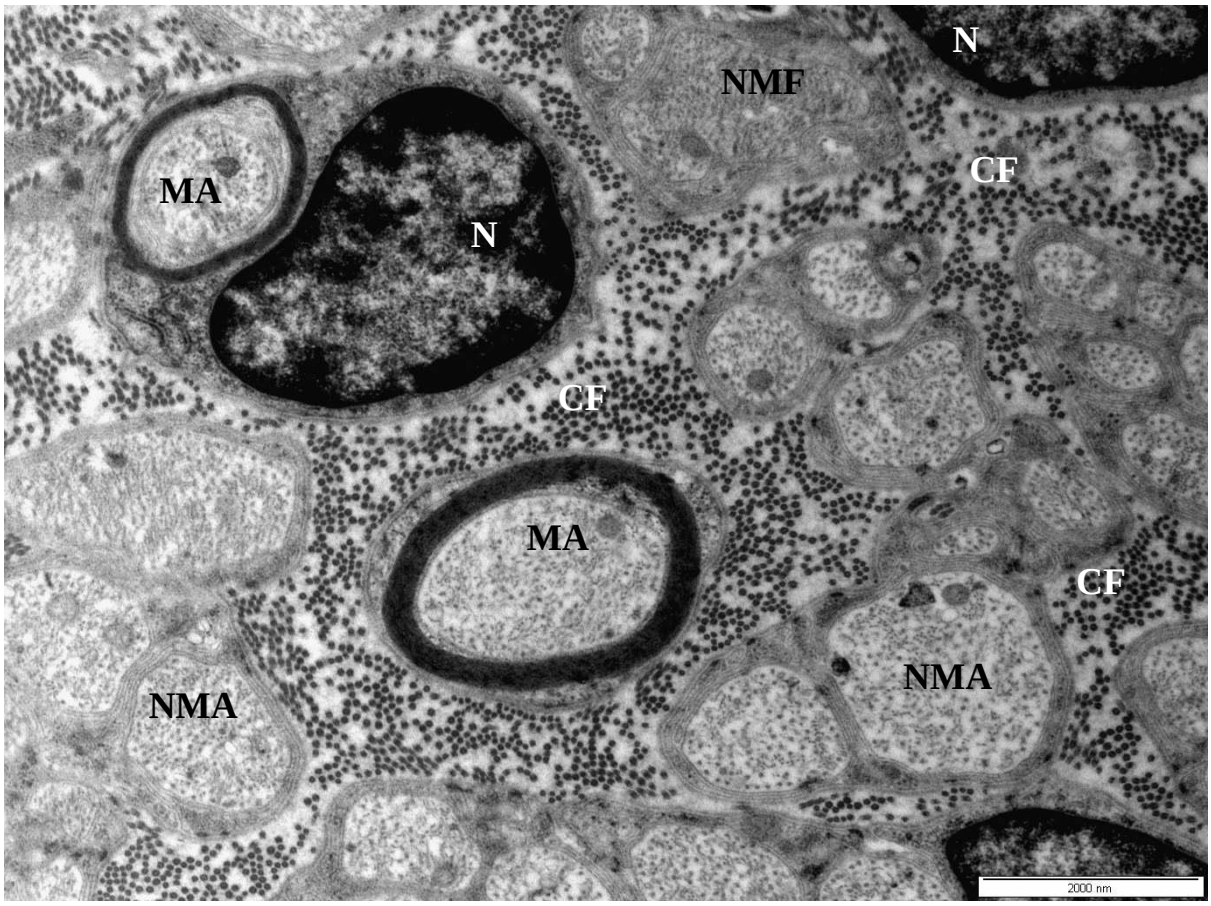

42

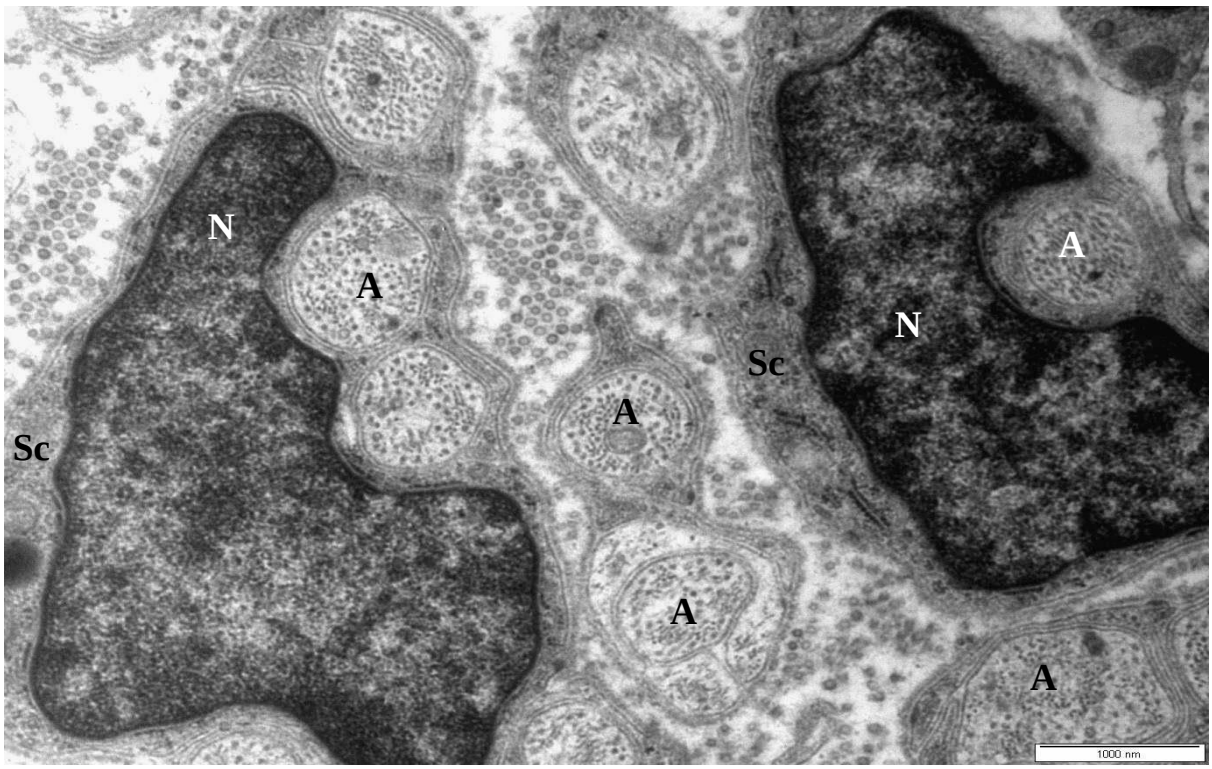

43

Fig. 42: Transmission electron micrograph of the CCG showing the neuropil containing myelinated axons (**MA**), non-myelinated axons (**NMA**) and collagen fibrils (**CF**). Note the distribution of the nuclei of Schwann cells (**N**) among the myelinated and non-myelinated axons. Image bar= 2000 nm.

Fig. 43: Transmission electron micrograph of the non-myelinated axons in the CCG neuropil showing multiple nerve fibres (**A**) of various sizes associated with the Schwann cell cytoplasm (**Sc**). collagen fibrils: (**CF**); Schwann cell nucleus: (**N**). Image bar= 1000 nm.

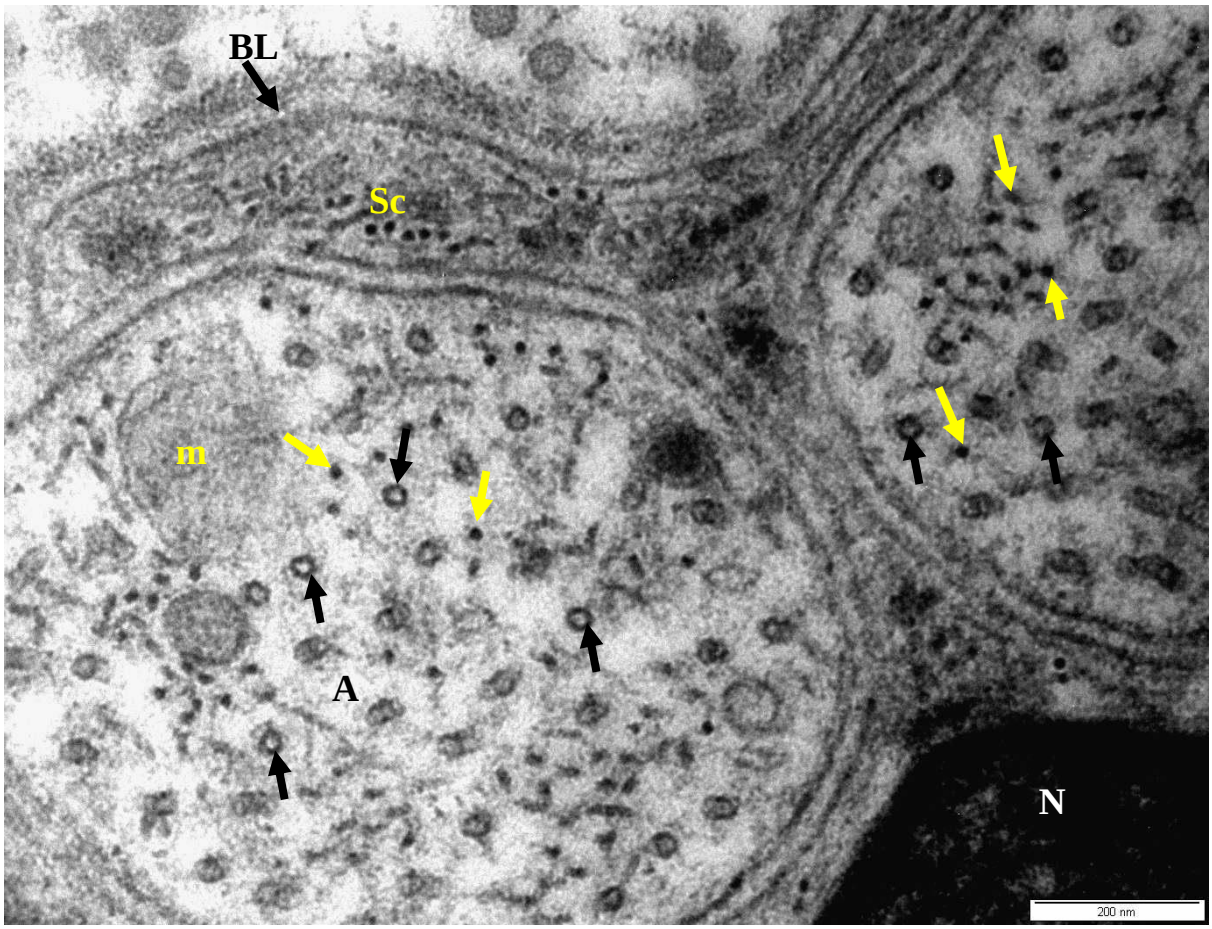

44

Fig. 44: Transmission electron micrograph of two non-myelinated axons (**A**) in the CCG neuropil associated with a Schwann cell cytoplasm (**Sc**). The axoplasm contains microtubules (**black arrows**), neurofilaments (**yellow arrows**) and mitochondria (**m**). Schwann cell nucleus: (**N**); Schwann cell basal lamina: (**BL**). Image bar= 200 nm.

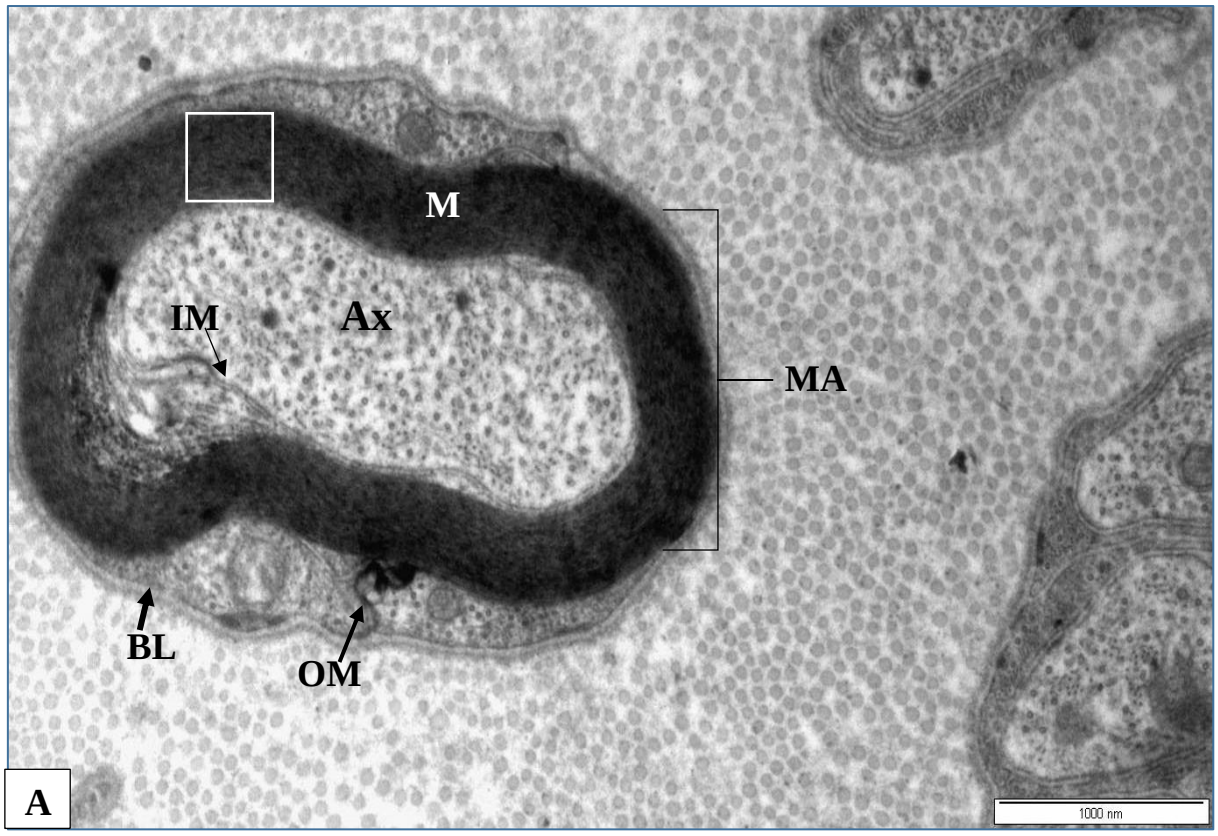

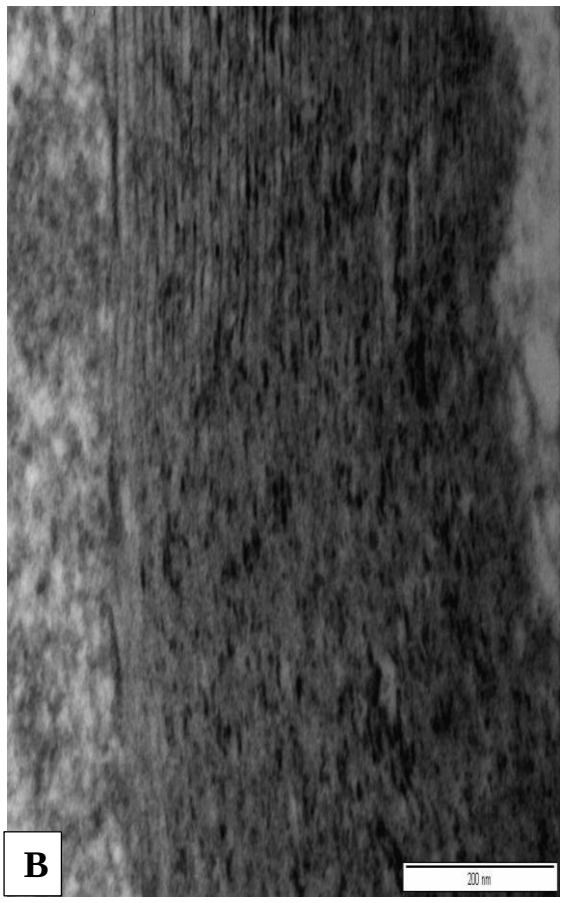

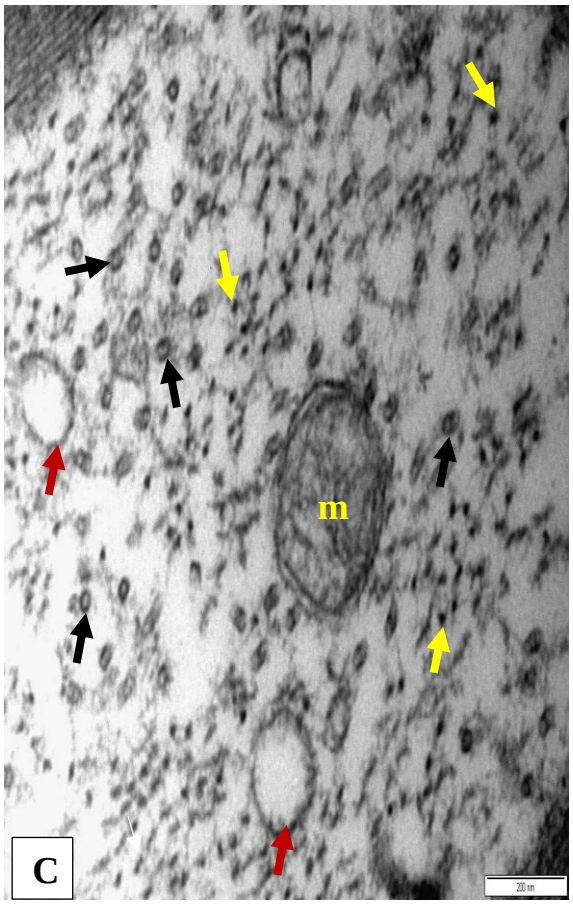

45

Fig. 45. A, B & C: Transmission electron micrographs of the myelinated axon (**MA**) in the CCG ganglionic stroma. **A**: Showing the axoplasm (**Ax**), Schwann cell basal lamina (**BL**), myelin sheath (**M**), outer mesaxon (**OM**) and inner mesaxon (**IM**). Image bar= 1000 nm. **B:** A higher magnification of the square in (**A**) showing compact myelin sheath. Image bar= 200 nm. **C:** Higher magnification of the axoplasm showing mitochondria (**m**), microtubules (**black arrows**), neurofilaments (**yellow arrows**) and clear vesicles (**red arrows)**. Image bar= 200 nm.

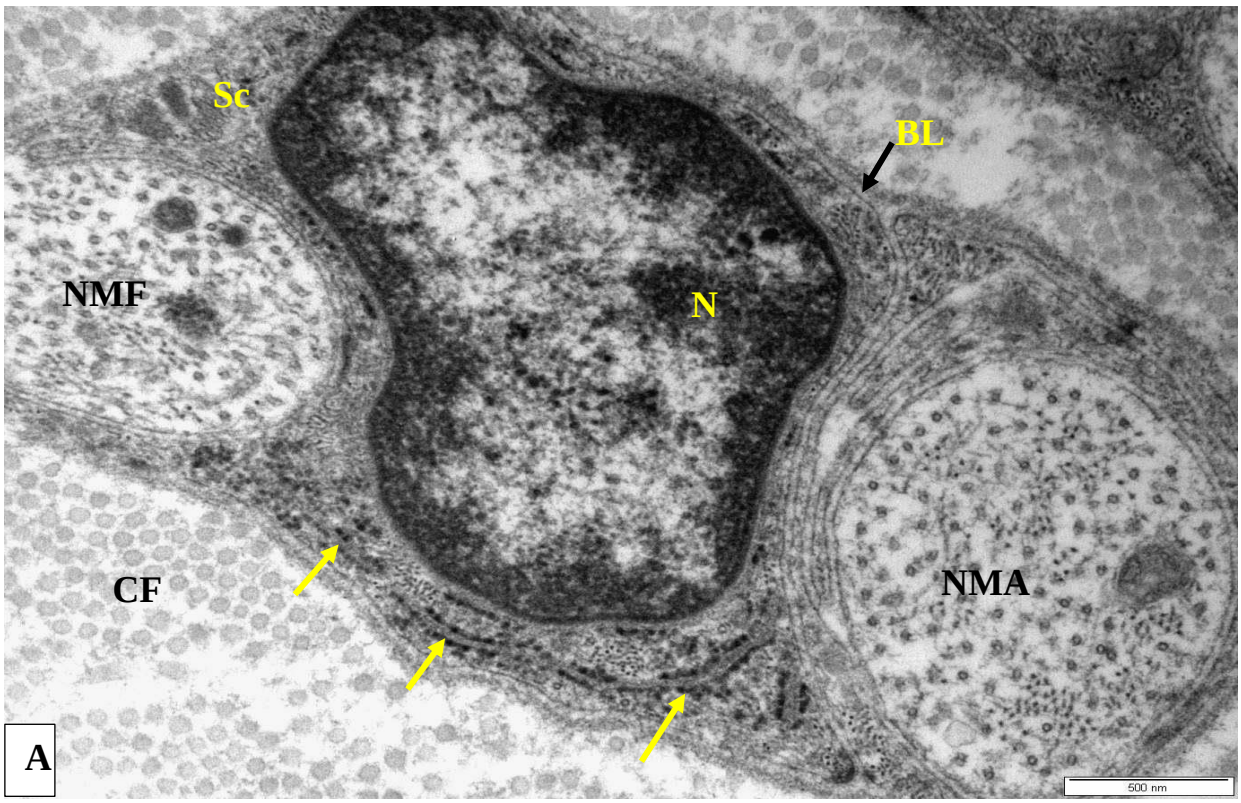

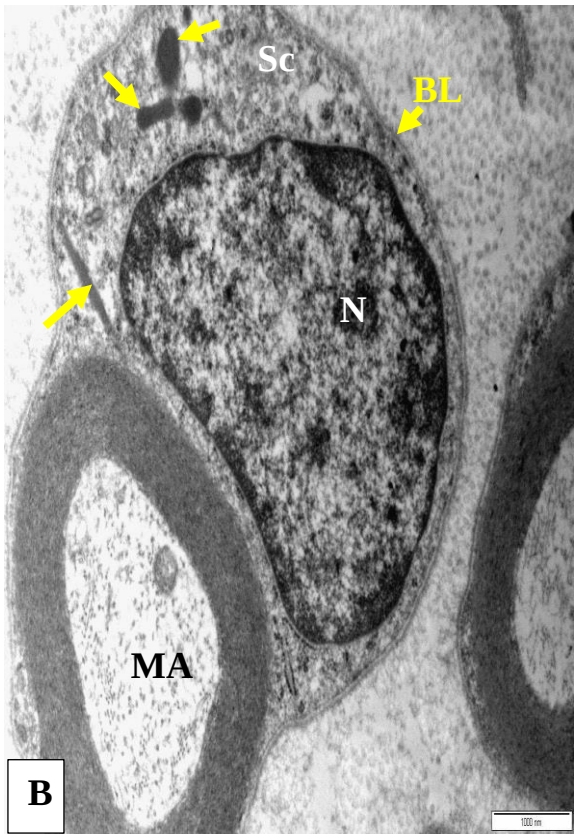

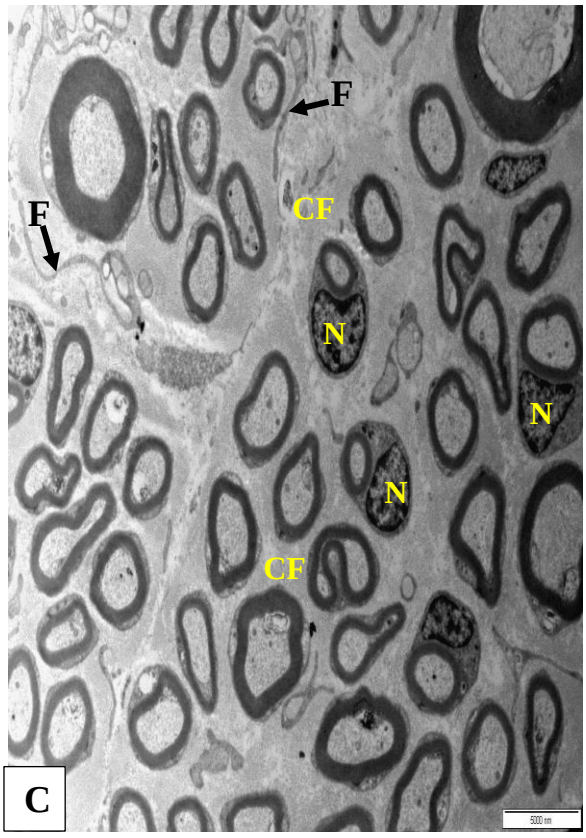

46

Fig. 46: A, B & C. Transmission electron micrographs of the CCG ganglionic stroma; **A:** showing the Schwann cell (**Sc**), nucleus (**N**), non-myelinated axons (**NMA**), rough endoplasmic reticulum (**yellow arrows**) and basal lamina (**BL**). Note the collagen fibrils (**CF**) surrounding the non-myelinated axons and Schwann cell. Image bar= 500 nm.

B: Showing myelinated axon (**MA**) ensheathed by Schwann cell (**Sc**). Schwann cell nucleus: (**N**). Schwann cell basal lamina: (**BL**). Note the dense bodies stacks (**yellow arrows**) in the cytoplasm of the Schwann cell. Image bar= 1000 nm. **C:** Showing the variable number of myelinated axon (**MA**) enclosed by a Schwann cell. Schwann cell nucleus: (**N**). Cytoplasmic extension of fibroblast: (**F**). Collagen fibrils: (**CF**). Image bar= 5000 nm.

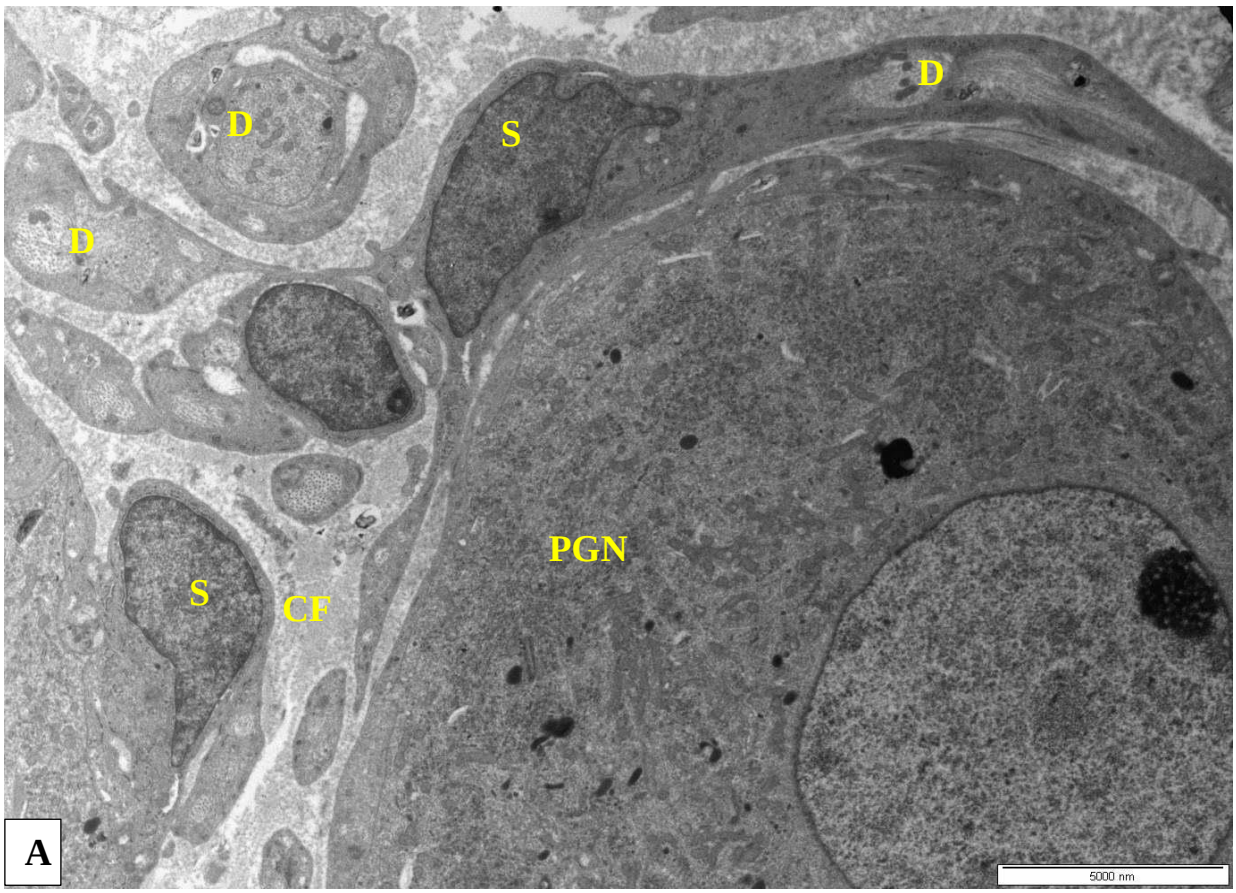

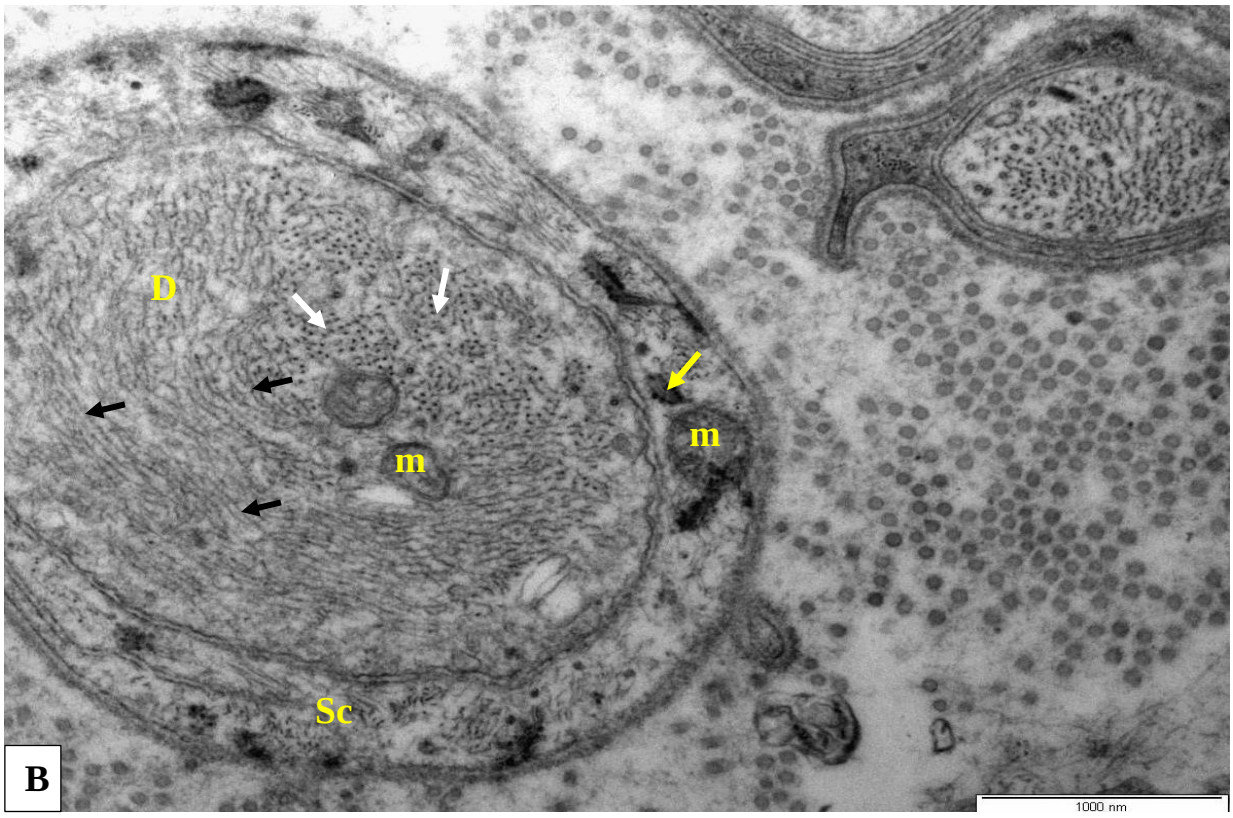

47

Fig. 47: A & B. Transmission electron micrographs of the neuropil of the CCG; **A:** showing variable number of dendrites (**D**), satellite glial cells (**S**), collagen fibrils (**CF**), principal ganglion neuron (**PGN**). Image bar= 5000 nm. **B:** Higher magnification of the dendrite (**D**) showing mitochondria (**m**), microtubules (**black arrows**) and neurofilaments (**white arrows**). Note that the cytoplasm of the Schwann cell (**Sc**) surrounding the dendrite displays mitochondria (**m**). Image bar= 1000 nm.

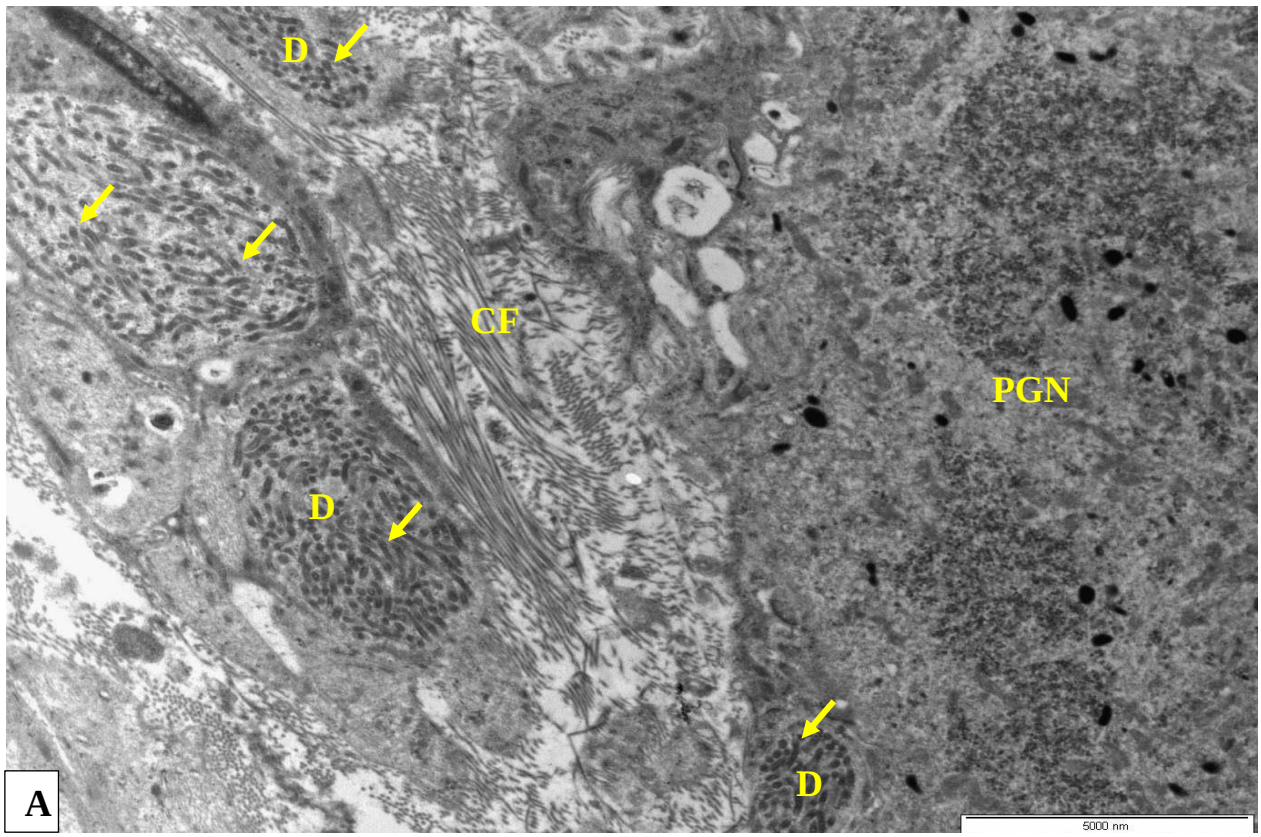

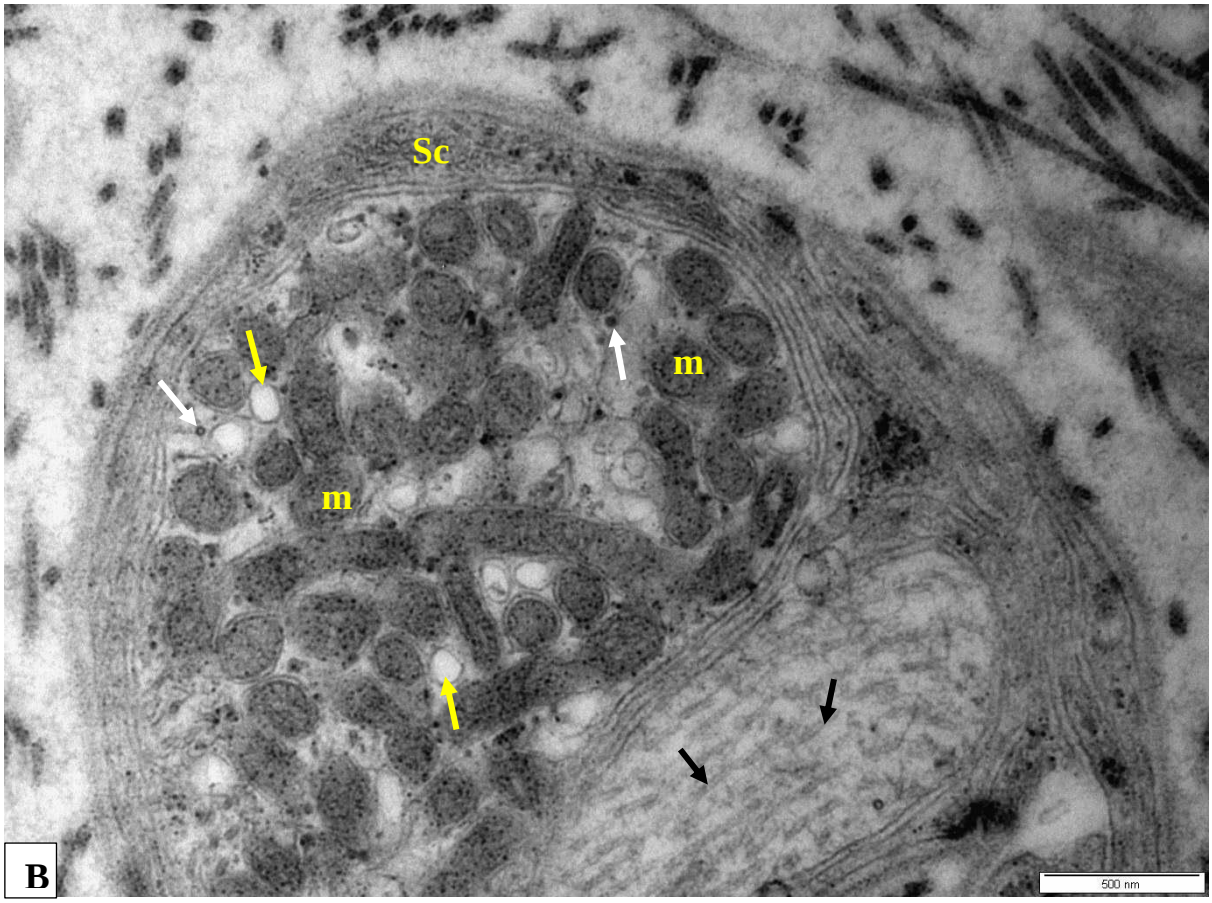

48

Fig. 48: A & B. Transmission electron micrographs of the neuropil of the CCG; **A:** The dendrites (**D**) showing a large number of dark mitochondria (**yellow arrows**). Collagen fibrils: (**CF**). Principal ganglion neuron (**PGN**). Image bar= 5000 nm. **B:** Higher magnification of the dendrite showing densely packed dark mitochondria (**m**), clear vesicles (**yellow arrows),** microtubules (**black arrows**) and neurofilaments (**white arrows**). Image bar= 500 nm.

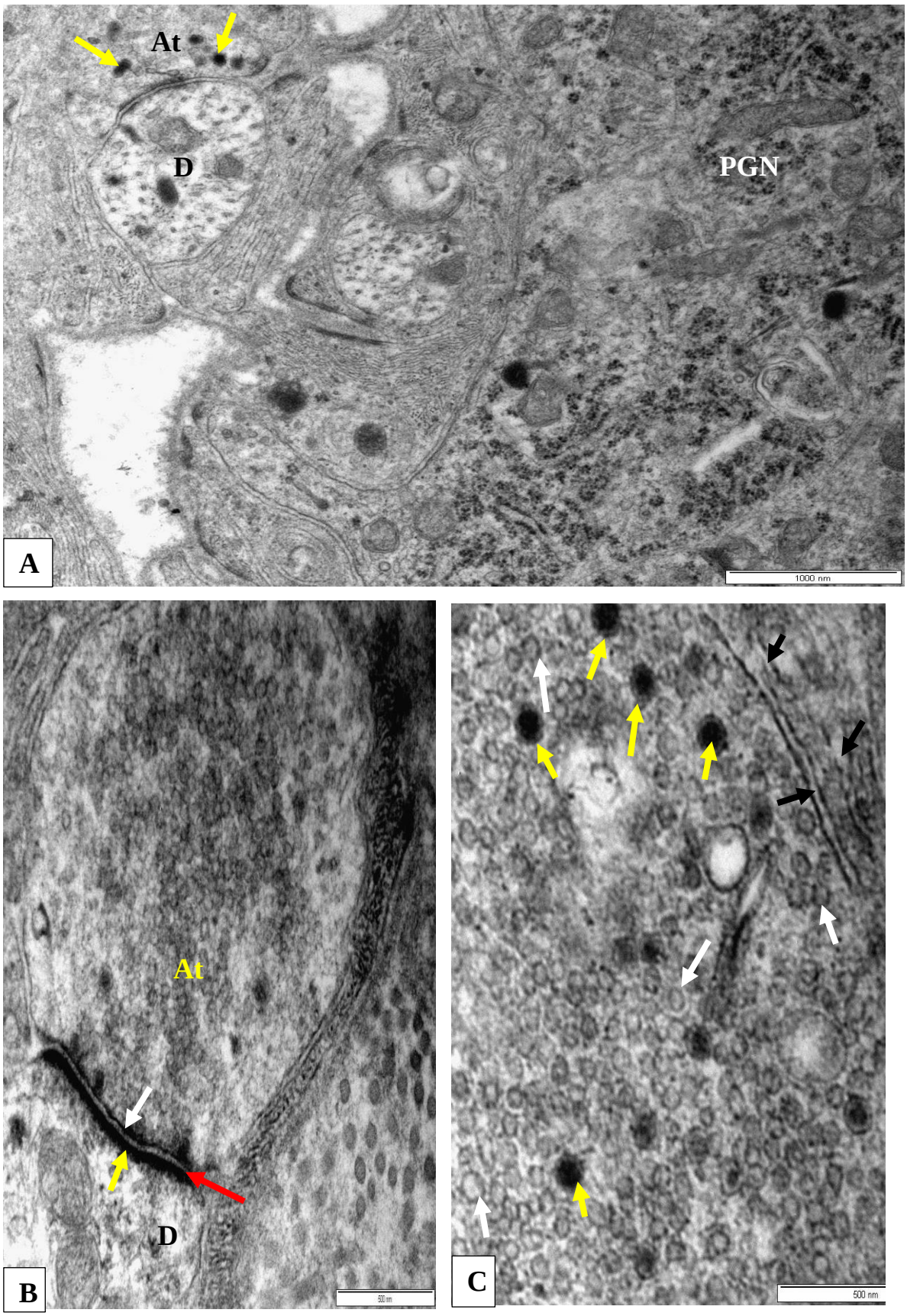

49

Fig. 49: A, B & C. Transmission electron micrographs of the CCG;
A: Showing an axon terminal (**At**) synapses with the base of a large dendrite (**D**). Large dense cored vesicles: (yellow **arrows**). Image bar= 1000 nm. **B:** Showing an axon terminal (**At**) synapses the base of a large dendrite (**D**). Note the presynaptic membrane **(white arrow),** postsynaptic membrane **(yellow arrow)** and synaptic cleft (**red arrow**). Image bar= 500 nm. **C:** Higher magnification of an axon terminal containing a mixture of small clear vesicles (**white arrows**), a few large dense cored vesicles (**yellow arrows**) and microtubules (**black arrows**). Image bar= 500 nm.

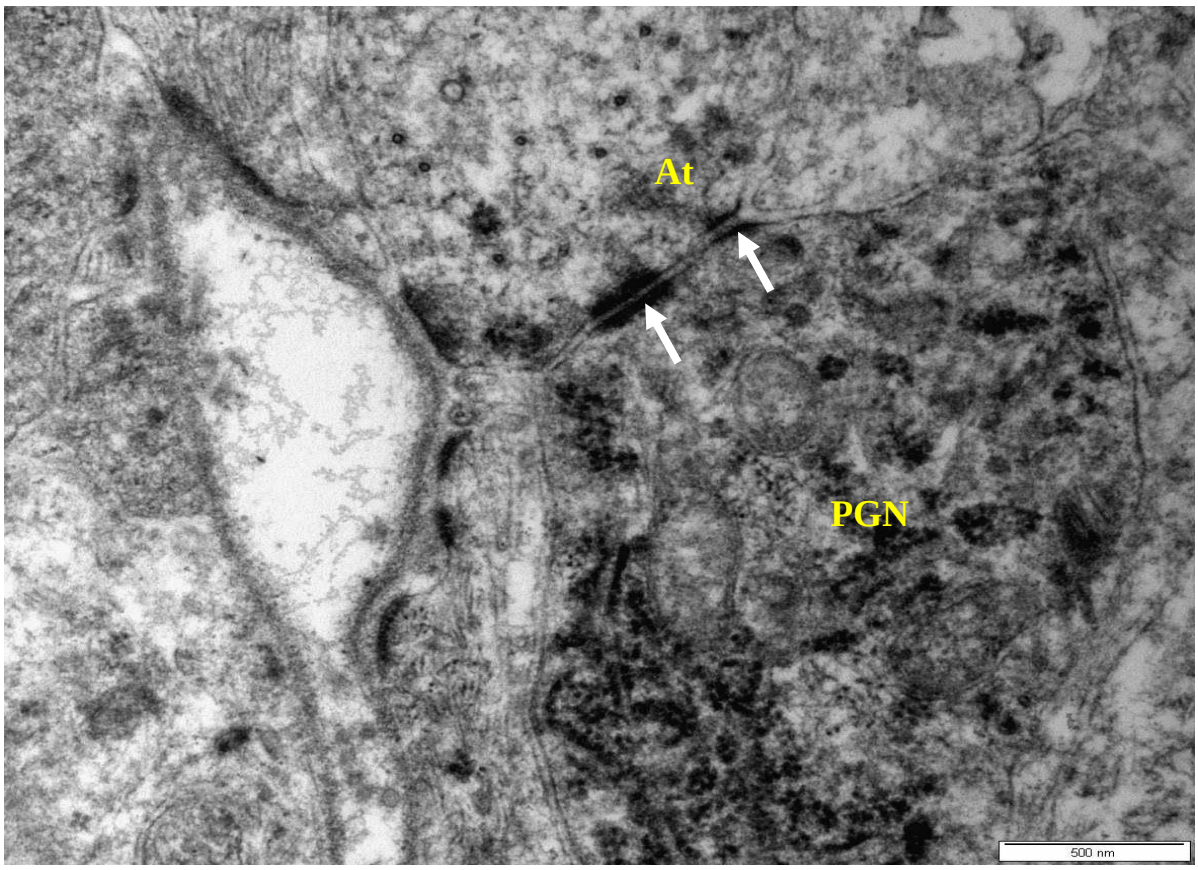

50

Fig. 50: Transmission electron micrographs of the of the CCG showing an axon terminal (**At**) in synaptic contacts (**white arrows**) within the soma of a principal ganglion neuron (**PGN**). Image bar= 500 nm.

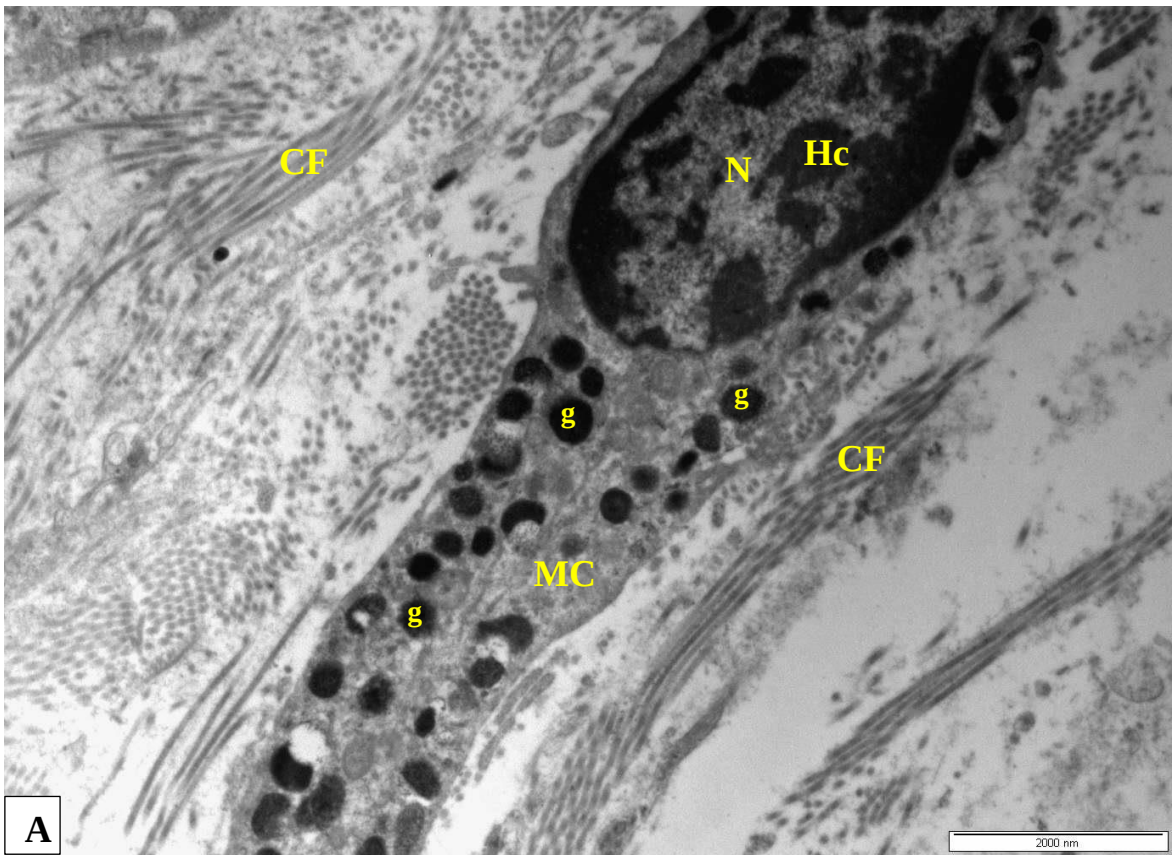

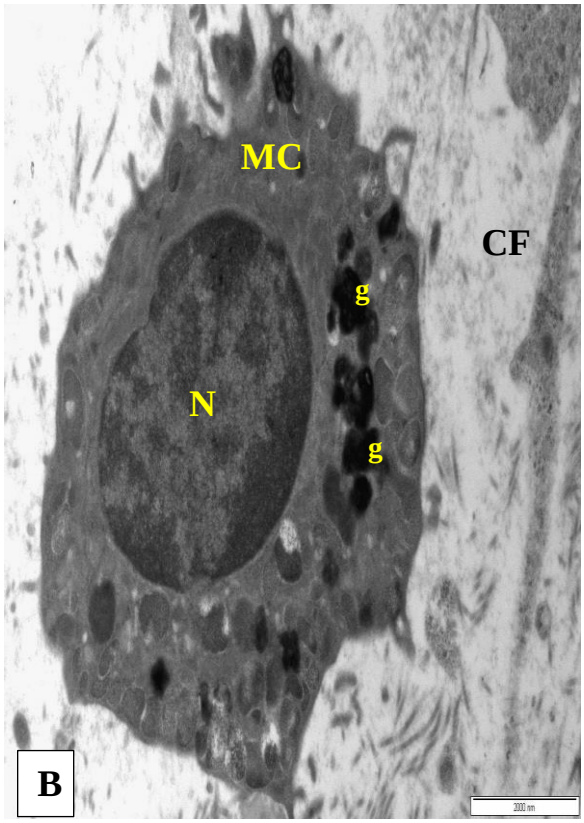

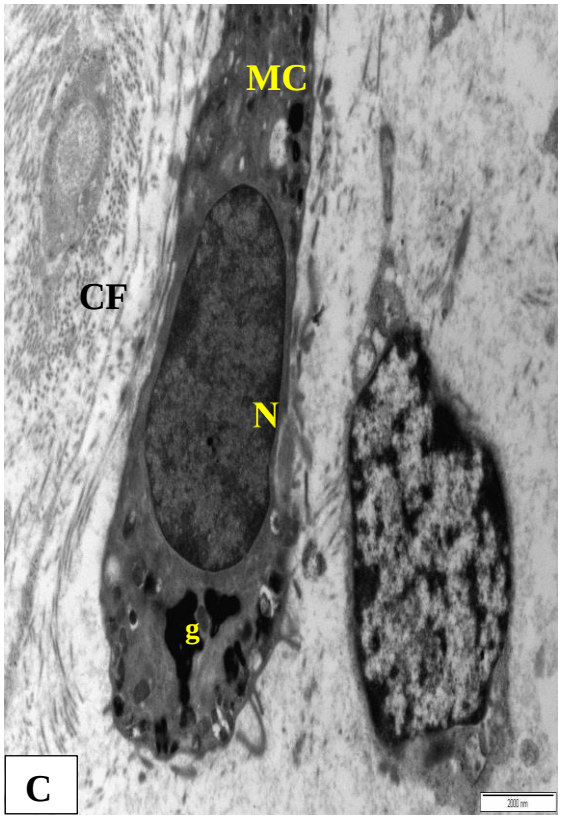

51

Fig. 51: A, B, &C: Transmission electron micrographs of a mast cell (**MC**) in the ganglionic stroma of the CCG. The cytoplasm of the mast cell showing rounded or oval densely-staining granules (**g).** The nucleus (**N**) with heterochromatin (**Hc**). The collagen fibrils (**CF**). Image bar= 2000 nm.

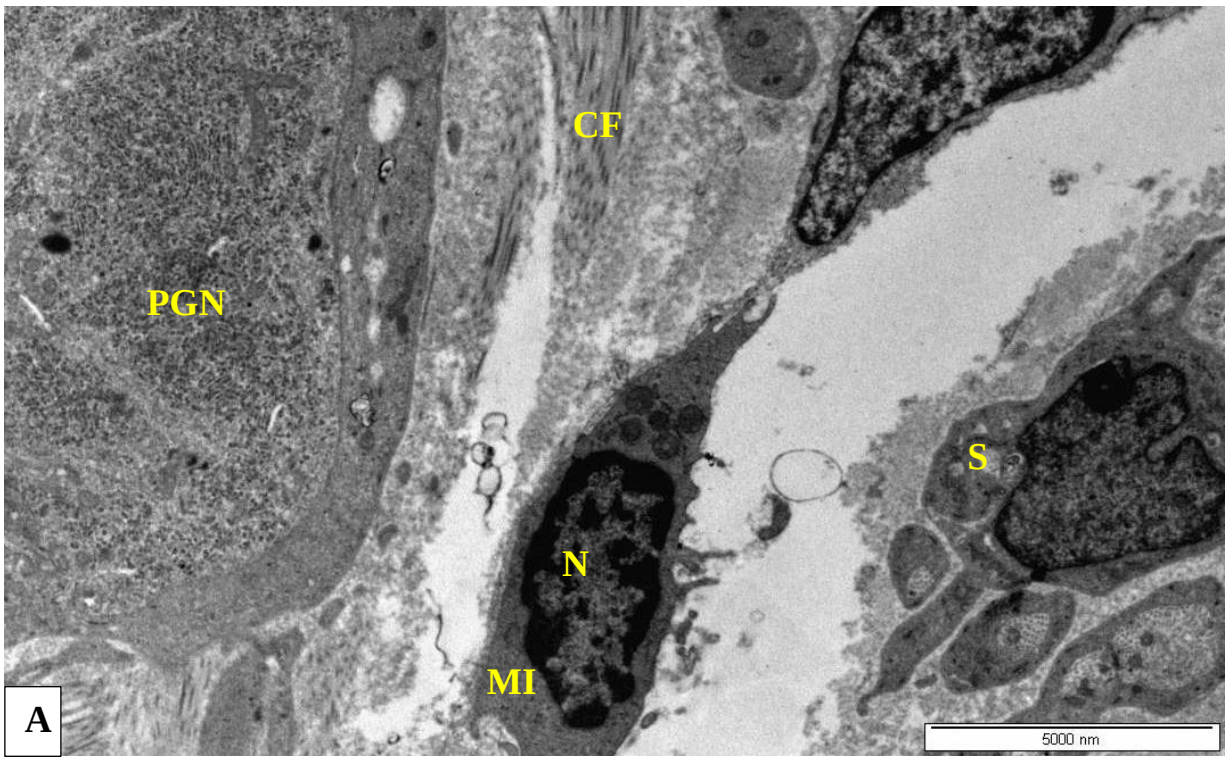

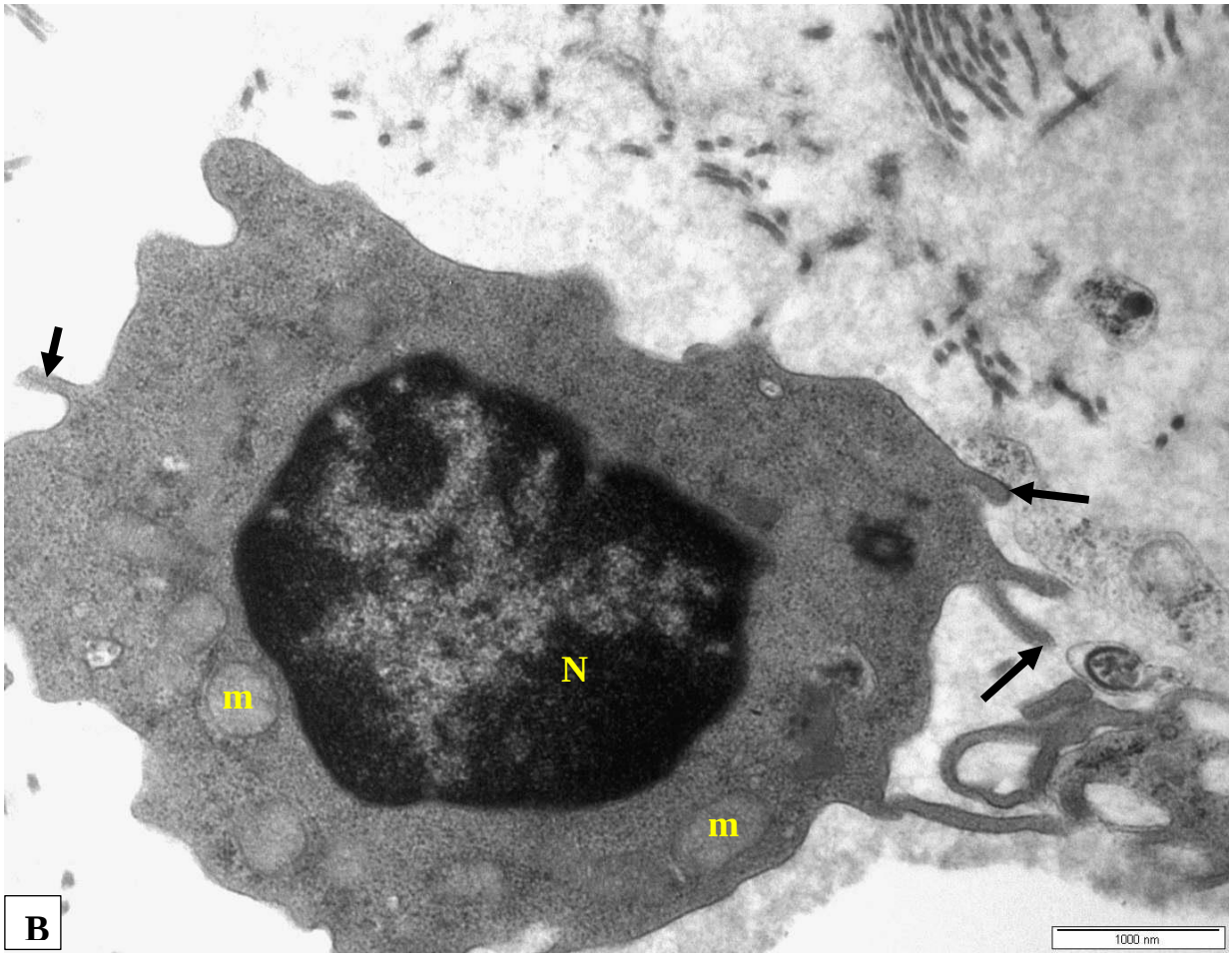

52

Fig. 52: A & B. A: Transmission electron micrographs of the microglial cells (**MI**) in the ganglionic stroma of the CCG. The principal ganglion neuron (**PGN**). The satellite glial cell (**S**). The collagen fibres (**CF**). Image bar= 5000 nm. **B:** The cytoplasm of the microglial cells showing numerous mitochondria (**m**) and the nucleus (**N**) and the cytoplasmic process (**black arrows**). Image bar= 1000 nm.

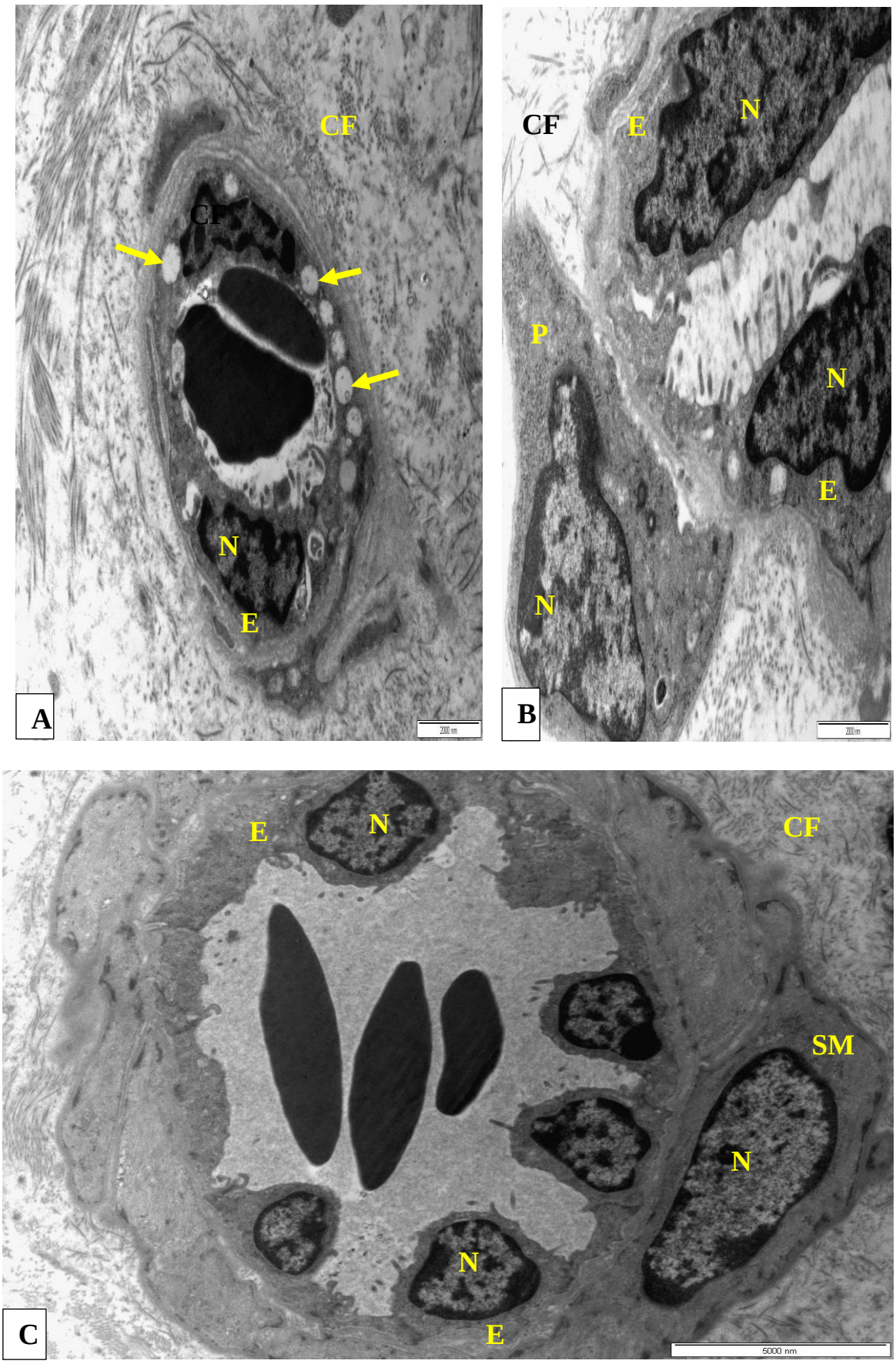

53

Fig. 53: A, B & C. Transmission electron micrographs of the CCG; **A:** Showing the first type of vasculature. The endothelial cell (**E**). The nucleus (**N**). The micropinocytotic vesicles **(Yellow arrows)**. The collagen fibrils (**CF**). Image bar= 2000 nm. **B:** Showing the endothelial cell (**E**) and a pericyte (**P**). The nucleus (**N**). The collagen fibrils (**CF**). Image bar= 2000 nm. **C:** Showing the second type of vasculature. The endothelial cell (**E**). The nucleus (**N**). The smooth muscle (**SM**). The collagen fibrils (**CF**). Image bar= 5000 nm.

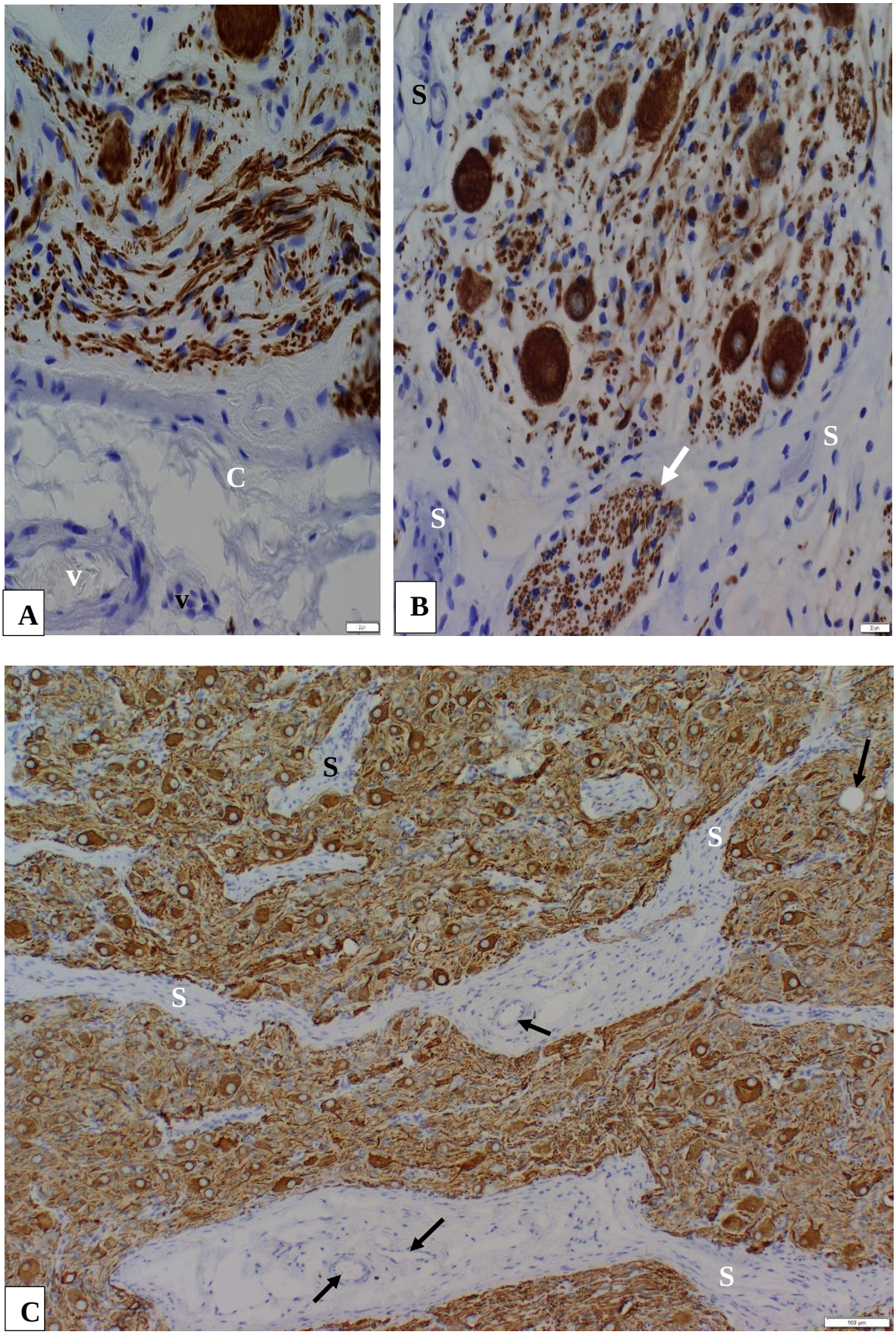

54

Fig. 54: A, B & C: Photomicrographs of the CCG; **A:** showing the negatively reacting capsule (**C**) and blood vessel (**V**) to the anti- neurofilament monoclonal antibodies (ANMA). Image bar= 20μm.

B: Showing a negatively reacting septa (**S**) of the CCG to the ANMA and a positively reacted nerve fibre within the septa (**white arrow**). Image bar= 20μm. **C:** Showing a negatively reacting septa (**S**) and blood vessels (**black arrows**) to the ANMA. Image bar= 100μm.

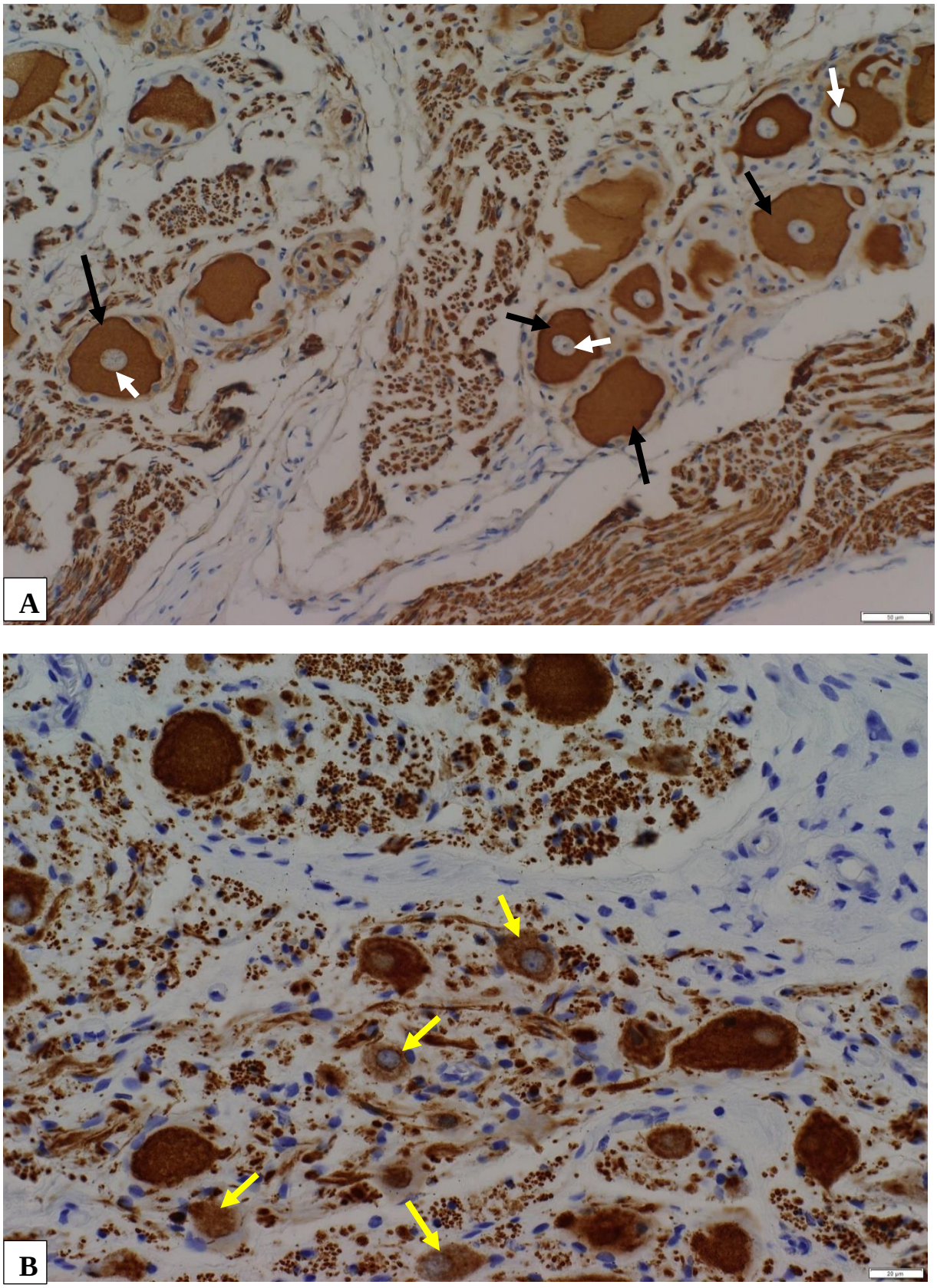

55

Fig. 55: A & B: Photomicrographs of the CCG ganglionic lobule; **A:** Showing a positive reactivity of the principal ganglion neurons (**black arrows**) to the ANMA. The nuclei (**white arrows**) showing negative reactivity. Image bar= 50μm. **B:** Showing low immunoreactivity (**yellow arrows**) of the small PGN to the ANMA. Image bar= 20μm

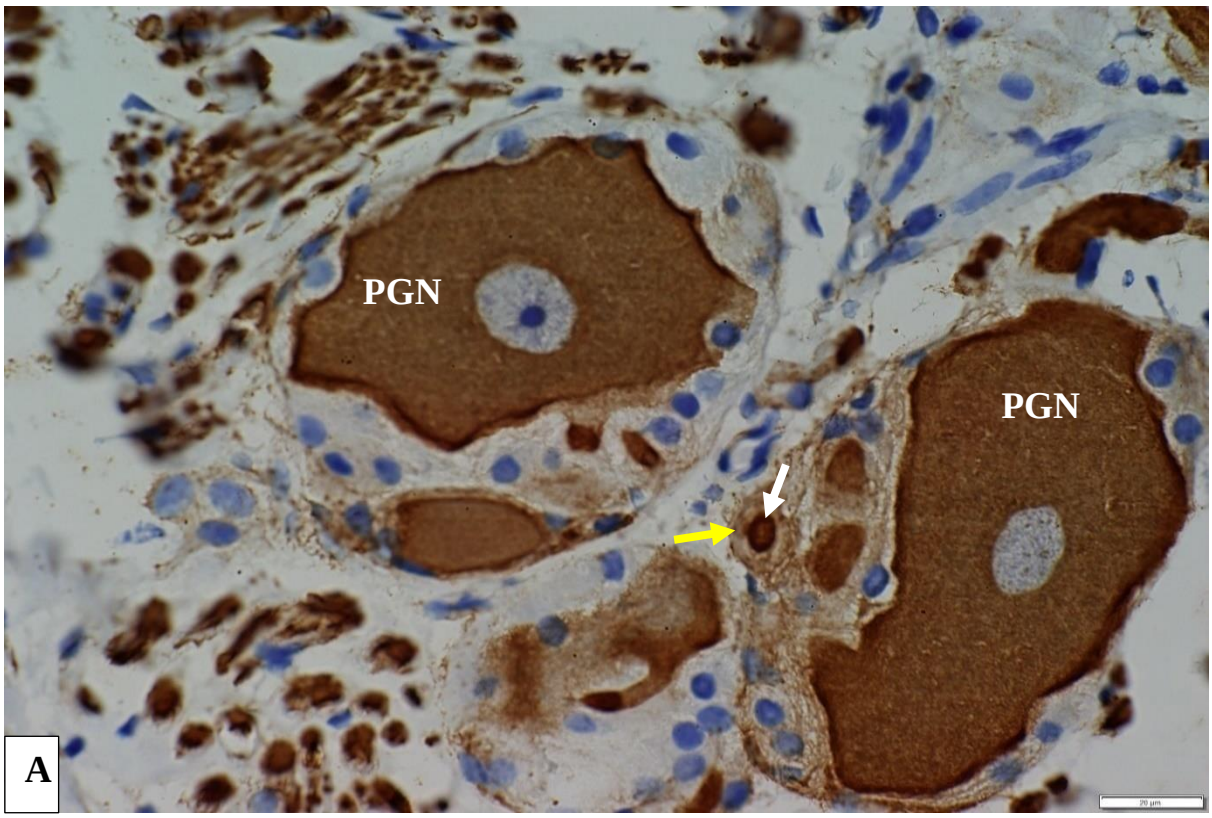

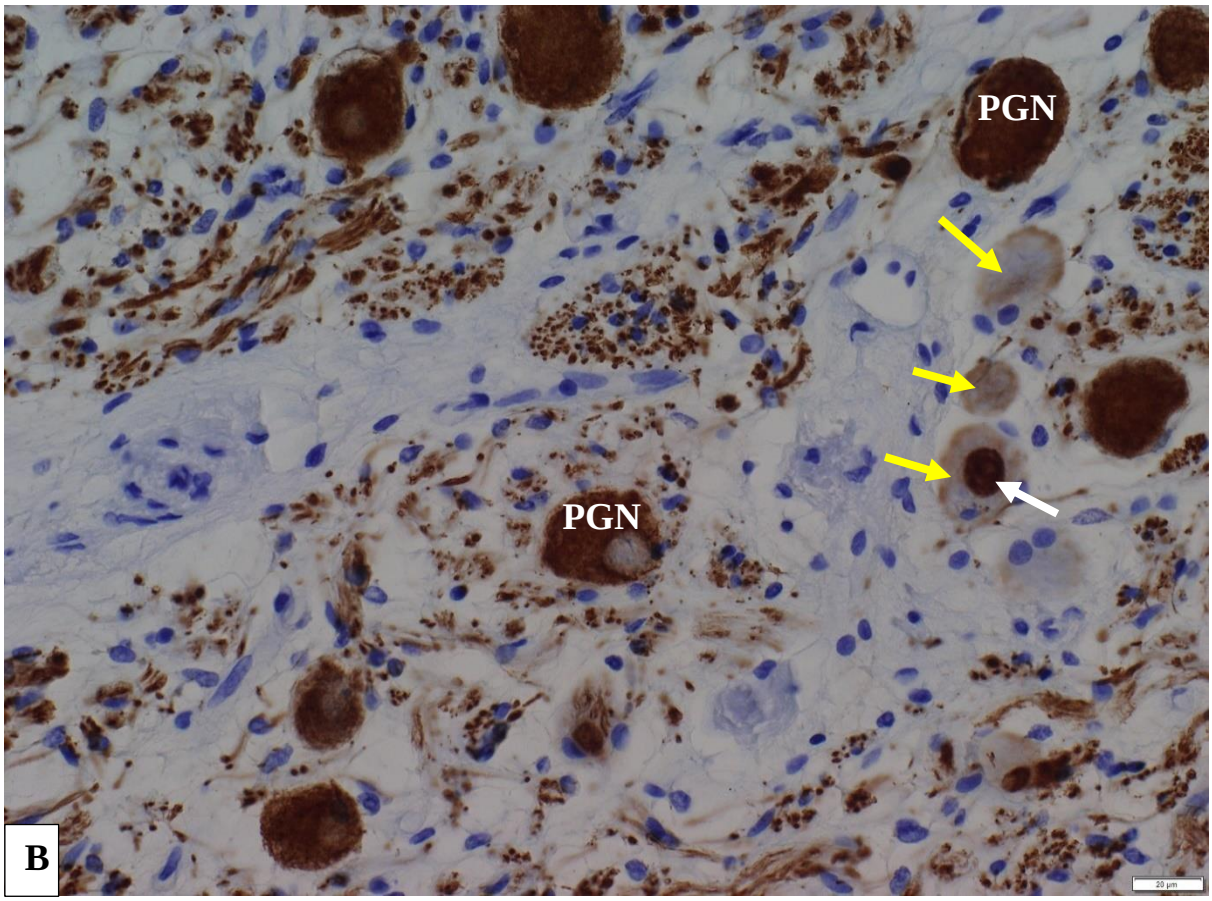

56

Fig. 56: A & B: Photomicrographs of the CCG ganglionic unit showing the principal ganglion neurons (**PGN).** The small intensely fluorescent cell's cytoplasm shows moderate reaction (**yellow arrows**), the strong positive reaction of the nucleus (**white arrows**) to the ANMA. Image bar= 20μm.

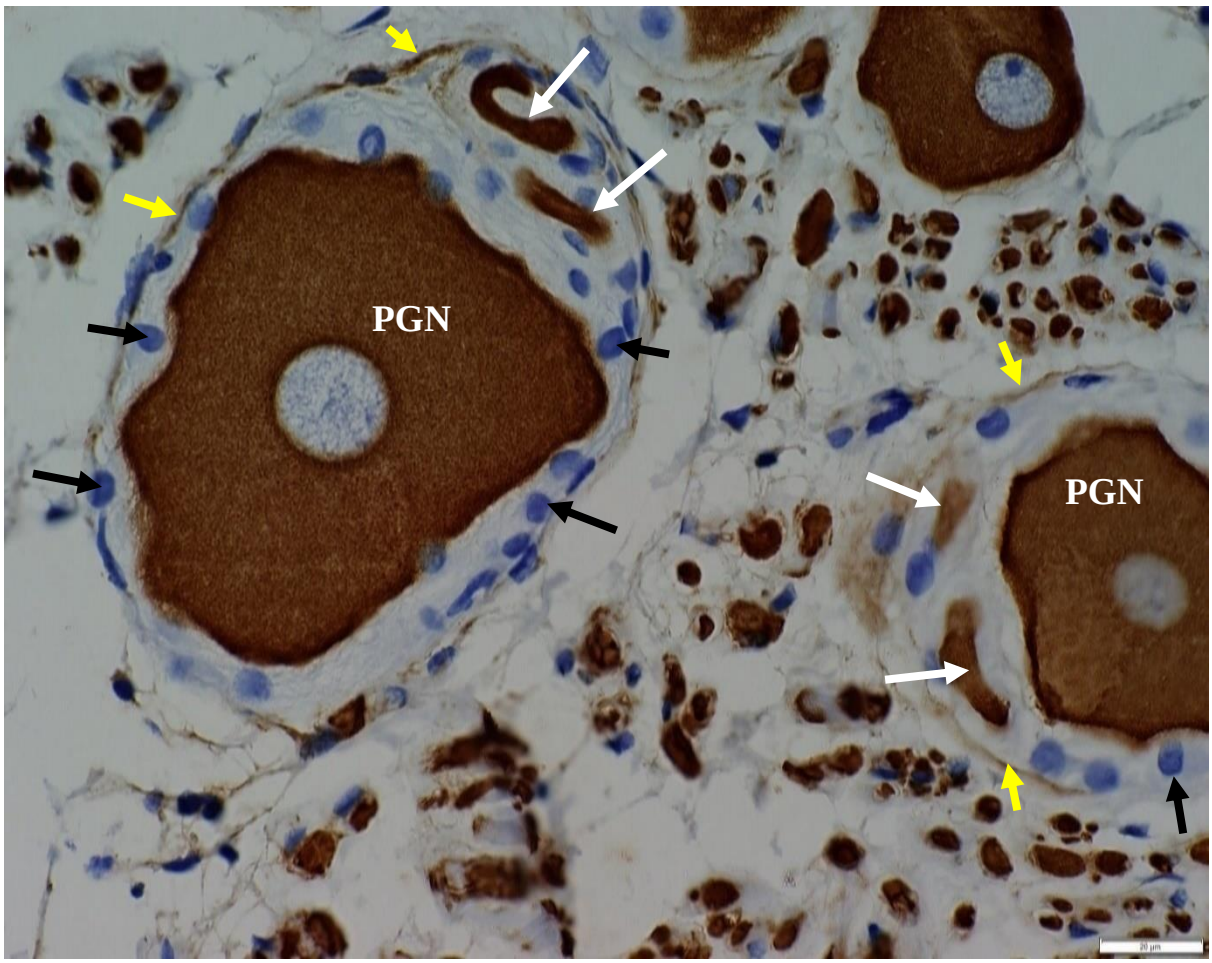

57

Fig. 57: Photomicrograph of a ganglionic unit of the CCG showing the positive reactivity of the principal ganglion neurons (**PGN**) and nerve fibres (**white arrows**) within the glial capsule to the ANMA. Note the weak reaction of the basal lamina (**yellow arrows**) of the glial capsule and the negative reaction of the satellite cells (**black arrows**). Image bar= 20µm.

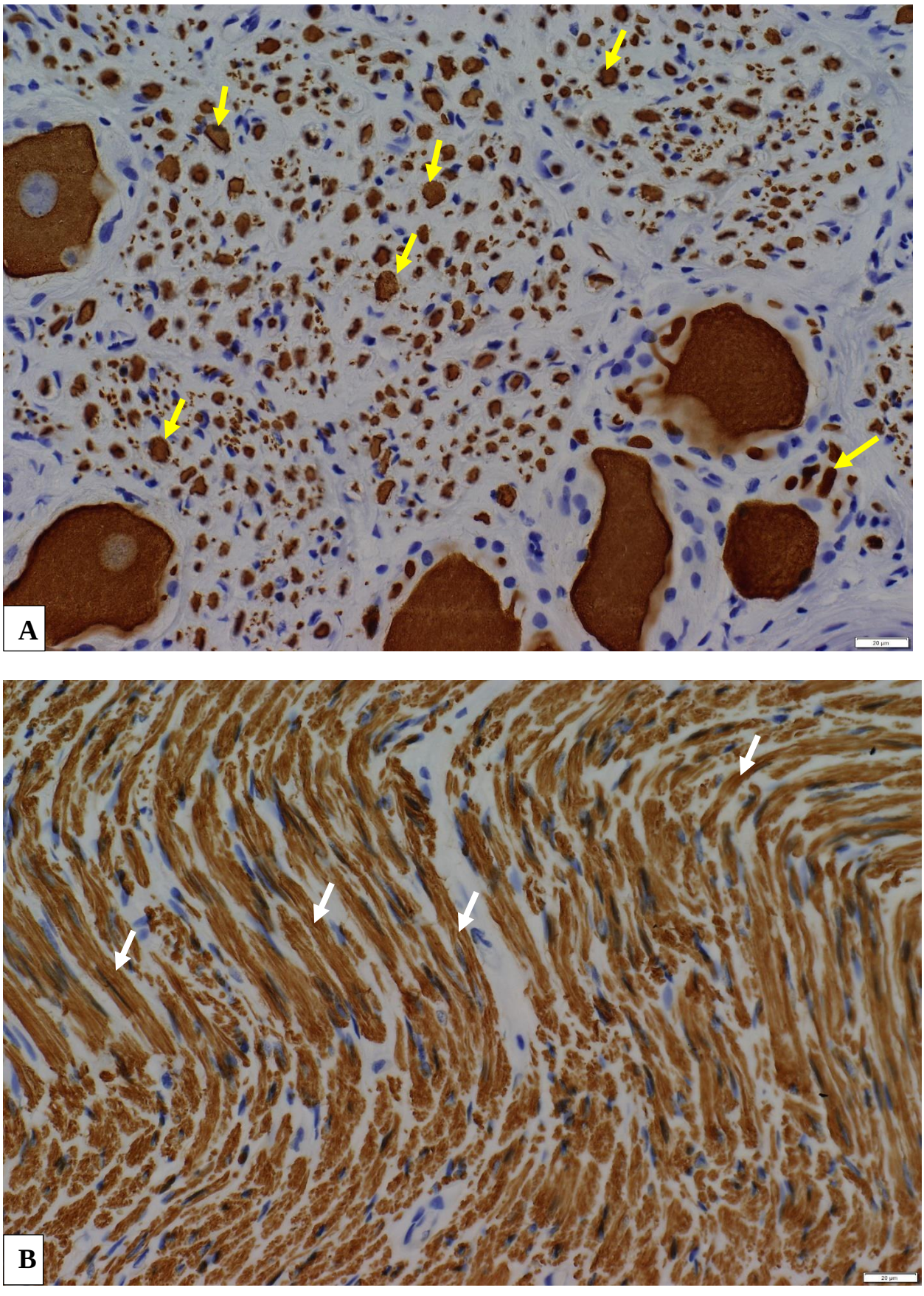

58

Fig. 58: A & B: Photomicrographs of a ganglionic lobule of the CCG; **A:** showing a positive reactivity of the myelinated axons (**yellow arrows**) within the stroma of the ganglionic lobule to the ANMA. Image bar= 20μm. **B:** Showing a positive reactivity of the non-myelinated axons (**white arrows**) within the stroma of the ganglionic lobule for the ANMA. Image bar= 20μm.

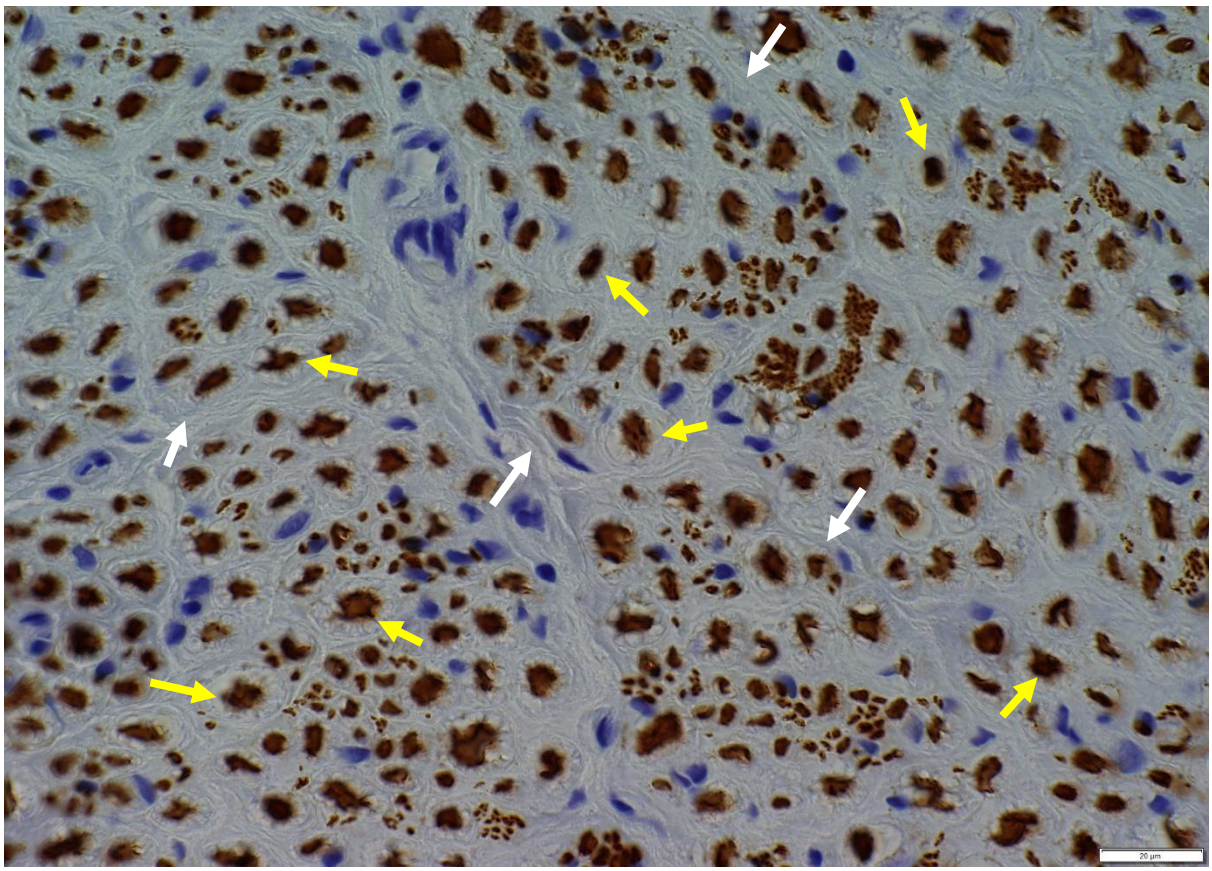

59

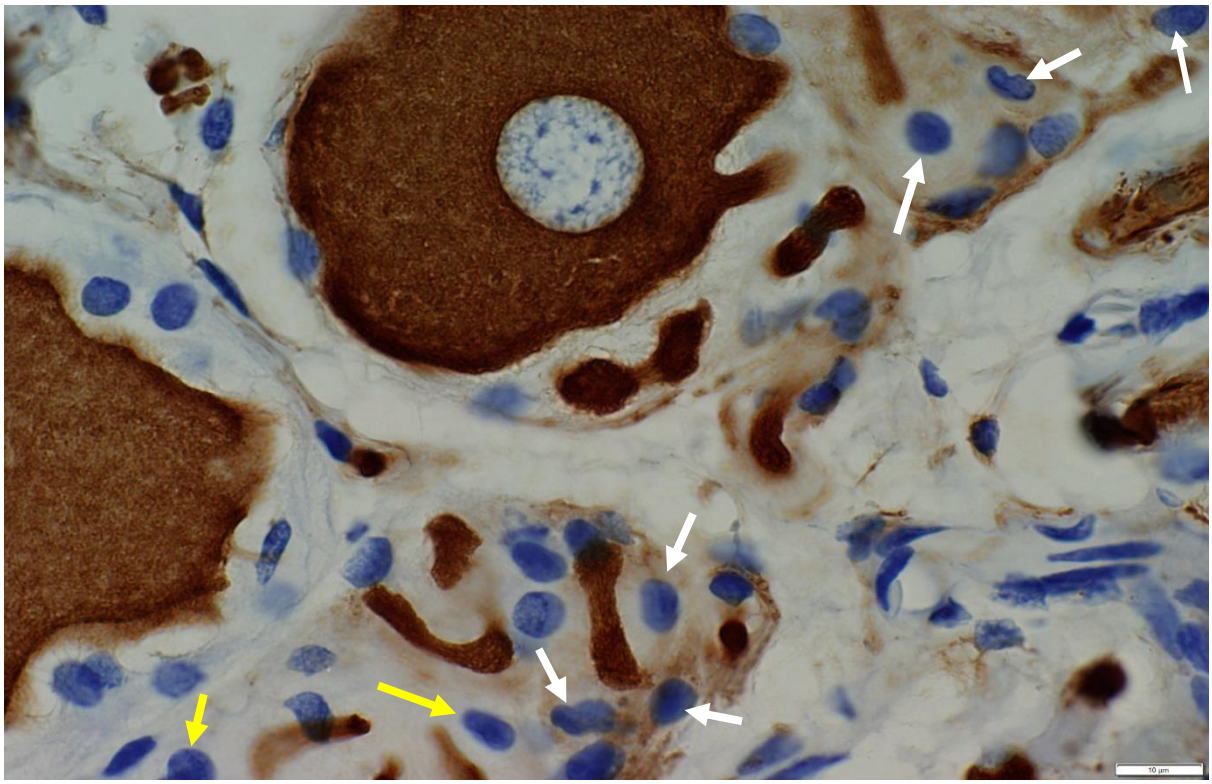

60

Fig. 59: A photomicrograph of the CCG stroma showing a negative reactivity of the perineurium (**white arrows**) and endoneurium (**yellow arrows**) to the ANMA. Image bar= 20μm.

Fig. 60: A photomicrograph of the ganglionic unit of the CCG showing the negative (**yellow arrows**) or weak (**white arrows**) reactivity of Schwann cells cytoplasm to the ANMA. Image bar= 10μm.

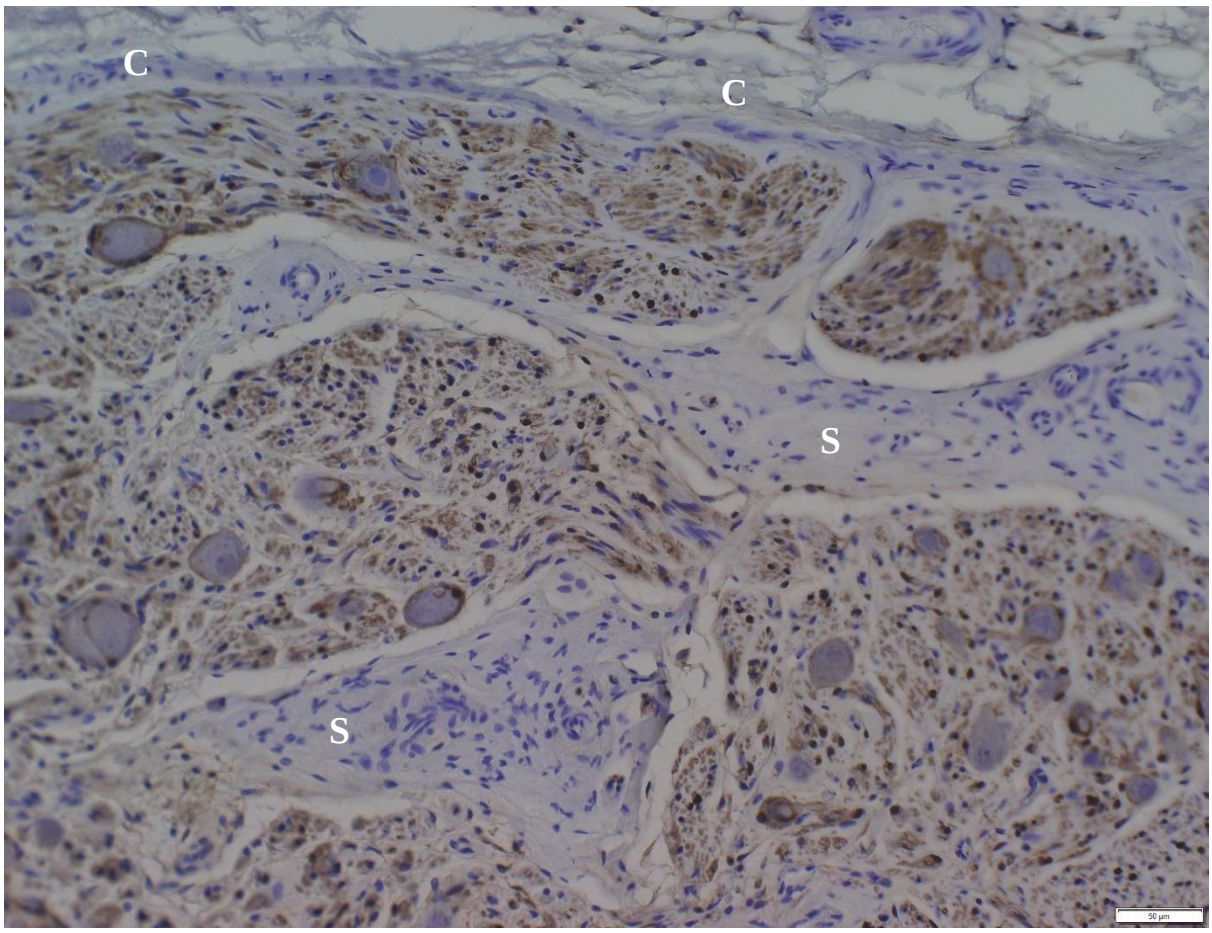

61

Fig. 61: A photomicrograph of the CCG showing a negative reaction of both the capsule (**C**) and septa (**S**) for S-100 protein. Image bar= 20µm.

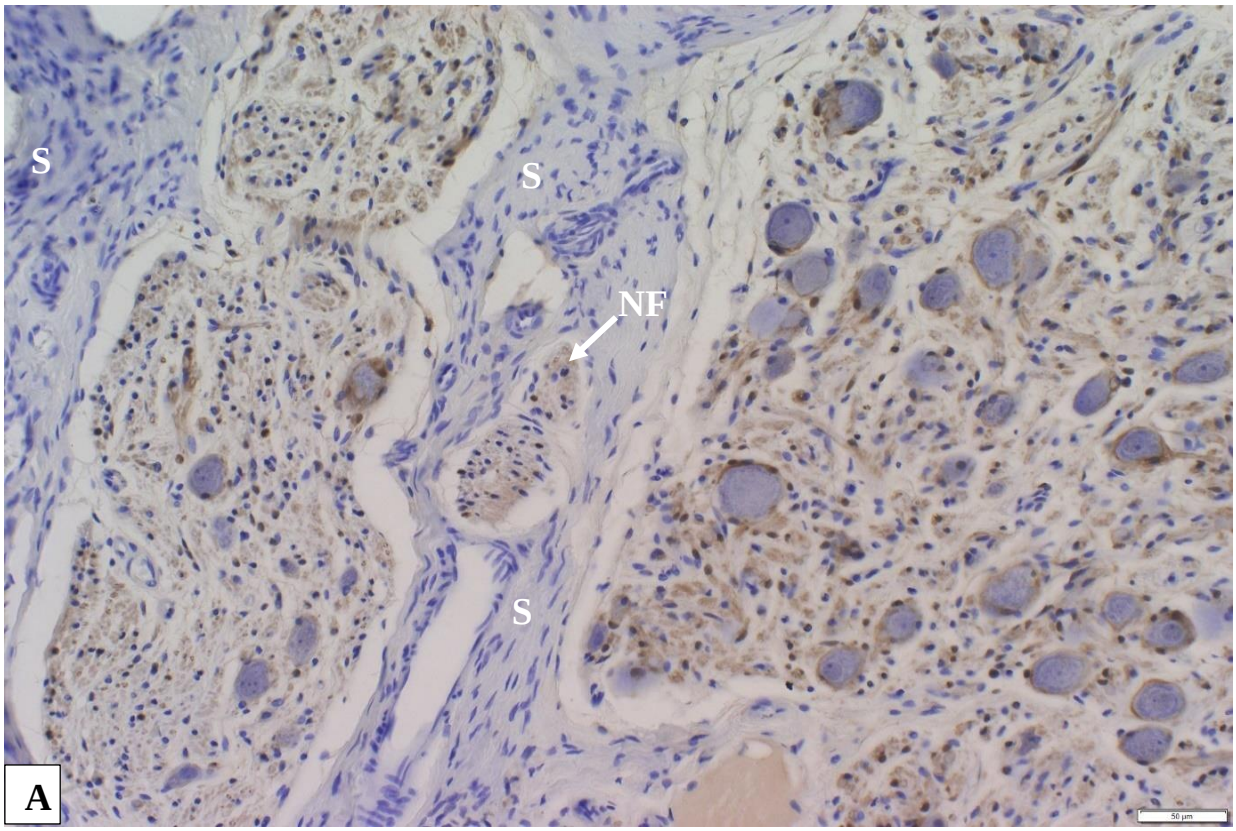

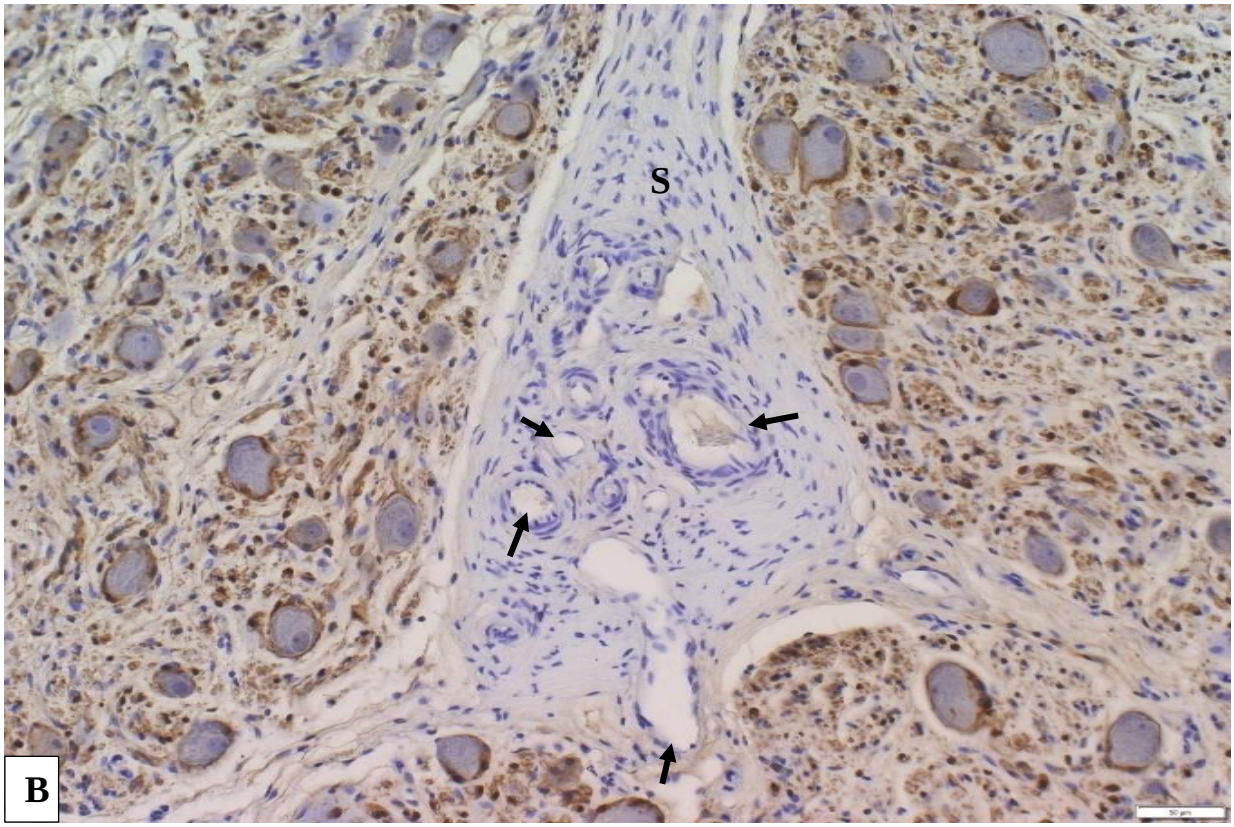

62

Fig. 62: A & B: photomicrographs of a negatively reactive septa (**S**) of the CCG to the S-100 protein. **A:** The nerve fibres (**NF**) within the septa showing a positive reaction to the S-100 protein. Image bar= 50μm. **B:** The blood vessels (**black arrows**) showing a negative reaction to the S-100 protein. Image bar= 50μm.

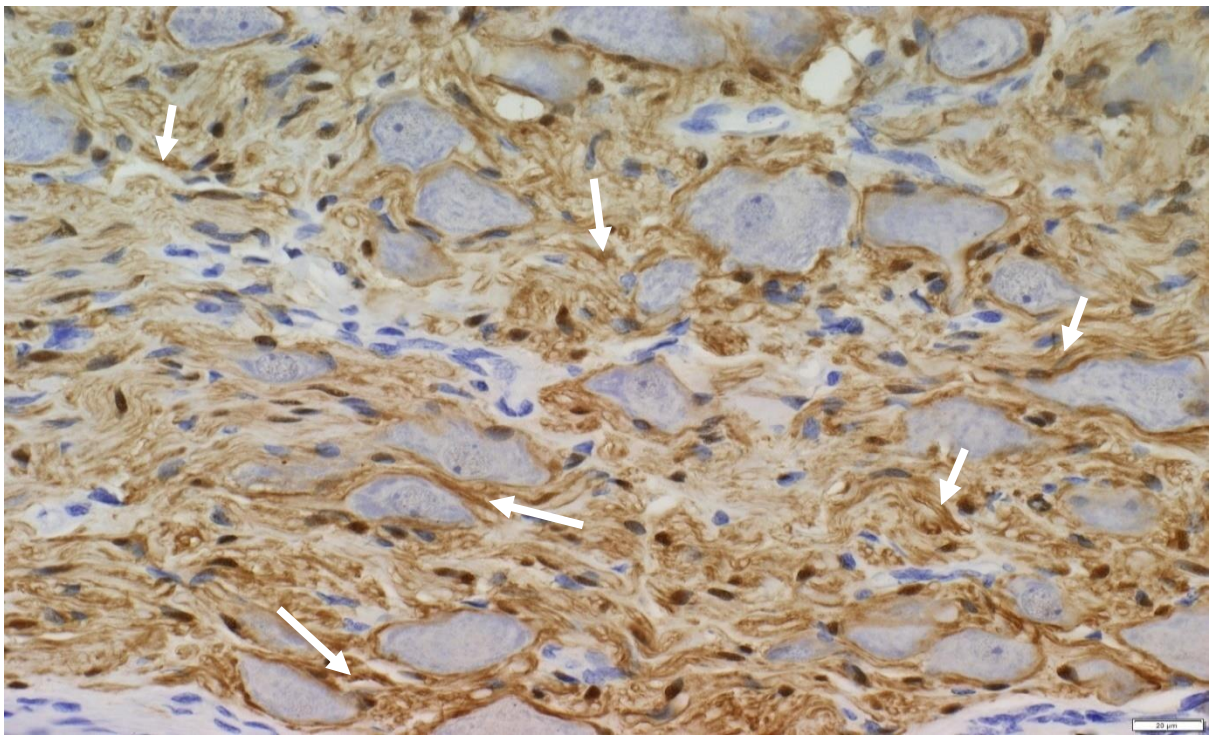

63

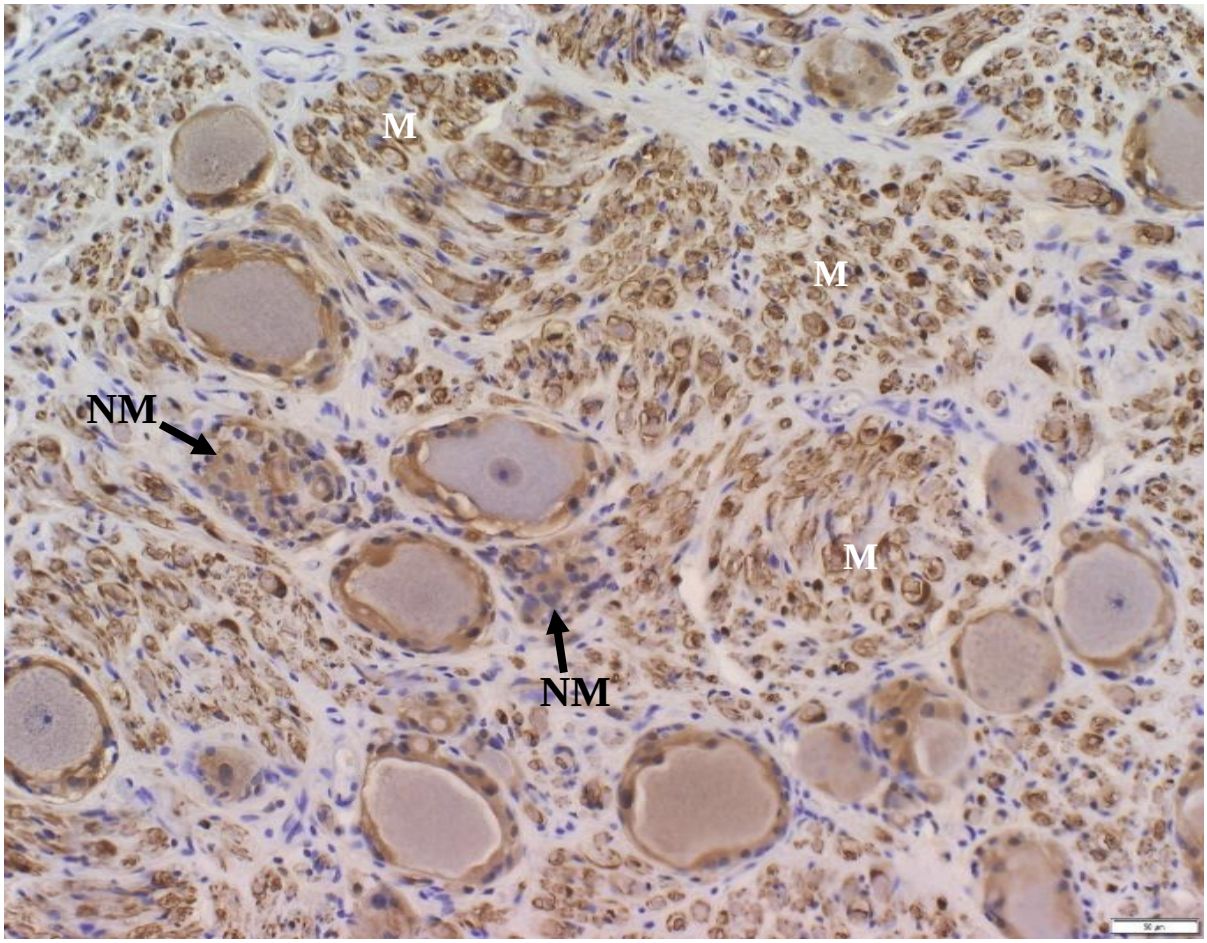

64

Fig. 63: A photomicrograph of the ganglionic lobule stroma showing a positive reactivity of the nerve fibres (**white arrows**) to the S-100 protein. Image bar= 20μm.

Fig. 64. A photomicrograph of the ganglionic lobule of the CCG; showing a positively reacting myelinated axons (**M**) and non-myelinated axons (**NM**) to S-100 protein. Image bar= 50μm.

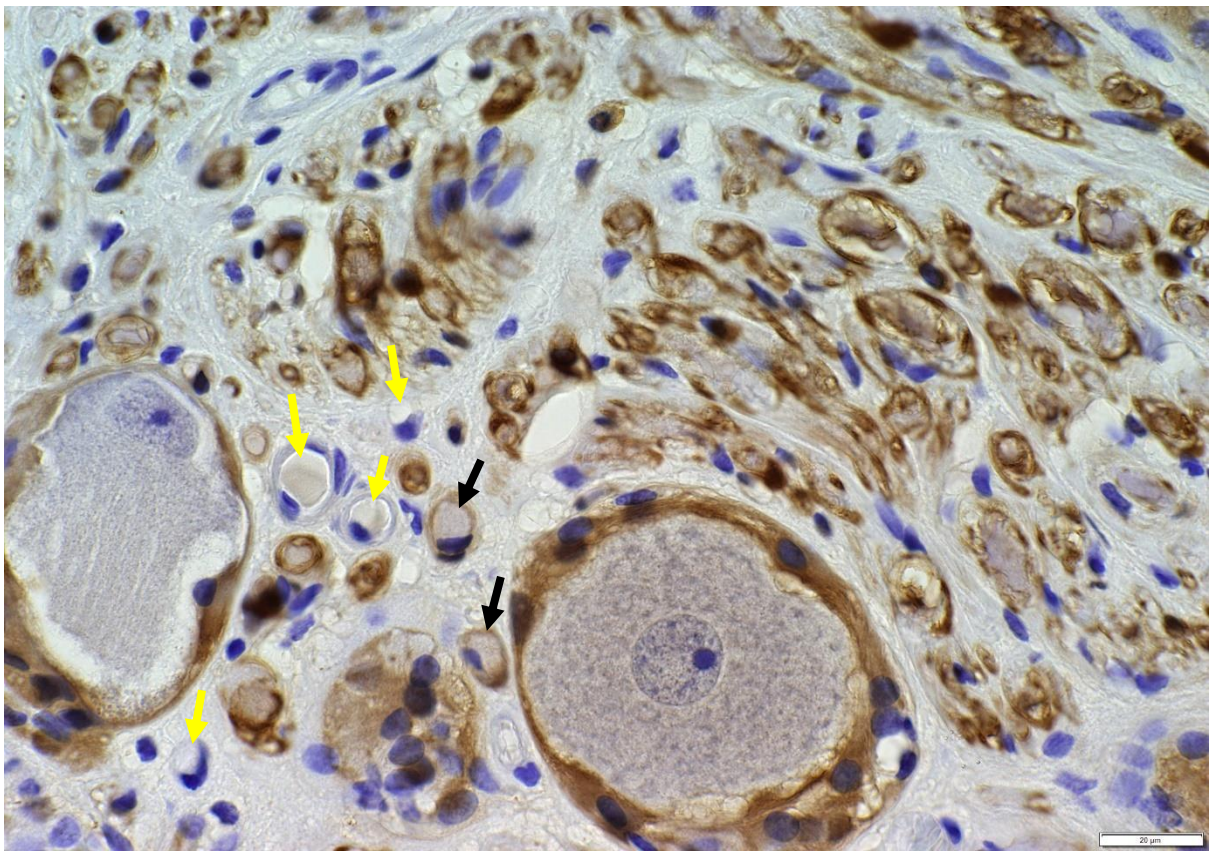

65

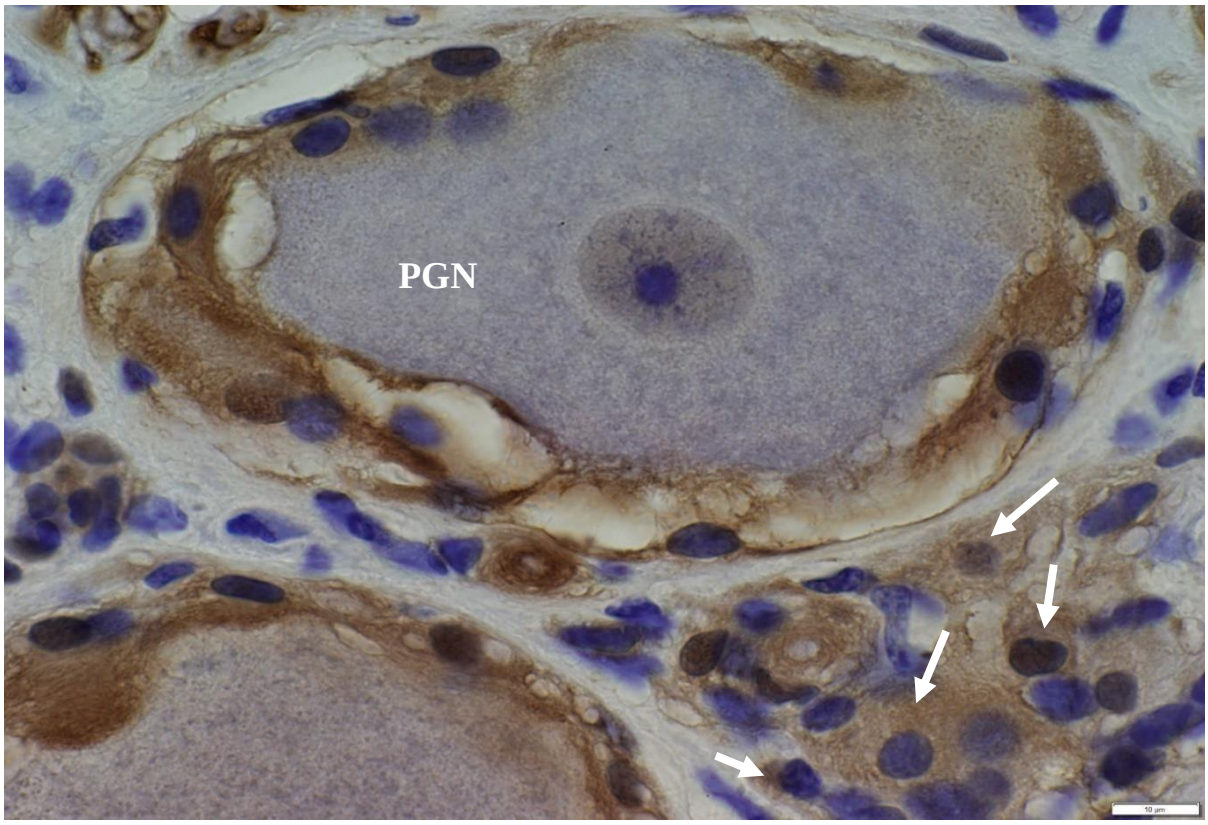

66

Fig. 65: A photomicrograph CCG stroma showing capillaries, either weakly positive (**black arrows**) or negative (**yellow arrows**) for S-100 protein. Image bar= 20μm.

Fig. 66: A photomicrograph of the CCG ganglionic unit showing a positive reaction of Schwann cells cytoplasm (**white arrows**) for S-100 protein. Image bar= 10μm.

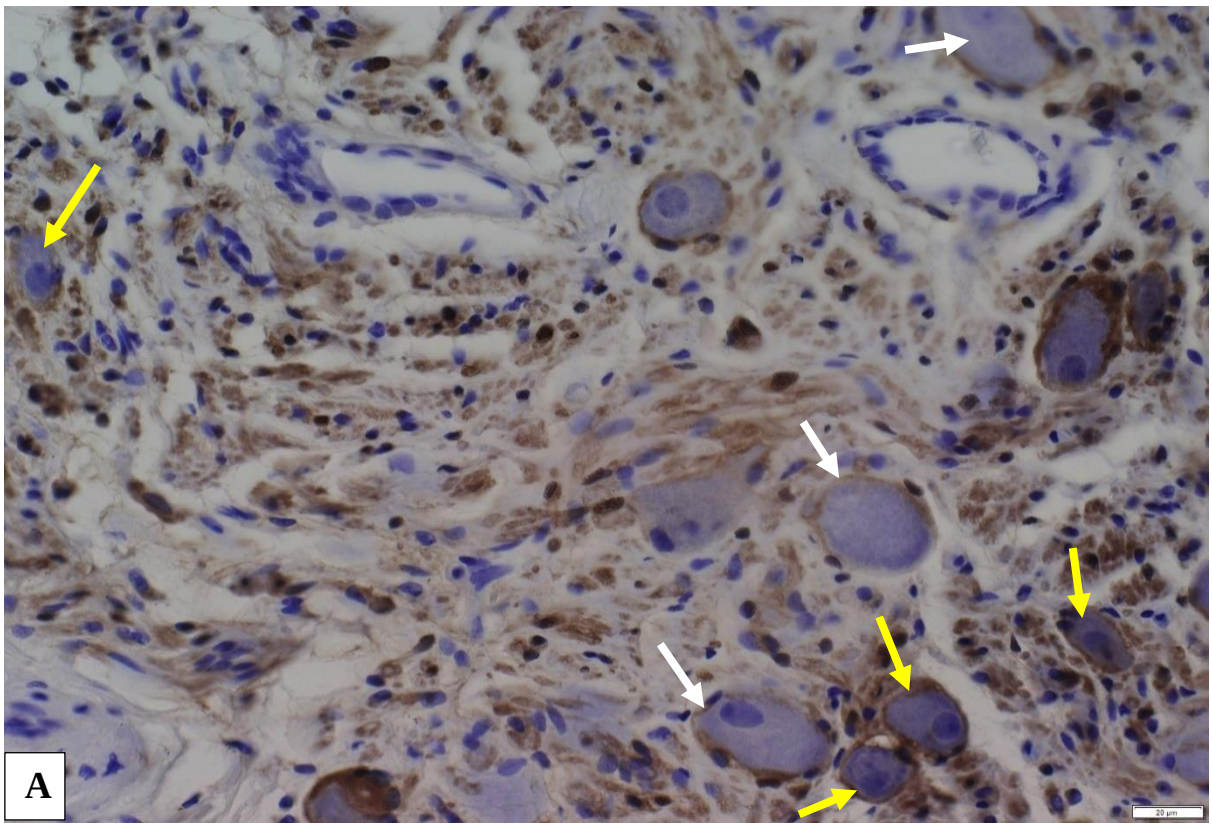

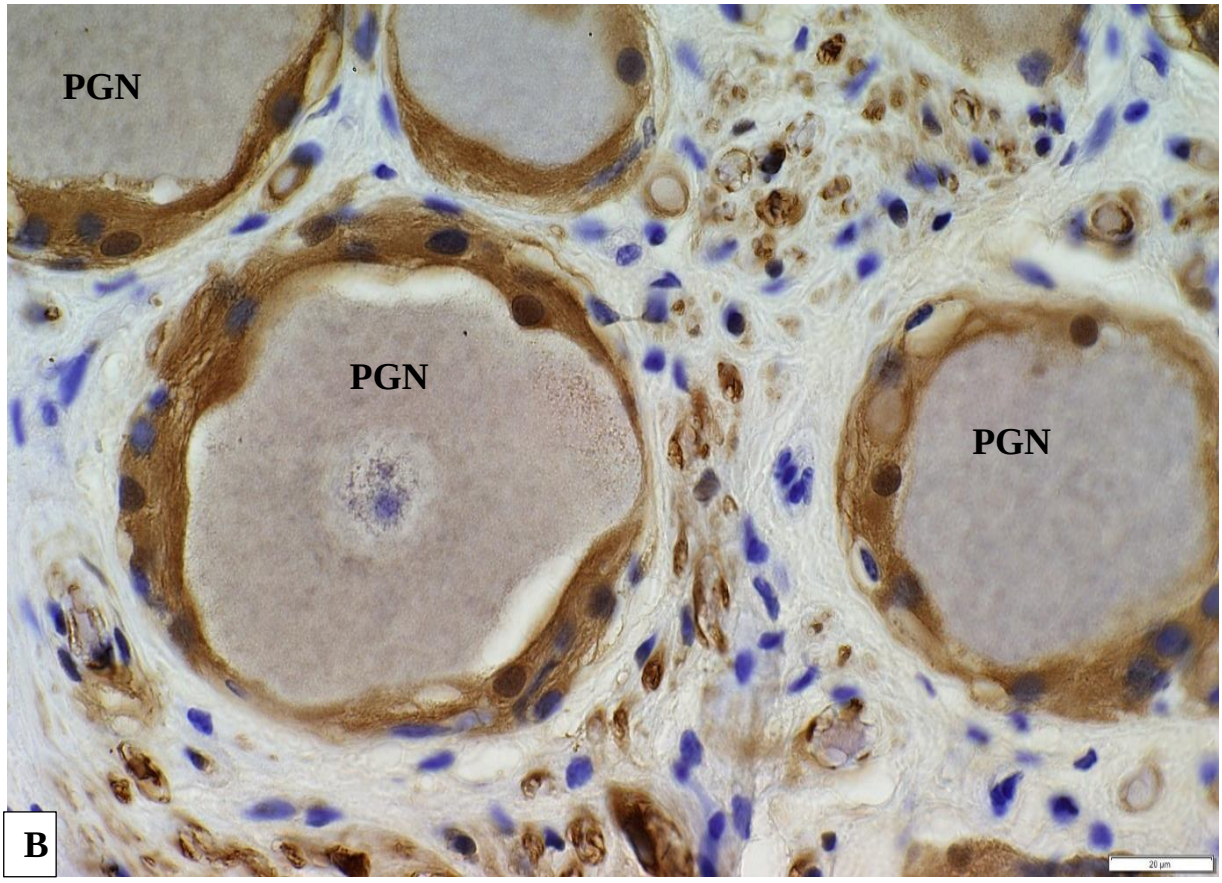

67

Fig. 67: A & B: Photomicrographs of the ganglionic lobule of the CCG; **A:** Showing small principal ganglion neurons (**yellow arrows**) and medium principal ganglion neurons (**white arrows**) negatively reacting to the anti S-100 protein. Image bar= 20μm. **B:** Showing a weak reaction of the large principal ganglion neurons (**PGN**) to the anti S-100 protein. Image bar= 10μm.

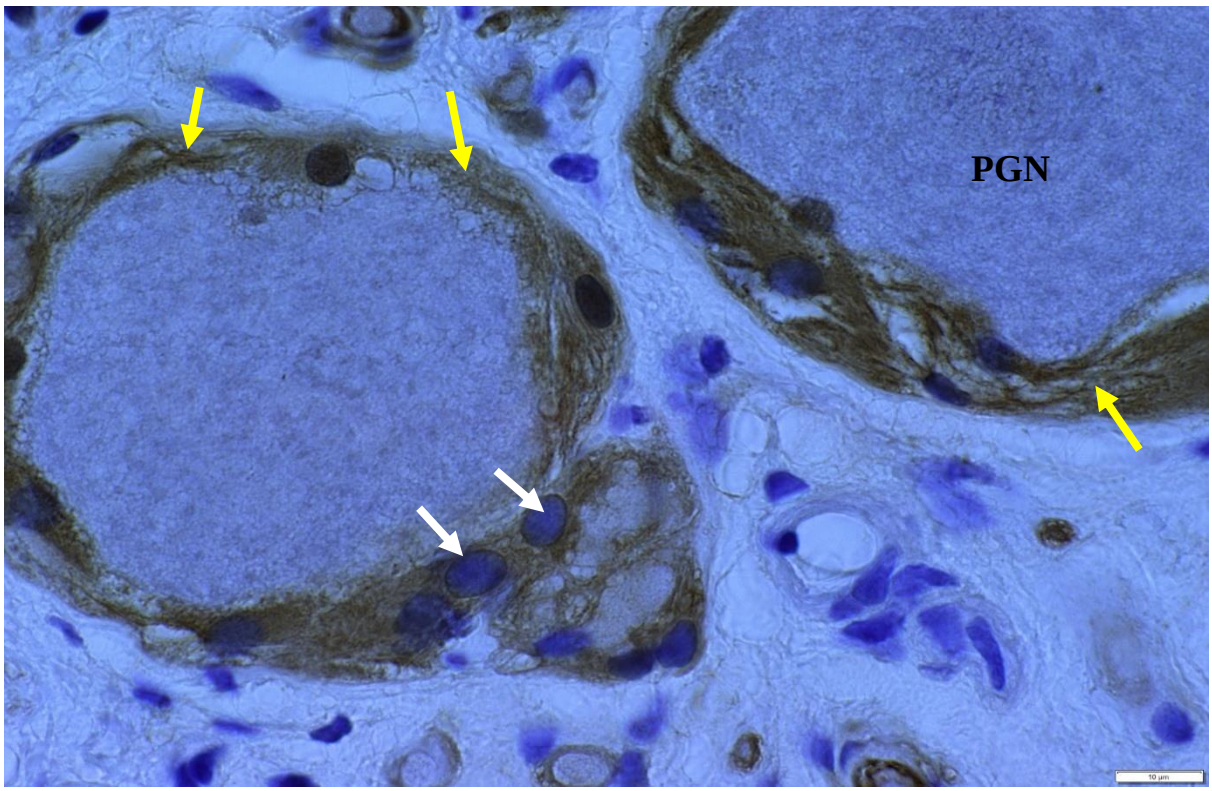

68

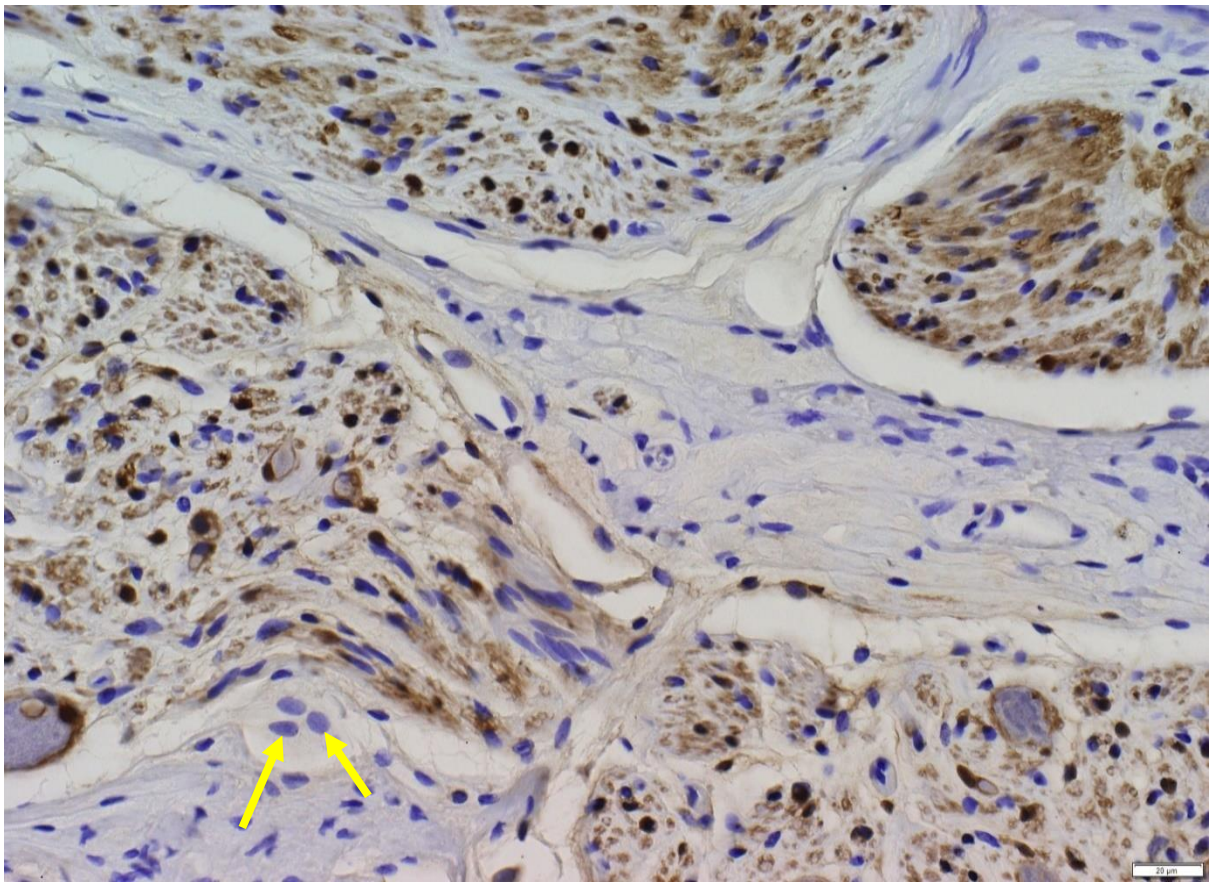

69

Fig.68: A photomicrograph of the ganglionic unit of the CCG showing a strong positive reaction of the glial capsule (**yellow arrows**) and satellite glial cells (**white arrows**) to the anti S-100 protein. Image bar= 20μm.

Fig. 69: A photomicrograph of the ganglionic lobule of the CCG showing a negatively reacted small intensely fluorescent cells (**yellow arrow**) to the S-100 protein. Image bar= 20μm.

CHAPTER FOUR

DISCUSSION

4.1. Gross Anatomy

In the present study, the CCG was located ventral to the caudal stylopharyngeal muscle and covered by the mandibular gland. It was lodged between the common carotid artery and the internal carotid artery, rostrolateral to the longus capitis muscle. It was related laterally to the vagus nerve and medially to the retropharyngeal lymph node. This position was similar to that observed by Cui-Sheng *et al.* (1998) in the bactrian camel and Nourinezhad *et al.* (2015) in the dromedary camels. On the contrary, in the yak, the CCG was found to be covered by the stylohyoid muscle (Shao *et al.* 2007).

The cranial cervical ganglia differed in color among the different animal species. It was either greyish (Shao *et al.* 2007), reddish (Ozgel *et al*., 2004; Najafi *et al.*, 2011) or white (Fioretto *et al.*, 2007; Ari *et al.,* 2010). The present study confirmed the findings of Fioretto *et al.* (2007) and Ari *et al.* **(**2010) in that the cranial cervical ganglia were white in colour.

The shape of the CCG was either oval (Getty, 1975; Cui-Sheng *et al.*, 1998; Cakir, 2001; Ozgel *et al*., 2004; Kabak *et al.*, 2005; Kabak 2007; Kabak and Onuk, 2010), spindle-shaped (Fioretto *et al.*, 2007; Nourinezhad *et al.*, 2016), fusiform (Fioretto *et al.*, 2003; shao *et al.*, 2007; Najafi *et al.*, 2011), rectangular (Ari *et al.,* 2010), or triangular (Najafi and Nejati, 2009). The present study agreed with the observation of Najafi and Nejati (2009) that the CCG was triangular in shape.

The present investigation recorded an average length, width and thickness (Mean ± SE) of the right CCG of the dromedary as 16.33±1.41 mm, 7.0±1.03 mm and 3.03±0.54 mm, respectively, whereas that of the left CCG had an average length, width and thickness (Mean ± SE) of 16.65±1.21 mm, 7.21±0.82 mm and 3.21±0.37 mm respectively. Our findings indicated that there were no differences in the measurements between the right and left CCG

and they were closely similar to the values obtained by Nourinezhad *et al.* (2015) which measured 14–18 mm in length and 6–8 mm in width in the same animal species. Cui-Sheng *et al.* (1998) reported that there were no obvious differences in the measurements and topography of cranial cervical ganglion between left and right sides of the animal within the same species. Kabak (2007) stated that there was a positive correlation between body size and the length and width of the CCG among different species of animals. However, Fioretto *et al.* (2007) added that the animal age was a factor affecting the ganglion measurements.

The current study agreed with the findings of Cui-Sheng *et al.* (1998) in the bactrian camel**,** Ozgel *et al*. (2004) in the donkey, Najafi and Nejati (2009) in sheep and Kabak and Onuk (2010) in the roe deer that the cranial cervical ganglion gave off three main branches. These were the external and internal carotid nerves and the jugular nerve. There was a variation in the number of the branches of the internal carotid nerve in the different animal species. The branches of the internal carotid nerve in ox consisted of seven to eight branches (Nourinezhad *et al.*, 2016). On the contrary, only three branches of the internal carotid nerve had been recognized in the sheep (Najafi and Nejati, 2009), Angora goats (Ari *et al.*, 2010), domestic pig (Kabak *et al*., 2005) and roe deer (Kabak and Onuk, 2010). In the dromedary camel, one or two branches had been identified (Nourinezhad *et al.*, 2015), whereas in the bactrian camel, five branches were noted (Cui-Sheng *et al.*, 1998). This investigation in the dromedary camel revealed five branches similar to these observed by Cui-Sheng *et al.* (1998) in the bactrian camel.

The external carotid nerve was composed of one branch which originates from the caudal end of the CCG and formed the carotid plexus on the carotid artery (Ari *et al.*, 2010; Najafi *et al.*, 2011; Nourinezhad *et al.*, 2015). Similar observations of the external carotid nerve were noted in this study.

Cui-Sheng *et al.* (1998) reported the presence of a communicating branch in the bactrian camel's CCG which originated from the rostroventral margin of the ganglion and connected it to the glossopharyngeal nerve. In this study, such a communicating branch was not observed.

4.2. Histology

The present study is the first report dealing with the histology of the CCG of the dromedary camel.

The histological findings of the CCG in the present study showed that the organization of the ganglion components was closely similar to that described previously by Gabella *et al*. (1988), Kiran (2002) and Eroschenko (2008) in the sympathetic ganglion in different mammals. Miolan and Niel (1996), Ribeiro *et al.* (2002) and Fioretto *et al*. (2007) reviewed that in large mammals, the CCG was a complex structure rather than a classical single paravertebral sympathetic ganglion as that found in laboratory animals. The present study confirmed these observations.

The CCG in most domestic mammals, was covered by a thick connective tissue capsule (Gabella *et al.*, 1988; Szurszewski and King, 1989; Szurszewski and Miller, 1994; Miolan and Niel, 1996; Schmidt, 1996; Ribeiro *et al*., 2002; Gagliardo *et al*., 2003; Ribeiro *et al*., 2004). Contrary to them, Gabella (1976) reported that the thick connective tissue capsule surrounding the ganglia of the sympathetic trunk arises from the epineurium of the associated nerves. Our findings in the present investigation confirmed the presence of a thick capsule which had been further subdivided into three distinct layers. The outer layer was very tough and composed mainly of collagenous fibers, the middle layer was relatively looser and contained ramifications of myelinated and nonmyelinated nerve fibres, whereas the inner most layer was highly cellular.

In domesticated mammals, the CCG is divided into well-defined compartments by capsular septa of connective tissue (Gabella *et al*., 1988;

Miolan and Niel, 1996; Ribeiro *et al*., 2002; Ribeiro *et al.*, 2004). Moreover, the previous authors stated that there were variations in the general architecture of the sympathetic ganglia in large mammals when compared with that of small laboratory rodents, such as rats and mice. The present study is in accord with their observations.

This study agreed with that of De Castro and Herreros (Cited by Gabella, 1976) who classified the neurons of the superior cervical ganglion (SCG) of the cat and man on the basis of their body size into three types; small, medium and large neurons. The present study showed significant differences between the diameter of the small, medium and large-sized principal ganglion neurons. Furthermore, in our investigation the PGNs were noted to be organized as follows; the small-sized PGNs occupied the middle region of the ganglia, followed by the medium and large-sized PGNs with numerous bundles of myelinated and non-myelinated nerve fibres, whereas the terminal ends of the CCG were made up exclusively of nerve bundles. De Castro and Herreros (Cited by Gabella, 1976) suggested that the large neurons provided the intrinsic innervation of the eye, whereas, the medium neurons provided vaso- and pilomotor fibres, however, the function of the small neurons was unclearly understood.

The present study, indicated eccentric, mono-nucleated PGNs, however, the central position of the nuclei was often recognized. Although, similar histological observations of the nuclei of PGN of the CCG have been reported by Gabella *et al.* (1988) in sheep, Ribeiro *et al.* (2002) in dog, Ribeiro (2006) in capybaras and Fioretto *et al.* (2007) in dog, cat and horse. PGNs with two nuclei have been also found in other group of animals including rabbit (Filichkina, 1981) and mice and rats (Dalsgaard and Elfvin, 1982; Purves, Rubin, Snider and Lichtman.1986; Smith, 1970). Ribeiro (2006) suggested that the occurrence of the was nuclei is an adaptation to some specific demands imposed on the cells with respect to protein synthesis. In contrast to this,

Filichkina (1981) reported that the bi-nucleated rabbit's superior cervical ganglion (SCG) cells did not show any increase in the total protein synthesis or axonal transport of proteins compared to the mono-nucleated SCG cells

The presence of lipofuscin granules in the peripheral region of the cytoplasm of the large PGNs had been observed by Gartner and Hiatt (2007); and Young, O'Dowd and Woodford (2014). A similar observation was noted in the present investigation. Brizzee, Ordy, and Kaack. (1974) mentioned that lipofuscin was a ubiquitous fluorescent pigment that accumulates with age in long-lived cells, such as neurons and cardiac myocytes. On the other hand, Gartner and Hiatt (2011) suggested that these pigment granules were thought to be secondary lysosomes involved in the degradation of unsaturated lipids and the detoxification of the end products of metabolism.

The present study showed the basic organization of the principal ganglion neuron and their satellite glial cells (SGCs). SGCs were observed encircling the principal ganglionic neurons and their processes. In this investigation, a positive correlation was noted between the number of the SGCs and the size of the PGNs. The SGCs together with the collagen fibers formed the glial capsule. Each principal ganglionic neuron and its own glial capsule formed a distinct ganglionic unit which was largely isolated from other similar units in the CCG by the ganglionic stroma. These results were similar to those observed in CCG of sheep (Gabella *et al.,* 1988), dog (Ribeiro et al., 2002) and cat and horse (Fioretto *et al*., 2007). Tropea, Johnson and Higgins (1988) claimed that the main function of the SGCs was the maintenance of the characteristic phenotype of PGNs. Hanani (2005, 2010) reviewed that the glial capsule could slow down the diffusion of most substances, and particularly large molecules, and had a partial control over the neuronal microenvironment.

In the present study, the thickness of the glial capsule and neuropil was greater around the large PGNs compared with the small PGNs. The thickness of the glial capsule varied extensively around the perikaryon of the individual

neuron. It was maximal at the level of the nucleus of a satellite glial cell, while it was sharply reduced in most of the other areas. These observations were in agreement with that reported by Pannese (1981) in sensory ganglia of mammals and Gabella *et al.* (1988) in the CCG of sheep. Gabella *et al.* (1988) were of the opinion that the matching of satellite glial cell number and PGN volume was achieved during development by satellite glial cell mitosis taking place long after the PGN had ceased dividing.

The present study showed that the neuropil wrapping the PGNs was formed of the glial capsule together with the myelinated and unmyelinated fibers. The nodes of Ranvier were seen between the internodal segments of the myelinated nerve fibres. This was in agreement with the previous observations of Banks (1993), Fawcett (1994), Haines (2013), and Young *et al.* (2014). Cui, Naftel, Lynch, Yang, Daley, Haines and Fratkin (2011) suggested that these nodes were able to carry out the complicated exchange of sodium and potassium ions across the membrane which was the basis of the conduction of the action potential. They added that the internodal segments of the myelinated nerve fibres might provide metabolic support for the attached thin membranous layer of myelin. Banks (1993), Fawcett (1994), Haines (2013), Young *et al.* (2014) described Schmidt-Lanterman clefts as cone-shaped discontinuities in the myelin sheath of the axons. According to Young *et al.* (2014) these clefts were not static and continually moving their position providing periodic exposure of the inner faces of the myelin sheath to the cytoplasm for the purpose of maintenance and molecular replacement.

In the present study, the small intensely fluorescent cells (SIF) in the CCG of the camel were similar to those noted in rabbits (Barton and Causey,1958), rats (Matthews and Raisman,1969) and dog, cat and horse (Fioretto *et al.*, 2007). They were characterized by rounded or polyhedral, and sometimes elongated shape with darkly staining, large central nucleus. The cytoplasm appeared pale and clear. Yokota (1973) suggested that there might

be two functional pathways for the SIF cells in the CCG in which some of them might operate as inter-neurons and the others were thought to be neuro-secretory cells. On the other hand, Miolan and Niel (1996) confirmed the suggestion of a neuro-endocrine role of the SIF.

4.3. Histometry

The present histometric study on CCG in the camel was done for the first time. The CCG capsule thickness ranged between 15-30 μm in rats, 30-70 μm in capybaras and 60-80 μm in horses (Ribeiro *et al*., 2004). Fioretto *et al*. (2007) reported that the thickness of the CCG capsule was 18.5 μm in cat, 21.5 μm in dog and 68.5 μm in horse. According to the present study the thickness of the capsule of the CCG of the camel was 155.92±19.43 μm. This study confirmed the previous studies in that there was a positive correlation between the animal size and the thickness of the ganglion capsule. The increased thickness in the ganglionic capsule in large mammals may be implicated in the protection of ganglion principal neurons.

The present study revealed that the mean diameter of the small, medium and large-sized PGNs of the CCG was 77.13±4.099, 127.154±7.444, and 250.22±37.154 respectively. De Castro and Herreros (Cited by Gabella, 1976) reported that the diameter of the small, medium and large-sized PGNs of the of the SCG in the cat and man ranged between 15-24 μm, 25-32 μm and 33-50 μm respectively. All values of diameter of the PGNs in the camel were larger than their corresponding ones in cat and man. This could be attributed to the differences in the animal size in the two cases.

4.4. Ultrastructure

The ultrastructure of the cranial cervical ganglion was early studied by many authors in many animal species; rabbit (Causey and Hoffman, 1956; Barton and Causey, 1958; Siegrist, *et al*., 1968); cat (Elfvin, 1963); rat (Matthews and Raisman, 1969); sheep (Gabella *et al*., 1988); dogs, cats and horses (Fioretto *et al*., 2007).

In the present study, the electron microscopy revealed the ultrastructure of the following cells of the ganglionic unit of the CCG: principal ganglion neurons, satellite glial cells, Schwann cells, microglial cells, fibroblasts, mast cells and pericytes, as well as the ultrastructure of myelinated and non-myelinated nerve fibres.

This investigation, central position of the nucleus of the principal ganglion neurons of the CCG in dromedary camel was found to be in accord with that described in the principal ganglion neurons of the CCG of rabbits, rats, dogs, cats and horses (Causey and Hoffman, 1956; Barton and Causey, 1958; Siegrist *et al*., 1968; Matthews and Raisman, 1969; Fioretto *et al.*, 2007), and the principal ganglion neurons of the sympathetic ganglia of many other animals (Banks, 1993; Aughey *et al.*, 2001).

Causey and Hoffman (1956), Barton and Causey (1958) stated that the nucleolemma of the principal ganglion neurons was a double membraned structure with numerous nuclear pores. They added that there was concentration of mitochondria at the perinuclear area. This was also true in the present study.

In the present study, the cytoplasm of the PGNs contained large amount of rough endoplasmic reticulum (Nissl's bodies), whereas the peripheral region of the PGNs was devoid of the cisterns of rough endoplasmic reticulum, and was occupied exclusively by free ribosomes, which were often aggregated in the form of small polysomes. This position of rough endoplasmic reticulum was similar to that observed by Gabella *et al.* (1988) in sheep. On the contrary, in sheep sympathetic ganglion, the cisterns of rough endoplasmic reticulum were found to be lying immediately beneath the cell membrane as subsurface cisterns (Siegesmund, 1968). Dixon (1963) suggested that these cisterns of rough endoplasmic reticulum might be structural basis for proteins synthesis.

In the present study, numerous pale mitochondria with different shapes; filamentous, rod-like, or spherical were evenly distributed throughout the

cytoplasm of the principal ganglion neurons. This was in agreement with the previous observations of Banks (1993), Fawcett (1994) Young *et al.* (2014) and Pannese (2015). Banks (1993) reported that the major function of the mitochondria was to produce energy, and hence it contained DNA and RNA and it might possess some genetic and protein synthesis potential. Sotelo (1967) suggested that the presence of a large number of mitochondria in the neurons reflected a high metabolic activity in the cell.

This investigation, large spherical and irregular lysosomes were often noted in the cytoplasm of the principal ganglion neuron. Similar findings had been reported by Leong and Wong (1989) in the stellate ganglion of the monkey. Banks (1993) suggested that the main function of the lysosomes was to regulate the cellular activities related to growth, nutrition, metabolism and differentiation.

Banks (1993), Fawcett (1994), Cui *et al.* (2011) Haines (2013) and Young *et al.* (2014) mentioned that the chief components of the neuronal cytoskeleton, were neurofilaments and microtubules. They were arranged in tracts that occupy the spaces among Nissl's bodies and other organelles throughout the perikaryon and along the length of the axon and dendrites. A similar observation was also noted in the present study. The main function of the neurofilaments, as described by Cui *et al.* (2011) and Young *et al.* (2014), was to provide structural support and the microtubules are involved in axonal transport of neurotransmitter substances, enzymes, membrane and other cellular constituents.

The present study showed that the plasma membrane of the principal ganglion neurons had numerous folds with irregular forms. These folds settled in the intercellular space and displayed shallow irregular grooves. These folds intermingled with corresponding ones of the satellite cells in the intercellular space. This was in agreement with the previous observations of Dixon (1963) in the trigeminal ganglion of the rats. Palay (1958) suggested that these folds

facilitated the diffusion of nutritional materials between the principal ganglion neuron and the satellite cell cytoplasm.

In the present study, the fibrous constituents of the neuropil of the camel CCG was built up of myelinated and non-myelinated axons separated by collagen fibrils. These observations support of the findings of Dixon (1963) in the trigeminal ganglion of the rat and Leong and Wong (1989) in the stellate ganglion of the monkey. On the contrary, these findings contradicted with that of Abdel-Magied (1995) in the dromedary camel, who reported the presence of only unmyelinated fibres in the neuropil of the CCG.

The present findings confirmed the observations of Dixon (1963), Leong and Wong (1989), Banks (1993) Fawcett (1994) and Haines (2013) that in the myelinated axons, the myelin sheath appeared as several layers of stacked membranes. Young *et al.* (2014) suggested that the layers of membrane of myelin sheath might be important sites for increasing the speed and efficiency of nerve impulse conduction.

In the present investigation, Schwann cells were large in size, measuring about 46.47±1.46 µm in width and about 67.20±2.01 µm in length. They had infoldings or grooves at their surfaces and were surrounded by a basal lamina. Organelles such as rough endoplasmic reticulum and mitochondria were seen throughout the cytoplasm of the Schwann cells. They also contained one to five homogeneous, dense bodies. Similar findings had already been reported by Leong and Wong (1989) in the Schwan cells of the stellate ganglion of the monkey. Hall (1997) explained that the Schwann cells provided essential trophic support to the neuron through the regeneration of the myelin. Bunge, Bunge and Eldridge (1986) reported that the basal lamina surrounding the Schwan cells was essential to link between the Schwann cells, the axon and the extracellular matrix.

In the present investigation two types of synapses were recognized. The first type was axodendritic synapse between the presumptive axon terminal and

the base or terminal end of a large dendrite, this was the most common type. The second type was axosomatic synapse on the surface of the soma of a principal ganglion neuron. On the contrary, only axodendritic synapses were present in sheep (Gabella *et al*., 1988), however, Matthews (1983) pointed out that in sympathetic ganglia, the dendrites may gain support from each other (dendrodendritic) and from cell bodies of principal ganglion neurons (dendrosomatic).

The presence of the large dense-cored vesicles and small clear vesicles were noted in the present study in the different types of nerve endings of the camel CCG, similar to those recognized by Abdel-Magied (1995) in the same animal, Elvin (1963) in cat and Yokota and Yamauchi (1974) in mouse. Matthews (1983) claimed that the small clear vesicles and the large dense-cored vesicles were responsible for storing acetylcholine, and enkephalin respectively. Abdel-Magied (1995) explained that both clear and dense-cored vesicles adhered to the presynaptic membrane, and released their content into the synaptic cleft.

In the present investigation, few dendrites in the neuropil also contained densely packed dark and cylindrical mitochondria interspersed with one or more patches of neurofilaments, and microtubules. These results were identical with those obtained by Abdel-Magied (1995) in the dromedary camel, Gabella *et al.* (1988) in sheep and Williams, Jew and Palay (1973) in cat. Sotelo (1967) attributed the presence of such structures in the CCG of the rat and cat to the high metabolic activity in the principal ganglion neuron. Knoche and Addicks (1976) suggested that these structures might be baroreceptors or chemoreceptors and they might be undergoing physiological changes of degeneration and regeneration. On the other hand, Abdel-Magied (1995) suggested that these structures could be mechanoreceptors.

In the present study, the microglial cells were observed within the stroma of the ganglionic units or in the neuropil adjacent to the PGNs. They were large

in size and irregular in shape with many cytoplasmic processes. They had dark cytoplasm with fine granules. This was in agreement with the previous observations of Leong and Wong (1989) in the stellate ganglion of the monkey. Fuchs and Auer (2010) reported that the major function of the microglia is to produce nitric oxide which is important for the innate immune defense against pathogens.

The mast cells observed within the stroma of the ganglionic units or in the neuropil in the present study had cytoplasm which was packed with densely staining round or oval granules. These observations were in agreement with that reported by Leong and Wong (1989) in the stellate ganglion of the monkey Additional to the well-known function of the mast cells in releasing histamine and heparin, Cui *et al.* (2011) suggested that the plasma membrane and the outer nuclear membrane of mast cells probably synthesize mediators of inflammation (prostaglandins and leukotrienes) from fatty acids of the membranes.

In the present study, the CCG of the dromedary camel was highly vascular and it showed two types of vasculature; the first type which resembled the blood capillaries was numerous and consisted of a single layer of endothelial cells. The second type was less numerous, larger in size and composed of an inner endothelial lining in addition to an outer layer of smooth muscles. These findings were similar to the observations of Leong and Wong (1989) in the stellate ganglion of the monkey.

4.5. Immunohistochemistry

The present study, was the first to clarify immunohistochemically the distributions of neurofilaments and S-100 protein in the cranial cervical ganglion of dromedary camel.

4.5.A. Neurofilaments

In this investigation, the neurofilaments were detected in the neuronal perikarya of large and medium-sized principal ganglion neurons, the

myelinated and non-myelinated fibres within connective tissue of the glial capsule or in the ganglionic unit stroma. Similar findings had been reported in the paravertebral sympathetic ganglia and trigeminal ganglia of the rats Trojanowski *et al.* (1986). Wang, Wu, Zhan, Ma, Yang, Yang and Li (2012) suggested that the main function of the neurofilament protein was to regulate the function and structure of linking proteins enzymes. They added that the neurofilament gene expression played an important role in nervous system development.

4.5.B. S-100 protein

In the present study, the cytoplasm of both satellite glial cells and Schwann cells, as well as the glial capsule showed a strong immunoreactivity for S-100 protein. This was in accord with the findings of Cocchia and Michetti (1981) in the superior cervical ganglion of rat, Vega *et al.* (1991) in dorsal root ganglion of rat, Albuerne, Mammola, Naves, Levanti, Germana and Vega (1998) in dorsal root, sympathetic and enteric ganglia of several mammalian species and Gonzalez-Martinez *et al.* (2003) in paravertebral and prevertebral sympathetic ganglia of human. Isobe, Ichimura and Okuyama (1989) suggested that the presence of S-100 protein in glial cells might be involved in the regulation of cell growth and differentiation.

The detection of S-100 protein in the neuronal perikarya of large principal ganglion neurons in our study was in accord with the observation of Vega *et al.* (1991) in dorsal root ganglion of rat. On the contrary, Albuerne *et al.* (1998) reported that the principal ganglion neurons in dorsal root, sympathetic and enteric ganglia of buffalo, sheep and pig were positively reacting with S-100 protein whereas, the principal ganglion neurons in dorsal root, sympathetic and enteric ganglia of cow, horse, dog and rabbit were negatively reacting with S-100 protein. Isobe *et al.* (1989) claimed that the main function of the S-100 protein was to regulate the biosynthesis of serotonin and catecholamine in neurons and other monoamine synthesizing cells.

CONCLUSION

This research was conducted to study the morphology and immunohistochemistry of the cranial cervical ganglion of the one-humped dromedary camel (*Camelus dromedarius*).

There were no differences in the topography, structure and immunoreactivity of the ganglion related to the sex and side.

The number and course of the nerves ramifications especially internal carotid nerves, were different from other species.

The ganglionic complex of the CCG had several ganglionic units which were designated as the structural and functional units composed of the PGNs and the neuropil.

The PGNs showed significant differences in their sizes ($p<0.05$), and as a result it had been divided into three types: small, medium and large- sized neurons.

The ultrastructural appearance of the PGNs showed organelles-rich cytoplasm which reflected the high activity of these cells.

Both neurofilaments and S-100 proteins were detected in various components of the CCG.

The PGNs and myelinated and unmyelinated axons were positively reacting with anti- neurofilament monoclonal antibodies.

The immunopositive reaction for S-100 protein as observed in the cytoplasm of large and intermediate sized PGNs, SGCs and Schwann cells in addition to myelinated and non-myelinated nerve fibres.

The CCG of the dromedary camel showed great differences in their gross anatomy, morphology and immunoreactivity compared to the other mammalian species.

RECOMMENDATIONS

Future research is needed to investigate:

1- Blood supply of the CCG.
2- Scanning electron microscopy of the CCG.
3- Transmission electron microscopy of the SIF cells.
4- Ultrastructural morphometry of the PGNs of the CCG.
5- Additional immunohistochemical substances such as calcitonin gene-related peptide, serotonin, peripherin, vimentin, PGP 9.5**,** NSE**,** substance P and laminin.

References

Abdel-Magied, E.M. (1995). Fine structure of nerve endings and junctions in the superior cervical ganglion of the camel (*Camelus dromedarius*). Anatomia Histologia Embryologia, **24:** 117–121.

Albuerne, M., Mammola, C. L., Naves, F. J., Levanti, B., Germana, G. and Vega, J. A. (1998). Immunohistochemical localization of S-100 proteins in dorsal root, sympathetic and enteric ganglia of several mammalian species, including man. Journal of Peripheral Nervous System, **3:** 243–253.

Ari, H.H., Soyguder, Z. and Cinaroglu, S. (2010). Macroanatomy of the cranial cervical ganglion in Angora goats. Veterinarni Medicina, 55, (**8):** 389–393.

Aughey, E., Fredric, L. and Frye, F.L. (2001). Comparative Veterinary Histology with Clinical Correlates. Manson Publishing Ltd.

Baljet, B. and Drukker, J. (1979). The extrinsic innervations of the abdominal organs in the female rat. Acta Anatomica (Basel), **104:** 243–267.

Banks, W. J. (1993). Applied Veterinary Histology. Third Edition. St. Louis. Mosby.

Barton, A.A. and Causey, G. (1958). Electron microscopic study of the superior cervical ganglion. Journal of Anatomy, **92:** 339–407.

Bell, R.L., Atweh, N., Ivy, M. and Possenti, P. (2001). Traumatic and iatrogenic Horner syndrome: case reports and review of the literature. Journal of Trauma, **51:** 400–404.

Boydell, P. (1995). Idiopathic Horner's syndrome in the golden retriever. Journal of Small Animal Practice, **36:** 382–384.

Bunge, R.D., Bunge, M.B. and Eldridge, C.F. (1986). Linkage between axonal ensheathment and basal lamina production by Schwann cells. Annual Review Neuroscience, **9:** 305–328

Brizzee, K.R., Ordy, J.M. and Kaack, B. (1974). Early appearance and regional differences in intraneuronal and extraneuronal lipofuscin accumulation with age in the brain of a nonhuman primate (*Macaca mulatta*). Journal of Gerontology, 29 **(4):** 366-381.

Cakir, A. (2001). The morphology of cranial cervical ganglion in the New Zealand rabbit. Veterinary Journal Ankara University, **48**: 83-87.

Cardinali, D.P., Vacas, M.I. and Gejman, P.V. (1981). The sympathetic superior cervical ganglia as peripheral neuroendocrine centers. Journal of Neural Transmission, **52:** 1–21.

Case, C. P. and Matthews, M.R. (1985). A quantitative study of structural features, synapses and nearest-neighbour relationships of small, granule-containing cells in the rat superior cervical sympathetic ganglion at various adult stages. Journal of Neuroscience. 15, **1:** 237-282.

Causey, G. and Hoffman, H. (1956). The ultrastructure of the synaptic area in the superior cervical ganglion. Journal of Anatomy, **90:**502-507.

Cocchia, D. and Michetti, F. (1981). S-100 antigen in satellite cells of the adrenal medulla and the superior cervical ganglion of the rat. An immunochemical and immunocytochemical study. Cell Tissue Research, **215:**103–112.

Coutard, M., Mertes, P., Mairose, P., Osborne-Pellegrin, M. and Michel, J.B. (2003). Arterial sympathetic innervation and cerebrovascular diseases in original rat models. Autonomic Neuroscience, **104:** 137–145.

Cui, D., Naftel, J. P., Lynch, J. C., Yang, G., Daley, W. P., Haines, D. E. and Fratkin, J. D. (2011). Atlas of Histology with Functional and Clinical Correlations. Lippincott Williams & Wilkins, a Wolters Kluwer business.

Cui-Sheng., Wang, J.L. and Xie, Z.M. (1998). The gross anatomy of the cranial cervical ganglion and its branches in the Bactrian camel (*Camelus bactrianus)*. Veterinary Research Communications **22**: 1–5.

Culling, C. F. A. (1975). Handbook of histological and Histochemical Techniques. Third Edition. Butterworth and Co. Ltd. London.

Dahl, D. (1983). lmmunohistochemical Differences between Neurofilaments in Perikarya, Dendrites and Axons. lmmunofluorescence Study with Antisera Raised to Neurofilament Polypeptides (ZOOK, 15OK, 7OK) Isolated by Anion Exchange Chromatography. Experimental Cell Research, **149:** 397–408.

Dalsgaard, C.J. and Elfvin, L.G. (1982). Structural studies on the connectivity of the inferior mesenteric ganglion of the guinea pig. Journal of Autonomic Nervous System, **5:** 265–278.

De Castro, F., Sanchez-Vives, M.V., Munoz-Martinez, E.J. and Gallego, R. (1995). Effects of postganglionic nerve section on synaptic transmission in the superior cervical ganglion of the guinea-pig. Neuroscience, **67:** 689–695.

Dixon, A. D. (1963). Fine structure of nerve-cell bodies and satellite cells in the trigeminal ganglion. American Association for Dental Research, **1919** (42): 990-999.

Donato, R., Cannon, B.R., Sorci, G., Riuzzi, F., Hsu, K., Weber, D. J. and Geczy, C.L. (2013). Published in final form as: Current Molecular Medicine, **13** (1): 24–57.

Drury, R. A. B. and Wallington, E. A. (1980). Carleton's Histological Techniques. Fifth Edition. Oxford University Press. New York. Toronto.

Elfvin, L. G. (1963). The ultrastructure of the superior cervical sympathetic ganglion of the cat. I. The structure of the ganglion cell processes

as studied by serial sections. Journal of Ultrastructure Research, **8:** 403-440.

Eroschenko, V. P. (2008). Di Fiore's Atlas of Histology with Functional Correlations. Eleventh Edition. Lippincott Williams & Wilkins.

Fawcett, D. W. (1994). Bloom and Fawcett A textbook of Histology. Twelfth Edition. Chapman, Hall: New York. London.

Fioretto, E. T., Guidi, W. L., Oliveira, P. C. and Ribeiro, A. A. C. M. (2003). Macrostructure of the cranial cervical ganglion complex and distal vagal ganglion during post-natal development in dogs. Brazilian Journal of Veterinary Research and Animal Science, **40:** 197-201.

Fioretto, E. T., de Abreu, R. N., de Souza Castro, M. F., Guidi, W. L. and Ribeiro, A. A. C. M. (2007). Macro- and Microstructure of the Superior Cervical Ganglion in Dogs, Cats and Horses during Maturation. Cells Tissues Organs, **186**:129-140.

Filichkina, N.M. (1981). Comparative radioautographic analysis of protein synthesis and slow transport in the axons of rabbit mono- and binuclear neurocytes. Arkh. Anat. Gistol. Embriol. **11:** 49–52.

Forssmann, W. G. (1964). Studien uber den Feinbau des Ganglion cervicale superius der Ratte. I. Normale Struktur. Acta anatomica, **59:** 106-140.

Fuchs, S. and Auer, M. (2010). Biochemistry and Histocytochemistry Research Developments. Nova Science Publishers, Inc. New York.

Gabella, G. (1976). Structure of the Autonomic Nervous System. London , Chapmam and Hall.

Gabella, G., Trigg, P. and McPhail, H. (1988). Quantitative cytology of ganglion neurons and satellite glial cells in the superior cervical ganglion of the sheep: relationship with ganglion neuron size. Journal of Neurocytology, **17:** 753–769.

Gabella, G. (2004). The Rat Autonomic Nervous System. London, Academic Press.

Gagliardo, K.M., Guidi, W.L., da Silva, R.A. and Ribeiro, A.A.C.M. (2003). Macro and microstructural organization of the dog's caudal mesenteric ganglion complex (*Canis familiaris).* Anatomia Histologia Embryologia, **32:** 236-243.

Gartner, L.P. and Hiatt, J. L. (2007). Color Textbook of Histology. Third Edition. Saunders, an imprint of Elsevier.

Gartner, L.P. and Hiatt, J. L. (2011). Concise Histology. Saunders, an imprint of Elsevier.

Getty, R. (1975): Sisson and Grossman's. The Anatomy of the Domestic Animals. Vol. 2. W.B. Saunders, Phidelphia. 1151–1155.

Gonzalez-Martinez, T., Perez-Pinera, P., Diaz-Esnal, B. and Vega, J.A. (2003). S-100 Proteins in the Human Peripheral Nervous System. Microscopy Research and Technique, **60:** 633–638.

Haines, D.E. (2013). Fundamental Neuroscience for Basic and Clinical Applications. Fourth Edition. Saunders, an imprint of Elsevier.

Hall, S.M. (1997). Axonal regeneration through acellular muscle grafts. Journal of Anatomy,**190:** 57-71.

Hanani, M. (2005). Satellite glial cells in sensory ganglia: from form to function. Brain Research Reviews, **48:** 457– 476.

Hanani, M. (2010). Satellite glial cells in sympathetic and parasympathetic ganglia: in search of function. Brain Research Reviews, **64:** 304-327.

Harman, D. (1989). Lipofuscin and ceroid formation: the cellular recycling system. Advances in Experimental Medicine and Biology, **266:** 3-15.

Hayakawa, T., Itoh, M., Miki, T., Kaneto, T., Tomiyama, H. and Takeuchi, Y. (2000). Sympathetic fibres innervating the extraocular muscles: cells of origin in the cat superior cervical ganglion. Okajimas Folia Anatomica Japnoica, **77:** 119–124.

Hedger, J.H. and Webber, R.H. (1976). Anatomical study of the cervical sympathetic trunk and ganglia in the albino rat (*Musnorvegicus albinos)*. Acta Anatomica, **96:** 206–217.

Heym, C. and Williams, T.H. (1979). Evidence for autonomic paraneurons in sympathetic ganglia of a shrew (*Tupaia glis*). Journal of Anatomy, **129**:151-164.

Hubbard, W.C., Robinson, J.C., Schmidt, K., Rohen, J.W., Tamm, E.R. and Kaufman, P.L. (1999). Superior cervical ganglionectomy in monkeys: effects on refraction and intraocular pressure. Experimental Eye Research, **68:** 637–639.

Hsu, S. M., Raine, L. and Fanger, H. (1981). Use of avidin-biotin peroxidase complex (ABC) in immunoperoxidase techniques. A comparison between ABC and unlabeled (PAP) procedures. Journal of Histochemistry Cytochemistry, **29:** 577-580.

Isobe, T., Ichimura, T. and Okuyama, T. (1989). Chemistry and Cell Biology of Neuron and Glia-Specific Proteins. Archives Histology and Cytology, **52:** 25-32.

Isobe, T., Ishioka, N. and Okuyama, T. (1981). Structural relation of two S-100 proteins in bovine brain subunit composition of S-100A protein. Europe Journal of Biochemistry, **115:** 469-474.

Isobe, T., Takahashi, K. and Okuyama, T. (1984). S-100 protein is present in neurons of the central and peripheral nervous system. Journal of Neurochemistry, **43:**1494–1496.

Kabak, M. (2007). The Gross Anatomy of the Cranial Cervical Ganglion in the Guinea Pig (*Cavia porcellus*). Veterinary Research Communications, **31:** 1–7.

Kabak, M. Orhan, I.O¨. and Hazıroglu, R.M. (2005). Macro anatomical investigations of the cranial cervical ganglion in domestic pig (*Sus*

scrofa domesticus). Anatomia, Histologia, Embryologia, **34:** 199–202.

Kabak, M. and Onuk, B. (2010). Macro anatomical investigations of the cranial cervical ganglion in roe deer (*Capreolus capreolus*). Ankara University Veterinary Fak Derg **57:** 1- 6

Kaemmer, D., Bozkurt, A., Otto, J., Junge, K., Klink, C., Weis, J., Sellhaus, B., O'Dey, D.M., Pallua, N., Jansen, M., Schumpelick, V. and Klinge, U. (2010). Evaluation of tissue components in the peripheral nervous system using Sirius red staining and immunohistochemistry: A comparative study (human, pig, rat). Journal of Neuroscience Methods, **190:** 112-116.

Kiran, S. (2002). Histogenesis of Neurons in Human Sympathetic Ganglia – A Light Microscopic Study. Journal of Anatomy Society of India, **51**(2): 148-155.

Knoche, H. and Addicks, K. (1976). Electron microscopic studies of the pressoreceptor fields of the carotid sinus of the dog. Cell and Tissue Research, **173:** 77-94.

Kokaia, M., Cenci, M.A., Elmer, E., Nilsson, O.G., Kokaia, Z. Bengzon, J. A. and Bjorklund, O. L. (1994). Seizure development and noradrenaline release in kindling epilepsy after noradrenergic reinnervation of the subcortically deafferented hippocampus by superior cervical ganglion or fetal locus coerulus grafts. Experimental Neurology, **130:** 351–361.

Ladizesky, M., Cutrera, R., Boggio, V., Mautalen, C.E. and Cardinali, D. (2000). Effect of unilateral superior cervical ganglionectomy on bone mineral content and density of rat's mandible. Journal of the Autonomic Nervous System, **78:** 113–116.

Lee, V. M. Y., Carden, M. J. and Trojanowski, J. Q. (1986). Novel Monoclonal Antibodies Provide Evidence for the in *situ* Existence of

a Non phosphorylated Form of the Largest Neurofilament Subunit. The Journal of Neuroscience**, 6** (3): 850-858.

Lee, V. M. Y., Carden, M. J., Schlaepfer, W.W. and Trojanowski, J. Q. (1987). Monoclonal Antibodies Distinguish Several Differentially Phosphorylated States of the Two Largest Rat Neurofilament Subunits (NF-H and NF-M) and Demonstrate their Existence in the Normal Nervous System of Adult Rats. The Journal of Neuroscience, **7** (11): 3474–3488.

Leong, S. K. and Wong, W. C. (1989). An ultrastructural study of the stellate ganglion of the pig-tailed monkey (*Macaca nemestrina*). Jounal of Anatomy, **164:** 1-18.

Liem, R. K. H., Yen, S. H., Salomon, G. B. and Shelanski, M. L. (1978). Intermediate filaments in nervous tissue. Journal of Cell Biology, **79:** 637-645.

Luebke, J.I. and Wright, L.L. (1992). Characterization of superior cervical ganglion neurons that project to the submandibular glands, the eyes, and the pineal gland in rats. Brain Research, **589:** 1–14.

Matthews, M. R. (1983). The ultrastructure of junctions in sympathetic ganglia of mammals. In: Autonomic Ganglia (L.-G. Elvin, ed.) Chichester: John Wiley and Sons, pp. 27-66.

Matthews, M.R. and Raisman, G. (1969). The ultrastructure and somatic efferent synapses of small granule-containing cells in the superior cervical ganglion. Journal of Anatomy, **105:** 255–282.

Matthews, M.R. (1989). Small intensely fluorescent cells and the paraneuron concept. Journal Electron Microscopy Technique, **12:** 408–416

Melian, C., Morales, M., Espinosa de los Monteros, A. and Peterson, M.E. (1996). Horner's syndrome associated with a functional thyroid carcinoma in a dog. Journal of Small Animal Practice, **37:** 591–593.

Miolan, J. and Niel, J. (1996). The mammalian sympathetic prevertebral ganglia: integrative properties and role in the nervous control of digestive tract motility. Journal of Autonomic Nervous System, **58:** 125–138.

Morgan, R.V. and Zanotti, S.W. (1989). Horner's syndrome in dogs and cats: 49 cases (1980–1986). Journal of the American Veterinary Medical Association, **194:** 1096–1099.

Najafi, G. and Nejati, V. (2009). Macro anatomical investigations of the cranial cervical ganglion of the sheep. Iranian Journal of Veterinary Research, **10** (2), 27: 186-188.

Najafi, G., Soltanalinejad, F. and Dehghani, D. (2011). Macrostructure of the Cranial Cervical Ganglion in the River Buffalo (*Bubalus Bubalis*). Veterinary Research Forum, **2** (3): 177-181.

Nourinezhad, J., Mazaheri, Y. and Biglari, Z. (2015). Detailed Anatomy of the Cranial Cervical Ganglion in the Dromedary Camel (*Camelus dromedarius)*. Anatomical Record, **298:** 1479–1491.

Nourinezhad, J., Mazaheri, Y. and Saberifar, S. (2016). Topography and morphology of the bovine cranial cervical ganglion and its branches. International Journal of Morphology, 34 ***(2)*:** 545-556

Ozgel, O., Kurtul, I. and Dursun, N. (2004). On the gross anatomy of the cranial cervical ganglion of the donkey (*Equus asinus*) in Turkey. Veterinary Research Communications, **28:** 261–266.

Palay, S. L. (1958). The morphology of the central nervous system. Experimental cell Research, **5:** 275-293.

Palay, S. L. and Palade, G. E. (1955). The fine structure of neurons. Journal of biophysical, biochemical and Cytology, **1:** 69-88.

Panciera, R.J., Ritchey, J.W., Baker, J.E. and Di Gregorio, M. (2002). Trigeminal and polyradiculoneuritis in a dog presenting with

masticatory muscle atrophy and Horner's syndrome. Veterinary Pathology, **39:** 146–149.

Pannese, E. (1981). The satellite cells of the sensory ganglia. Advances in Anatomy Embryology and Cell Biology, **65:** 1–111.

Pannese, E. (2015). Neurocytolog: Fine Structure of Neurons, Nerve Processes and Neuroglial Cells. Second Edition. Springer, Switzerland.

Peters, A., Palay, S.L. and Webster de, F. (1991) The Fine Structure of the Nervous system: Neurons and Their Supporting Cells. Second Edition. New York, Oxford University Press

Pomeroy, S.L. and Purves, D. (1988). Neuroglia relationships observed over intervals of several months in living mice. Journal of Cell Biology, **107:** 1167–1175.

Purves, D. and Wigston, D.J. (1983). Neural units in the superior cervical ganglion of the guinea-pig. Journal of Physiology, **334:** 169–178

Purves, D., Rubin, E., Snider, W.D. and Lichtman, J. (1986). Relation of animal size to convergence, divergence and neuronal number in peripheral sympathetic pathways. Journal of Neuroscience, **6:** 158-163.

Ribeiro, A.A.C.M., Elias, C.F., Liberti, E.A., Guidi, W.L. and de Souza, R.R. (2002). Structure and ultrastructure of the celiac-mesenteric ganglion complex in the domestic dog *(Canis familiaris)*. Anatomia, Histologia, Embryologia, **31:** 344–349.

Ribeiro, A.A.C.M., Davis, C. and Gabella, G. (2004). Estimate of size and total number of neurons in superior cervical ganglion of rat, capybara and horse. Anatomia, Histologia, Embryologia, **208:** 367–380.

Ribeiro, A.A.C.M. (2006). Size and number of binucleate and mononucleate superior cervical ganglion neurons in young capybaras. Anatomy and Embryology, **211:** 607–617.

Shao, B.P., Ding, Y.P., Xie, Z.H., Yu, H.X., Saberi, B. and Wang, J.L. (2007). The cranial cervical ganglion and its branches in the yak (*Bos grunniens)*. The Veterinary Journal, **173:** 176-179.

Shao, B. P., Ding, Y. P. and Wang, J. L. (2011). The cranial cervical ganglion and its branches in the white yak (*Bos grunniens*). Anatomia Histologia Embryologia, **40:** 321–325.

Sadoshima, S., Busija, D. M. and Brody, D. H. (1981). Sympathetic nerves protect against stroke in stroke-prone hypertensive rats: a preliminary report. Hypertension, **3:** 124–127.

Sadoshima, S. and Heistad. D. (1982) Sympathetic nerves protect the blood-brain barrier in stroke-prone spontaneously hypertensive rats. Hypertension, **4:** 904–907.

Santer, R.M. (2001). Sympathetic neuron numbers in ganglia of young and aged rats. Journal of Autonomic Nervous System, **33:** 221–222.

Schlaepfer, W. W. and Freeman, L. A. (1978). Neurofilament proteins of rat peripheral nerve and spinal cord. Journal of Cell Biology, **78:** 653-662.

Schmidt, R.E. (1996). Neuropathology of human sympathetic autonomic ganglia. Microscopy Research Technique, **35:** 107–121.

Sedaghat, F. and Notopoulos, A. (2008). S100 protein family and its application in clinical practice. Hippokratia Quarterly Medical Journal, **12** (4): 198–204.

Shaibani, A., Khawar, S., Shin, W., Cashen, T.A., Schirf, B., Rohany, M., Kakodkar, S. and Carroll, T.J. (2006). First results in an MR imaging-compatible canine model of acute stroke. American Journal of Neuroradiology, **27:** 1788–1793.

Siegesmund, K. A. (1968). The fine structure of subsurface cisterns. Anatomical Record, **162:** 187-196.

Siegrist, G., Dolivo, M., Dunant, Y., Foroglou-Kerameus, C., de Ribaupierre, F. and Rouiller, C. (1968). Ultrastructure and function of the chromaffin cells in the superior cervical ganglion of the rat. Journal of Ultrastructure Research, **25:** 381-407.

Smith, S. W. (1959). Reticular and areticular Nissl bodies in sympathetic neurons of a lizard. Journal of Biophysical and Biochemical Cytology **6:** 77-90.

Smith, R.B. (1970). Binucleate neurons in the human foetal heart. Experientia **26:** 772.

Sotelo, C. (1967). Dendritic profiles filled with mitochondria in the lateral vestibular nucleus of the rat. Anatomical Record, **157:** 326-330.

Suvarna, S. K., Layton, C. and Bancroft, J. D. (2013). Bancroft's Theory and Practice of Histological Techniques. Seventh Edition. Churchill Livingstone, Elsevier.

Szurszewski, J.H. and King, B.F. (1989). Physiology of prevertebral ganglia in mammals with special reference to inferior mesenteric ganglion; in S.G. Schultz, J.D. Wood, B.B. Rauner (eds): Handbook of Gastrointestinal Physiology. Bethesda, American Physiological Society, pp 519–577.

Szurszewski, J.H. and Miller, S.M. (1994). Physiology of the prevertebral ganglia; in L.R. Johnson (eds): Physiology of the Gastrointestinal Tract. New York, Raven Press, pp 795–878.

Trojanowski, J. Q., Obrocka, M. A. and Lee, V. M. Y. (1985). Distribution of neurofilament subunits in neurons and neuronal processes: immunohistochemical studies of bovine cerebellum with subunit-specific monoclonal antibodies. The Journal of Histochemistry and Cytochemistry, **33** (6): 55-563.

Trojanowski, J. Q., Walkenstein, N. and Lee, V. M. Y. (1986) Expression of neurofilaments subunits in neurons of the central and peripheral

nervous system: An immunohistochemical study with monoclonal antibodies. Journal of Neuroscience, 6 **(3):** 650-660.

Tropea, M. A., Johnson, M. I. and Higgins, D. (1988). Glial cells promote dendritic growth in the rat sympathetic neurons in *vitro*. Glia, **1**: 380-392.

Turkmenoglu, I. and Dursun, N. (2003). Koyunda ganglion cervicale craniale uzerine makroanatomik calismalar. Turkish Journal of Veterinary and Animal Sciences, **27:** 1019–1021.

Vega, J. A., del Valle-Soto, M. E., Calzada, B. and Alvarez-Mendez, J. C. (1991). Immunohistochemical localization of S-100 protein subunits (alpha and beta) in dorsal root ganglia of the rat. Cellular Molecular Biology, **37** (2):173-181.

Wang, H., Wu, M., Zhan, C., Ma, E., Yang, M., Yang, X. and Li, Y. (2012). Neurofilament proteins in axonal regeneration and neurodegenerative diseases. Neural Regeneration Research, 7 (8): 620-626.

Webster, H.D. (1975). Development of peripheral myelinated and unmyelinated nerve fibres. In: Dyck, P.J., Thomas, P.K., Lambert, E.H. (Eds.), Peripheral Neuropathy. Saunders, Philadelphia.

Williams, T.H., Jew, J. and Palay, S.L. (1973), Morphological plasticity in the sympathetic chain. Experimental Neurology, **39:** 181-203.

Wilson, R. T. (1984). The camel. First Edition. Longman Group Ltd. London. New York.

Wolf, R., Howard, O. M., Dong, H. F., Voscopoulos, C., Boeshans, K., Winston, J., Divi, R., Gunsior, M., Goldsmith, P., Ahvazi, B., Chavakis, T., Oppenheim, J.J. and Yuspa, S.H. (2008). Chemotactic activity of S-100A7 (Psoriasin) is mediated by the receptor for advanced glycation end products and potentiates inflammation with highly homologous but functionally distinct S100A15. Journal of Immunology, **181** (2):1499–1506.

Yokota, R. (1973). The granule-containing cell somata in the superior cervical ganglion of the rat, as studied by a serial sampling method for electron microscopy. Zeirschrift f**ü**r Zellforschung mikroskopische Anatomie, **141:** 331-345.

Yokota, R. and Yamauchi, A. (1974). Ultrastructure of the mouse superior cervical ganglion with particular reference to the pre- and postganglionic elements covering the soma of its principal neurons. American Journal of Anatomy, **140:** 281-298.

Young, B. and Heath, J. W. (2000). Wheater's Functional Histology. Fourth Edition. Churchill Livingstone, an imprint of Elsevier limited.

Young, B., O'Dowd, G. and Woodford, PH. (2014). Wheater's Functional Histology. A Text and Colour Atlas. Sixth Edition. Churchill Livingstone, an imprint of Elsevier Ltd.

APPENDIX

Capsule thickness

Animals = Animal 1

Descriptive Statistics[a]

	N	Range	Minimum	Maximum	Mean	Std. Deviation
Capsule thickness	5	19.48	162.46	181.94	171.7800	8.15939
Valid N (listwise)	5					

a. Animals = Animal 1

Animals = Animal 2

Descriptive Statistics[a]

	N	Range	Minimum	Maximum	Mean	Std. Deviation
Capsule thickness	5	45.31	121.69	167.00	138.0540	21.34983
Valid N (listwise)	5					

a. Animals = Animal 2

Animals = Animal 3

Descriptive Statistics[a]

	N	Range	Minimum	Maximum	Mean	Std. Deviation
Capsule thickness	5	55.92	143.94	199.86	181.4400	23.61092
Valid N (listwise)	5					

a. Animals = Animal 3

Animals = Animal 4

Descriptive Statistics

	N	Range	Minimum	Maximum	Mean	Std. Deviation
Capsule thickness	5	47.87	120.70	168.57	146.7940	17.57866
Valid N (listwise)	5					

a. Animals = Animal 4

Animals = Animal 5

Descriptive Statistics

	N	Range	Minimum	Maximum	Mean	Std. Deviation
Capsule thickness	5	96.33	111.65	207.98	141.5560	38.12738
Valid N (listwise)	5					

a. Animals = Anima 5

Size of principal neurons of cranial cervical ganglion

Value Label		N
Size of neuron	Small size`	25
	Medium size	25
	Large size	25
Animal number	Animal number 1	15
	Animal number 2	15
	Animal number 3	15
	Animal number 4	15
	Animal number 5	15

Descriptive Statistics

Dependent Variable: Size of principal neurons of cranial cervical ganglion

Size of neuron	Animal number	Mean	Std. Deviation	N
Small size`	Animal number 1	81.2360	8.90358	5
	Animal number 2	76.4160	11.88921	5
	Animal number 3	74.0800	5.32717	5
	Animal number 4	81.4820	10.25699	5
	Animal number 5	72.4820	6.09138	5
	Total	77.1392	8.90070	25
Medium size	Animal number 1	138.9580	20.56258	5
	Animal number 2	129.5200	17.23854	5
	Animal number 3	124.1900	25.96878	5
	Animal number 4	119.9420	17.91535	5
	Animal number 5	123.1600	13.15645	5
	Total	127.1540	18.99789	25
Large size	Animal number 1	271.3440	39.79357	5
	Animal number 2	256.2980	22.89306	5
	Animal number 3	290.6320	33.72207	5
	Animal number 4	240.0940	38.47397	5
	Animal number 5	192.7380	21.95154	5
	Total	250.2212	44.92712	25
Total	Animal number 1	163.8460	85.91553	15
	Animal number 2	154.0780	79.85142	15
	Animal number 3	162.9673	98.51551	15
	Animal number 4	147.1727	73.71828	15
	Animal number 5	129.4600	52.92833	15
	Total	151.5048	78.47443	75

Tests of Between-Subjects Effects

Dependent Variable: Size of principal neurons of cranial cervical ganglion

Source	Type III Sum of Squares	df	Mean Square	F	Sig.
Corrected Model	425762.834[a]	14	30411.631	60.932	.000
Intercept	1721527.832	1	1721527.832	3449.196	.000
Size	396703.289	2	198351.644	397.411	.000
Animal No	11925.852	4	2981.463	5.974	.000
Size * Animal No	17133.692	8	2141.712	4.291	.000
Error	29946.589	60	499.110		
Total	2177237.254	75			
Corrected Total	455709.423	74			

a. R Squared = .934 (Adjusted R Squared = .919)

Post Hoc Tests

Size of animals

Multiple Comparisons

Dependent Variable: Size of principal neurons of cranial cervical ganglion

LSD

(I) Size of neuron	(J) Size of neuron	Mean Difference (I-J)	Std. Error	Sig.	99% Confidence Interval
					Lower Bound
Small size`	Medium size	-50.0148*	6.31892	.000	-66.8249
	Large size	-173.0820*	6.31892	.000	-189.8921
Medium size	Small size`	50.0148*	6.31892	.000	33.2047
	Large size	-123.0672*	6.31892	.000	-139.8773
Large size	Small size`	173.0820*	6.31892	.000	156.2719
	Medium size	123.0672*	6.31892	.000	106.2571